AD NUMBER

AD873340

LIMITATION CHANGES

TO:

Approved for public release; distribution is unlimited. Document partially illegible.

FROM:

Distribution authorized to U.S. Gov't. agencies and their contractors; Critical Technology; APR 1970. Other requests shall be referred to Army Missile Command, Attn: AMSMI-RD, Redstone Arsenal, AL 35809. Document partially illegible. This document contains export-controlled technical data.

AUTHORITY

usamc, ltr, 15 nov 1972

(Revision)

REPORT NO. RD-TR-70-8

NORMAL FORCE EFFECTIVENESS OF SEVERAL FIN PLANFORMS WITH STREAMWISE GAPS AT MACH NUMBERS OF 0.8 TO 5.0

by

C. W. Dahlke
W. Pettis

April 1970

This document is subject to special export controls and each transmittal to foreign governments or foreign nationals may be made only with prior approval of this Command, ATTN: AMSMI-RD.

U.S. ARMY MISSILE COMMAND
Redstone Arsenal, Alabama 35809

DISCLAIMER NOTICE

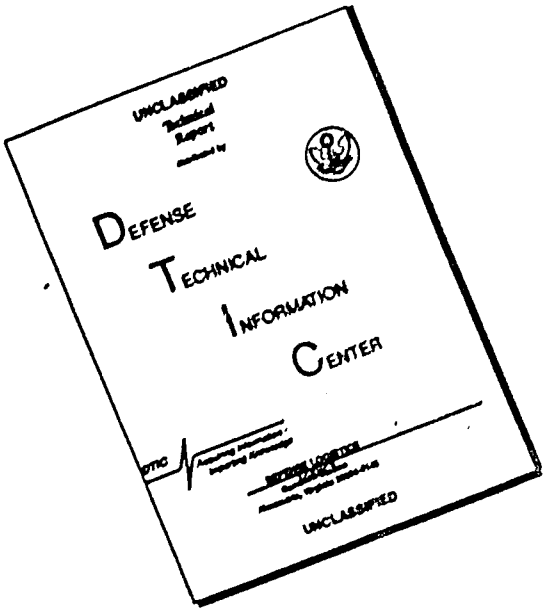

THIS DOCUMENT IS BEST QUALITY AVAILABLE. THE COPY FURNISHED TO DTIC CONTAINED A SIGNIFICANT NUMBER OF PAGES WHICH DO NOT REPRODUCE LEGIBLY.

24 April 1970

Report No. RD-TR-70-8
(Revision)

NORMAL FORCE EFFECTIVENESS OF SEVERAL FIN PLANFORMS WITH STREAMWISE GAPS AT MACH NUMBERS OF 0.8 TO 5.0

by

C. W. Dahlke
W. Pettis

DA Project No. 1M262301A206
AMC Management Structure Code No. 5221.11.14800

Advanced Systems Laboratory
Research and Engineering Directorate
U. S. Army Missile Command
Redstone Arsenal, Alabama 35809

Abstract

This report contains the results and analysis of a series of wind-tunnel tests for several rectangular and one delta fin planform with streamwise gaps between the fin root chord and body. The tests were conducted at free-stream Mach numbers from 0.8 to 1.5 with fin to body gap variation of 0.00 to 0.25 body diameter. The normal force effectiveness for the fin-gap configuration is presented as normal force coefficient slopes at zero angle of attack. Small gaps are shown to cause significant loss in fin effectiveness especially at transonic Mach numbers.

Contents

Illustrations

Table

Figure

Illustrations (Concluded)

Symbols

A_{ref}	reference area, $\frac{\pi}{4} D^2$
b	fin exposed semi span
C	fin chord
C_A	axial force coefficient
C_m	pitching moment coefficient
C_N	normal force coefficient
C_{N_α}	$dC_N/d\alpha$
D	body diameter
G	fin-body gap
M	Mach number
X_{cp}	center of pressure percent chord from trailing edge
t	fin maximum thickness
subscripts	
0	zero angle of attack
∞	free-stream conditions

I. Introduction

The Aerodynamics Branch, Advanced Systems Laboratory, Research and Engineering Directorate, Army Missile Command, is currently conducting a supporting research project in stability margin management. The purpose of the project is to establish methods and design data which will allow the aerodynamic design engineer to provide a configuration having a desired stability margin variation with Mach number. The desired variation is that one which trajectory simulation requires for greatest accuracy or minimum dispersion.

One problem area is the large increase in stability margin which occurs through the transonic velocity regime. For high acceleration vehicles this occurs early in the trajectory. Any path errors introduced at this point cause large dispersions in unguided rocket vehicles and complicate the control gains required for guided vehicles. The ability to reduce or eliminate this transonic stability increase is highly desirable and an important requirement in stability margin management.

Most of the transonic stability increase is due to the fins used to stabilize the vehicle. The stability of a fin-stabilized rocket is a function of the fin-normal force and center of pressure. Generally, the best planform for accomplishing a reduction in the transonic stability margin is the low aspect ratio rectangular planform. The lower the aspect ratio, the lower is the transonic rise in normal force.

There are times in missile design, however, when the lower aspect ratio cannot be tolerated at the extremes of the flight Mach number regime. For these cases higher aspect ratio fins may be required than are desirable at transonic speeds. When trade-offs between fin aspect ratio and fin area give unsatisfactory transonic static margin, other methods of reducing the transonic fin lift may be desirable. One method of doing this is using more than four-multiple fins [1]. The use of multiple fins, however, may be precluded by the increase of cost and structural complexity, and multiple fins may cause undesirable weight penalities. Another method of decreasing the fin lift is allowing bleed between the fin root chord and the body surface through fin-body gaps, thereby allowing equalization of fin-body interaction pressure.

This report presents the results of wind-tunnel tests conducted at Mach numbers from 0.8 to 4.5 of four configurations with three rectangular and one delta fin configuration with root-chord-body gaps from 0.0 to 0.25 body diameter over an angle of attack range of from -4 to 8 degrees. These tests were part of an overall program designed to study the methods of varying transonic stability.

2. Apparatus

Wind-tunnel tests were conducted at two facilities during this study. The transonic portion of the test was conducted at the 1-foot transonic tunnel [2], Propulsion Wind Tunnel Facility, Arnold Engineering Development Center (AEDC), Arnold Air Force Station, Tennessee, and the supersonic portion at Ballistic Research Laboratories (BRL) tunnel No. 1 [3]. Aerodynamic forces and moments were measured with the Army Missile Command VHB-2-4 six-component strain gage balance. This balance has a 10-pound normal force and a 5-pound side force capacity.

The basic model is a 4-caliber tangent ogive nose with an 8-caliber cylindrical afterbody. The model diameter is 1.1 inches. The model is uniquely designed to measure the forces and moments on the aft 2 calibers of length only. This balanced section is designed so that a split barrel section may be replaced with other barrels having fins mounted on them. The total normal force measured is the cylinder loading by the induced pressure distribution due to the nose, the cylinder loading due to the presence of the fins, and the fins in the presence of the body. The configurations tested are described in Table I and Figures 1 and 2.

TABLE I. GEOMETRY OF MODEL FIN CONFIGURATIONS

Configuration	Total Span / D	Root Chord / D	Gap / D	AR without Gap
FD. 00	1.955	1.273	0.00	1.50
FD. 06	2.075		0.06	
FD. 12	2.195		0.12	
FD. 20	2.355		0.20	
F4. 00	1.856	0.856	0.00	1.00
F4. 08	2.016		0.08	
F4. 16	2.176		0.16	
F4. 25	2.356		0.25	
F7. 00	1.955	1.273	0.00	0.75
F7. 06	2.075		0.06	
F7. 12	2.195		0.12	
F. 720	2.355		0.20	

TABLE I. GEOMETRY OF MODEL FIN CONFIGURATIONS (Concluded)

Configuration	Total Span / D	Root Chord / D	Gap / D	AR without Gap
F8.00	1.636	1.273	0.00	0.50
F8.04	1.716		0.04	
F8.12	1.876		0.12	
F8.20	2.036		0.20	
0000	Instrumented Afterbody only, D = 1.1 in.			

NOTES: FD – delta fin
F4, F7, and F8 – rectangular rin
16 finned configurations

The model configurations were chosen to give some variation in fin planform as well as fin to body gap variation. Two basic planforms, rectangular and delta, were chosen and sized to fit within the constraints normally imposed on typical Army missile design. Fin configurations F4, F7, and F8 had rectangular planforms with aspect ratios of 1.0, 0.75, and 0.50 respectively. A single delta fin planform had an aspect ratio of 1.5; however, the root chord and span are identical to the rectangular fin F7. All configurations were tested with the fins in a cruciform arrangement at the same roll attitude. The roll attitude was with the fins arranged in the vertical and horizontal lifting planes such that the vertical plane was always at a geometric zero yaw angle.

3. Procedure

All configurations except F7 were tested at Mach numbers of 0.8 to 1.4 at AEDC, and all configurations were tested at Mach numbers of 1.75 to 3.0 at BRL. Data were acquired for all runs at angles of attack including and varying between -4 and 8 degrees in 1-degree increments. Half-degree increments were taken between -2 and 2 degrees. The wind-tunnel operating conditions in the transonic portion at AEDC [4] result in Reynolds numbers of from 0.38 to 0.45×10^6 per inch. A constant Reynolds number of 0.48×10^6 per inch at all Mach numbers was maintained at BRL during the supersonic test.

The relative deflections between the forebody and the instrumented afterbody are accounted for in data reduction. The estimated precisions of measurements are as follows:

$C_N = \pm 0.004$ $C_m = \pm 0.003$

$C_A = \pm 0.004$ $M_\infty = \pm 0.003$

$q_\infty = \pm 3$ psf $\alpha = \pm 0.1$ deg

4. Results and Discussion

The results of the present investigation are based upon two wind-tunnel tests: A transonic test at AEDC [4], and a supersonic test at BRL with the same model used at both facilities (Figures 1 and 2). The basic data plots of normal force C_N, pitching moment C_m and axial force C_A coefficients versus model angle of attack, and pitching moment versus normal force coefficients are contained in the appendix.

Figures 3 through 18 present the summary of the results for all Mach numbers of the various configurations. These are presented in the form of normal force coefficient slope C_{N_α}, center of pressure X_{cp}, and axial force coefficient C_{A_0} at zero angle of attack.

a. Normal Force Effectiveness

Figures 3 through 6 present the slope of the normal force coefficient $dC_N/d\alpha$ at zero angle of attack as a function of free-stream Mach number.

The C_{N_α} presented represents the total normal force effectiveness of basic fin lift, body upwash, fin-body carryover, fin-body gap effects, and the small component of cylinder lift especially around $M_\infty = 1$ (Figure 18).

The normal procedure for determining fin effectiveness on missile configurations experimentally is to make measurements of the body without fins first, then make measurements of this same body with fins attached. The fin effectiveness can then be determined by taking the difference between these two measurements at the same free-stream flow conditions. This technique requires that the model instrumentation have load capacity much higher than loads produced by the fins. Accuracy is sacrificed by having to take the difference, since the body lift is usally of the same order of magnitude as the fin effectiveness for typical missile configurations. Definition of the effects of adding streamwise

gaps between the body and fin requires better accuracy than that achieved through the above procedure.

Because of the uniqueness of the model used in this study (Figure 1), the body forces are small compared to the fin effectiveness. Figure 18 presents the normal force coefficient slope as a function of Mach number for the instrumented cylindrical section of the body. The effects of fin gaps on the normal force effectiveness can be shown without the complication of making subtraction of the body alone from the total measured effectiveness. The summary data for the body without fins are contained in Figure 18, and Figures A-16 (a-d) of the appendix contain the basic wind-tunnel results if it is desired to determine the fin effectiveness alone.

Normal force effectiveness shown in Figures 3 through 6 are in the form of the best estimate of the slope $dC_N/d\alpha$ at zero angle of attack. The slopes were determined by a fifth-order polynomial curve fit of data points for -4 deg $\leq \alpha \leq 4$ deg, and were checked at each Mach number for all configurations by graphical hand sloping methods. For configuration F8 (smallest fin) the data are highly nonlinear with respect to angle of attack, and some interpretation had to be made to the use of the slopes from the polynominal fit. In all cases the C_{N_α} represents the best estimate of the true slope at zero angle of attack. For fins F4, F8, and FD (Figures 3, 5, and 6) both transonic and supersonic tests were conducted; however, for F7 (Figure 4) there were no transonic tests conducted. It can be seen from Figures 3 through 6 that the effect of increasing gap from 0.0 to 0.25 body diameters causes a general reduction of the normal force effectiveness throughout the Mach number range, but most reduction occurs transonically and at low supersonic Mach numbers. This could be especially useful when it is desired to reduce the missile static margin variation throughout the Mach number range.

Figures 7 through 10 show the normal force effectiveness C_{N_α} as a function of the ratio of gap distance to the body diameter, G/D, for various Mach numbers. These figures are simply cross plots of Figures 3 through 6, but they demonstrate how the small gap has significant effect with the change in effect becoming less significant as the gap increases. The influence of the post attaching the fins to the body has not been isolated for this study. The posts are cylindrical (Figure 2), and the normal force contributed by them is expected to be insignificant at small α. The influence of the post on body upwash and carryover, however, is not known at this time.

A theoretical model is being developed that utilizes a modified linear theory to predict the fin effectiveness for fins with streamwise gaps. These data will be used to make comparison with this theory in a report at a later date.

b. Center of Pressure

Figures 11 through 14 present the center of pressure X_{cp} expressed in percent root chord from the fin trailing edge for each configuration as a function of Mach number. The X_{cp} are determined from the slope of the pitching moment C_m versus the normal force C_N curves at $C_N = 0$. For the transonic data the moment reference center is 9.518 body diameters from the model nose (Station 10.47) or 2.484 body diameters from the fin trailing edge. The center of pressure from the trailing edge is

$$X_{cp} = 2.484 + dC_m \Big/ dC_N \Big|_{\alpha = 0} .$$

For the supersonic data the moment reference center is at the fin trailing edge and

$$X_{cp} = dC_m \Big/ dC_N \Big|_{\alpha = 0} .$$

It can be seen by comparing the transonic to the supersonic data that there is some disagreement betwee. the AEDC and the BRL levels of X_{cp}: If the change in body-alone X_{cp} were accounted for, the transonic-body-alone effects would partly account for this difference. Some differences could also be attributed to accuracy involved in transferring moments during the wind-tunnel data reduction process.

c. Axial Force

Figures 15 through 17 present the zero angle of attack axial force coefficient as a function of Mach number for fins F4, F8, and FD will all gaps. The axial force was not obtained at the supersonic Mach numbers for fins F4, F7, and F8 because of an error in instrumentation. For axial force computations, the body without fins must be considered -- even though it was neglected for normal force effectiveness — because of base and friction drag components. The base drag was determined from the average of two static pressure orifices mounted on the model base. The values of C_{A_0} in Figures 15 through 17 are computed from:

$$C_{A_0} = C_{A_0}{}_{\text{FIN + BODY}} - C_{A_0}{}_{\text{BODY}}$$

5. Conclusions

This study has been conducted to determine the effect of adding streamwise gaps between the fin root chord and a body of revolution. Based on the results of a series of wind-tunnel tests at both transonic and supersonic Mach numbers, the following conclusions are made:

1) The fin effectiveness is significantly reduced by adding streamwise gaps between the fin and body of missile configurations.

2) The largest reduction of fin effectiveness occurs at the transonic and low supersonic Mach numbers, tending to flatten the C_{N_α} versus Mach number variation.

3) Small gaps cause large reduction in fin effectiveness, with a lower rate of change in effectiveness reduction at larger gaps.

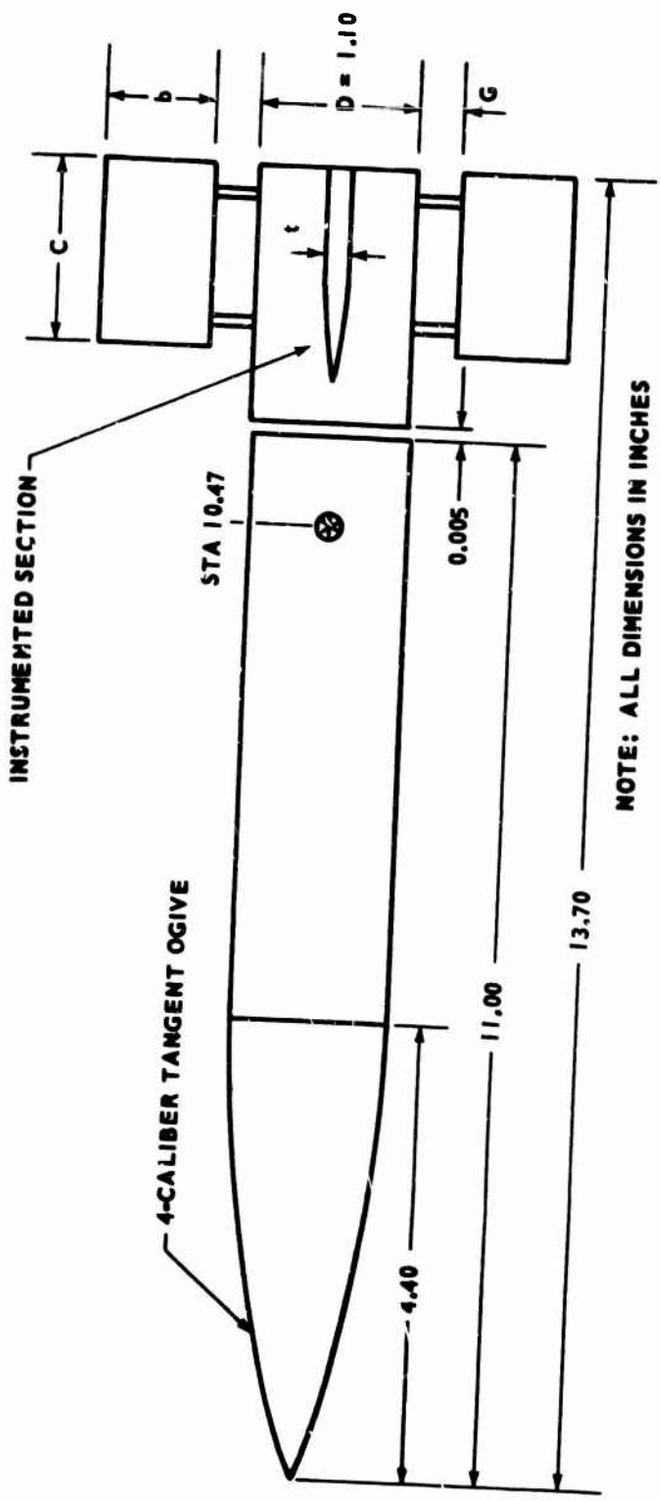

FIGURE 1. MODEL GEOMETRY

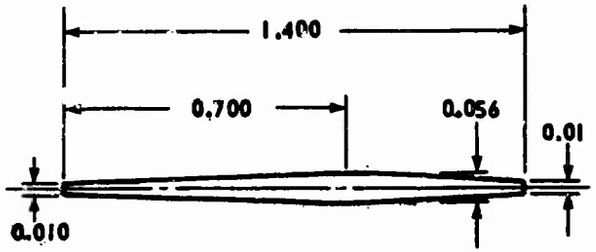

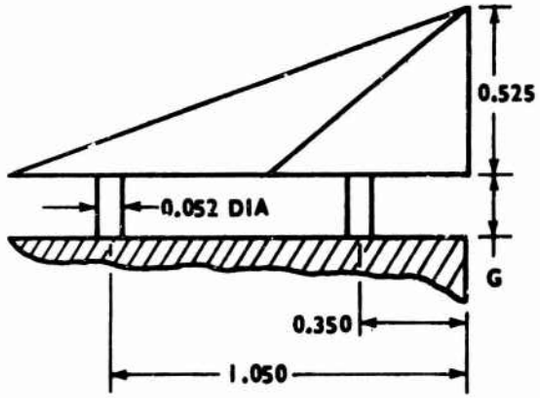

CONFIGURATION	G
FD.00	0
FD.06	0.066
FD.12	0.132
FD.20	0.220

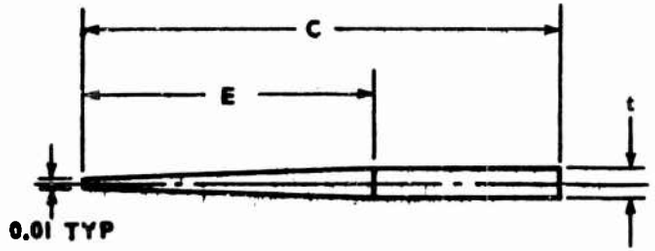

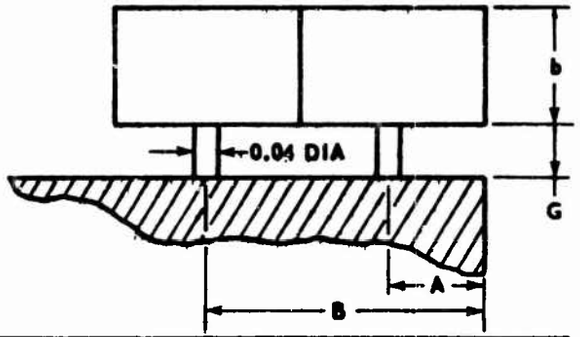

CONFIGURATION	C	b	t	G	A	B	E
F4.00 F4.08 F4.16 F4.25	0.942	0.471	0.063	0 0.068 0.176 0.275	0.242	0.706	0.520
F7.00 F7.06 F7.12 F7.20	1.400	0.525	0.056	0 0.066 0.132 0.220	0.350	1.050	0.350
F8.00 F8.06 F8.12 F8.20	1.400	0.350	0.056	0 0.066 0.132 0.220	0.350	1.050	0.350

FIGURE 2. FIN GEOMETRY

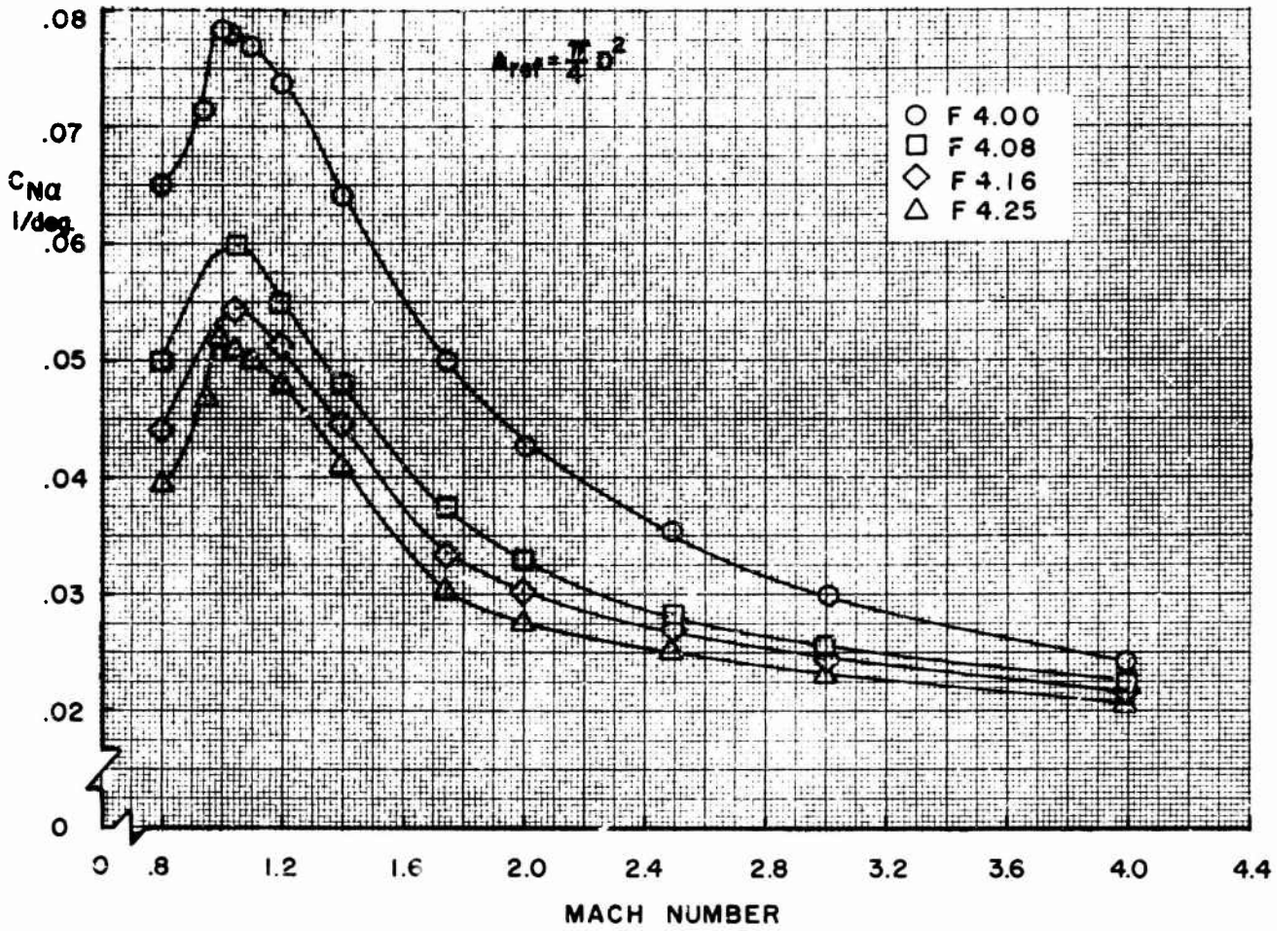

FIGURE 3. NORMAL FORCE COEFFICIENT SLOPE VERSUS MACH NUMBER, F4

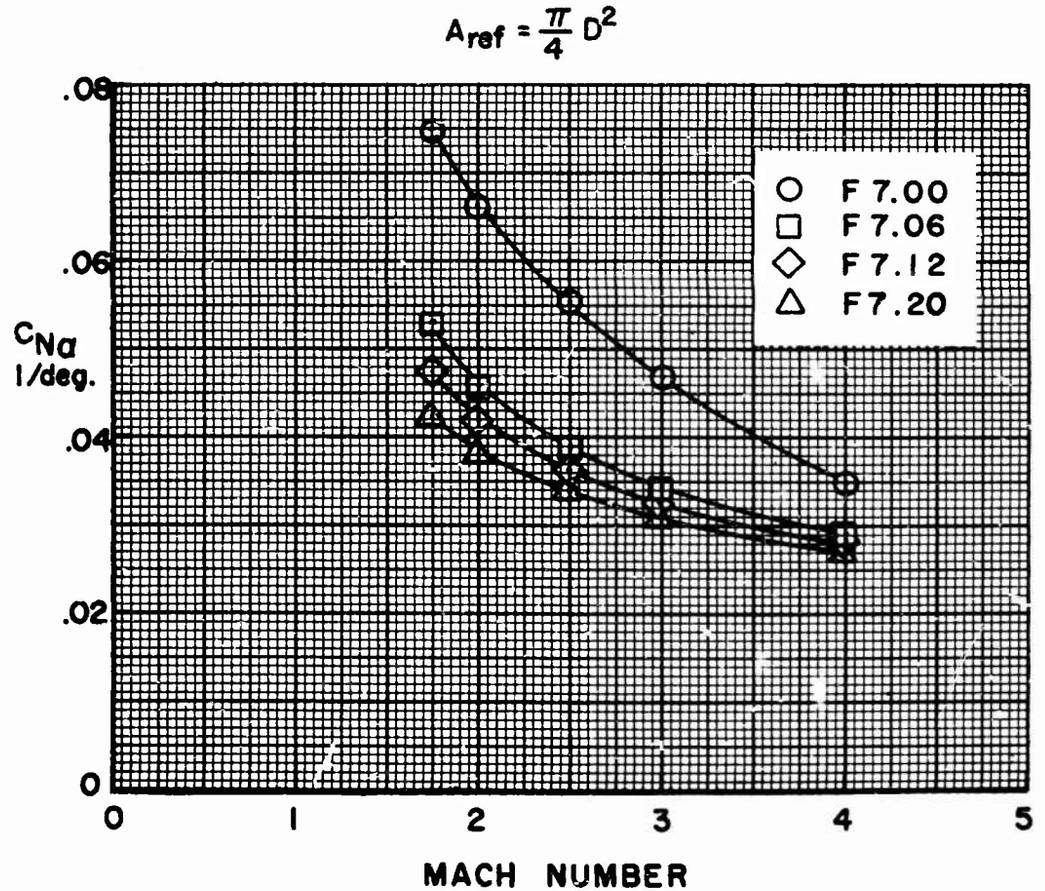

FIGURE 4. NORMAL FORCE COEFFICIENT SLOPE VERSUS MACH NUMBER, F7

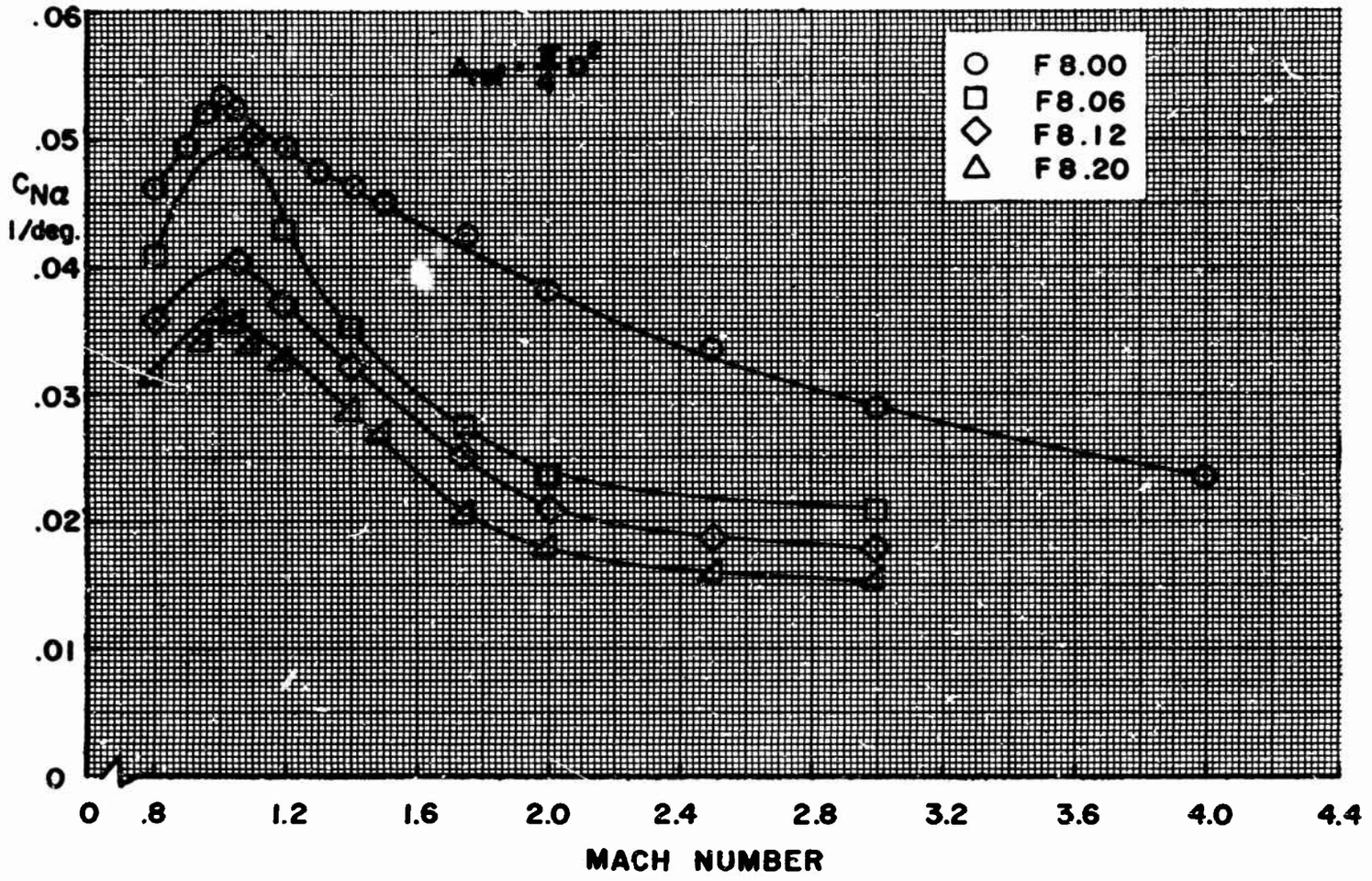

FIGURE 5. NORMAL FORCE COEFFICIENT SLOPE VERSUS MACH NUMBER, F8

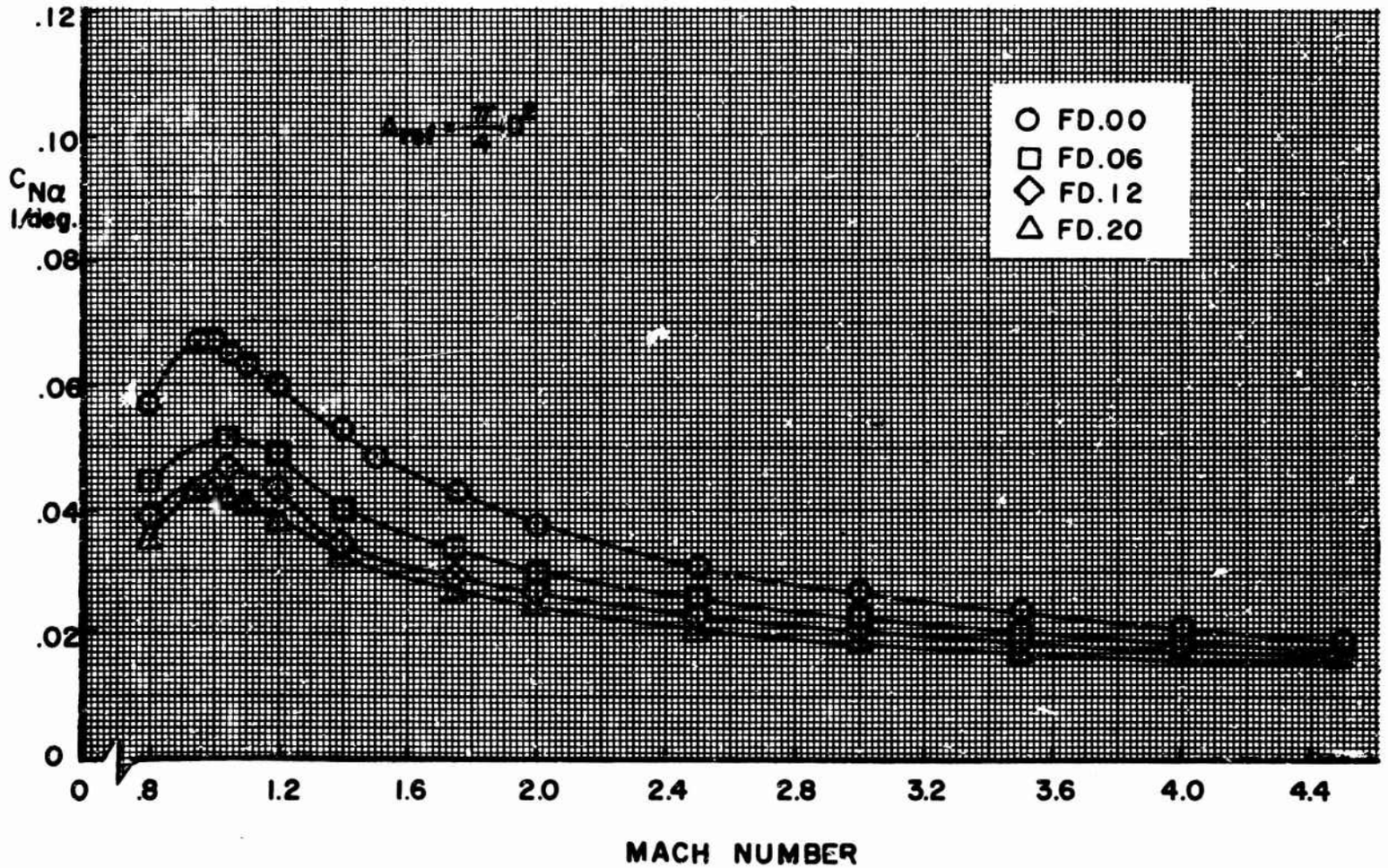

FIGURE 6. NORMAL FORCE COEFFICIENT SLOPE VERSUS MACH NUMBER, FD

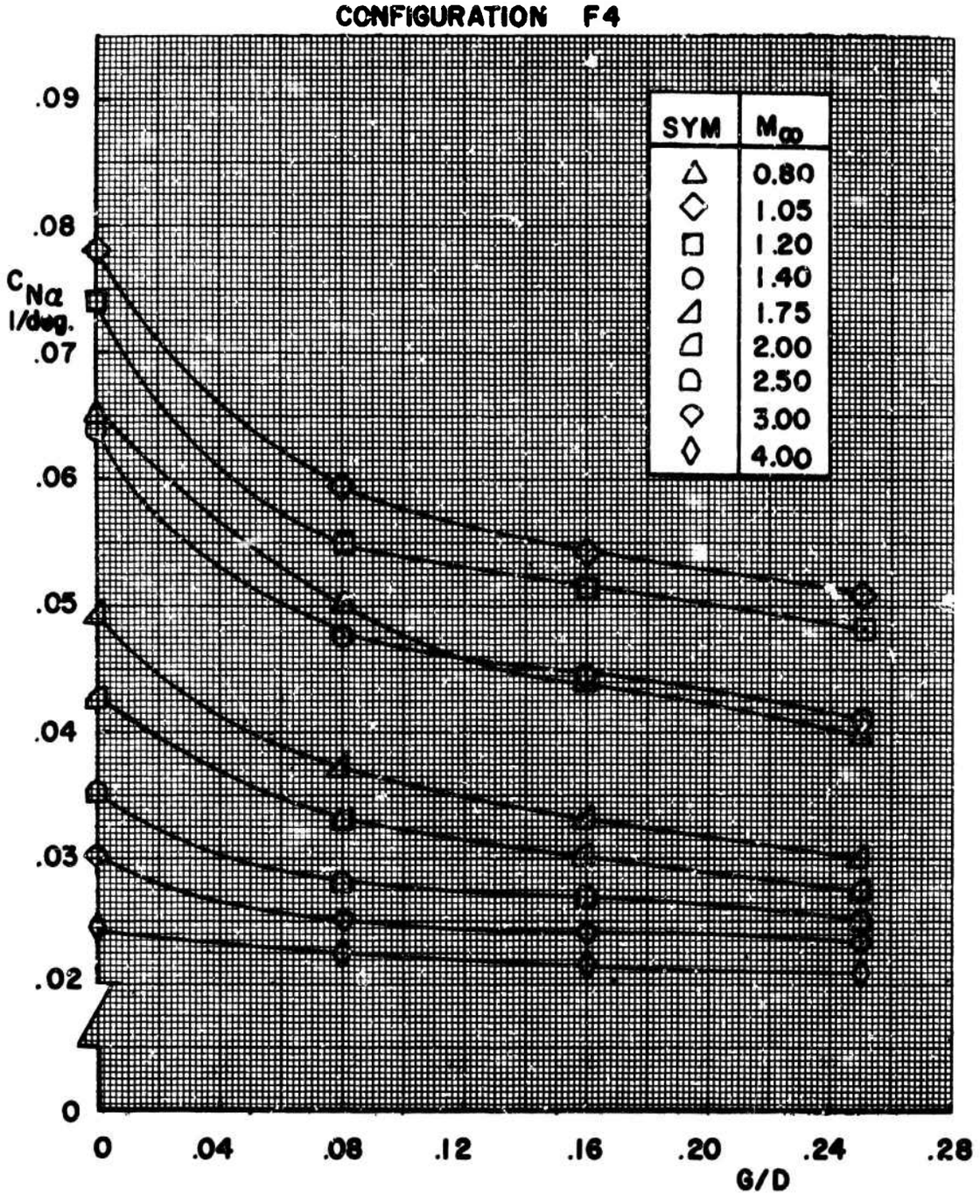

FIGURE 7. NORMAL FORCE COEFFICIENT SLOPE VERSUS GAP-TO-DIAMETER RATIO, F4

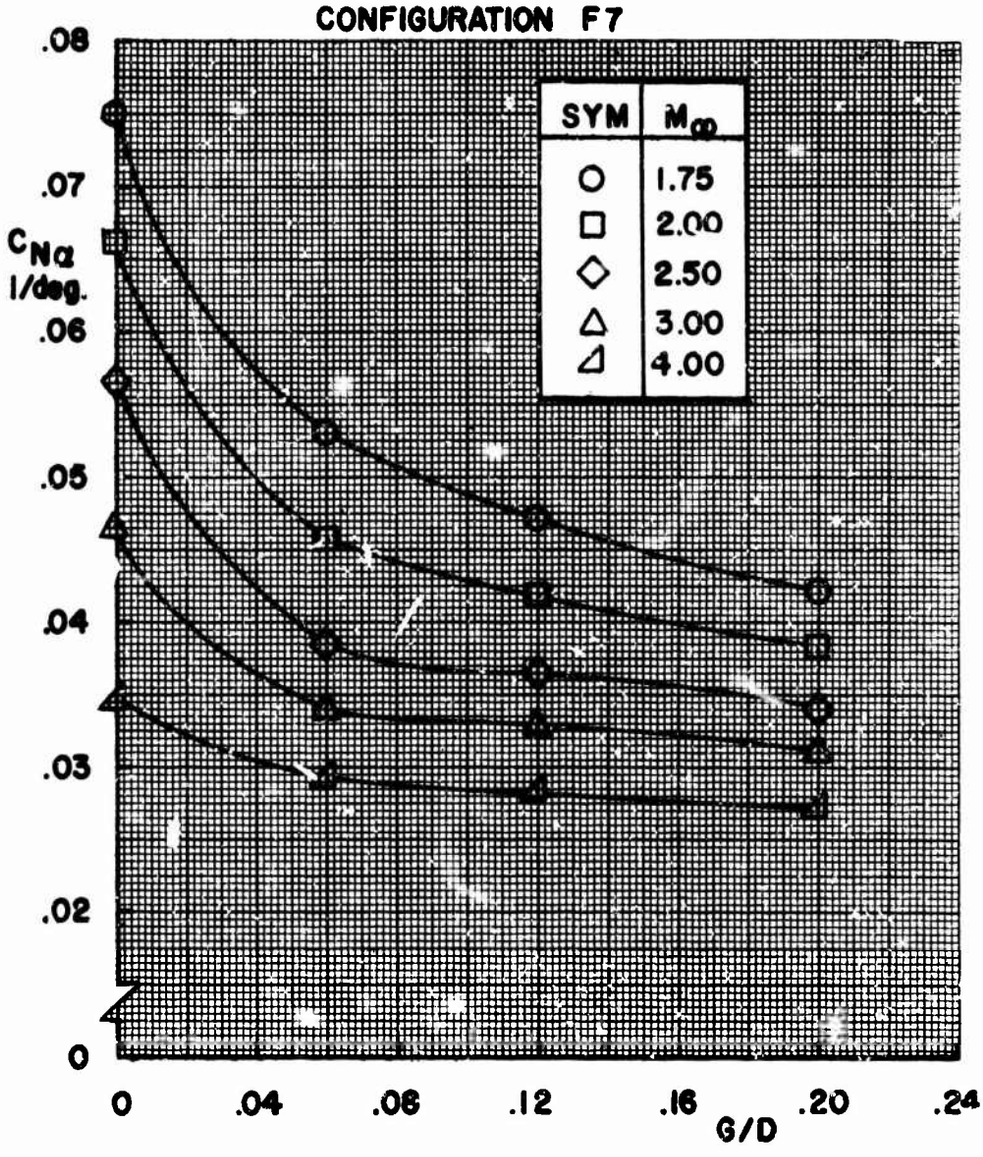

FIGURE 8. NORMAL FORCE COEFFICIENT SLOPE VERSUS GAP-TO-DIAMETER RATIO, F7

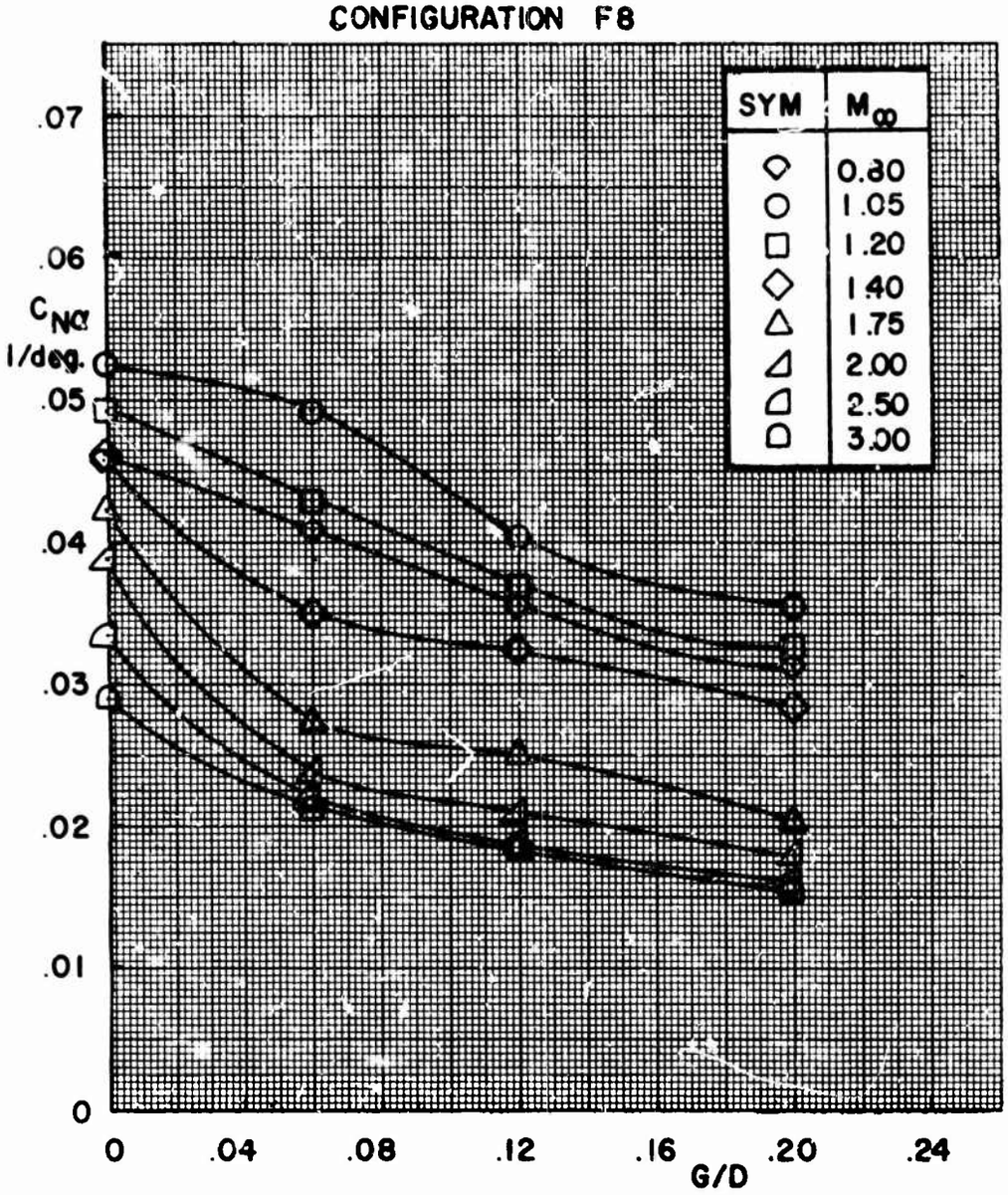

FIGURE 9. NORMAL FORCE COEFFICIENT SLOPE VERSUS GAP-TO-DIAMETER RATIO, F8

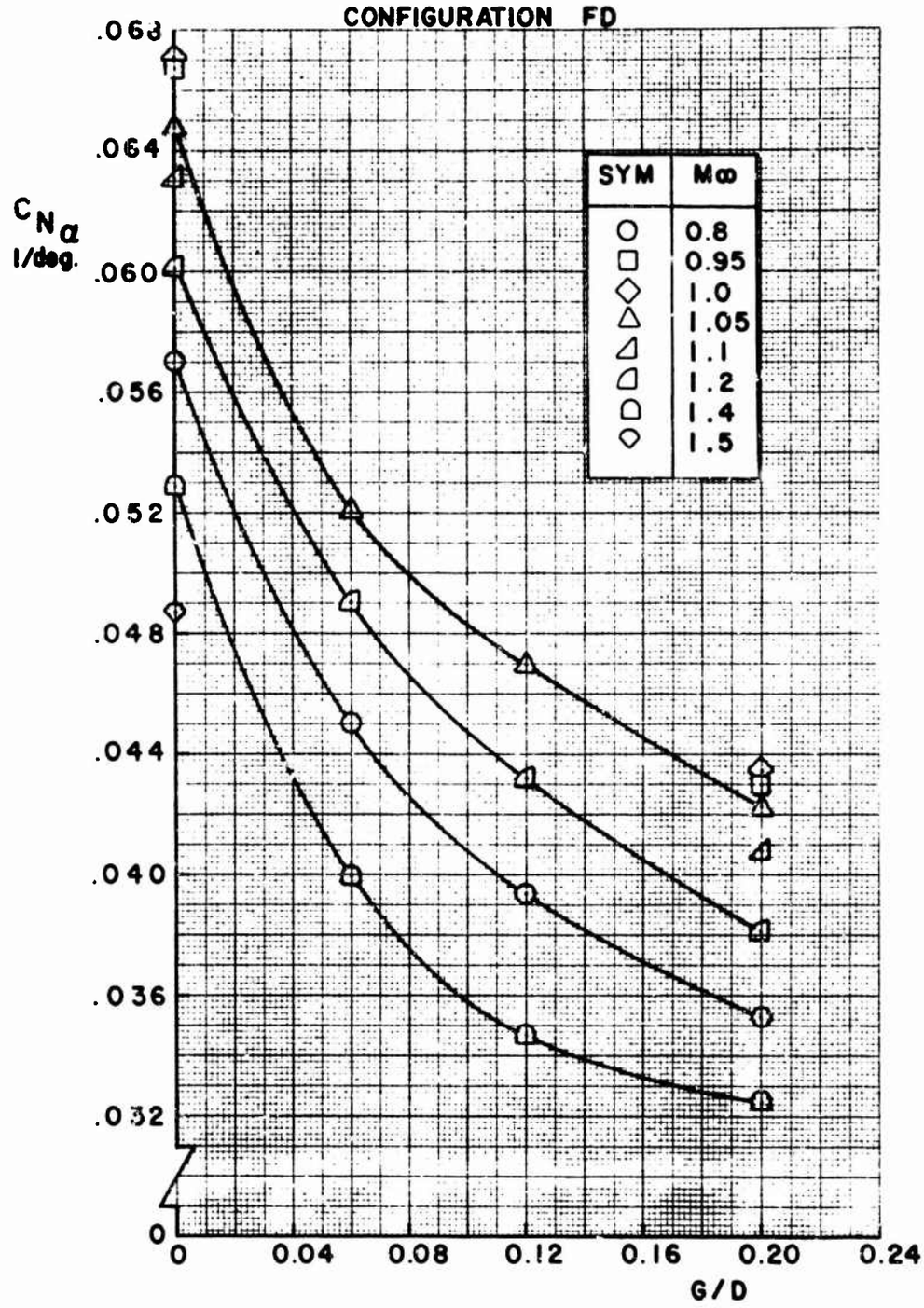

FIGURE 10. NORMAL FORCE COEFFICIENT SLOPE VERSUS GAP-TO-DIAMETER RATIO, FD

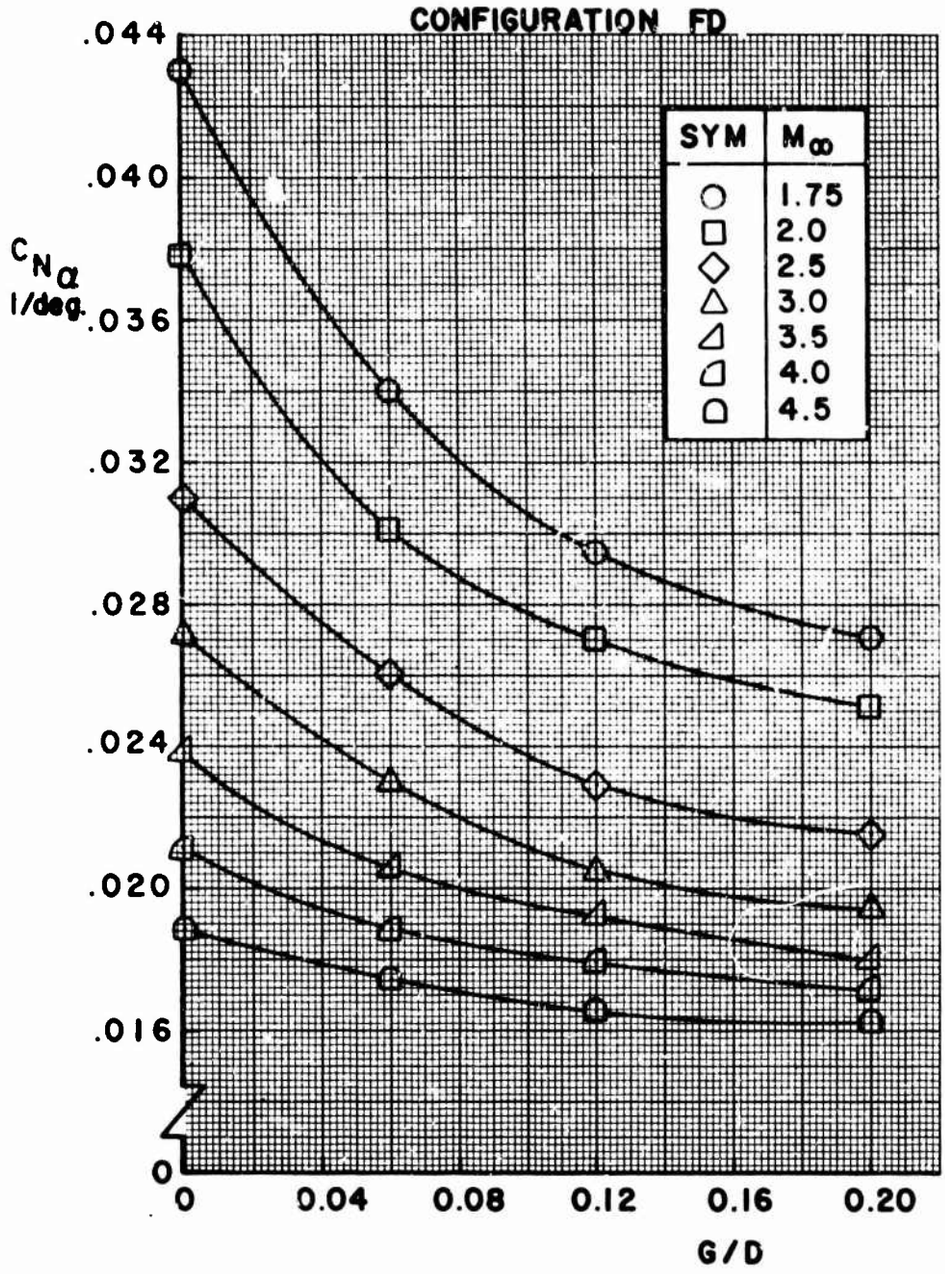

FIGURE 10. NORMAL FORCE COEFFICIENT SLOPE VERSUS GAP-TO-DIAMETER RATIO, FD (Concluded)

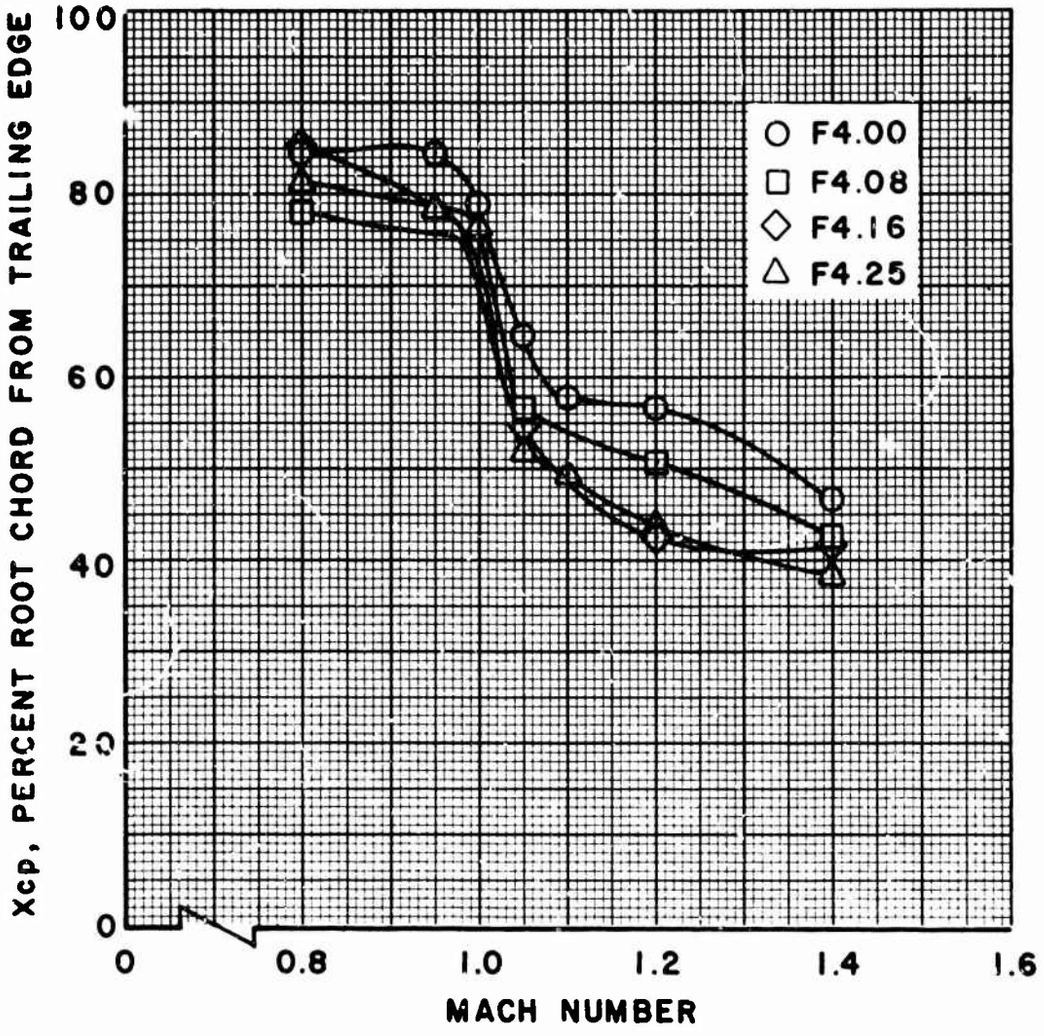

FIGURE 11. CENTER OF PRESSURE VERSUS MACH NUMBER, F4

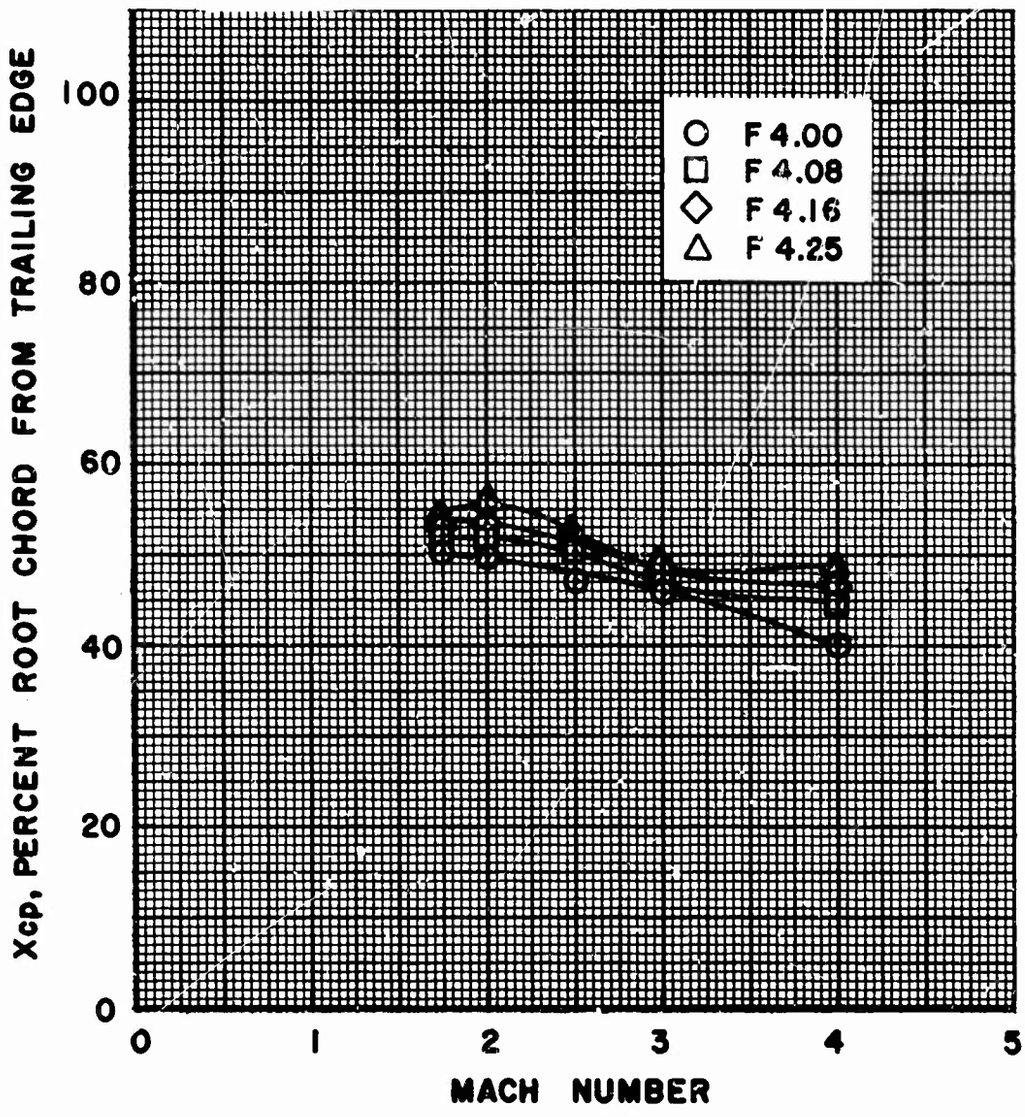

FIGURE 11. CENTER OF PRESSURE VERSUS MACH NUMBER F4 (Concluded)

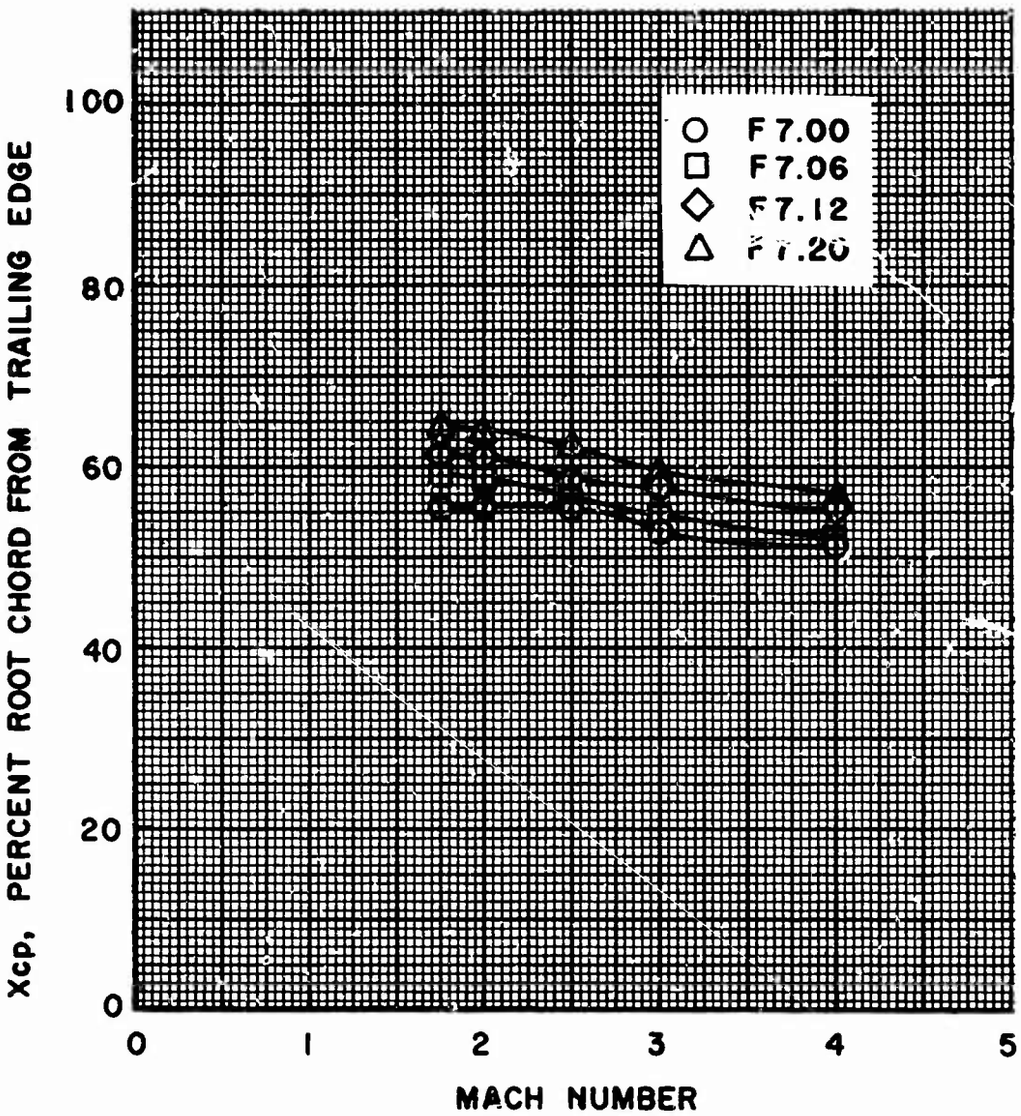

FIGURE 12. CENTER OF PRESSURE VERSUS MACH NUMBER, F7

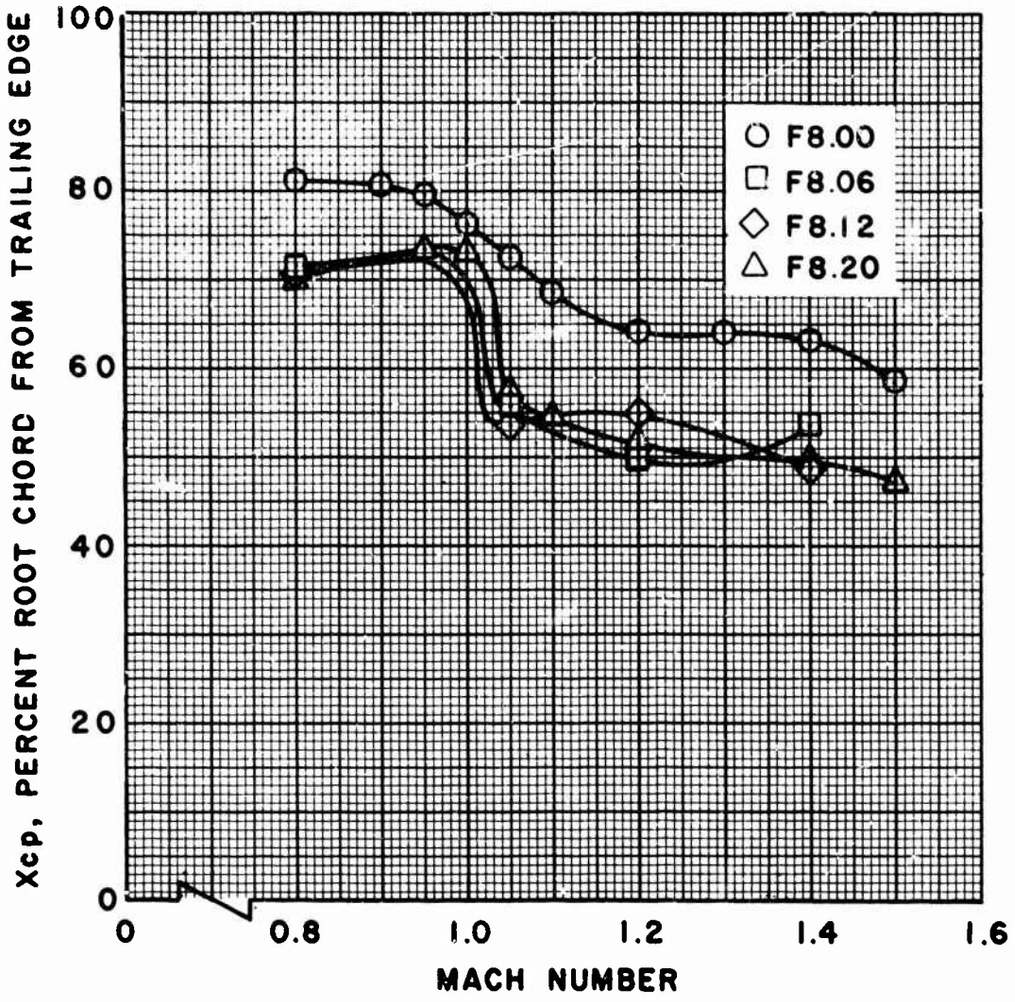

FIGURE 13. CENTER OF PRESSURE VERSUS MACH NUMBER, F8

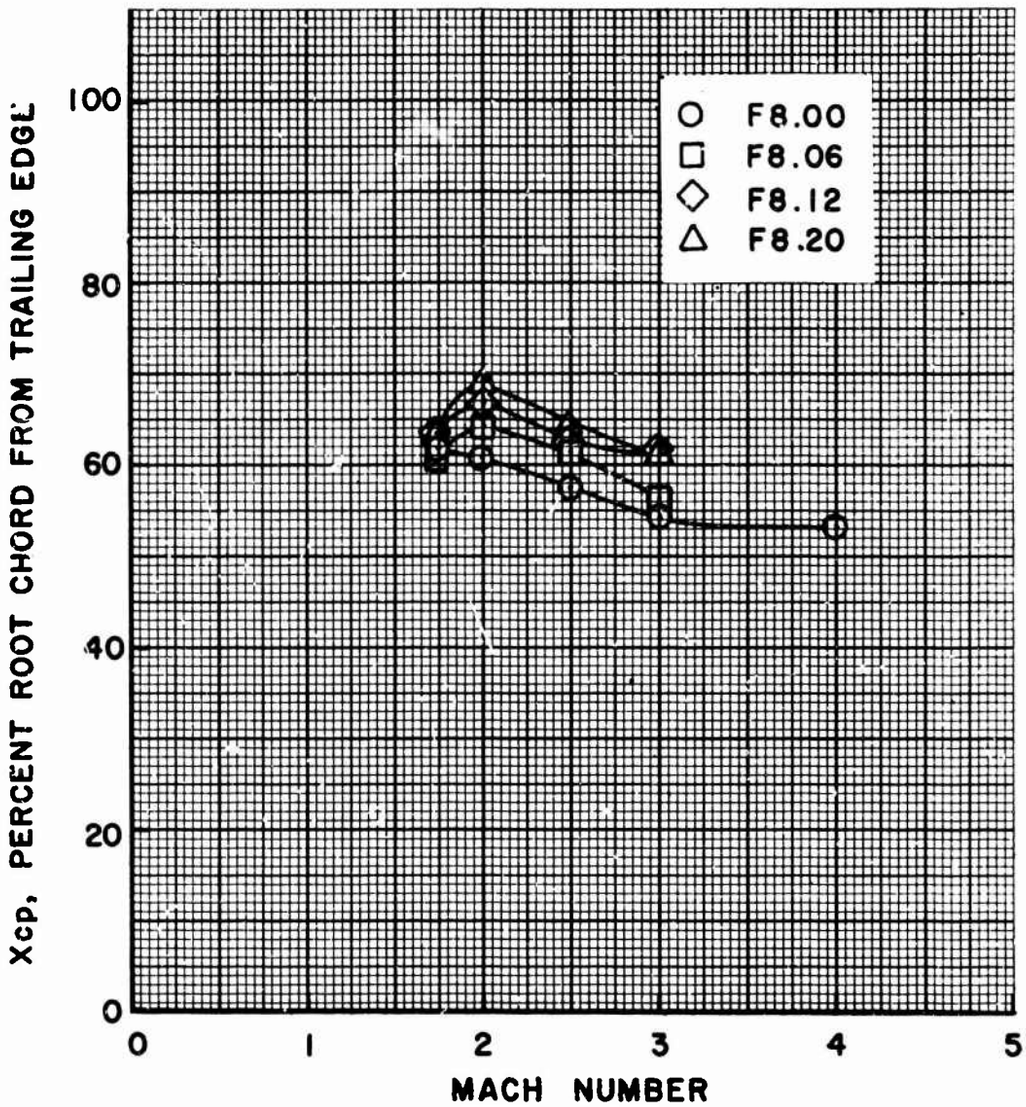

FIGURE 13. CENTER OF PRESSURE VERSUS MACH NUMBER, F8 (Concluded)

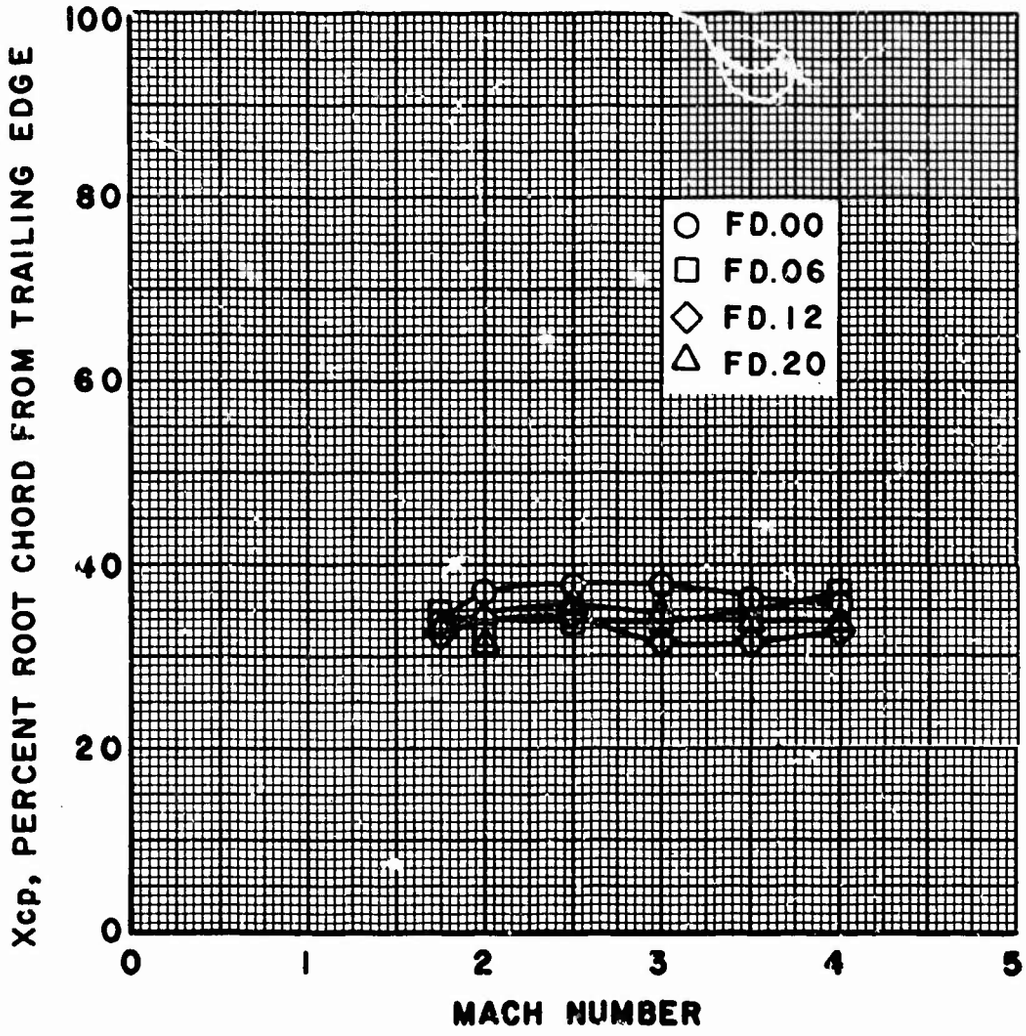

FIGURE 14. CENTER OF PRESSURE VERSUS MACH NUMBER, FD

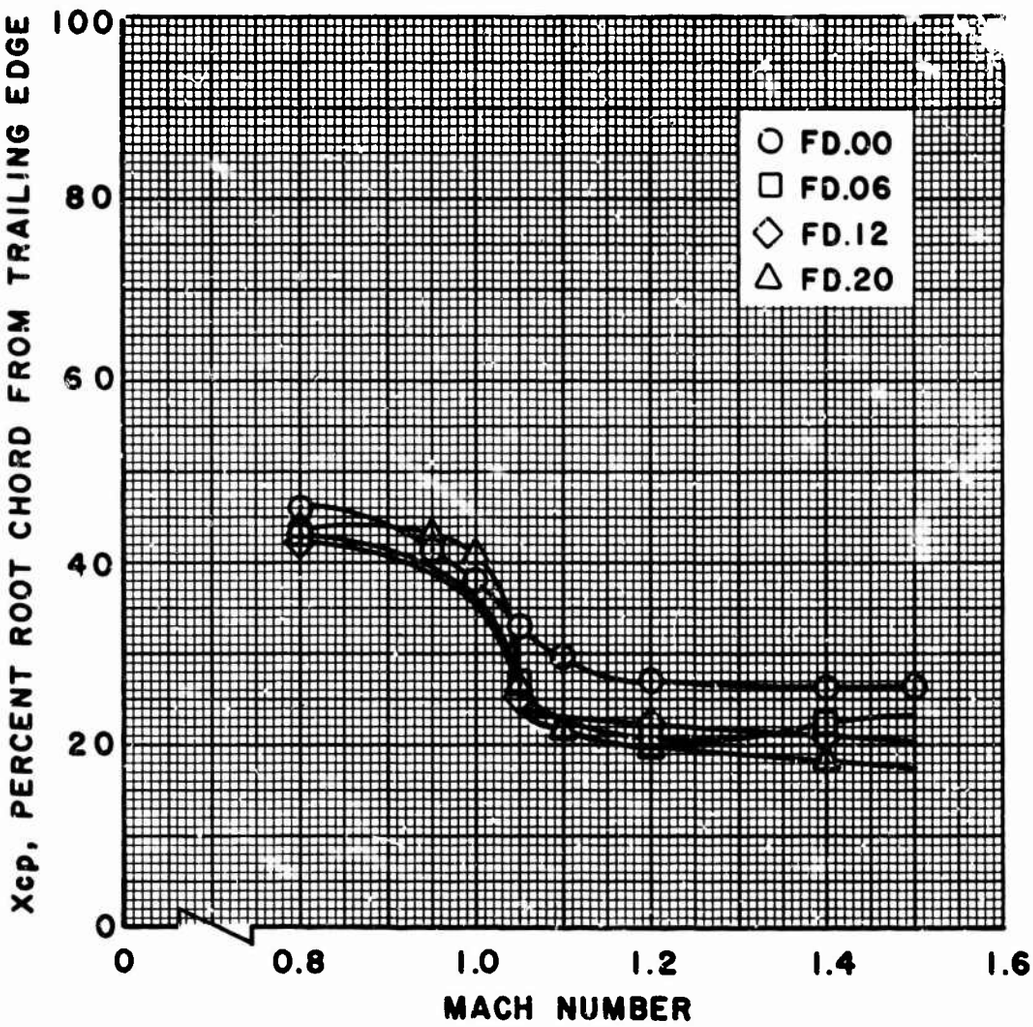

FIGURE 14. CENTER OF PRESSURE VERSUS MACH NUMBER, FD (Concluded)

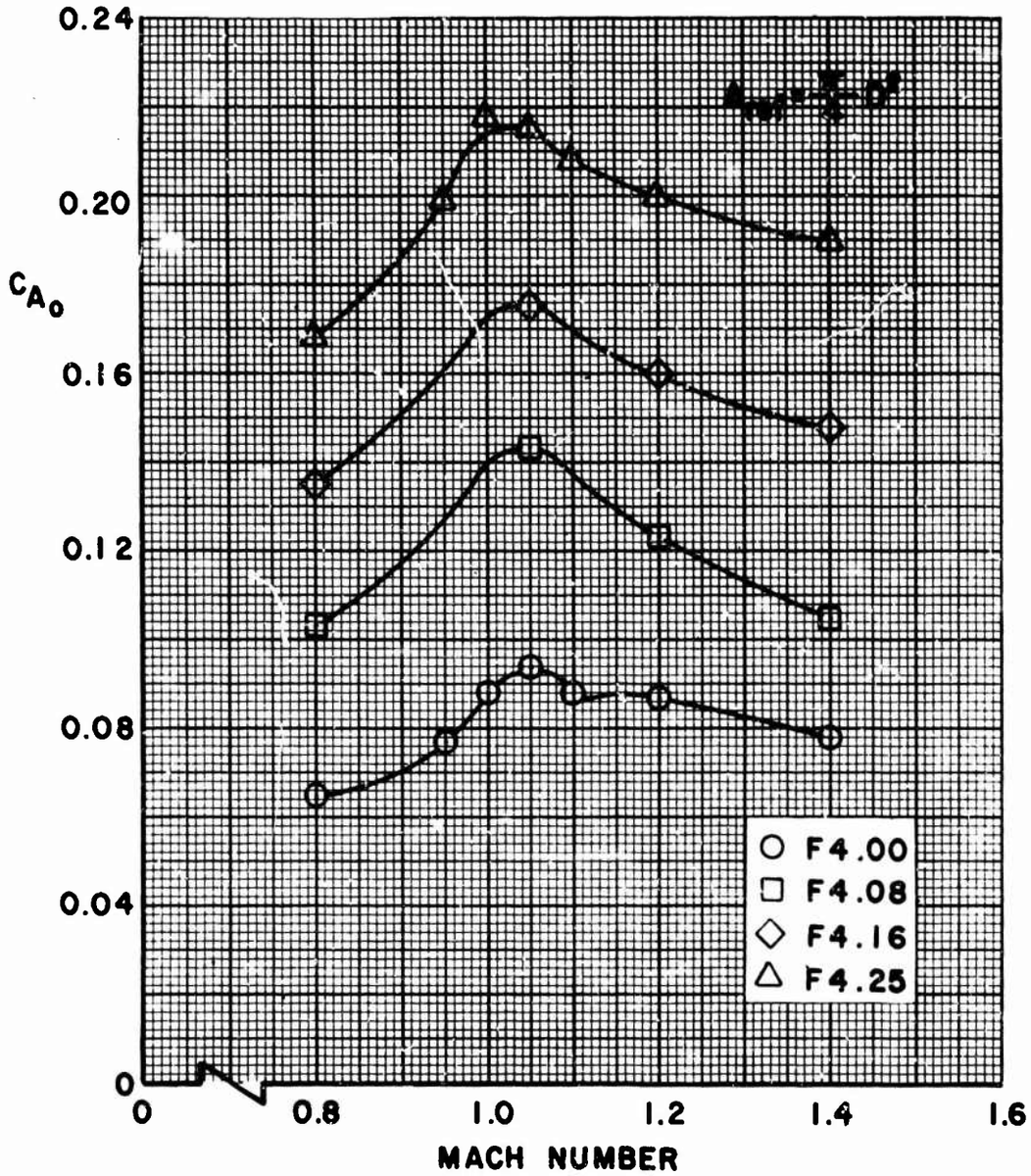

FIGURE 15. AXIAL FORCE VERSUS MACH NUMBER, F4

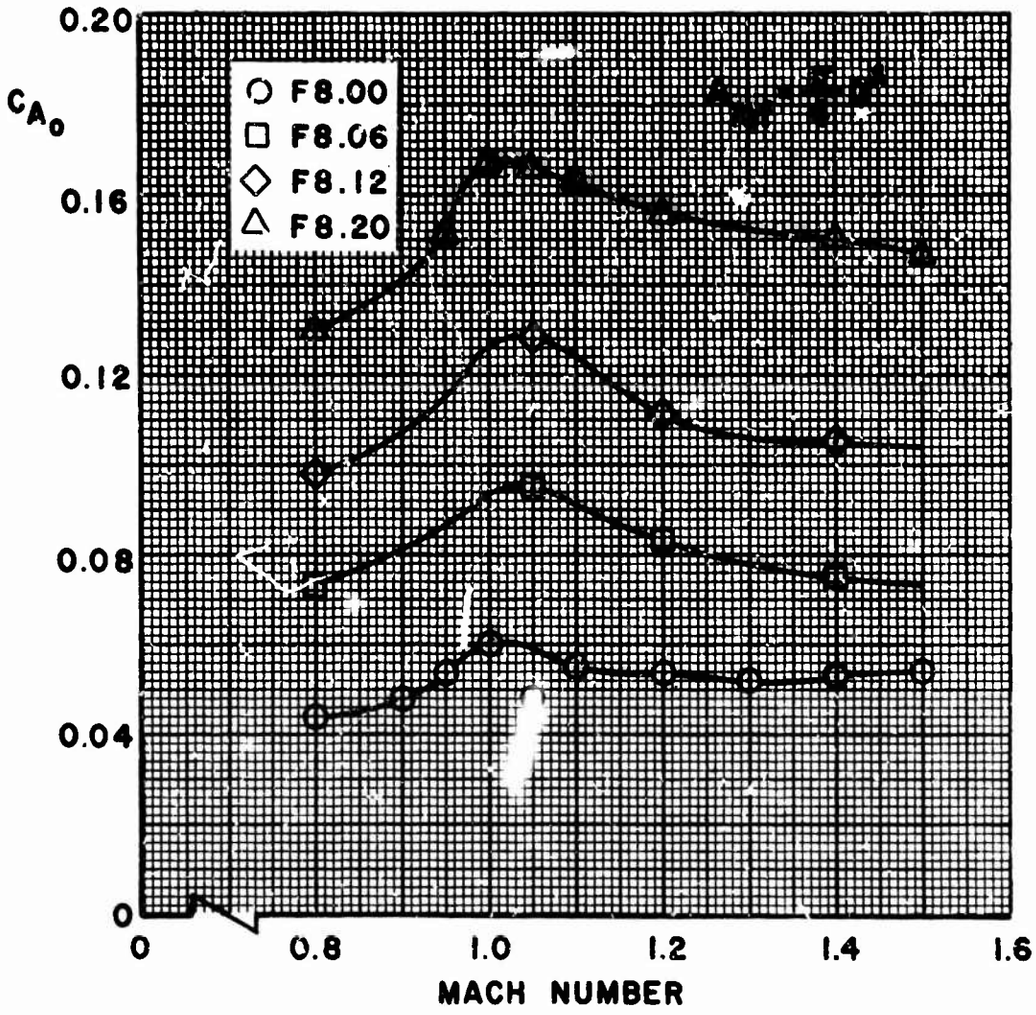

FIGURE 16. AXIAL FORCE VERSUS MACH NUMBER, F8

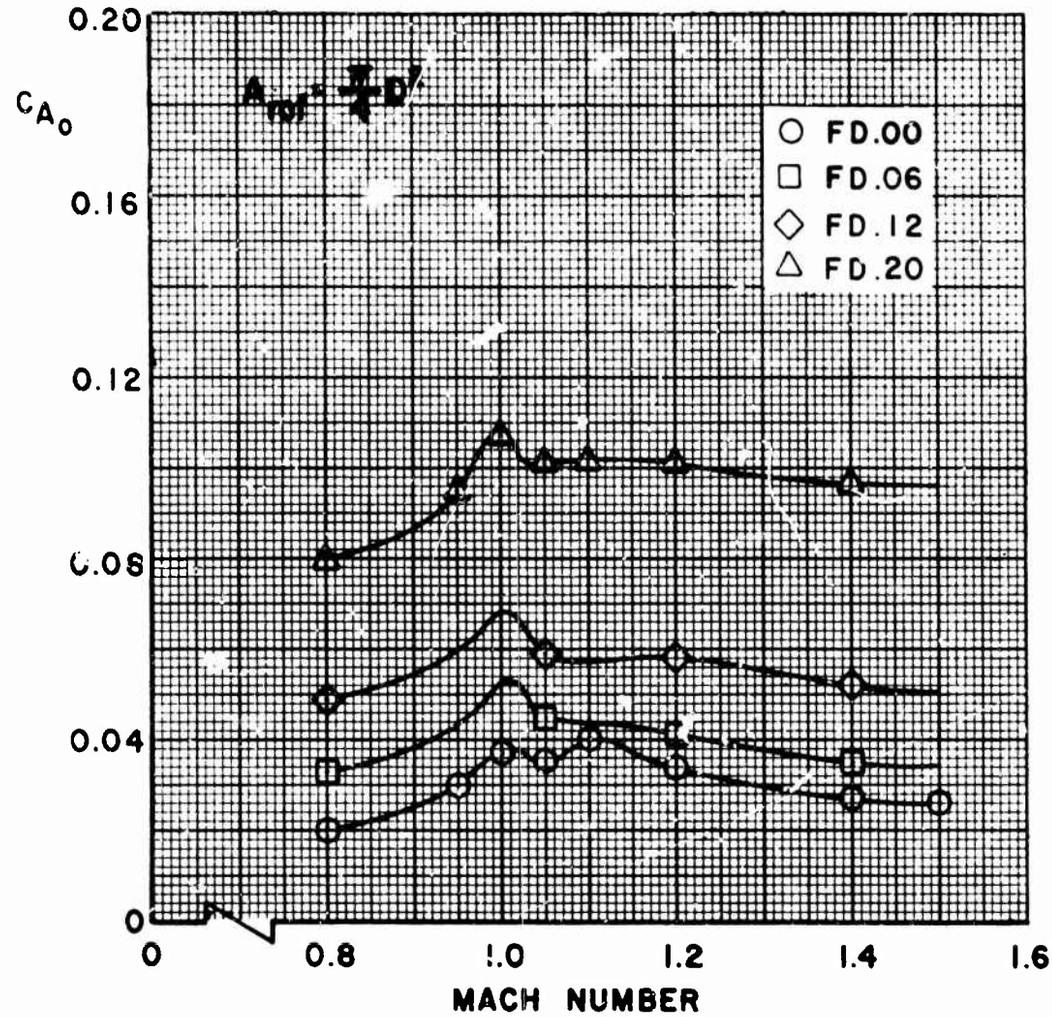

FIGURE 17. AXIAL FORCE VERSUS MACH NUMBER, FD

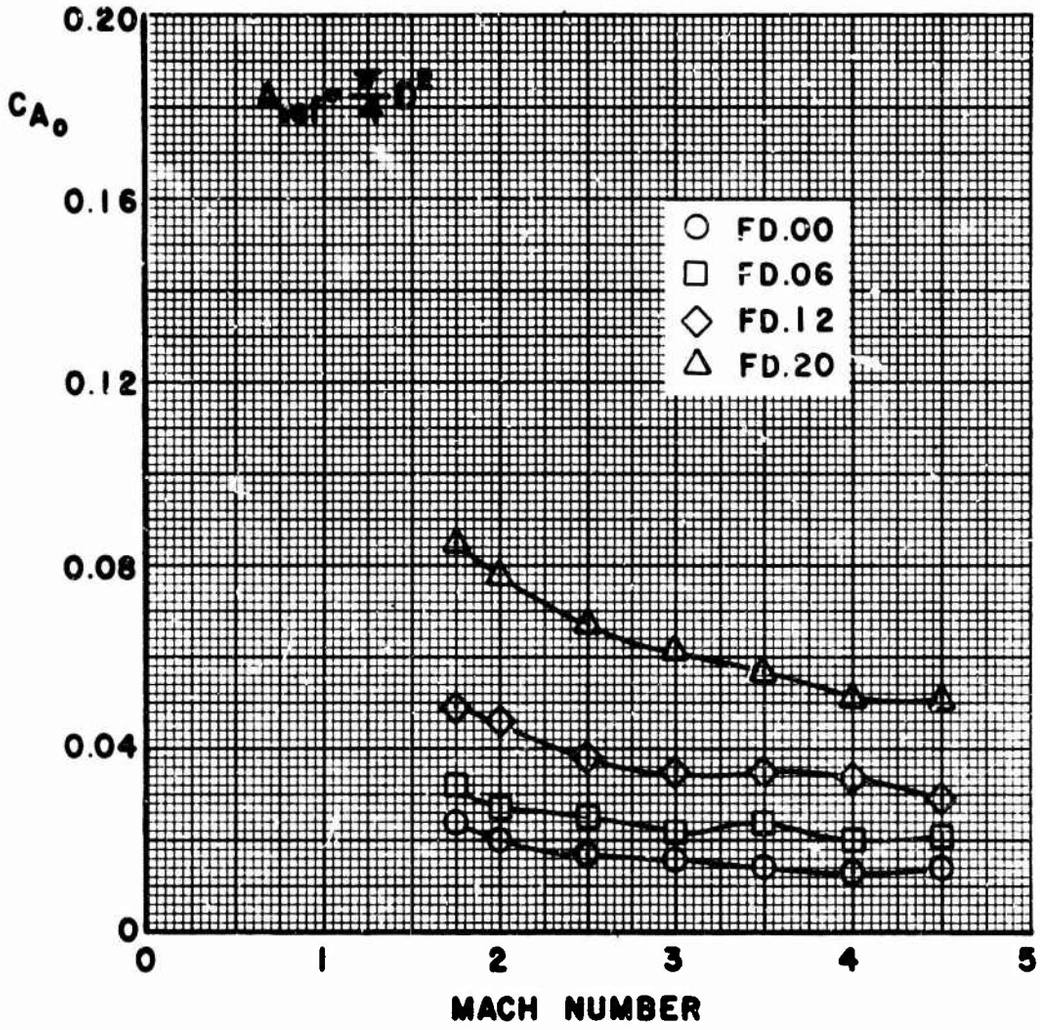

FIGURE 17. AXIAL FORCE VERSUS MACH NUMBER, FD (Concluded)

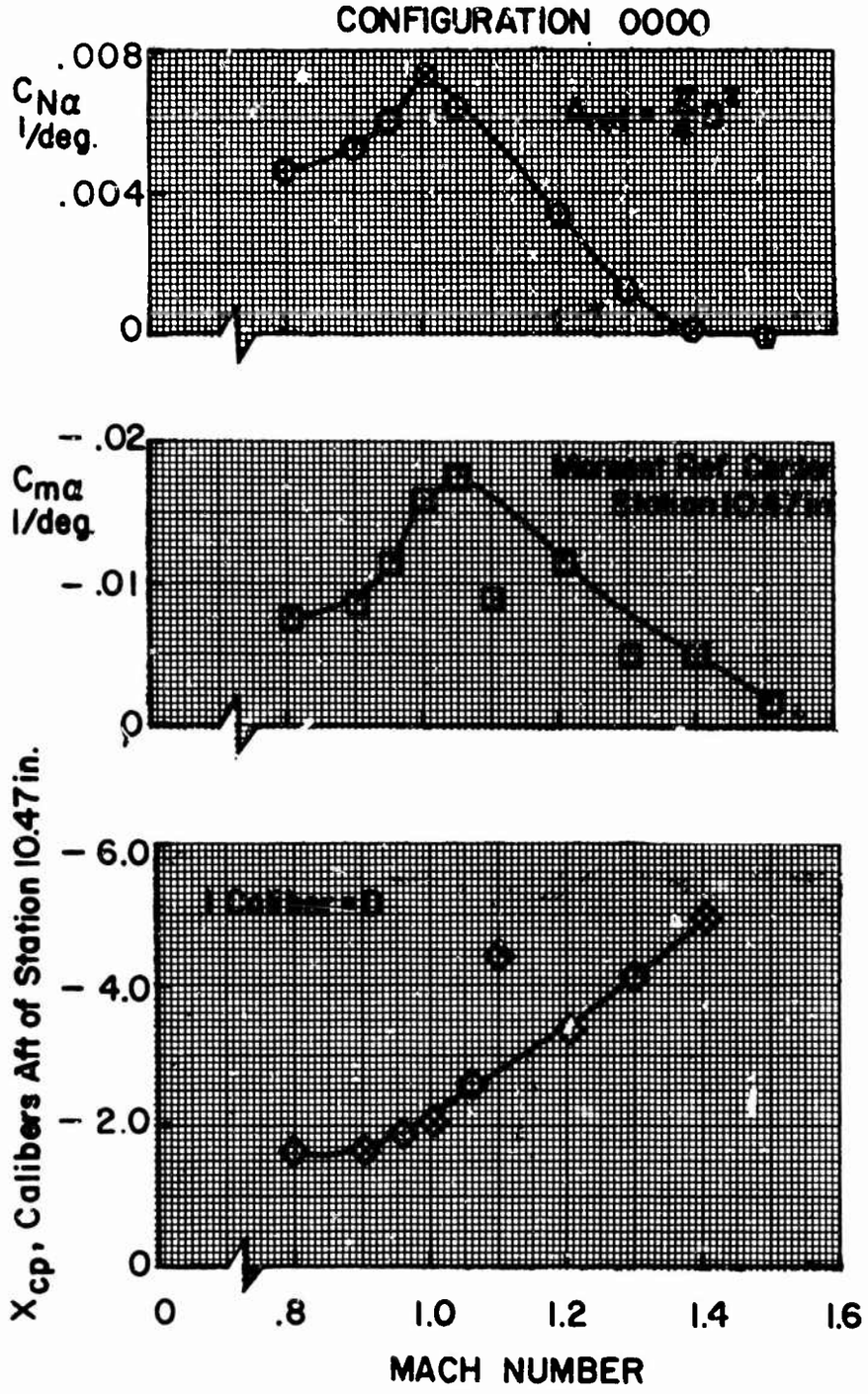

FIGURE 18. AERODYNAMIC COEFFICIENTS, AFTERBODY ONLY, 0000

Appendix
Results from Wind-Tunnel Tests

The results from a series of wind-tunnel tests are presented herein. Figures A-1 through A-4 present the normal force coefficient versus angle of attack at all Mach numbers and configurations. Figures A-5 through A-8 present the pitching moment coefficient versus angle of attack, and Figures A-9 through A-12 present the pitching moment versus normal force coefficient. Figures A-13 through A-15 present the axial force coefficient versus angle of attack at all Mach numbers for all configurations. Figures A-16a through A-16d) contain all coefficients for the body without fins.

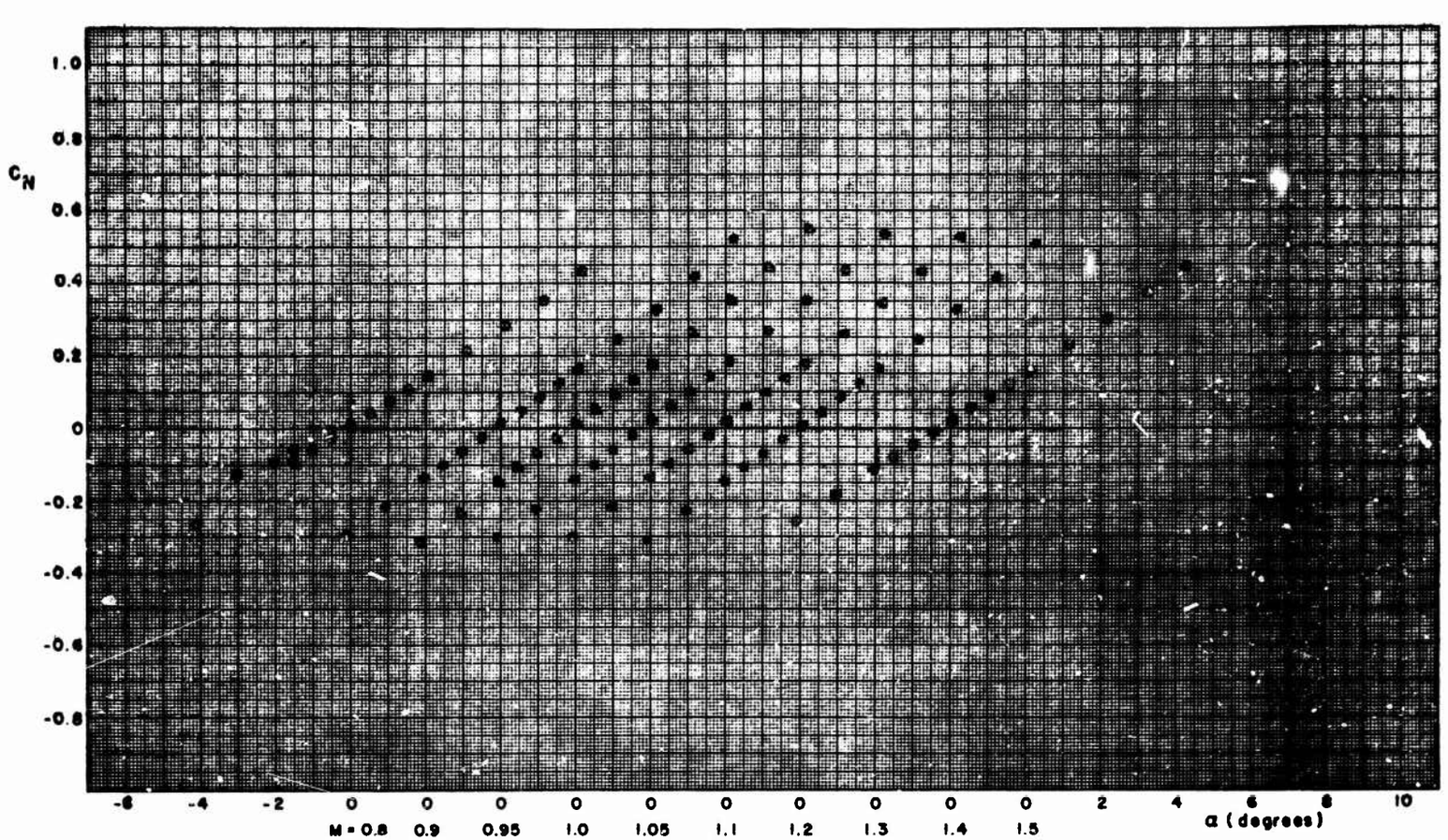

FIGURE A-1. NORMAL FORCE COEFFICIENT VERSUS ANGLE OF ATTACK, F4.00

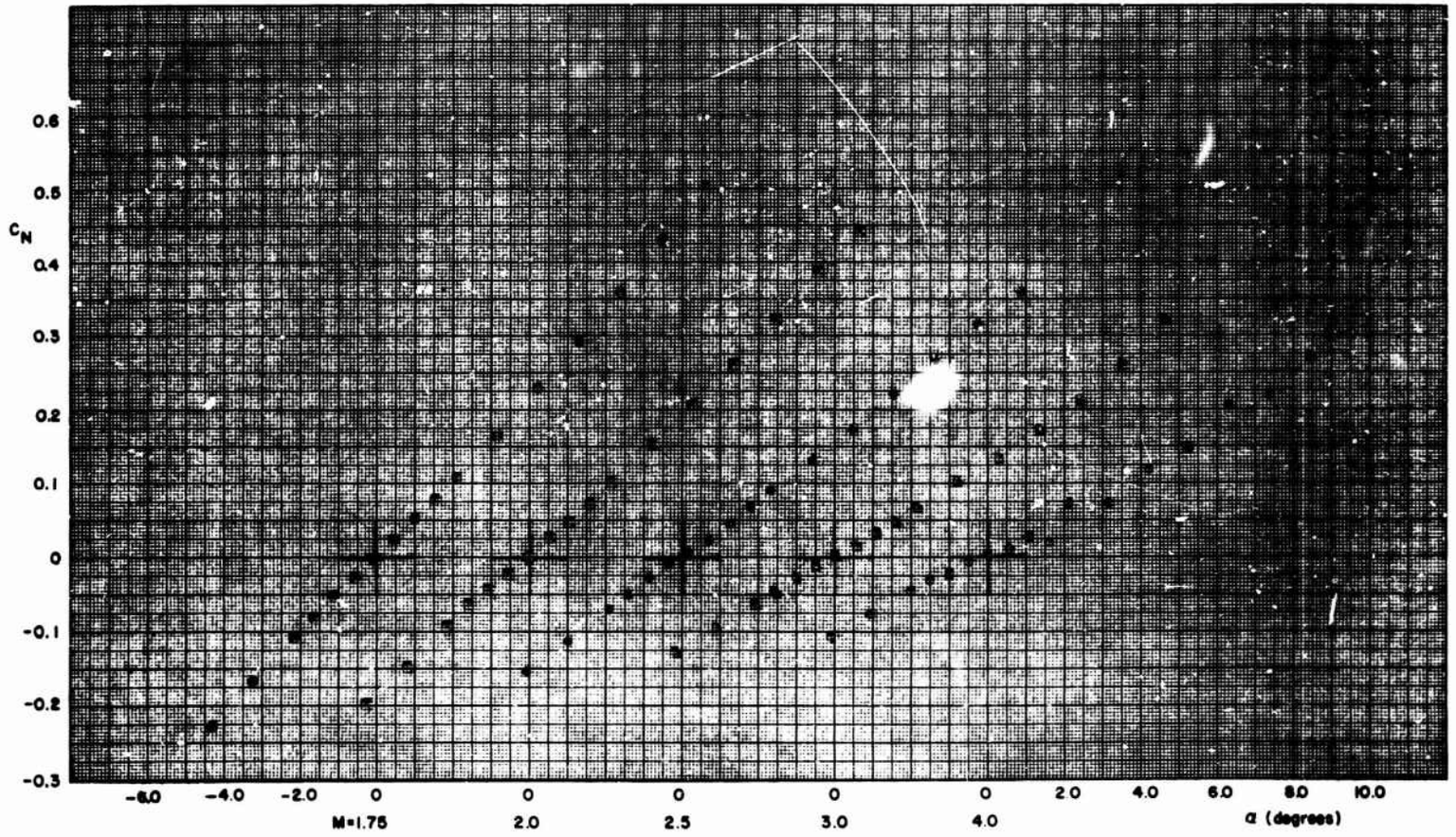

FIGURE A-1. NORMAL FORCE COEFFICIENT VERSUS ANGLE OF ATTACK, F4.00 (Continued)

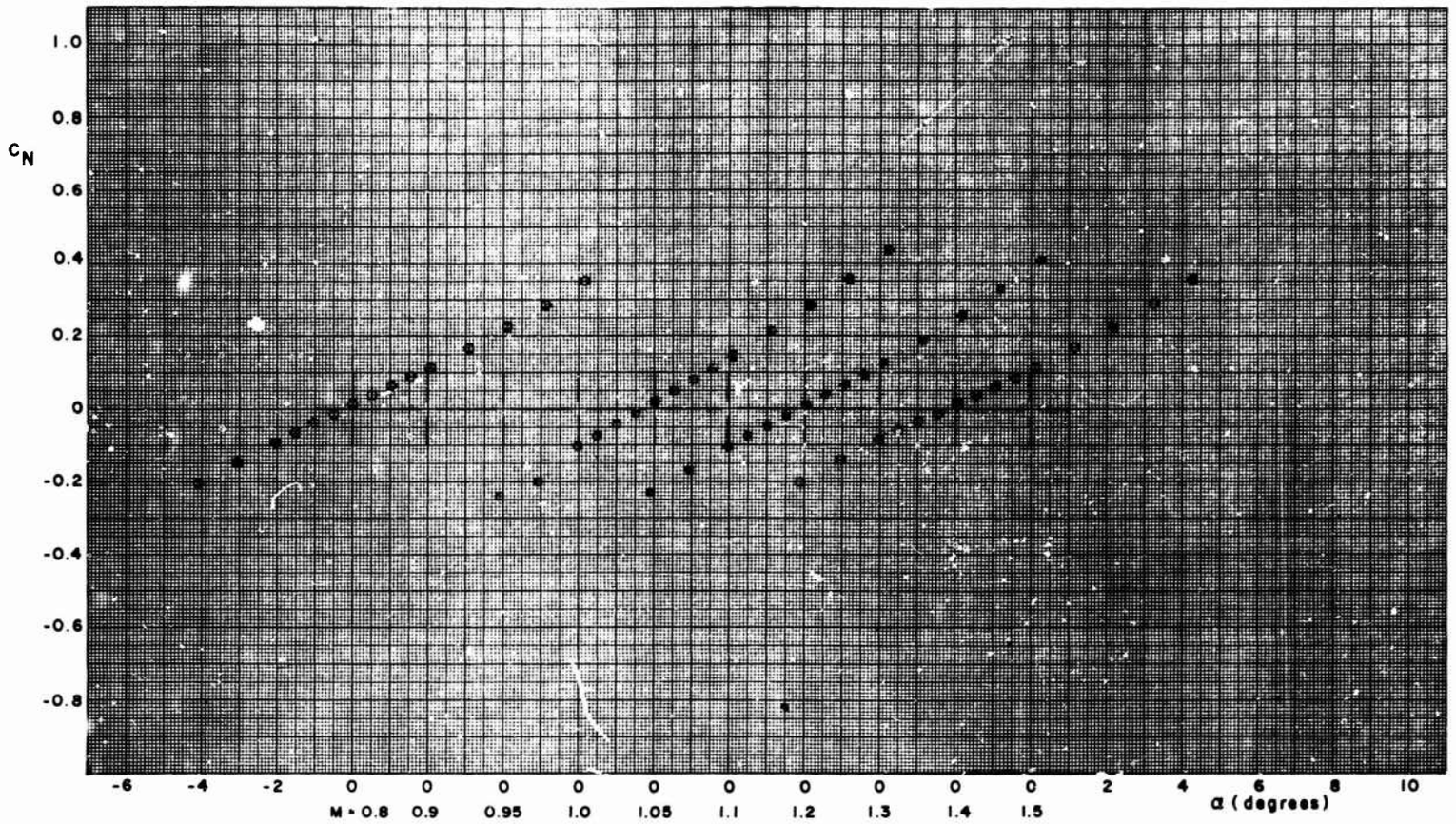

FIGURE A-1. NORMAL FORCE COEFFICIENT VERSUS ANGLE OF ATTACK, F4.08 (Continued)

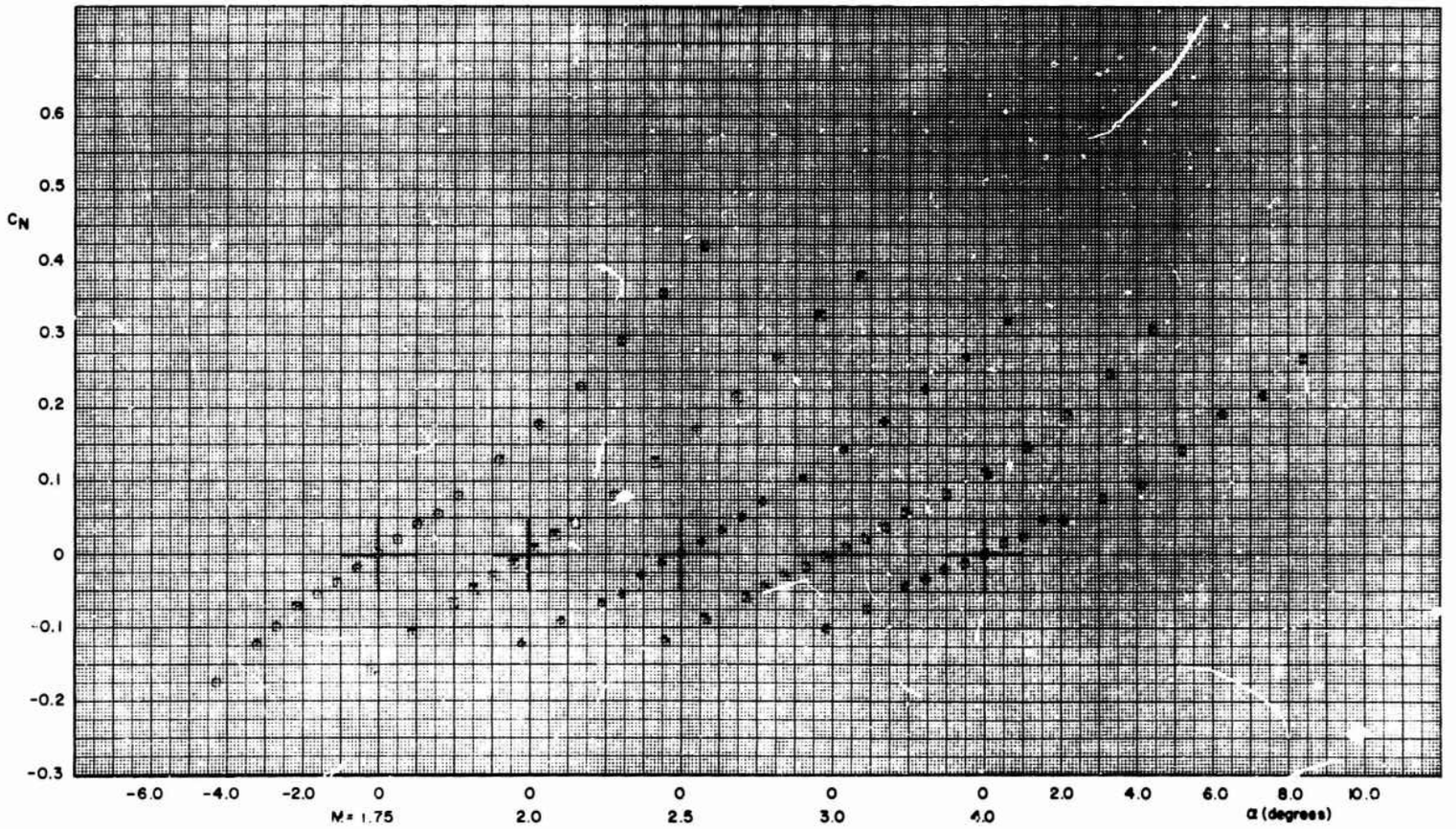

FIGURE A-1. NORMAL FORCE COEFFICIENT VERSUS ANGLE OF ATTACK, F4.08 (Continued)

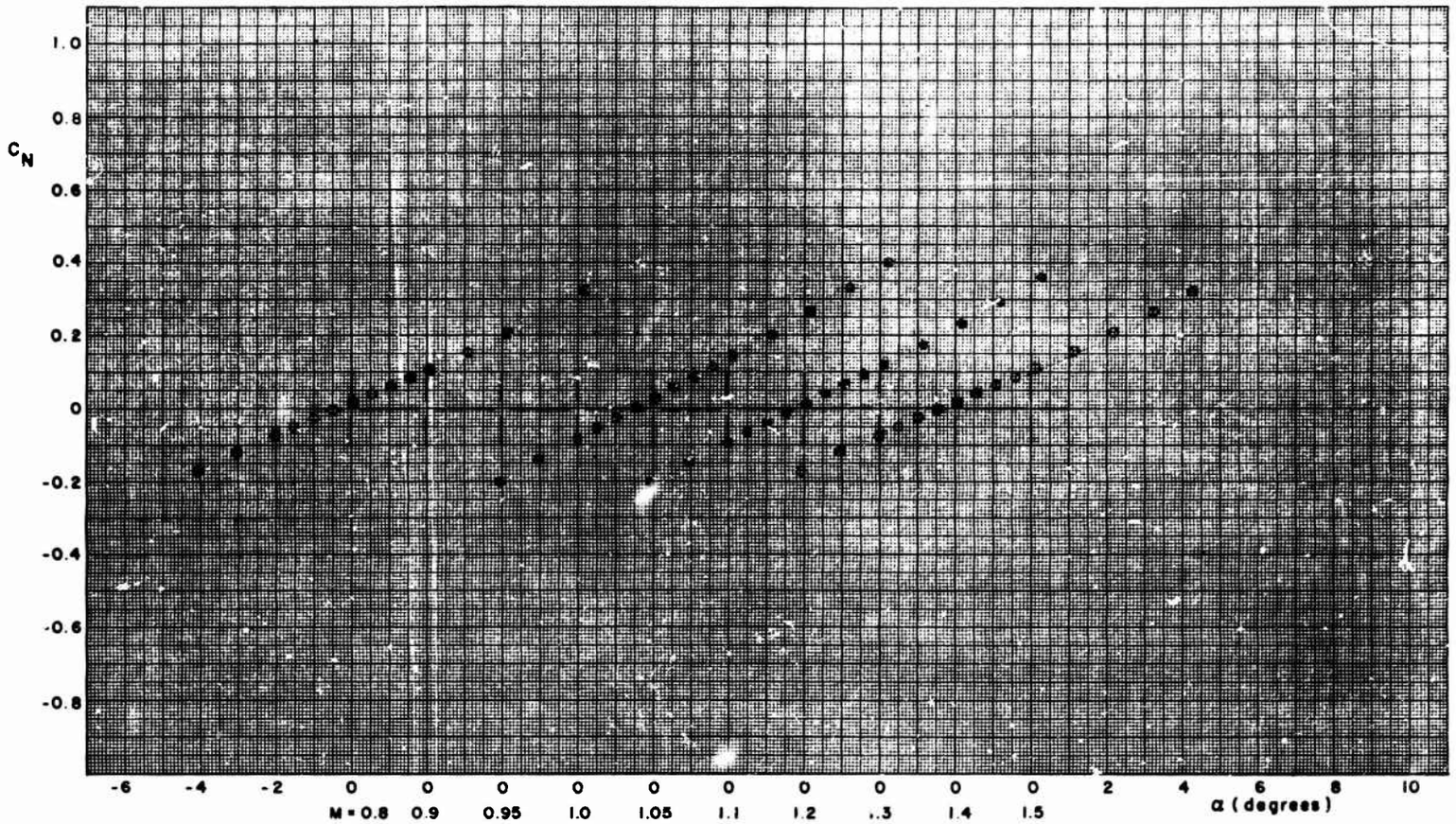

FIGURE A-1. NORMAL FORCE COEFFICIENT VERSUS ANGLE OF ATTACK, F4.16 (Continued)

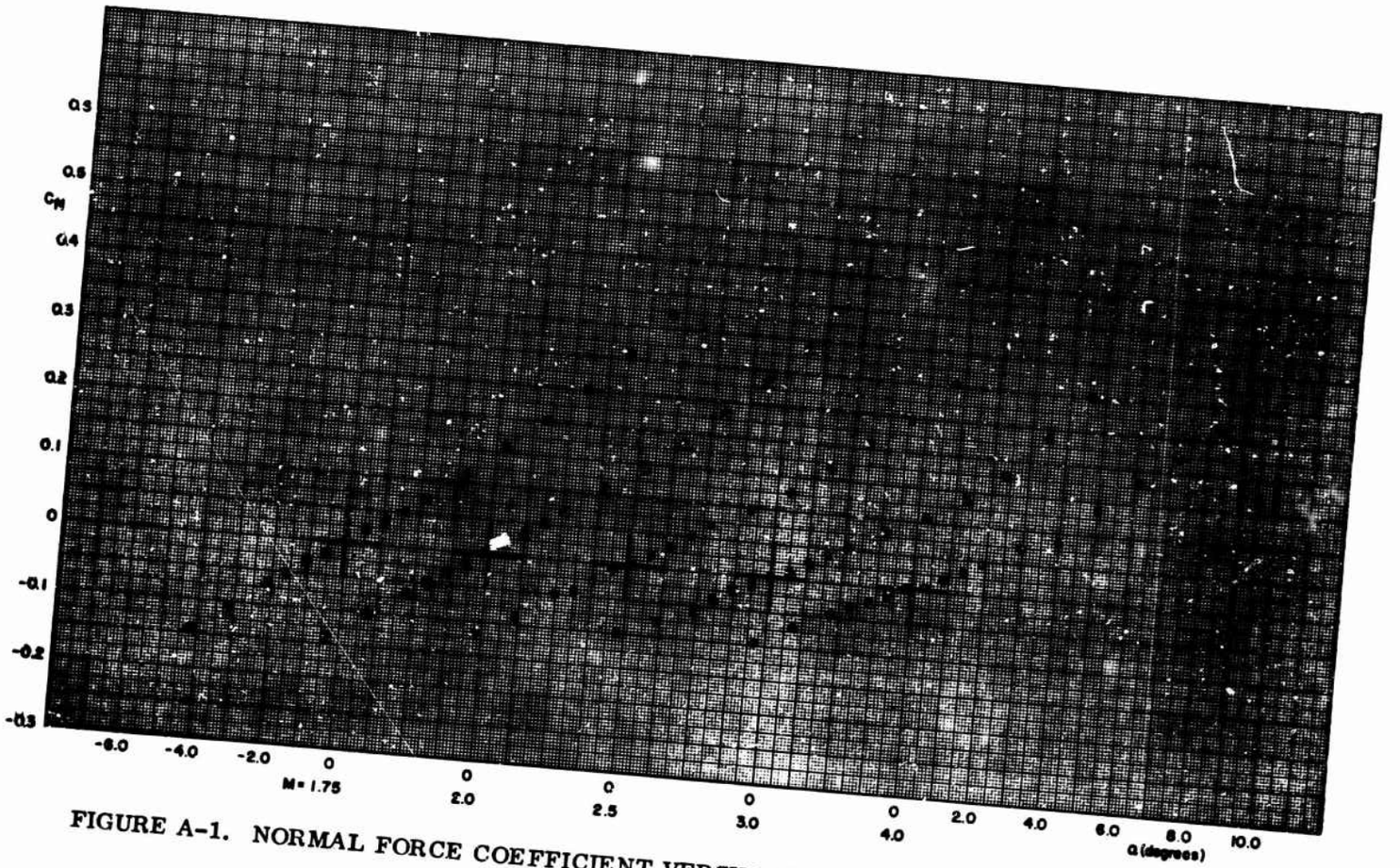

FIGURE A-1. NORMAL FORCE COEFFICIENT VERSUS ANGLE OF ATT :K, F4.16 (Continued)

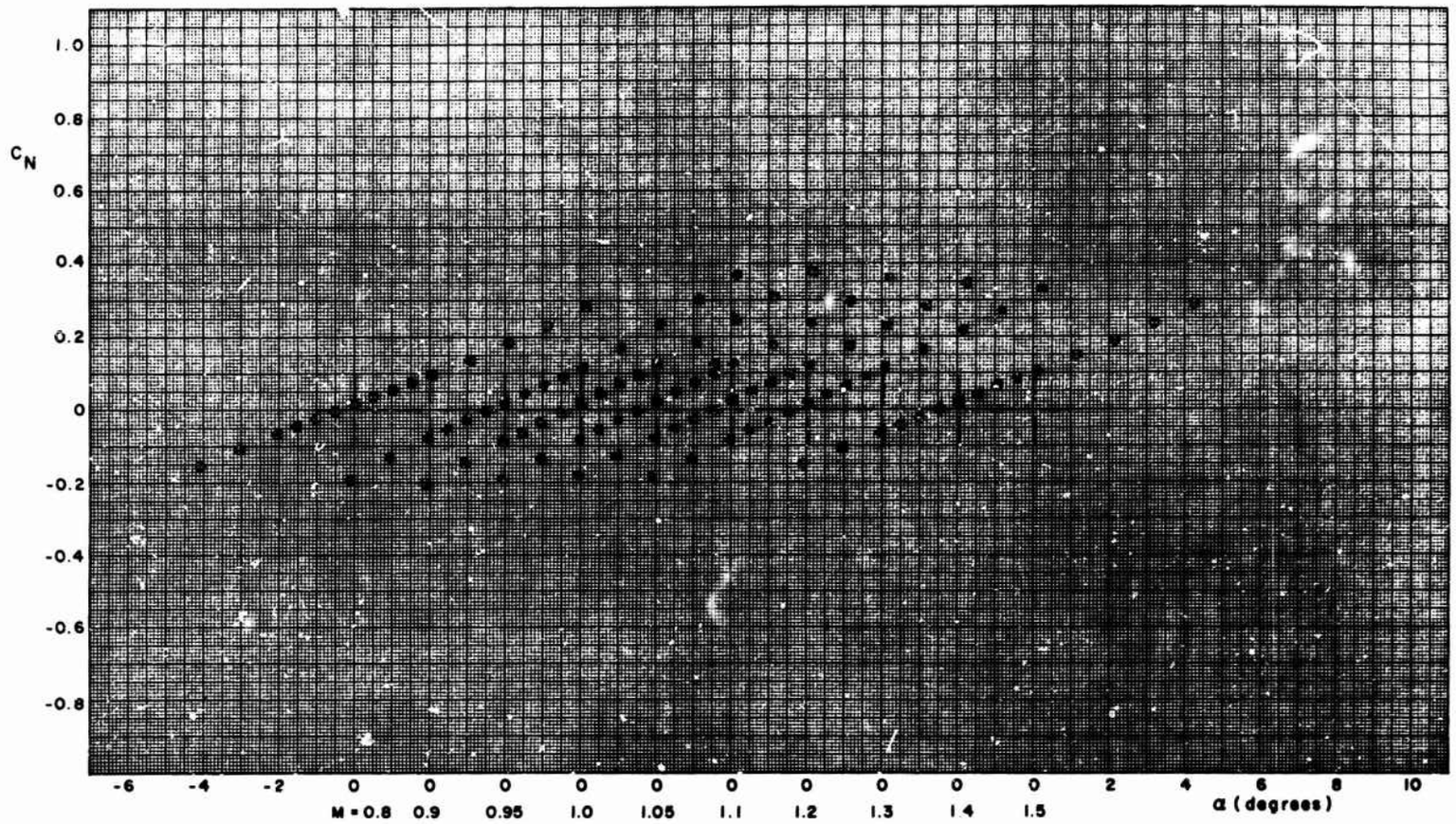

FIGURE A-1. NORMAL FORCE COEFFICIENT VERSUS ANGLE OF ATTACK, F4.25 (Continued)

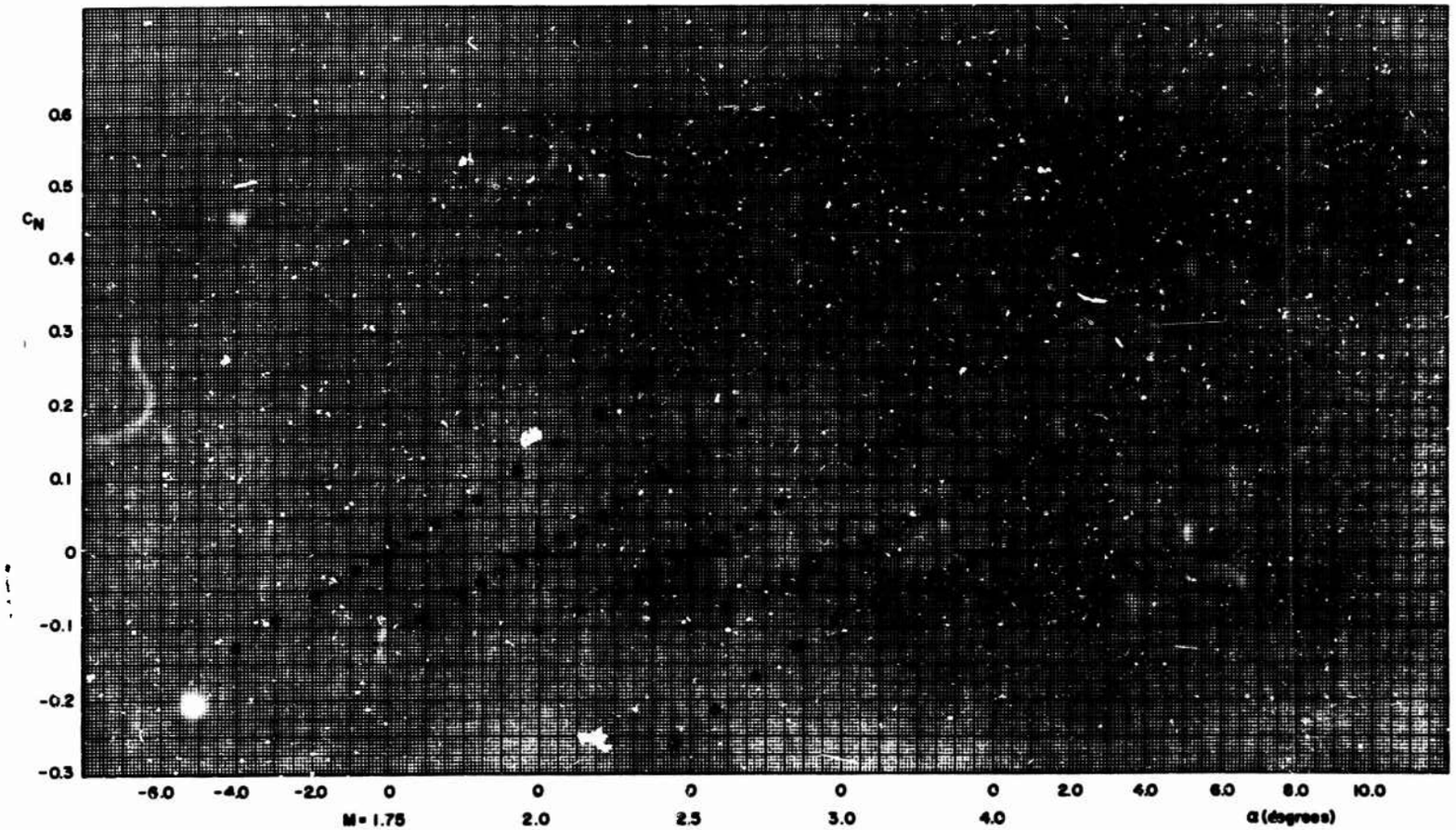

FIGURE A-1. NORMAL FORCE COEFFICIENT VERSUS ANGLE OF ATTACK, F4.25 (Concluded)

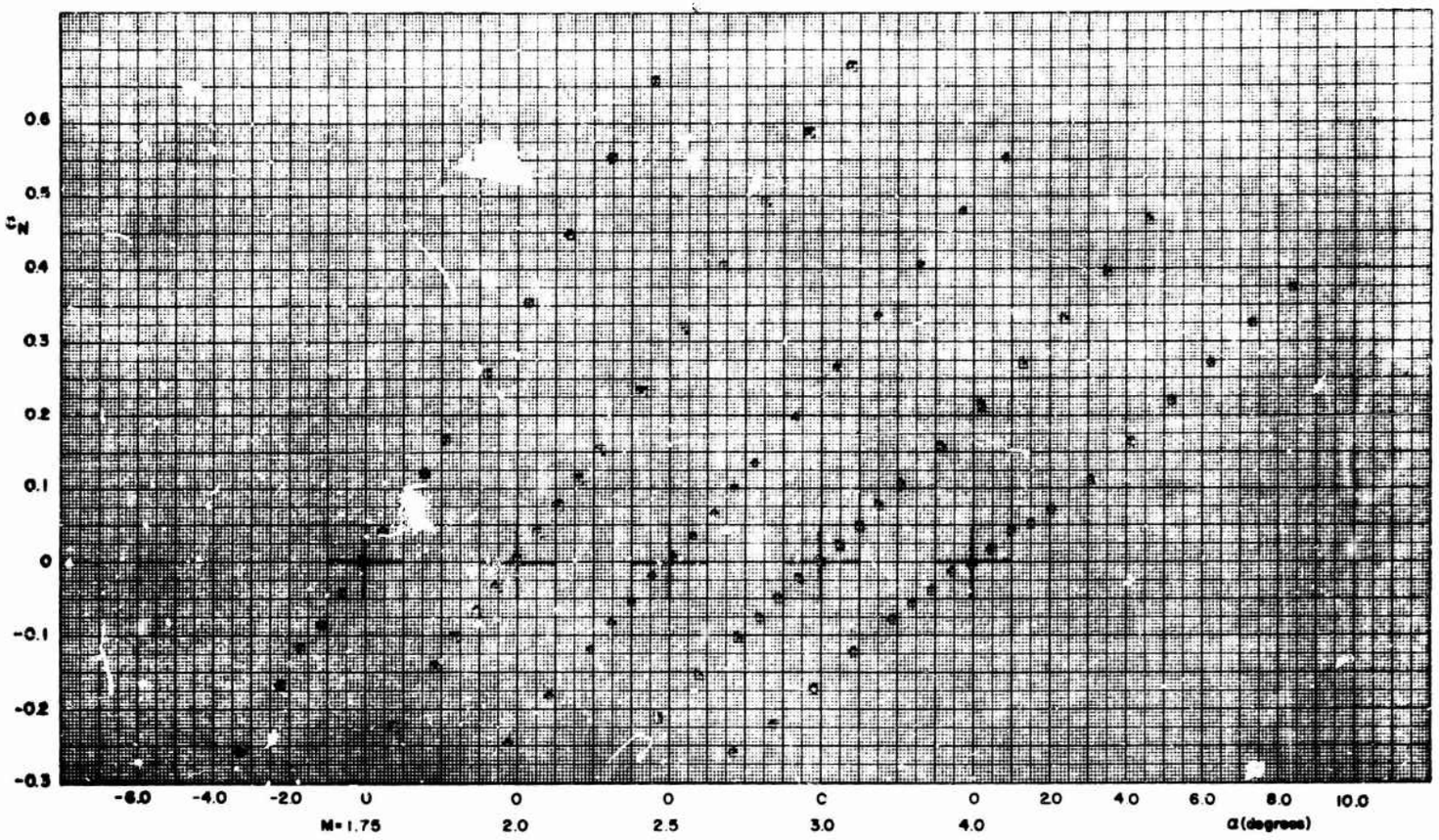

FIGURE A-2. NORMAL FORCE COEFFICIENT VERSUS ANGLE OF ATTACK, F7.00

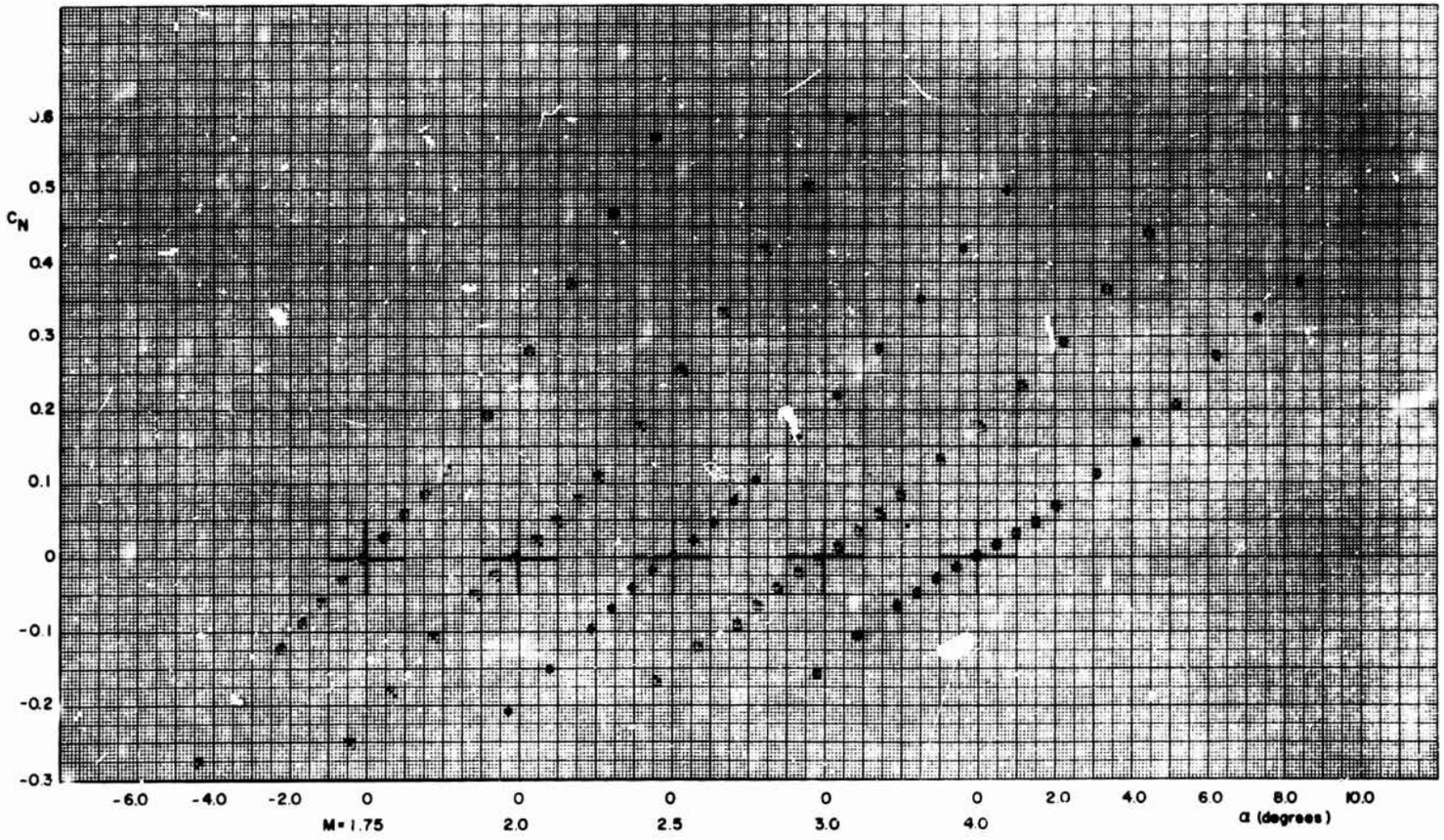

FIGURE A-2. NORMAL FORCE COEFFICIENT VERSUS ANGLE OF ATTACK, F7.06 (Continued)

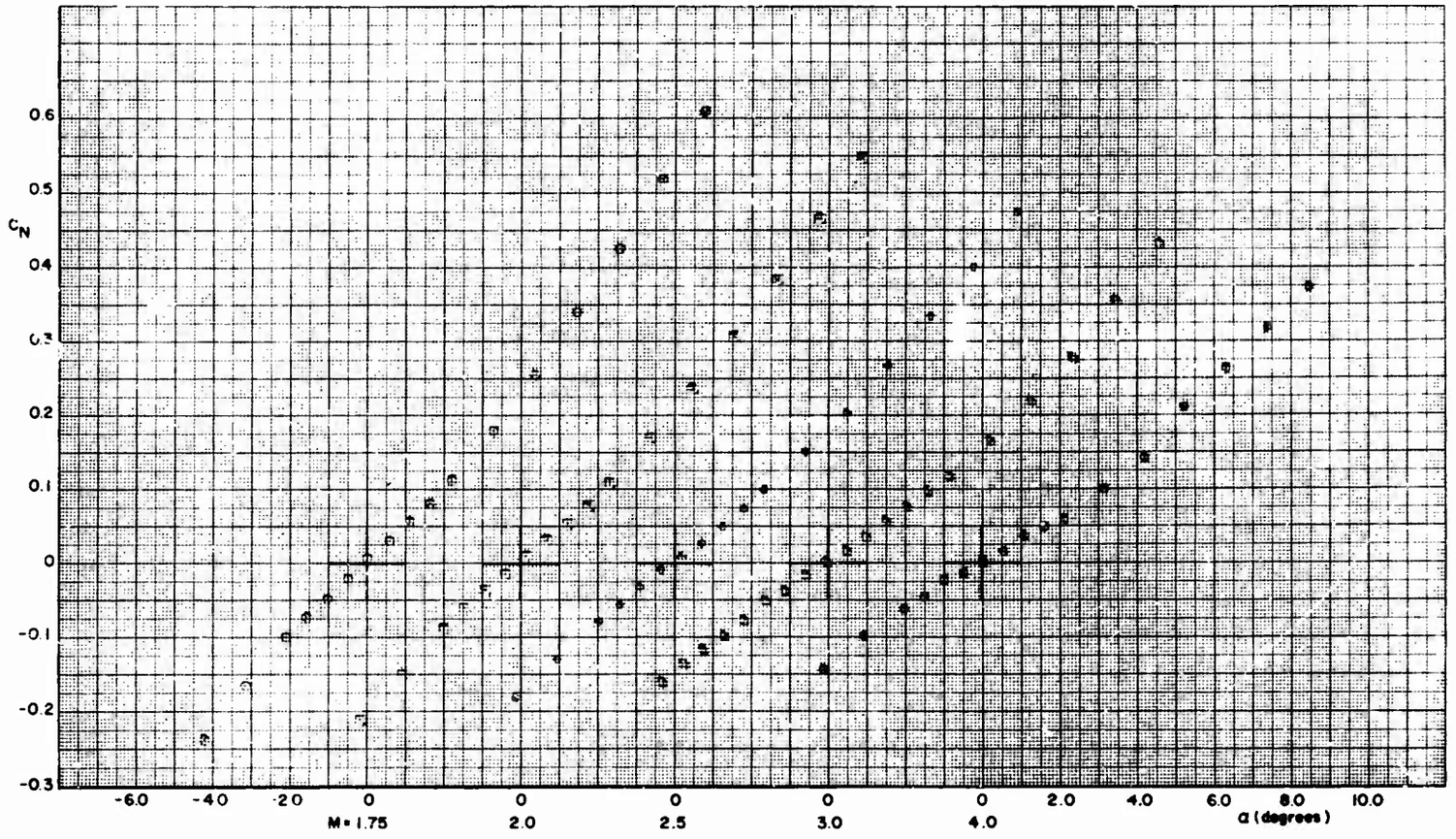

FIGURE A-2. NORMAL FORCE COEFFICIENT VERSUS ANGLE OF ATTACK, F7.12 (Continued)

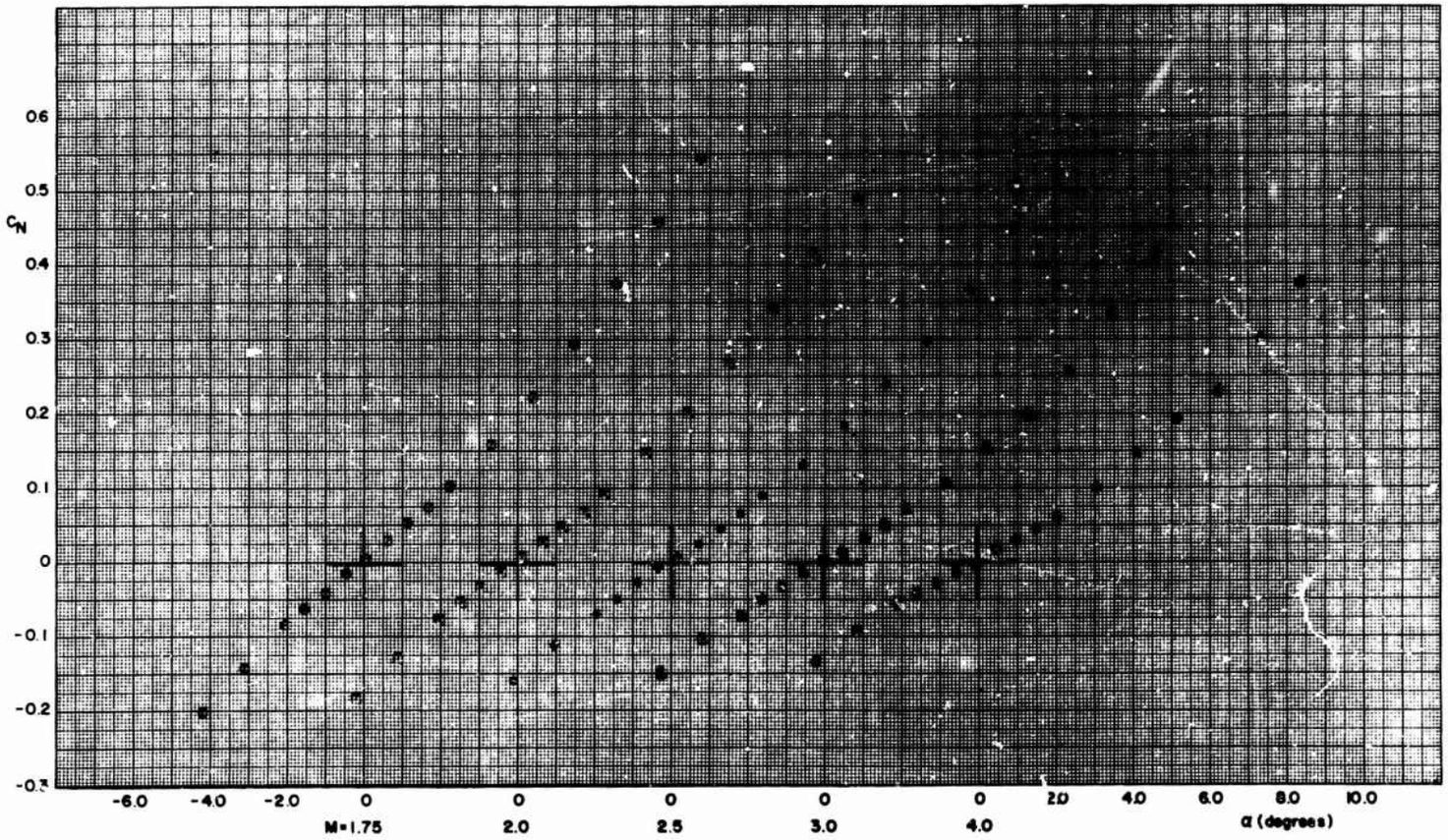

FIGURE A-2. NORMAL FORCE COEFFICIENT VERSUS ANGLE OF ATTACK, F7.20 (Concluded)

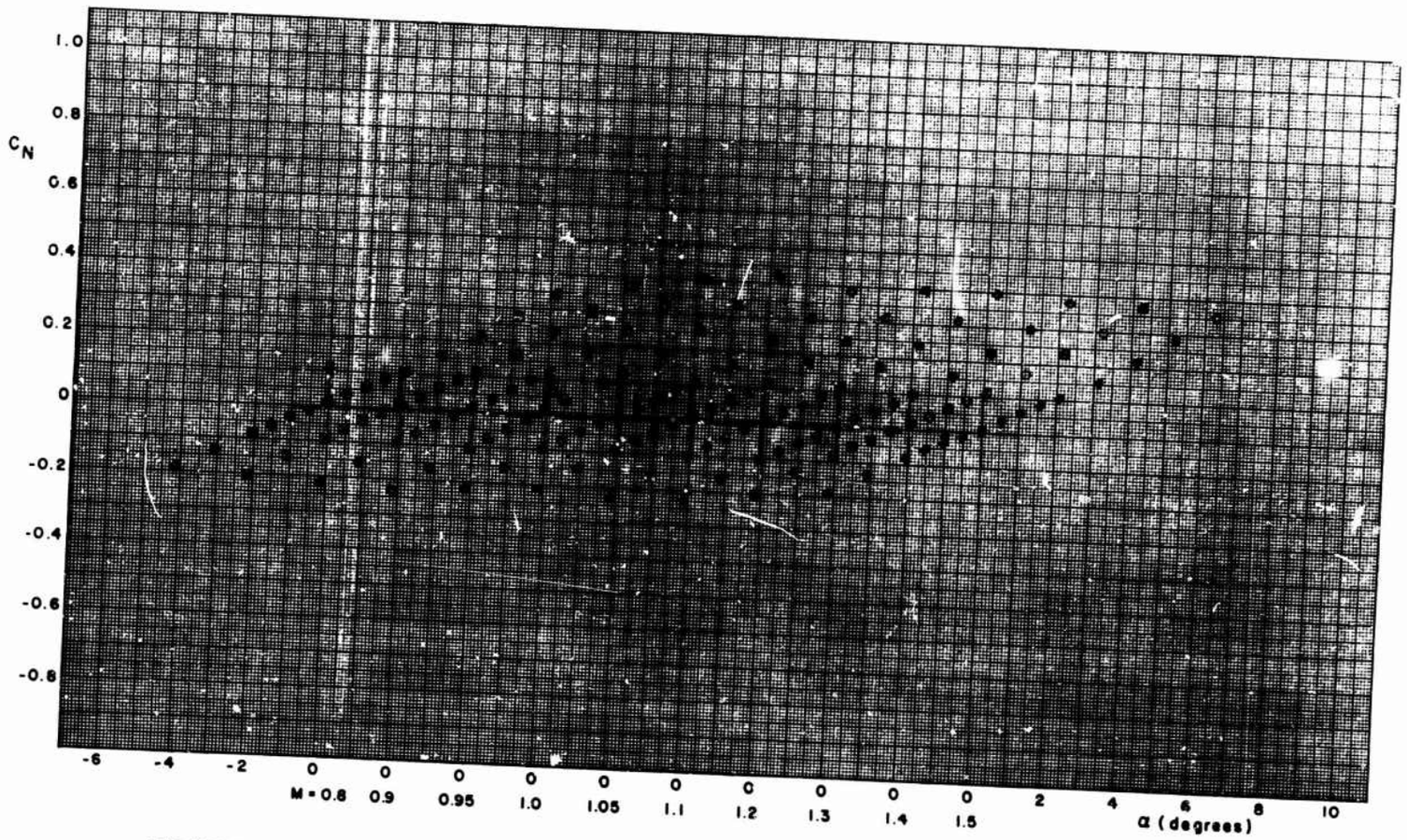

FIGURE A-3. NORMAL FORCE COEFFICIENT VERSUS ANGLE OF ATTACK, F8.00

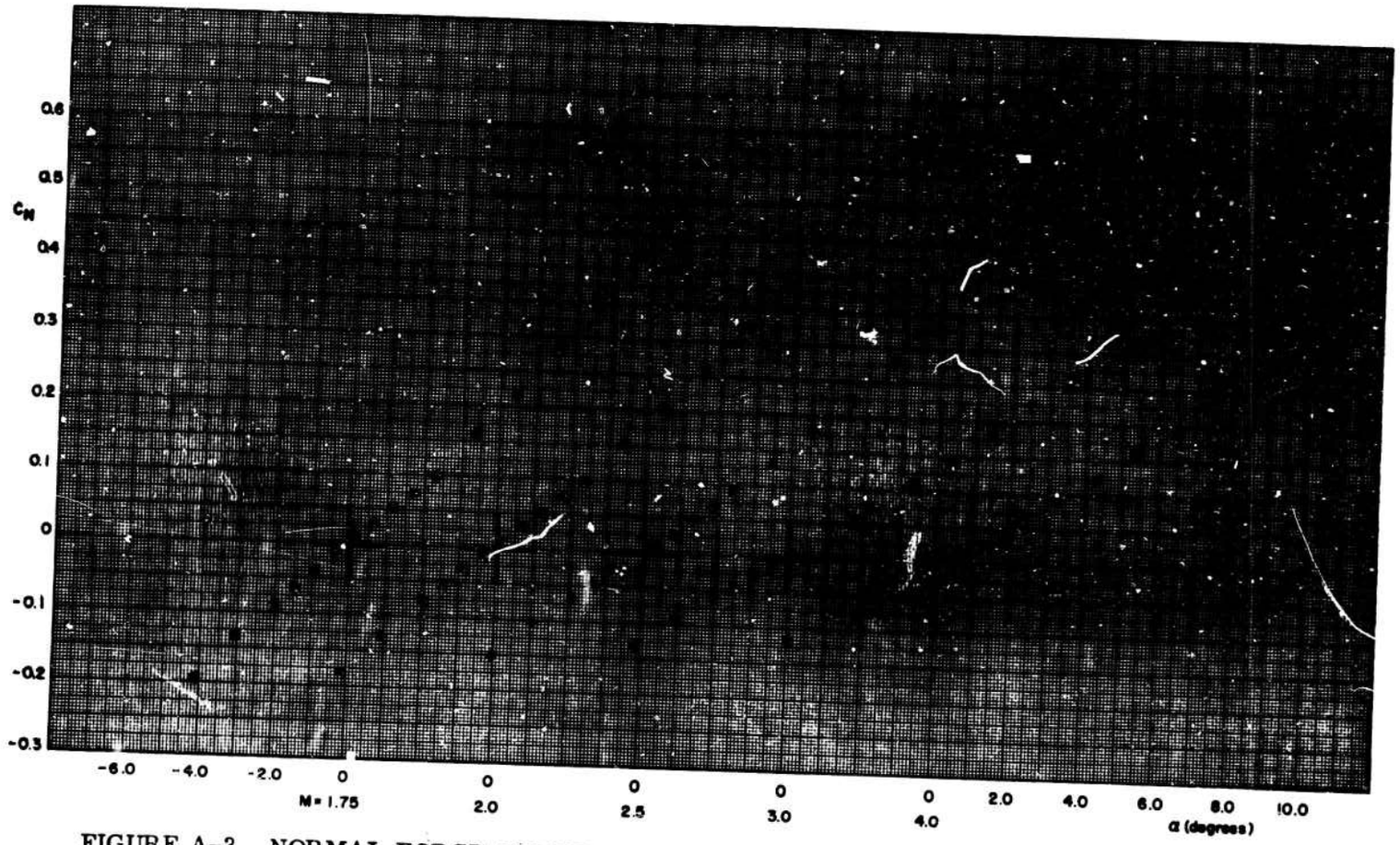

FIGURE A-3. NORMAL FORCE COEFFICIENT VERSUS ANGLE OF ATTACK, F8.00 (Continued)

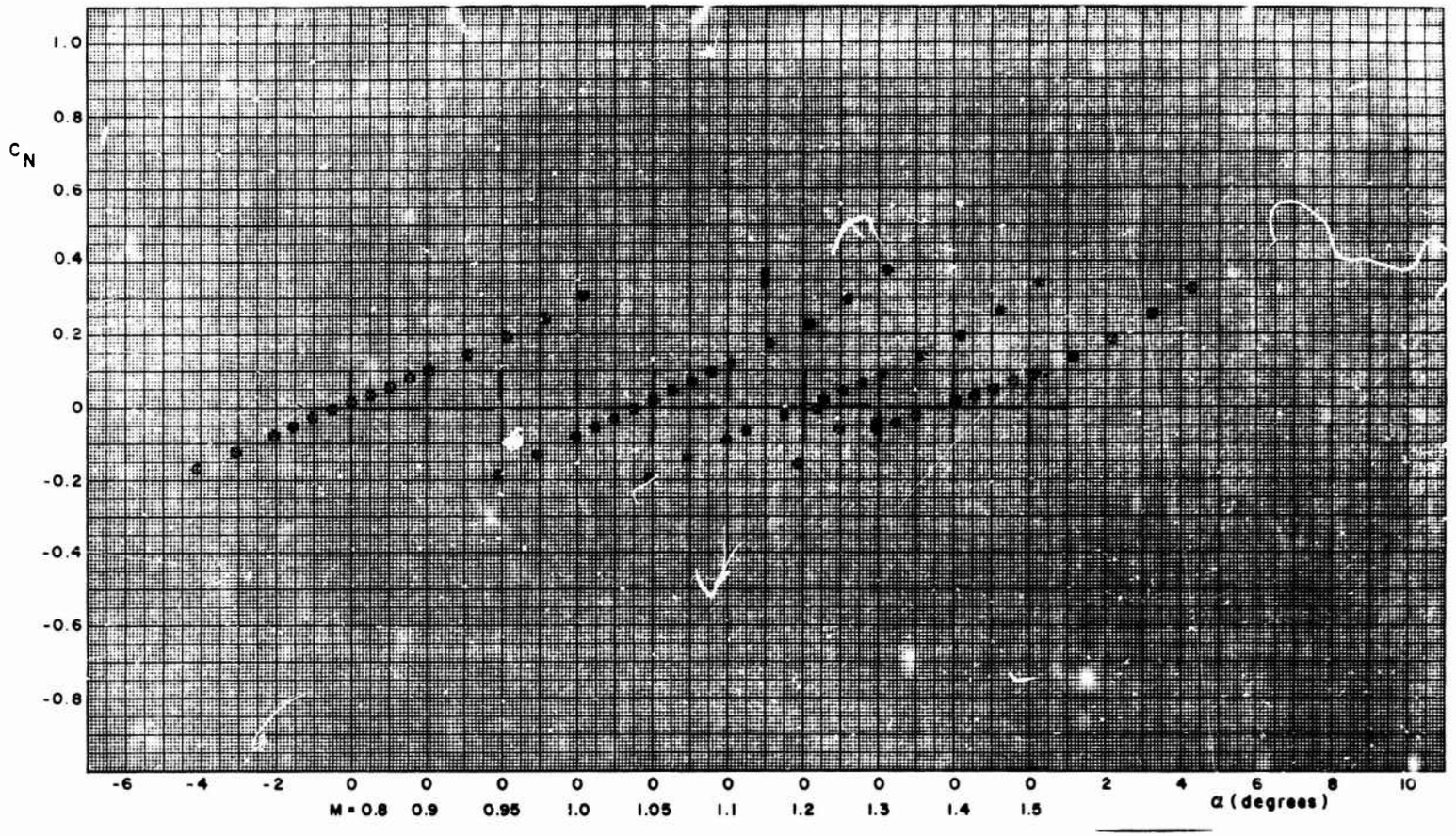

FIGURE A-3. NORMAL FORCE COEFFICIENT VERSUS ANGLE OF ATTACK, F8.06 (Continued)

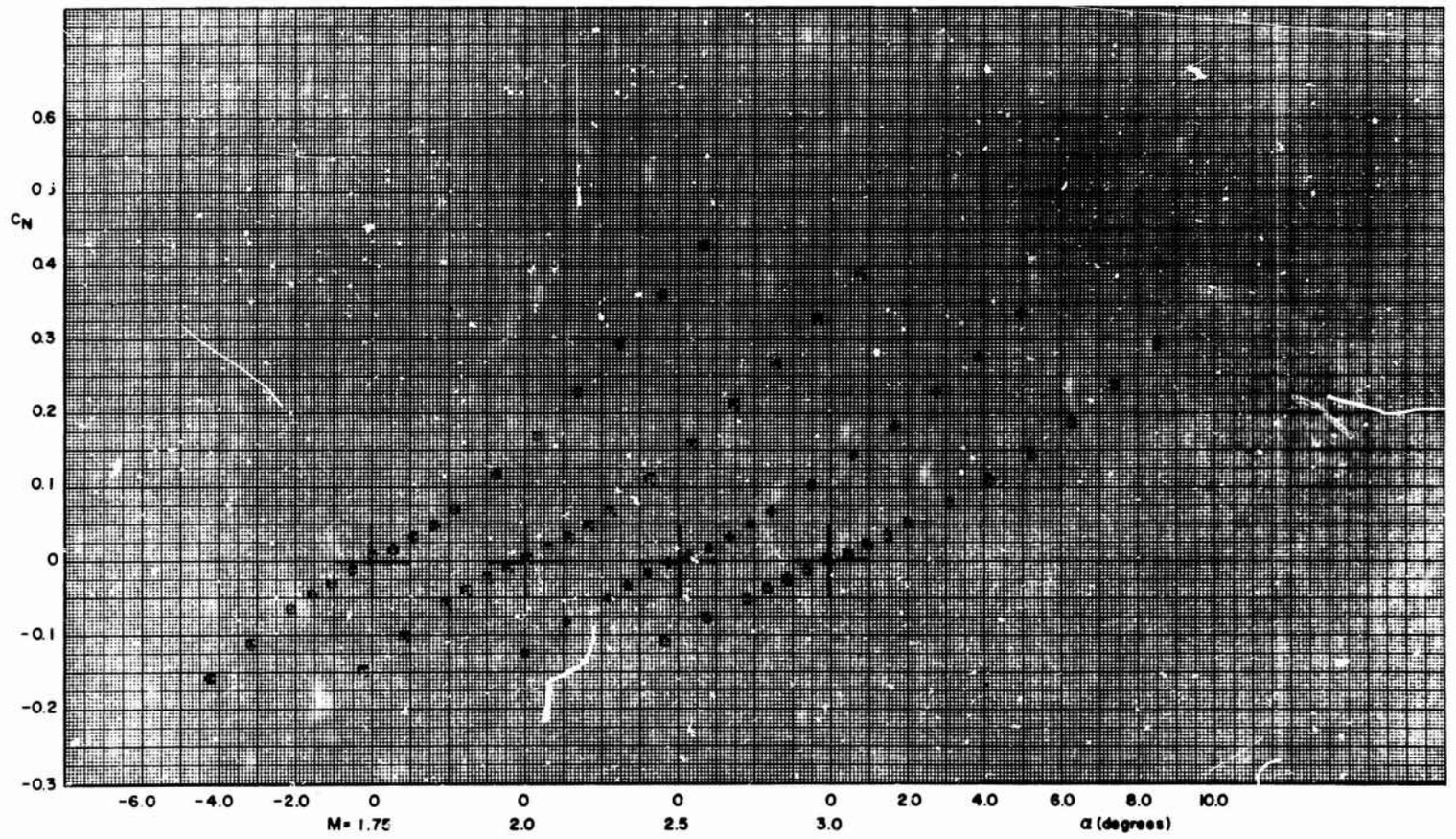

FIGURE A-3. NORMAL FORCE COEFFICIENT VERSUS ANGLE OF ATTACK, F8.06 (Continued)

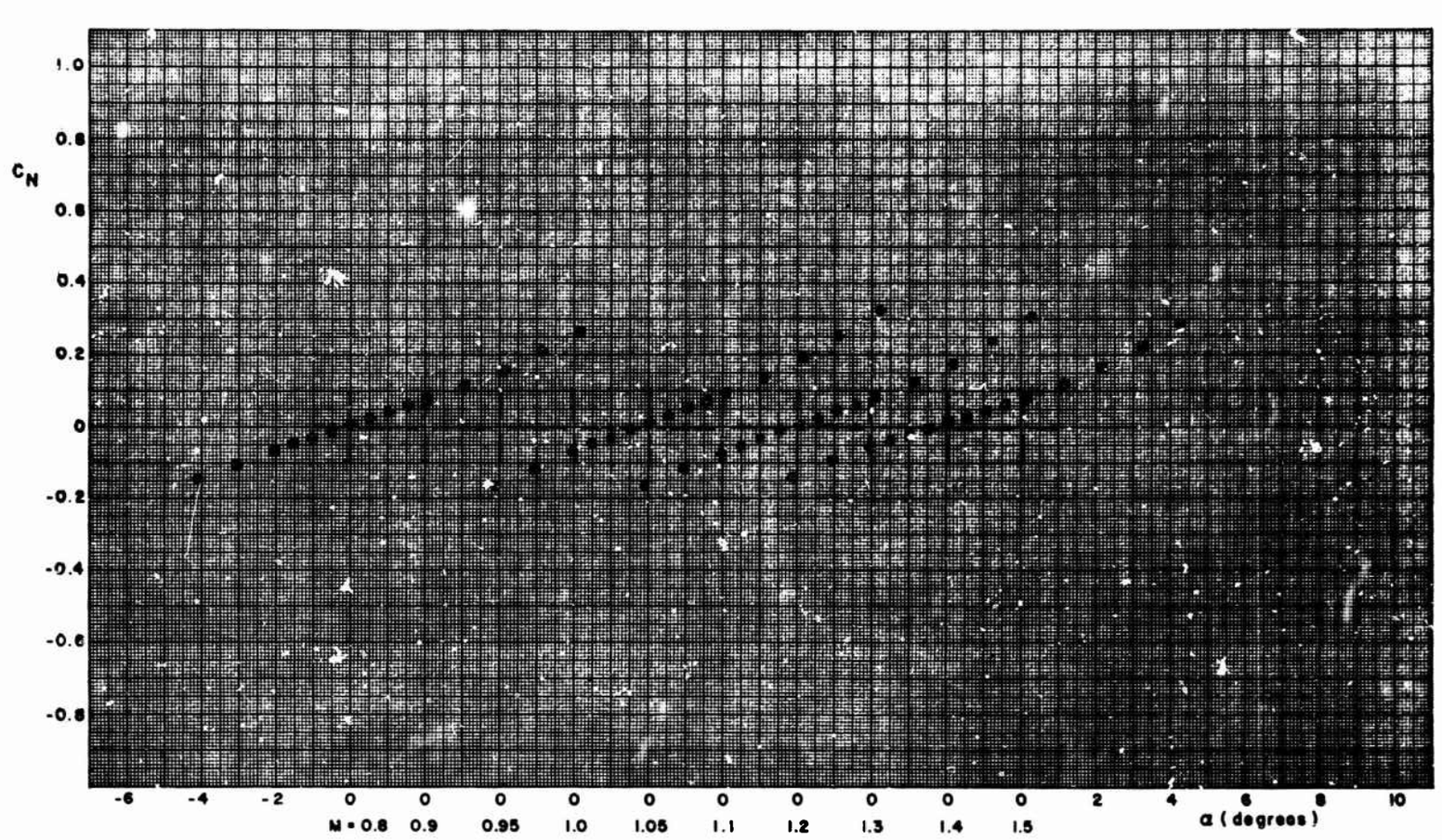

FIGURE A-3. NORMAL FORCE COEFFICIENT VERSUS ANGLE OF ATTACK, F8.12 (Continued)

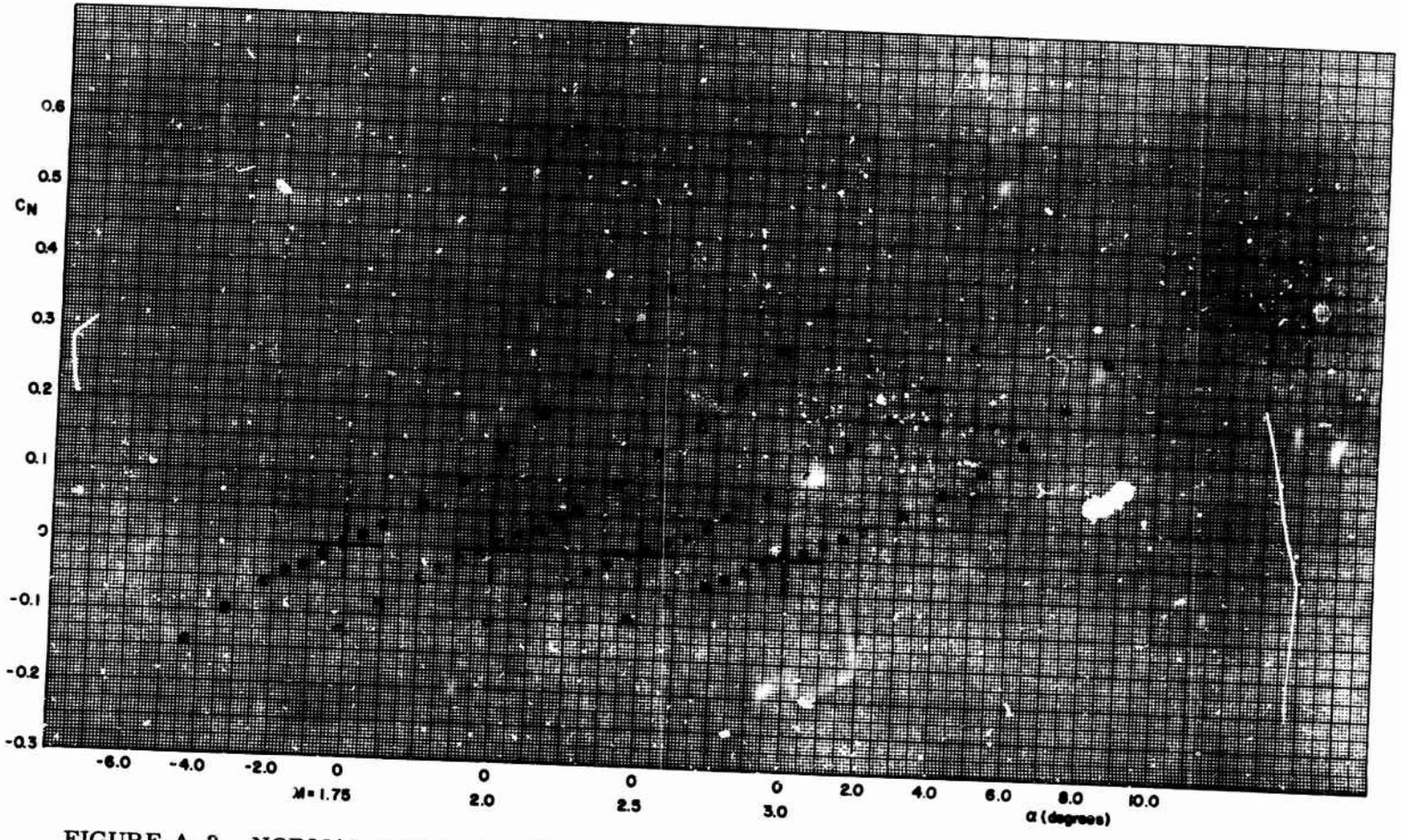

FIGURE A-3. NORMAL FORCE COEFFICIENT VERSUS ANGLE OF ATTACK, F8.12 (Continued)

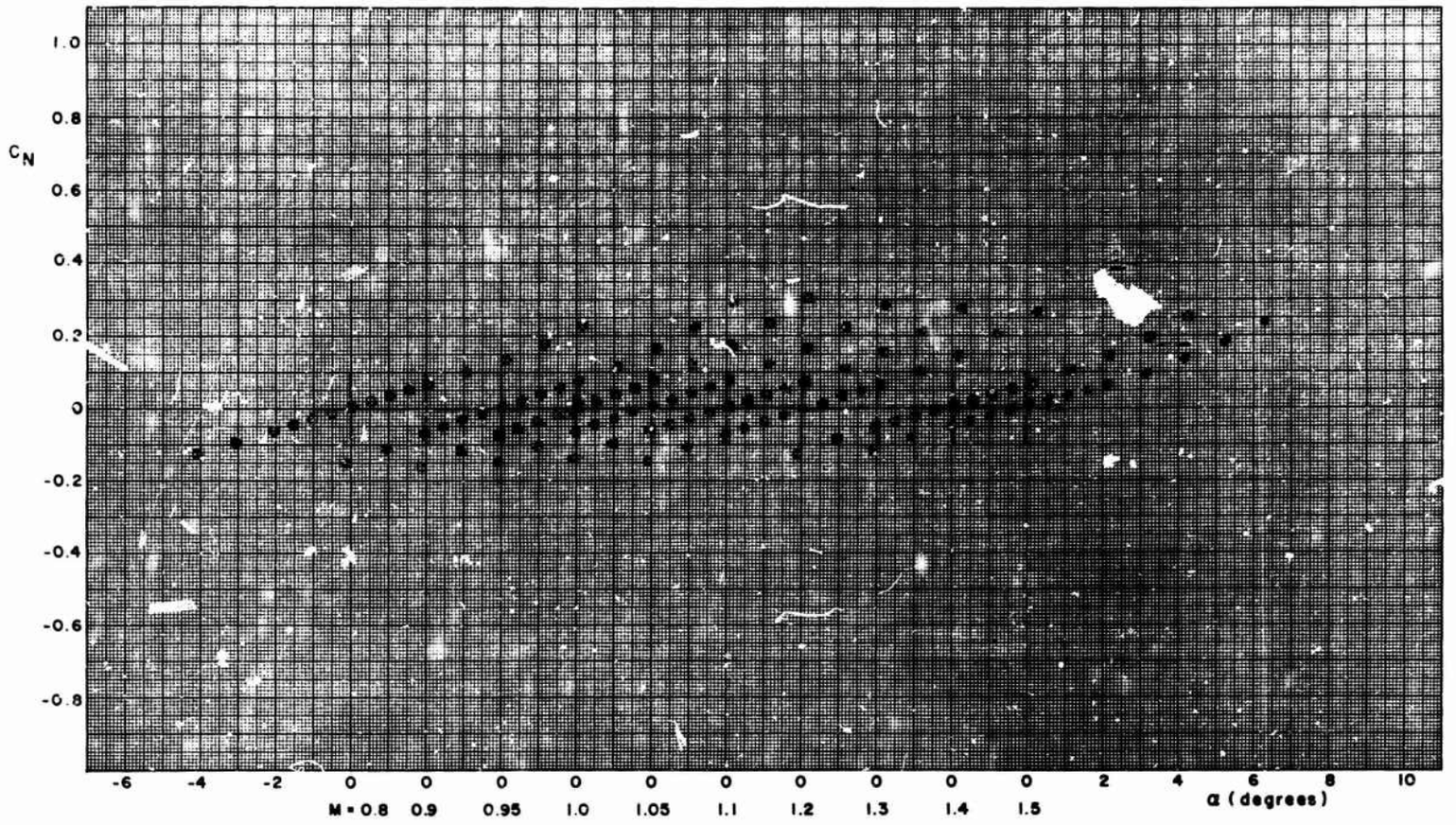

FIGURE A-3. NORMAL FORCE COEFFICIENT VERSUS ANGLE OF ATTACK, F8.20 (Continued)

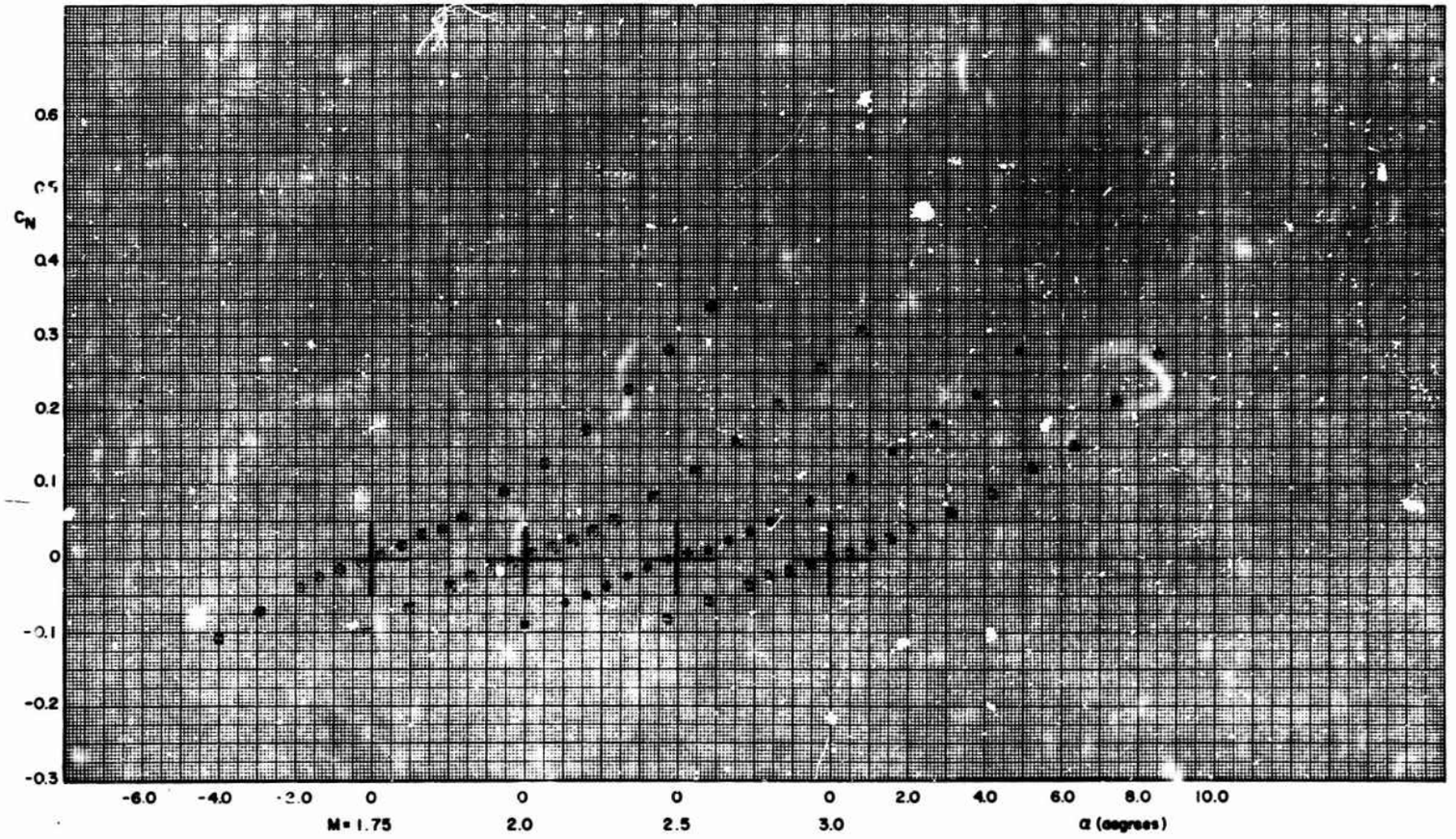

FIGURE A-3. NORMAL FORCE COEFFICIENT VERSUS ANGLE OF ATTACK, F8.20 (Concluded)

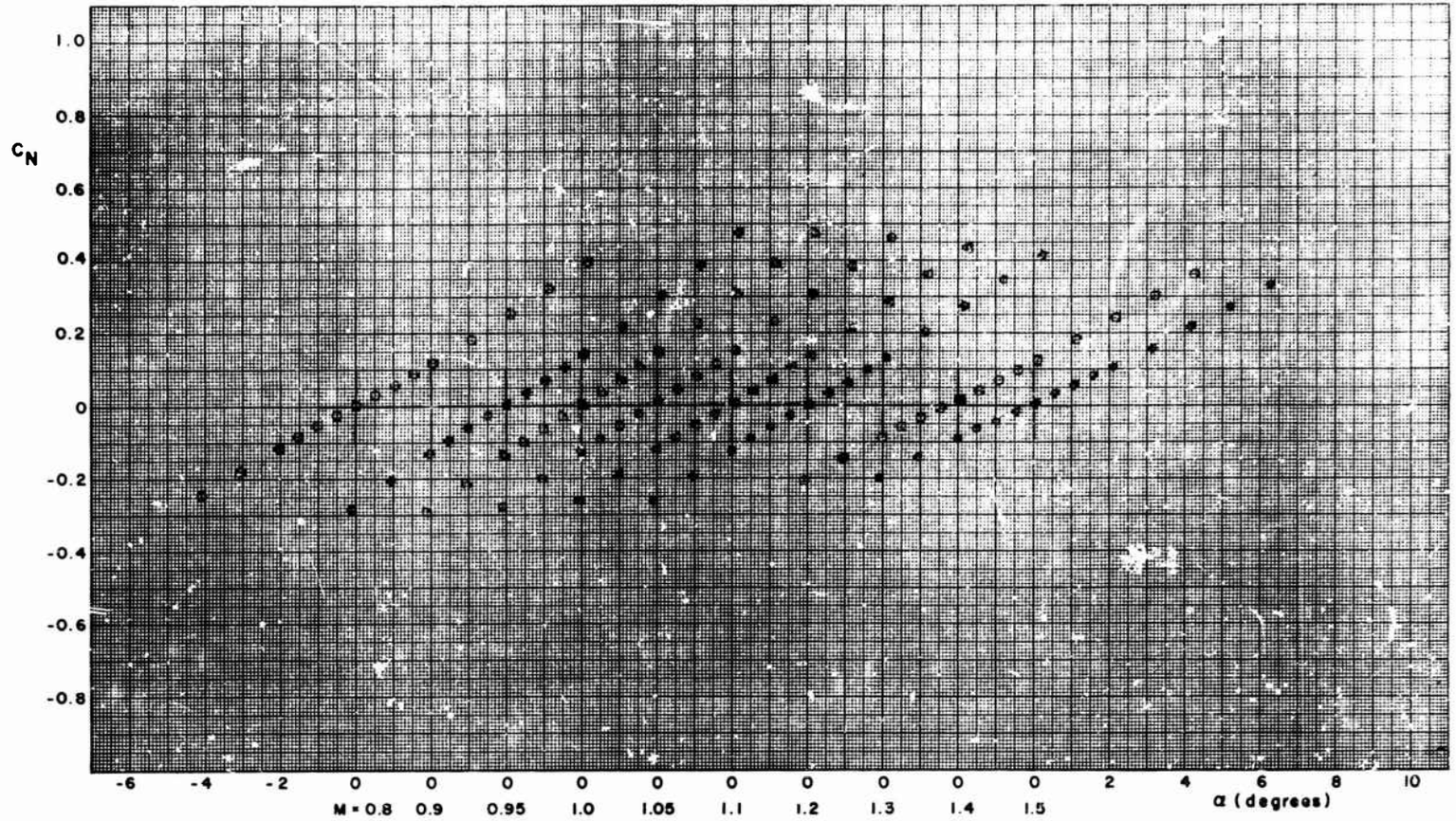

FIGURE A-4. NORMAL FORCE COEFFICIENT VERSUS ANGLE OF ATTACK, FD. 00

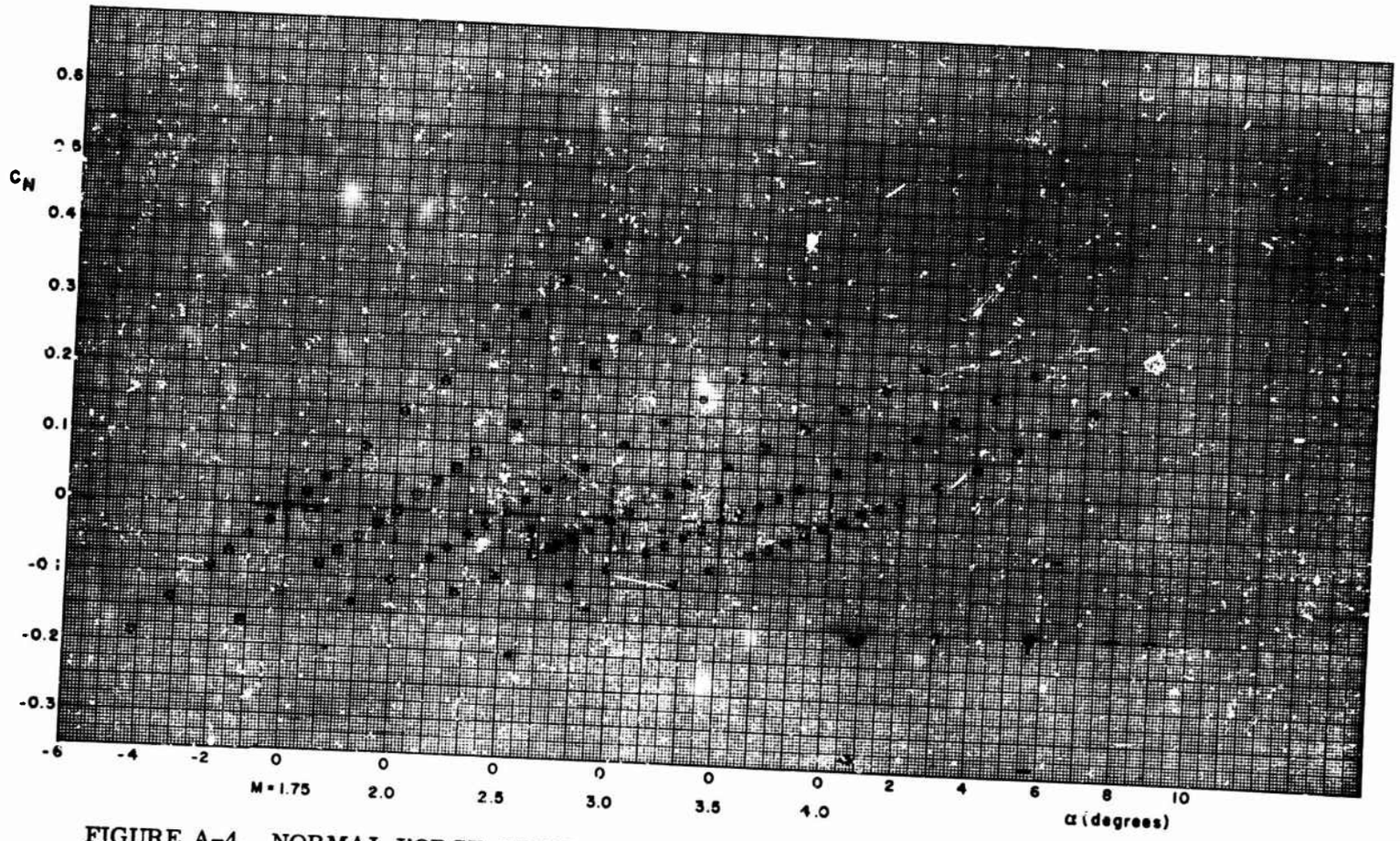

FIGURE A-4. NORMAL FORCE COEFFICIENT VERSUS ANGLE OF ATTACK, FD. 00 (Continued)

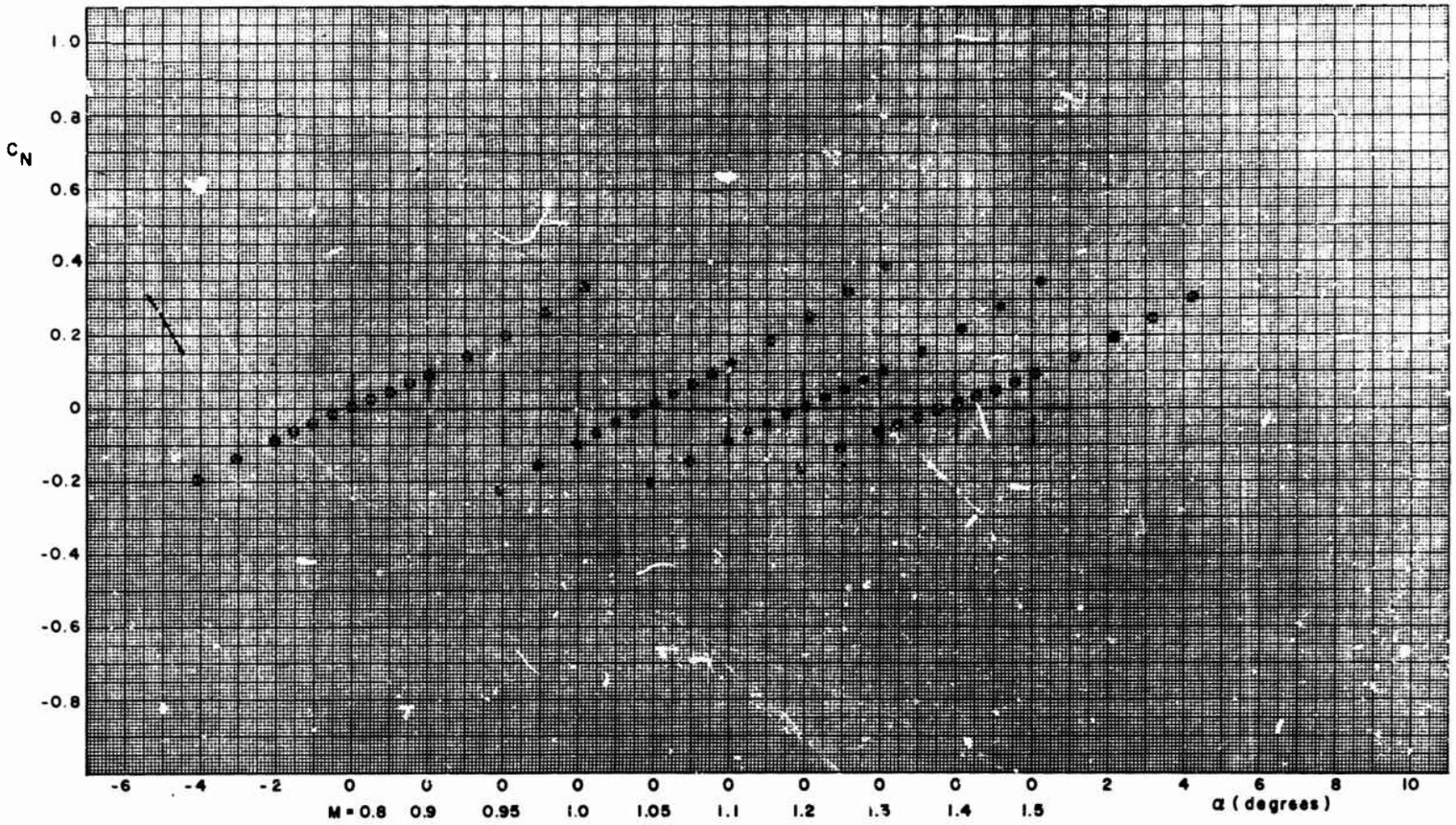

FIGURE A-4. NORMAL FORCE COEFFICIENT VERSUS ANGLE OF ATTACK, FD. 06 (Continued)

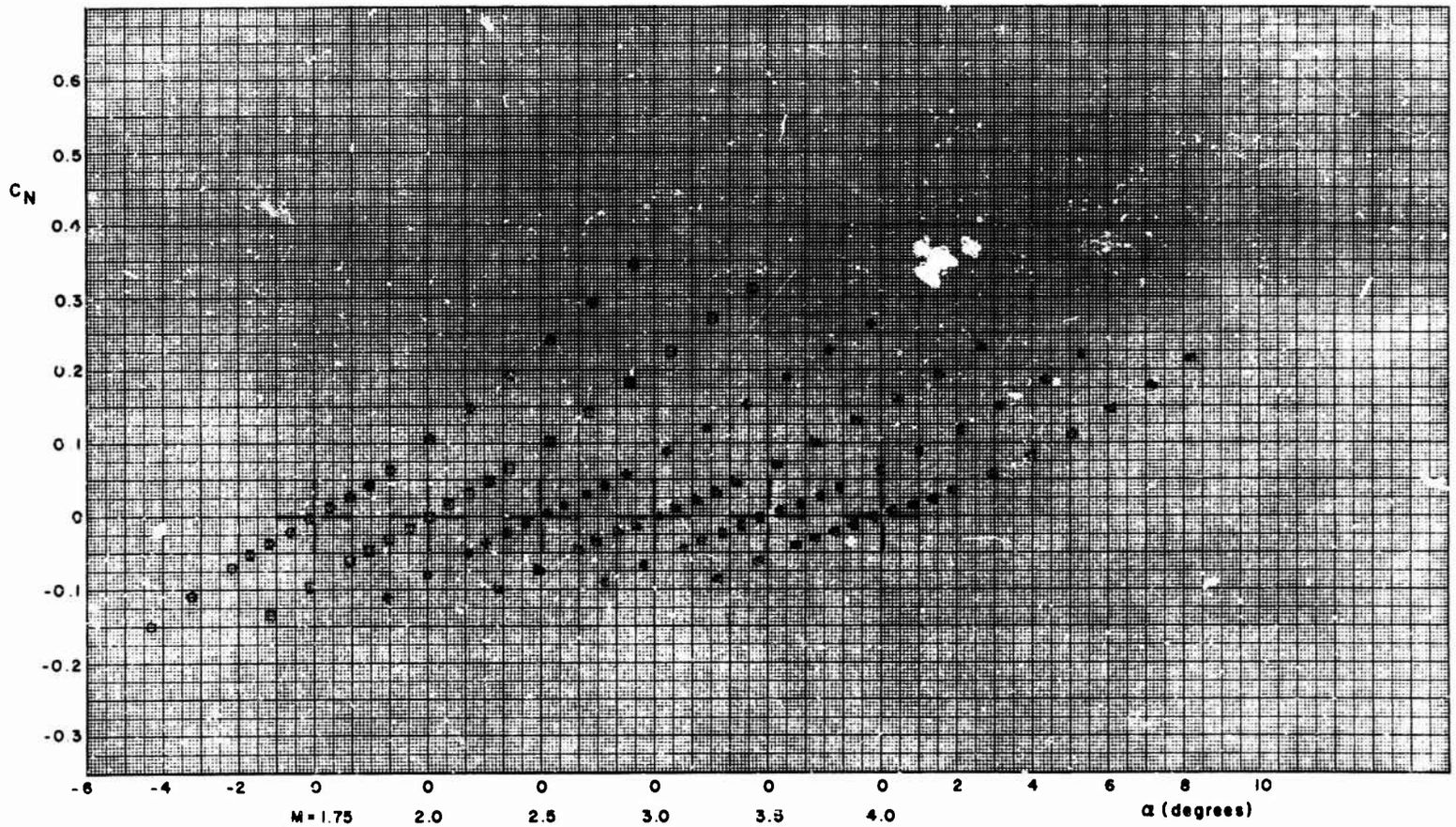

FIGURE A-4. NORMAL FORCE COEFFICIENT VERSUS ANGLE OF ATTACK, FD. 06 (Continued)

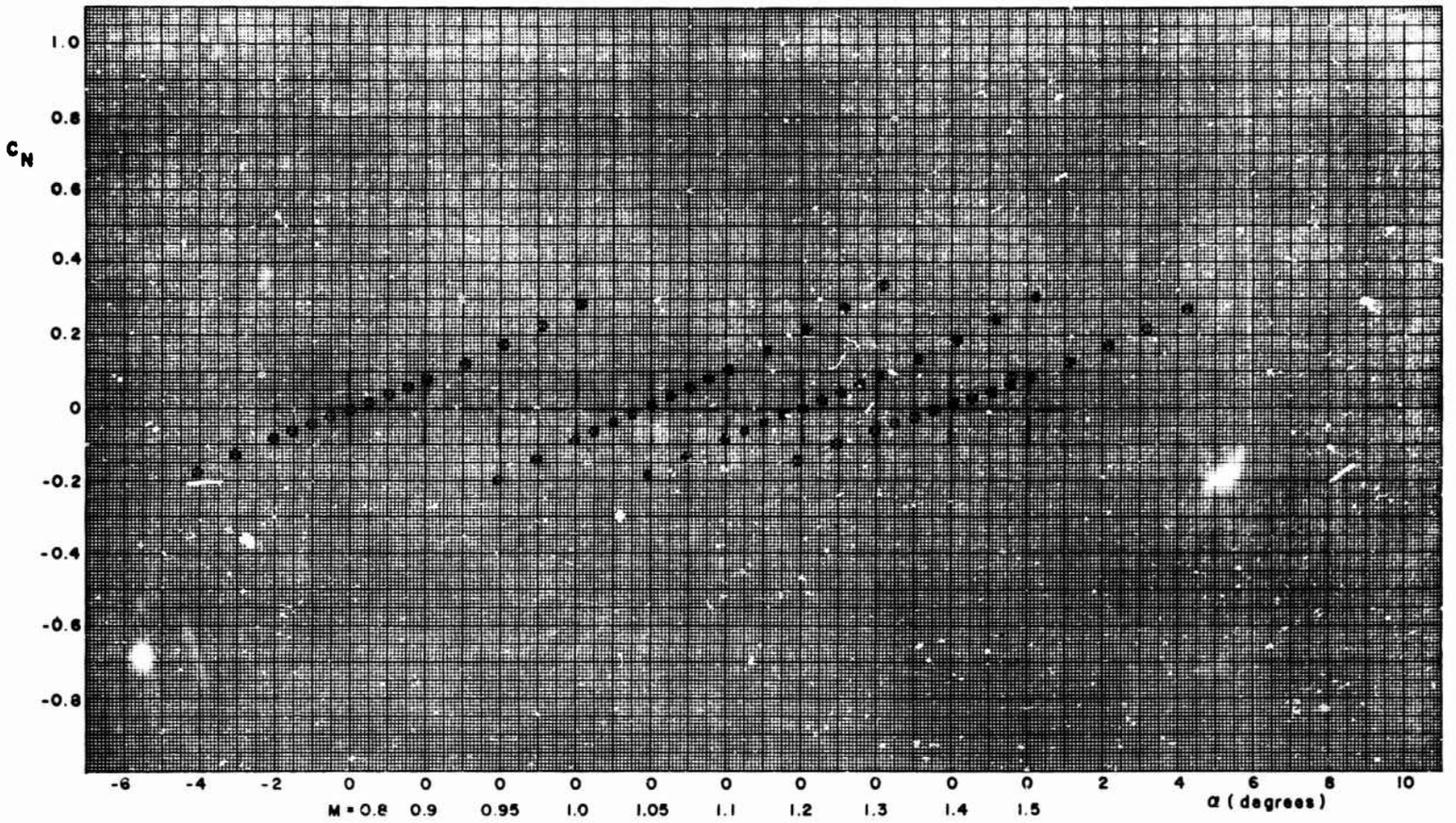

FIGURE A-4. NORMAL FORCE COEFFICIENT VERSUS ANGLE OF ATTACK, FD. 12 (Continued)

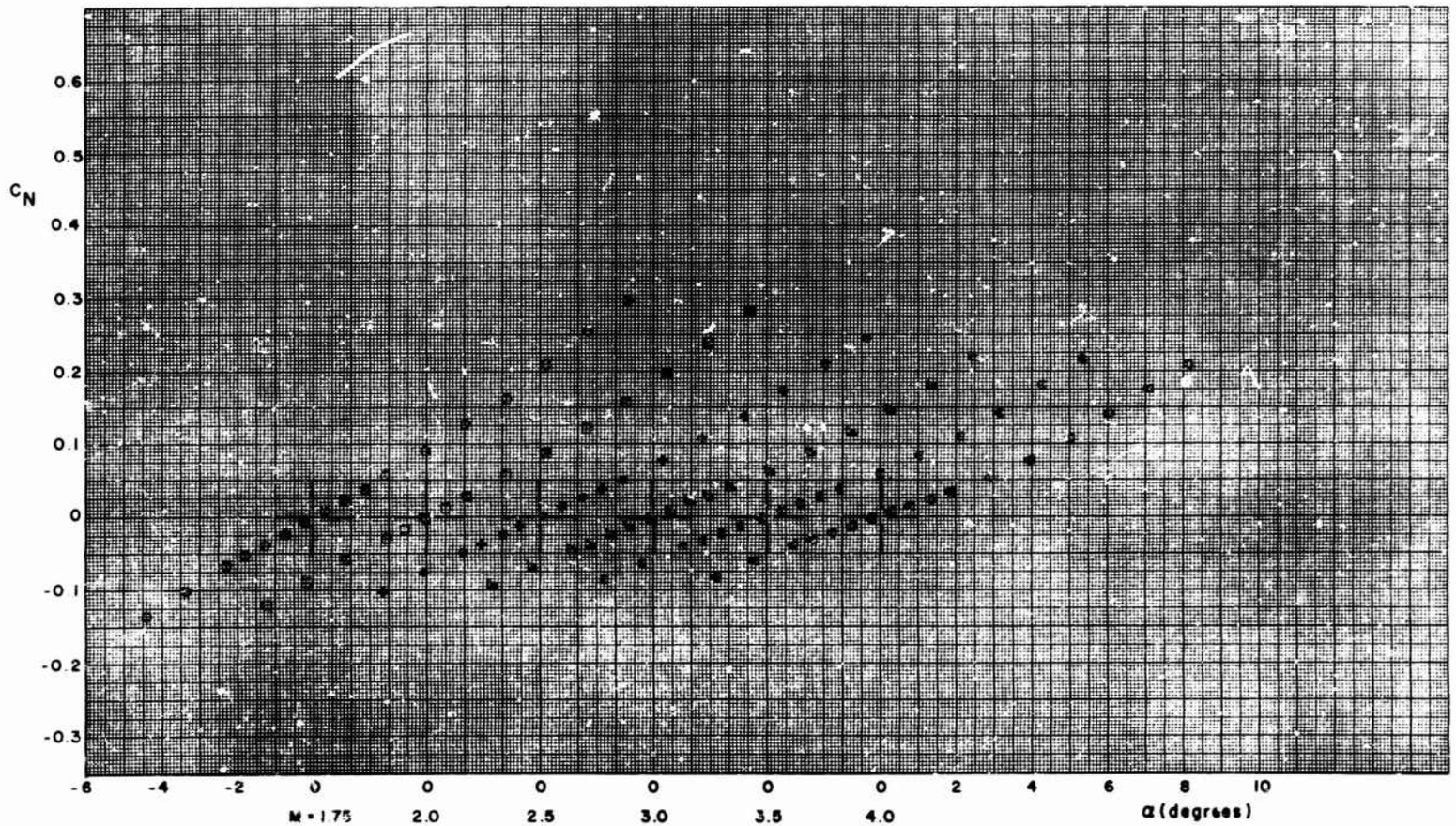

FIGURE A-4. NORMAL FORCE COEFFICIENT VERSUS ANGLE OF ATTACK, FD. 12 (Continued)

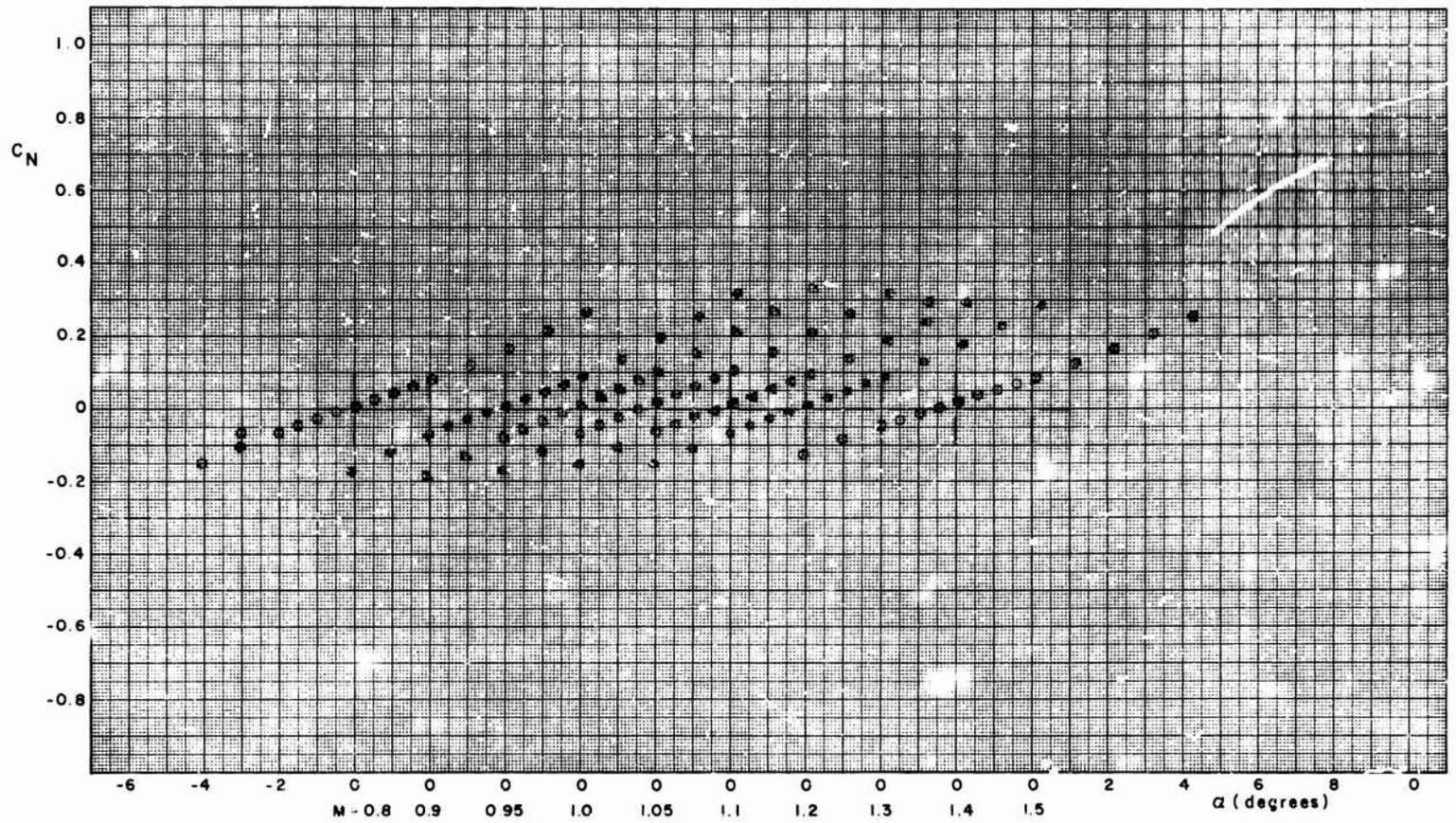

FIGURE A-4. NORMAL FORCE COEFFICIENT VERSUS ANGLE OF ATTACK, FD-20 (Continued)

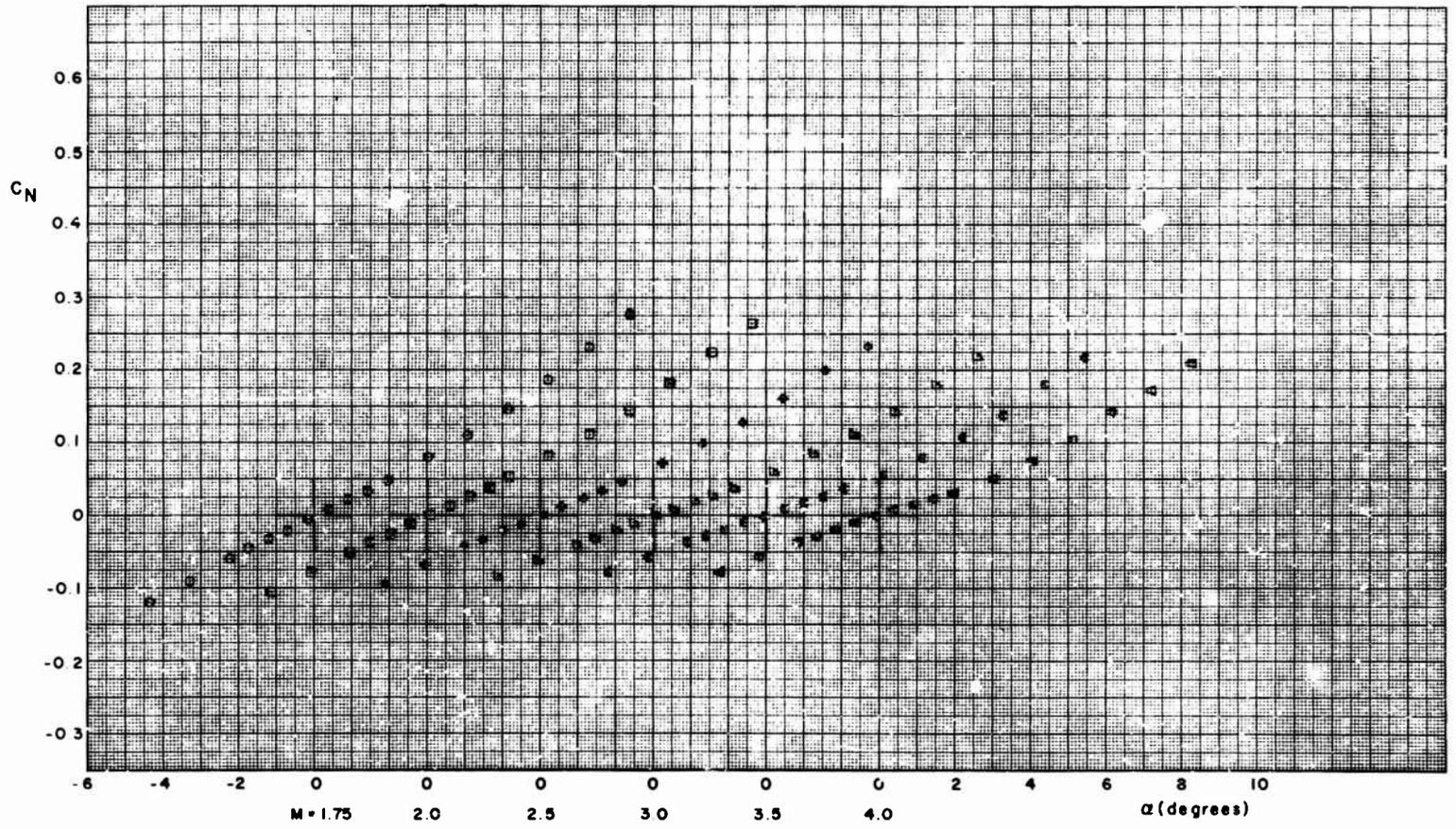

FIGURE A-4. NORMAL FORCE COEFFICIENT VERSUS ANGLE OF ATTACK, FD.20 (Concluded)

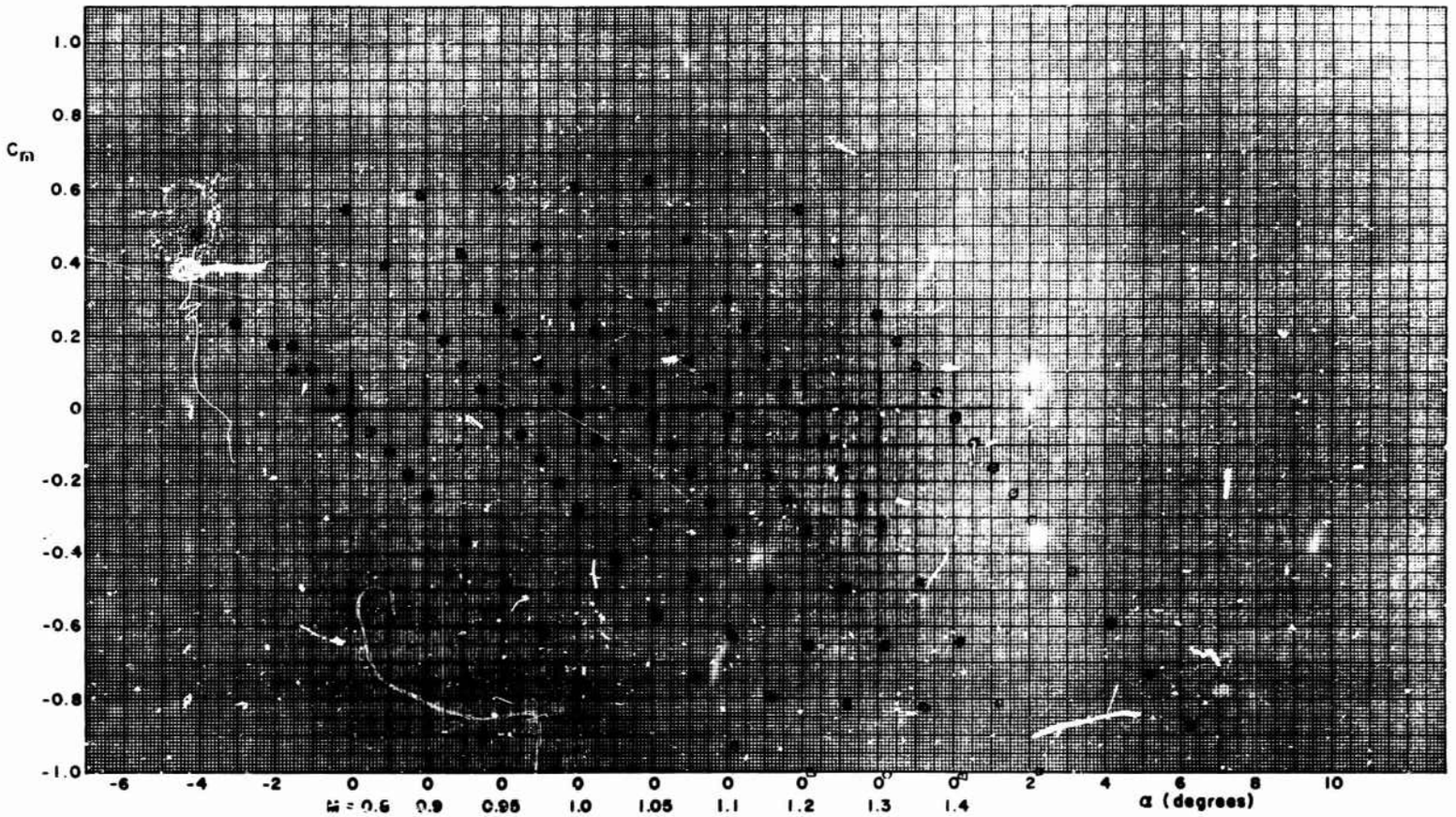

FIGURE A-5. PITCHING MOMENT VERSUS ANGLE OF ATTACK, F4.00

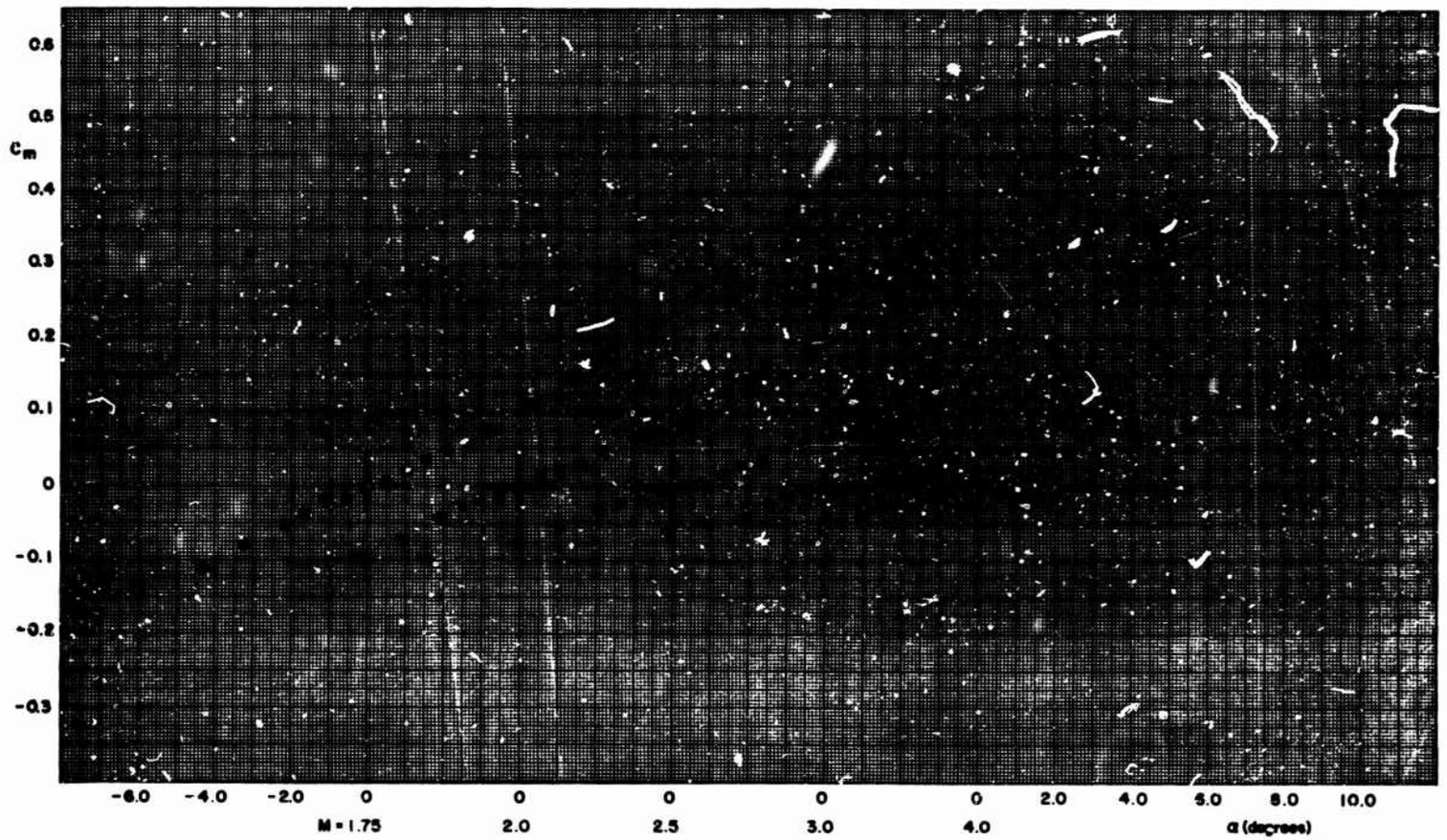

FIGURE A-5. PITCHING MOMENT VERSUS ANGLE OF ATTACK, F4.00 (Continued)

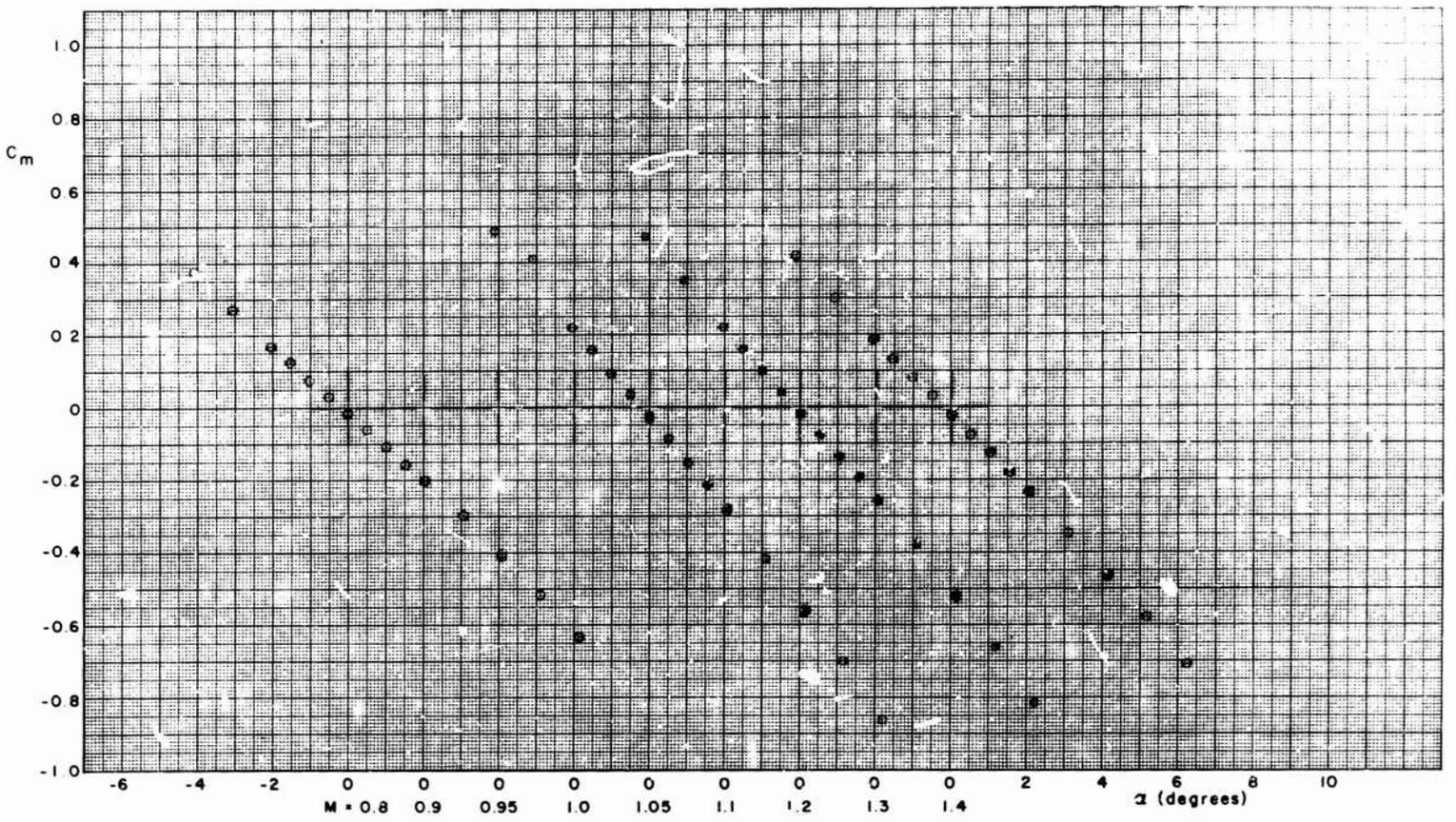

FIGURE A-3. PITCHING MOMENT VERSUS ANGLE OF ATTACK, F4.08 (Continued)

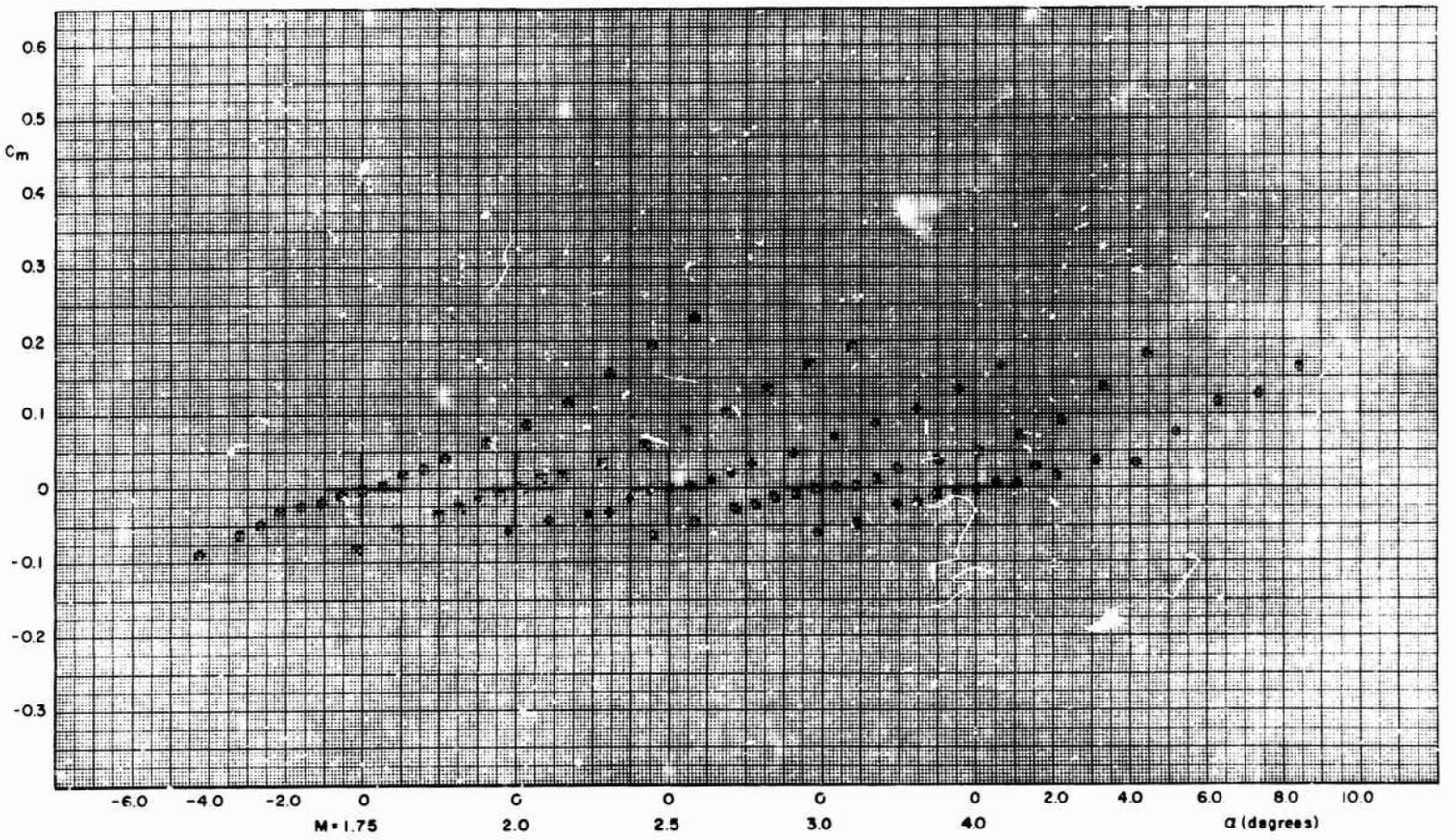

FIGURE A-5. PITCHING MOMENT VERSUS ANGLE OF ATTACK, F4.08 (Continued)

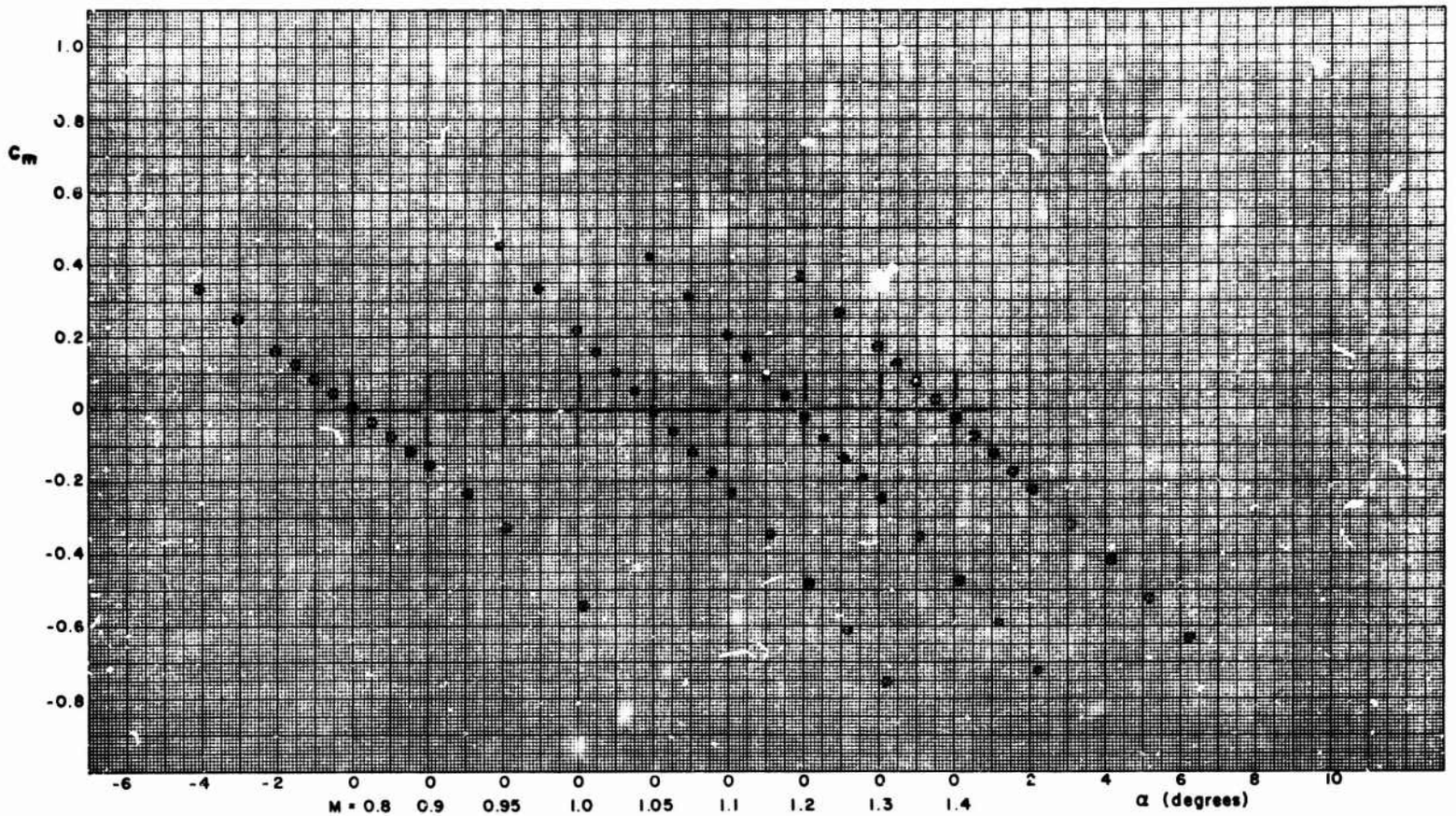

FIGURE A-5. PITCHING MOMENT VERSUS ANGLE OF ATTACK, F4.16 (Continued)

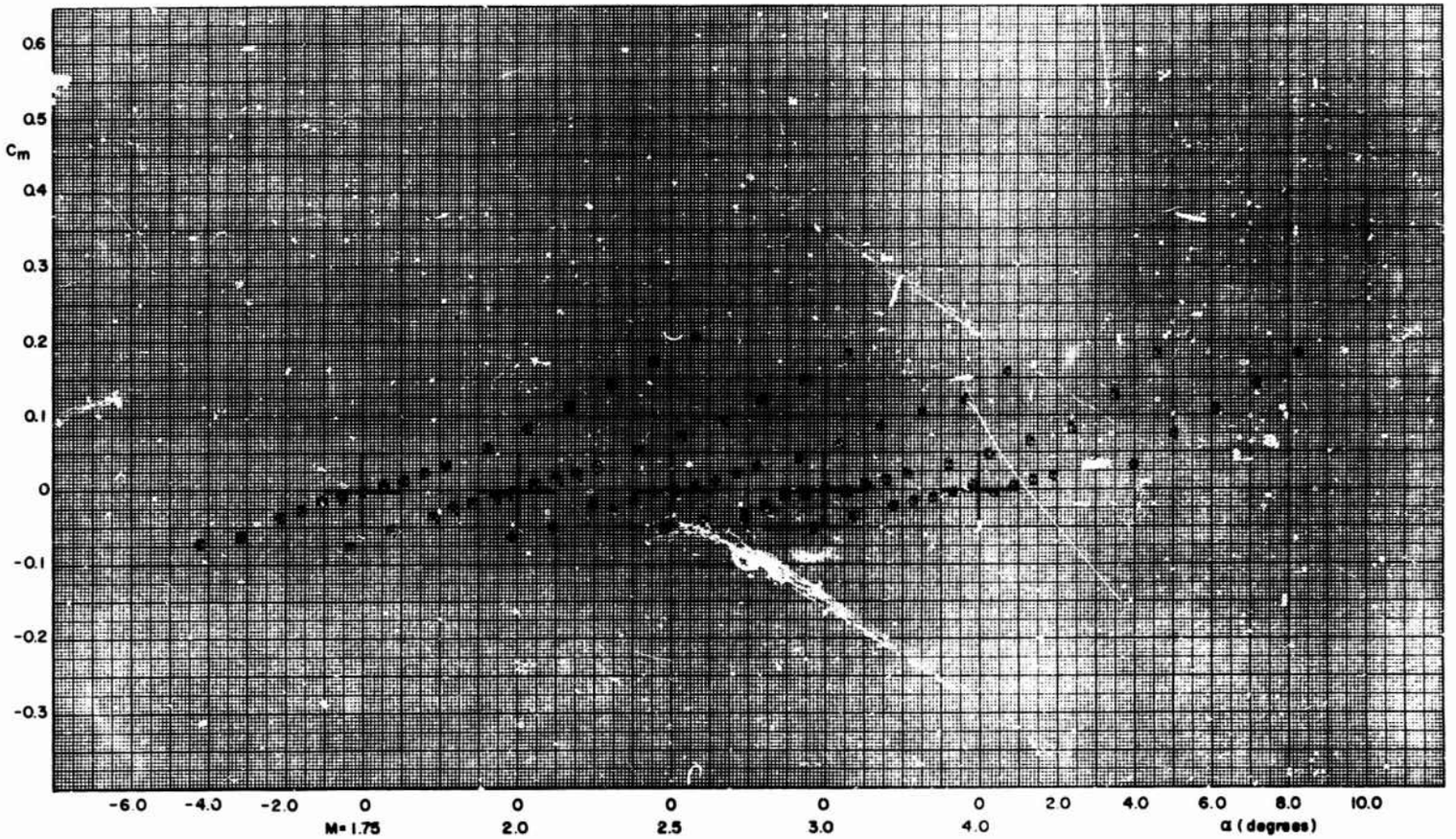

FIGURE A-5. PITCHING MOMENT VERSUS ANGLE OF ATTACK, F4.16 (Continued)

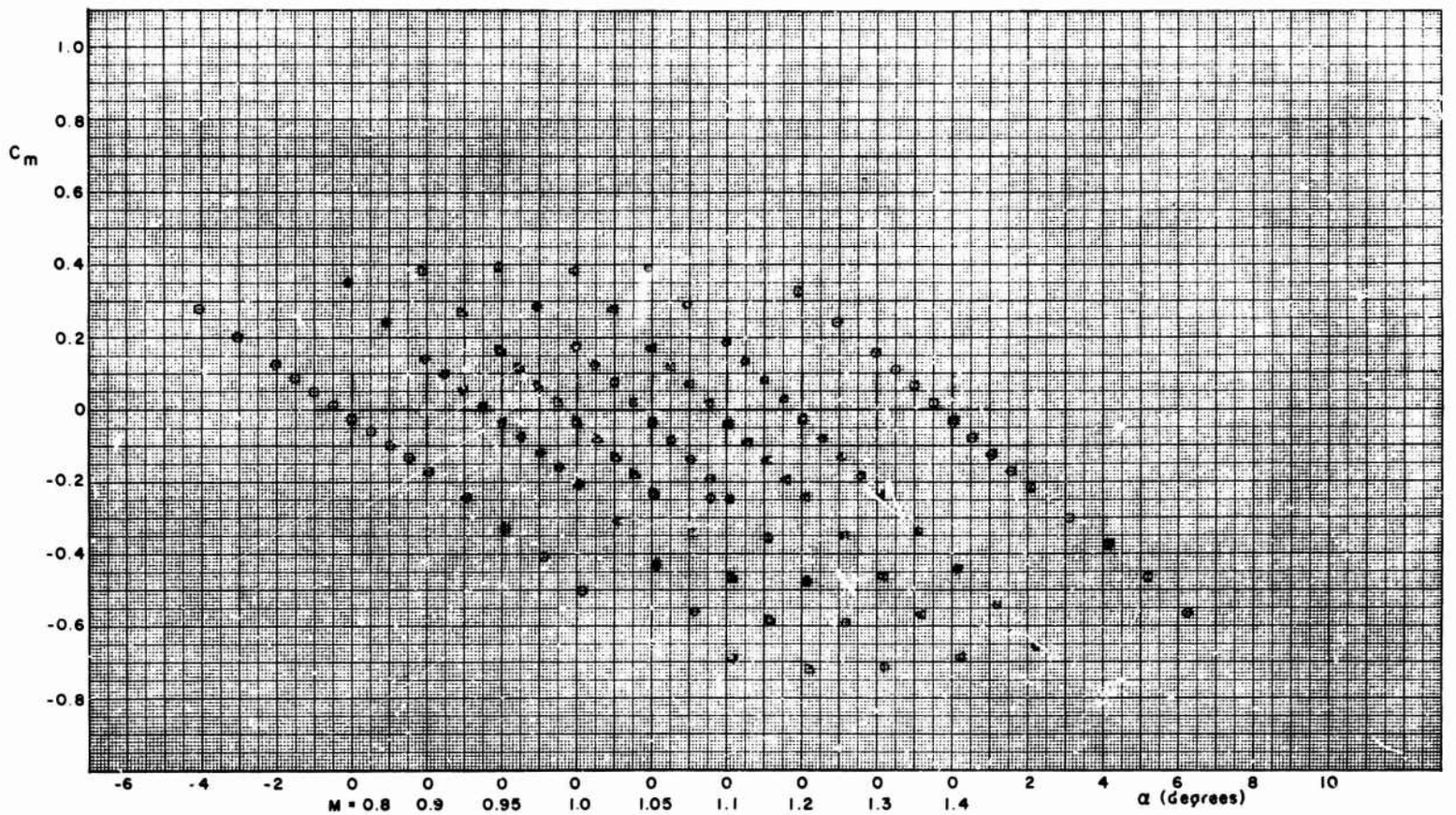

FIGURE A-5. PITCHING MOMENT VERSUS ANGLE OF ATTACK, F4.25 (Continued)

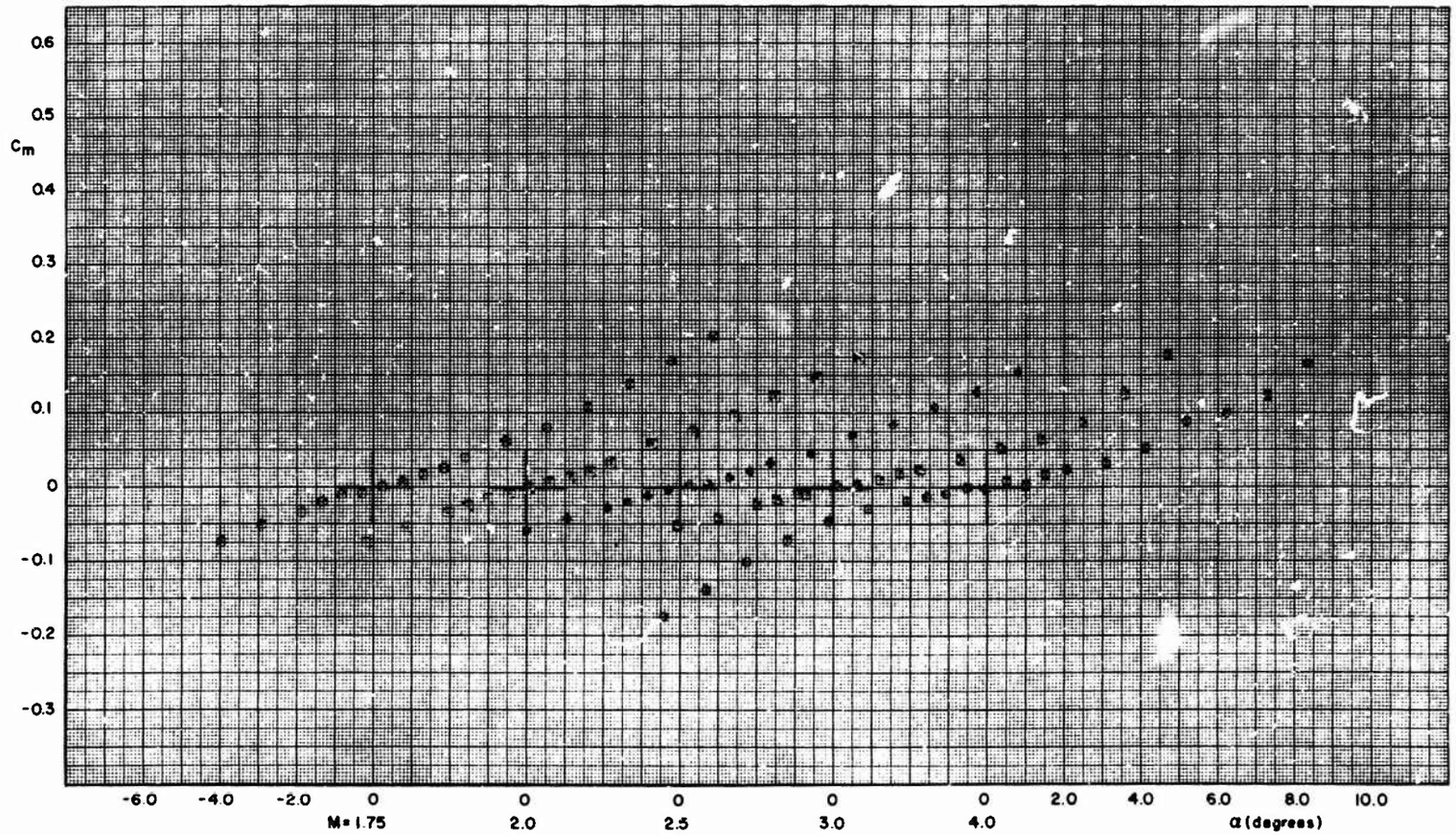

FIGURE A-5. PITCHING MOMENT VERSUS ANGLE OF ATTACK, F4.25 (Concluded)

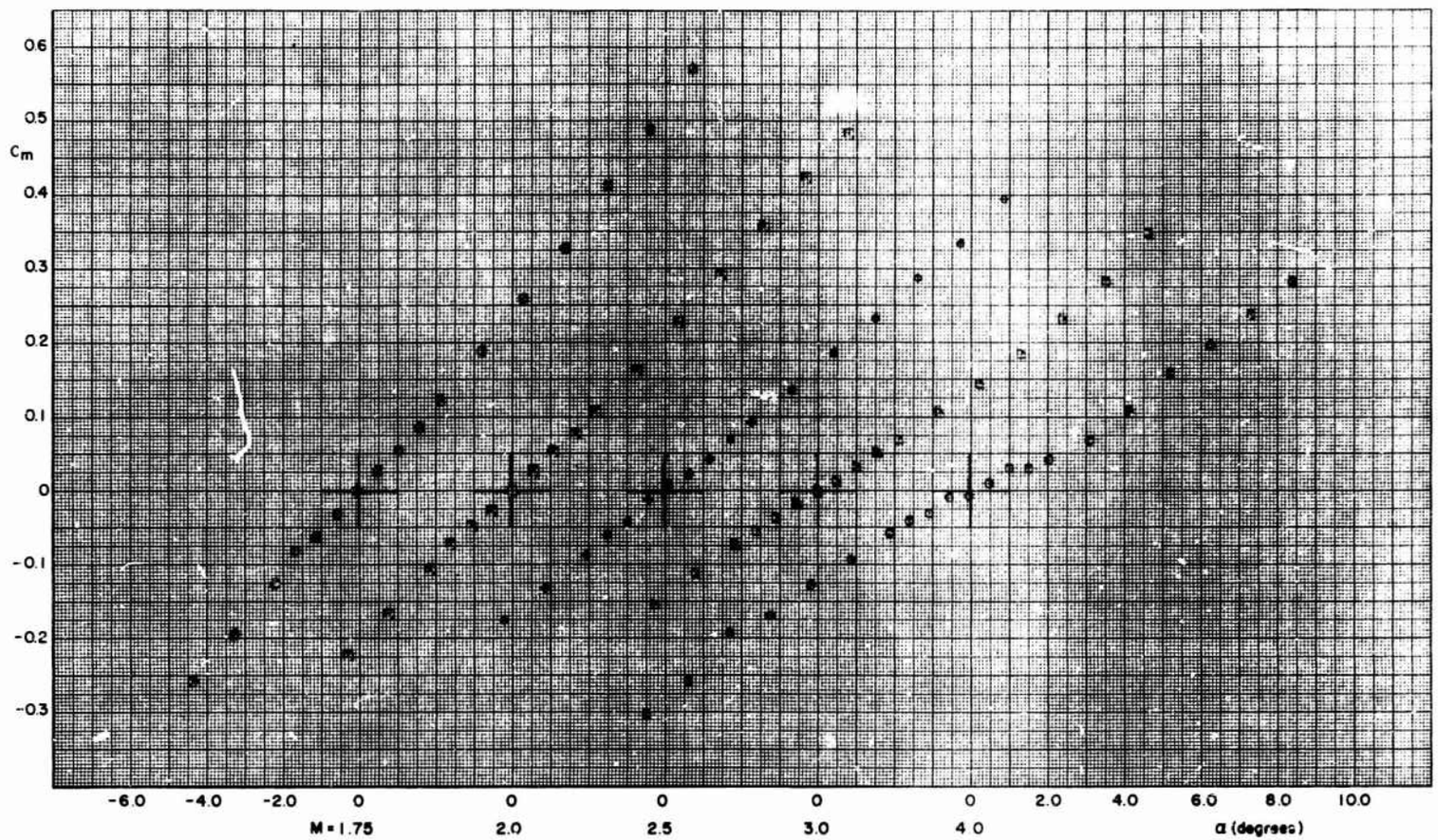

FIGURE A-6. PITCHING MOMENT VERSUS ANGLE OF ATTACK, F7.00

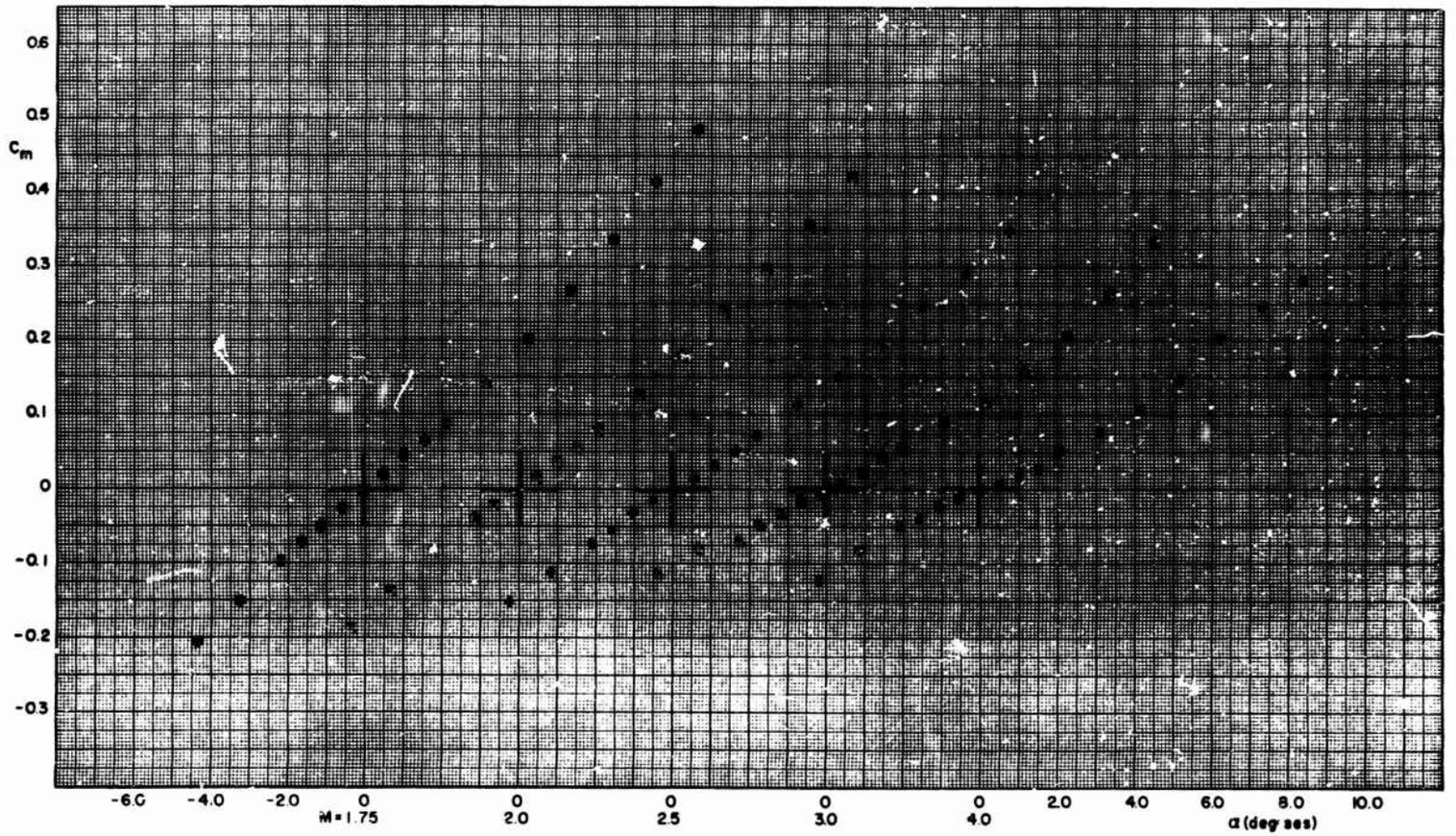

FIGURE A-6. PITCHING MOMENT VERSUS ANGLE OF ATTACK, F7.06 (Continued)

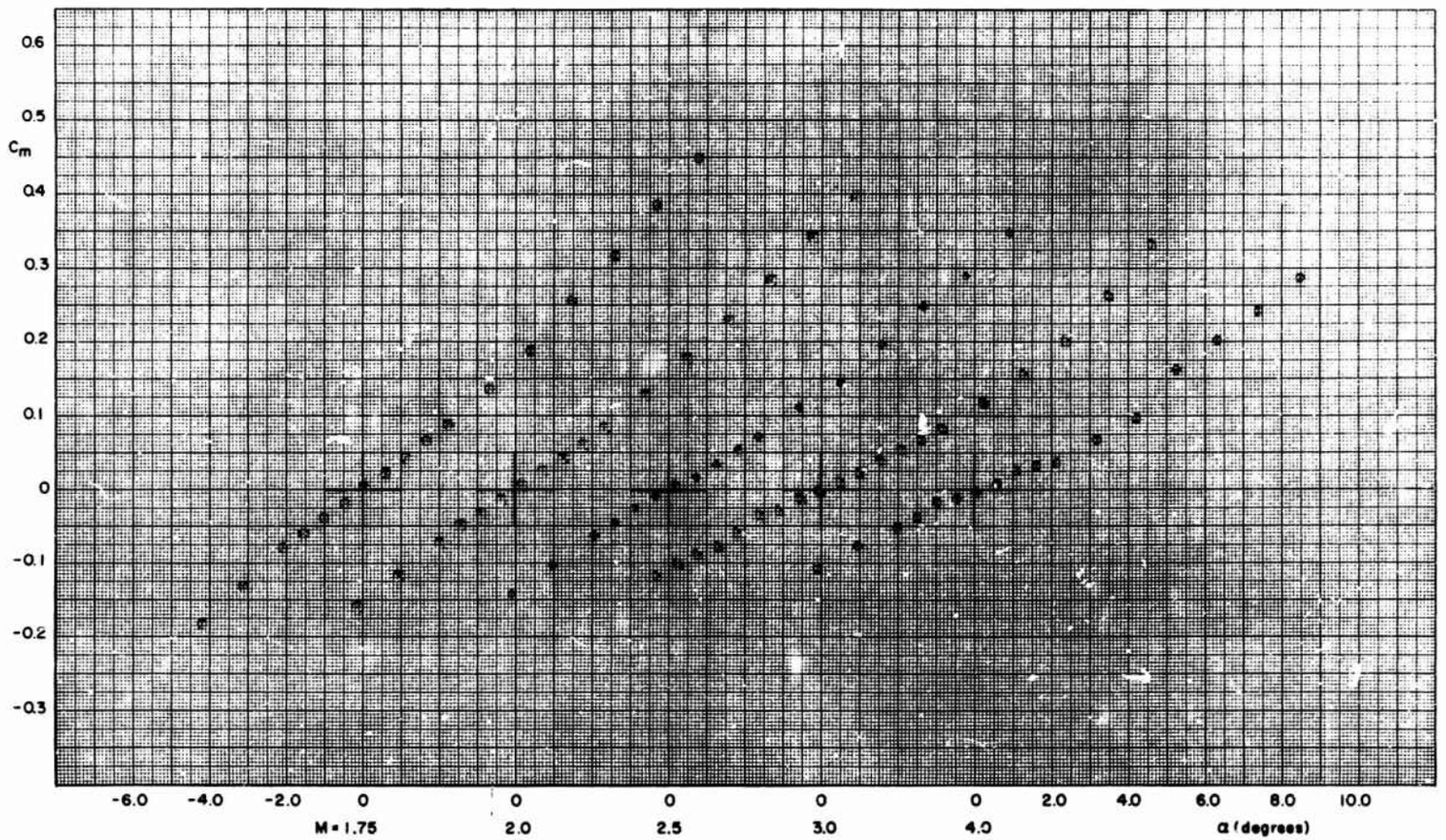

FIGURE A-6. PITCHING MOMENT VERSUS ANGLE OF ATTACK, F7 2 (Continued)

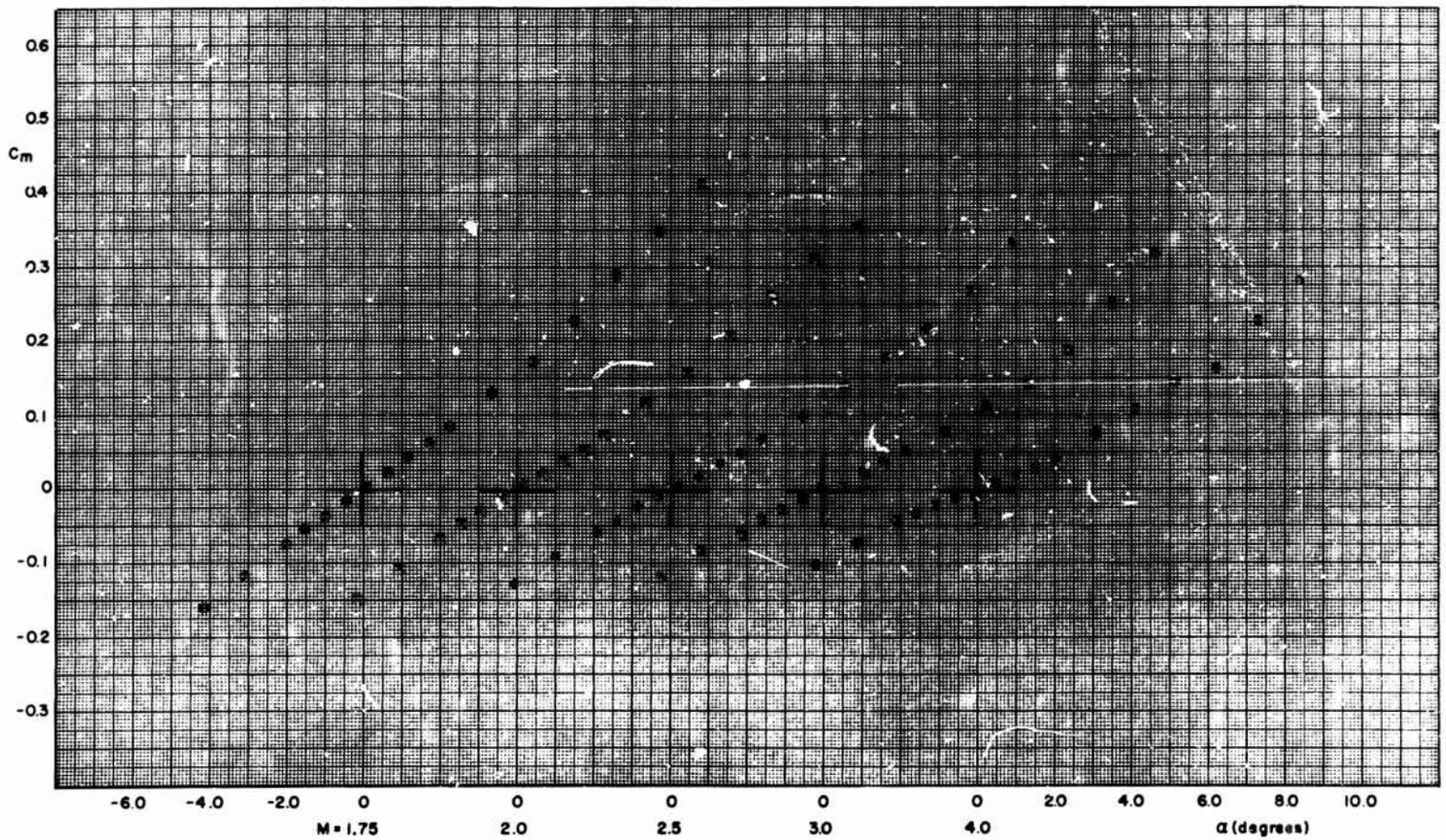

FIGURE A-6. PITCHING MOMENT VERSUS ANGLE OF ATTACK, F7.20 (Concluded)

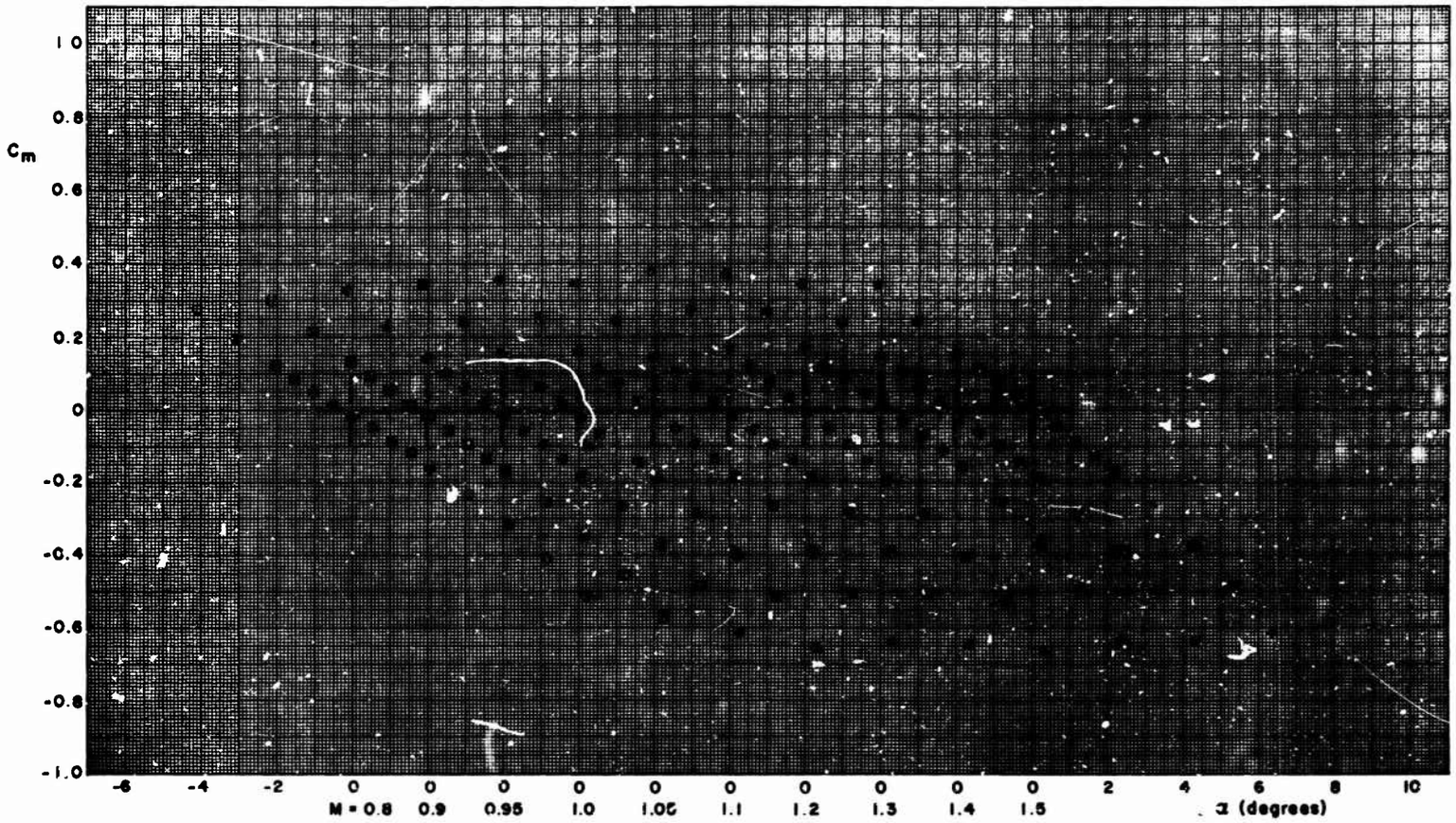

FIGURE A-7. PITCHING MOMENT VERSUS ANGLE OF ATTACK, F8.00

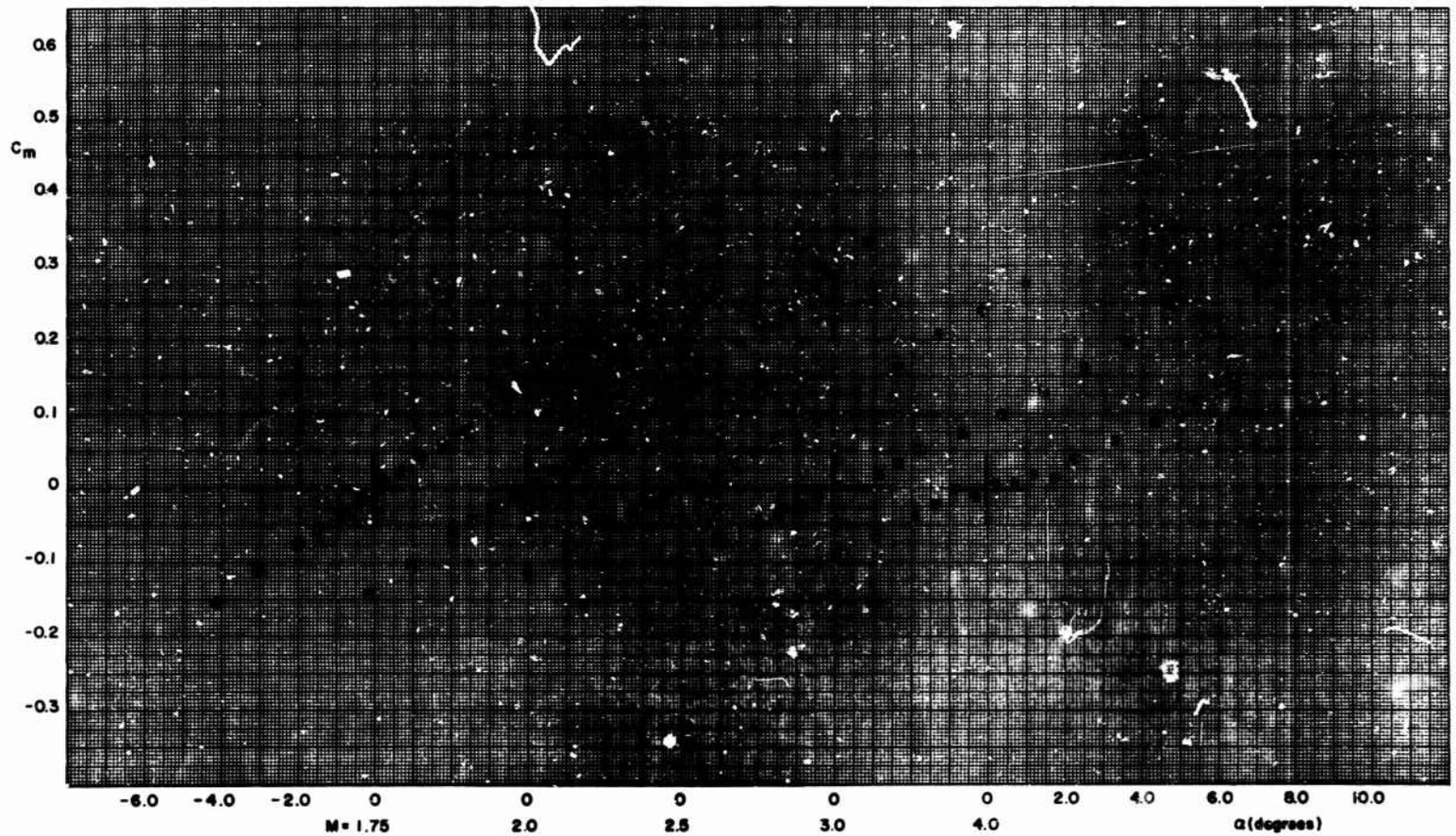

FIGURE A-7. PITCHING MOMENT VERSUS ANGLE OF ATTACK, F8.00 (Continued)

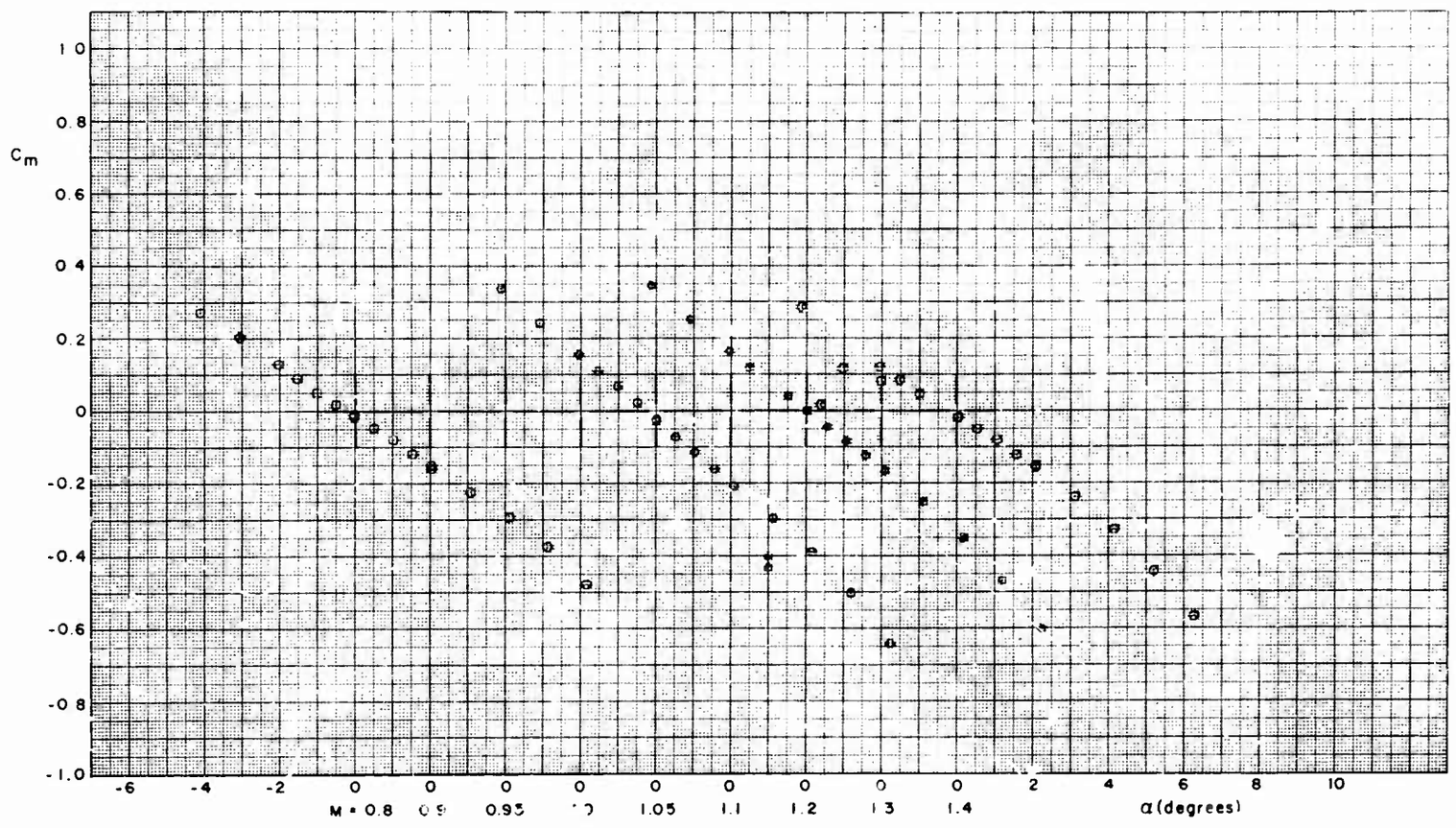

FIGURE A-7. PITCHING MOMENT VERSUS ANGLE OF ATTACK, F8.06 (Continued)

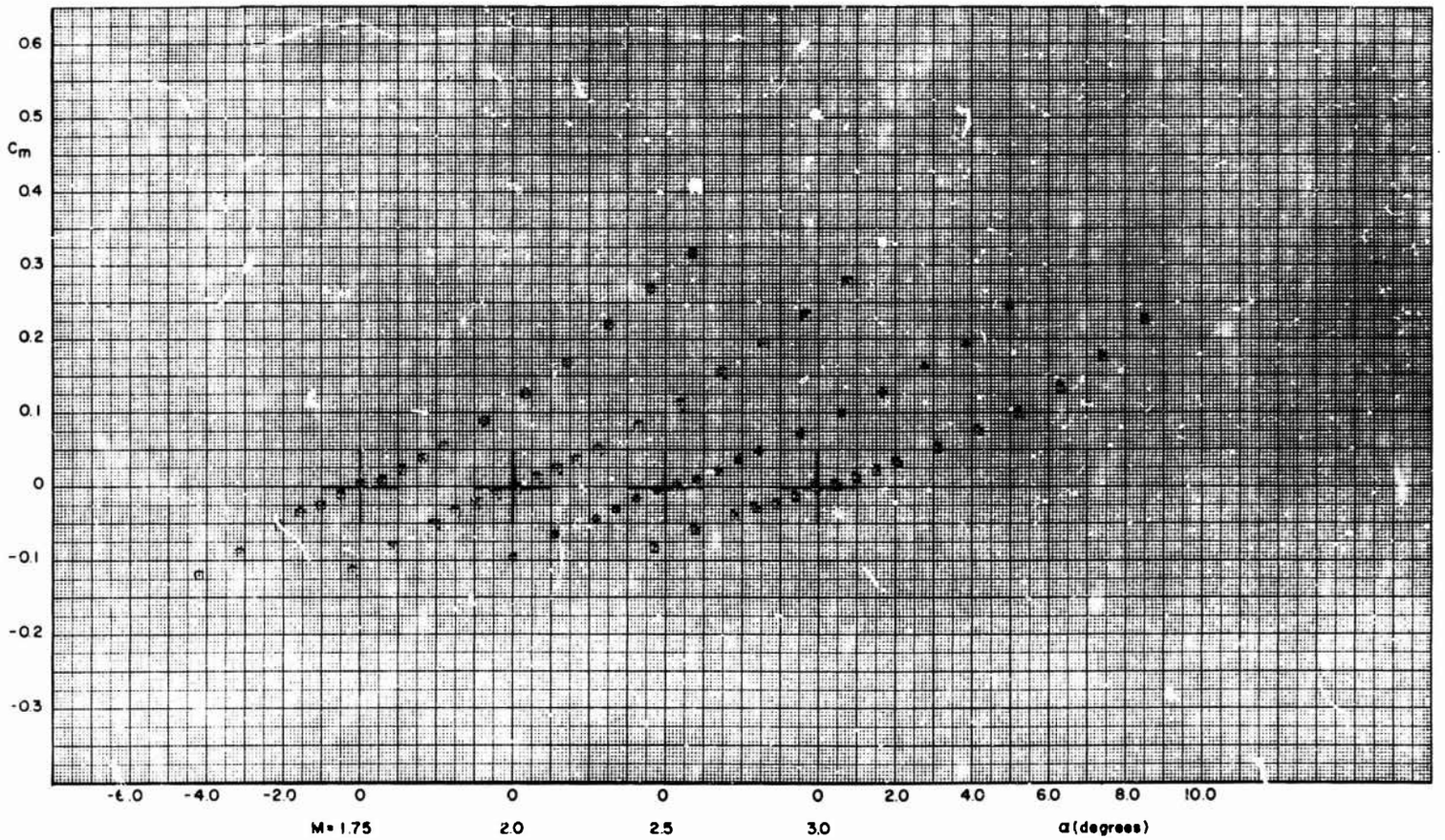

FIGURE A-7. PITCHING MOMENT VERSUS ANGLE OF ATTACK, F8.06 (Continued)

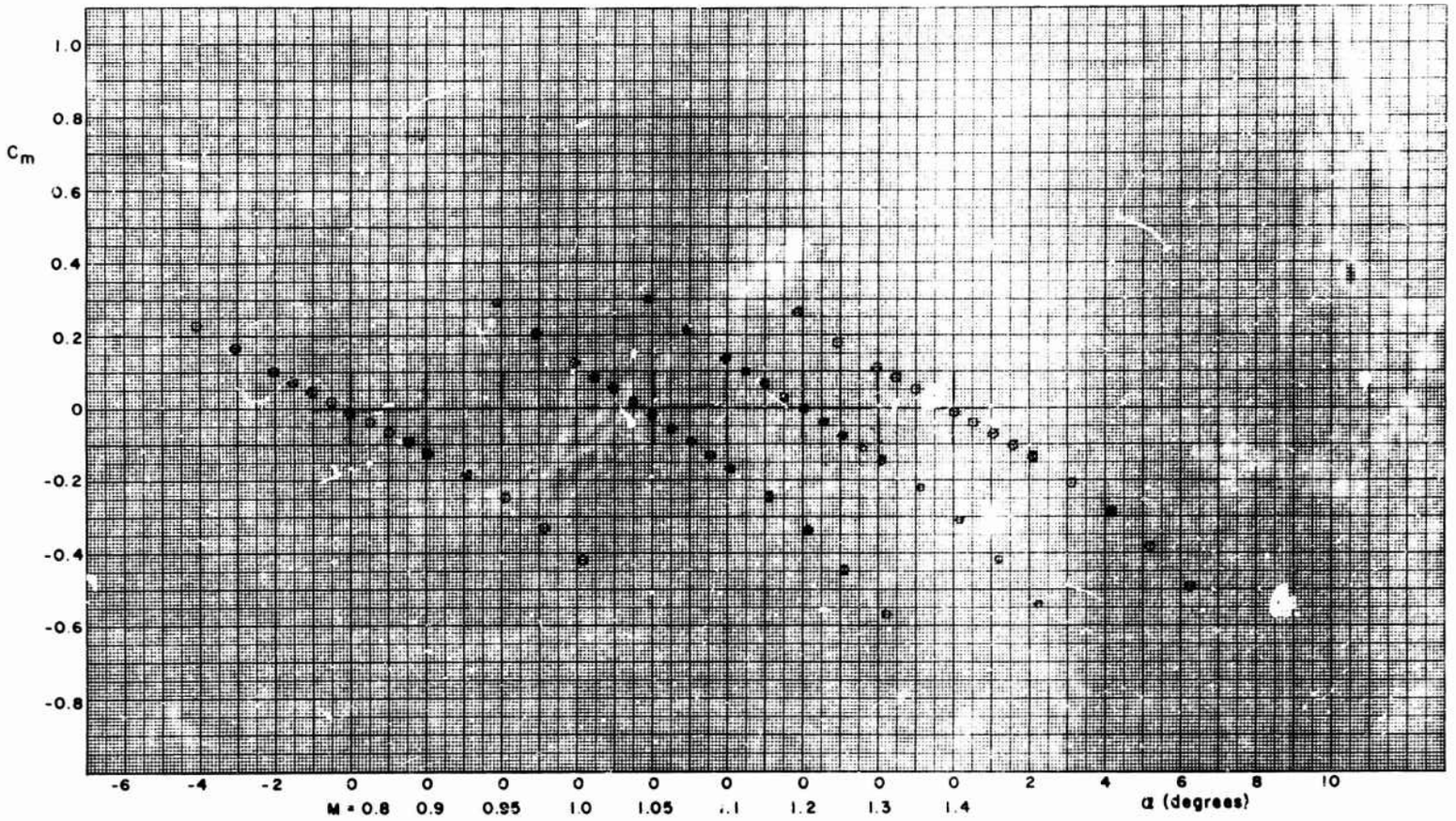

FIGURE A-7. PITCHING MOMENT VERSUS ANGLE OF ATTACK, F8.12 (Continued)

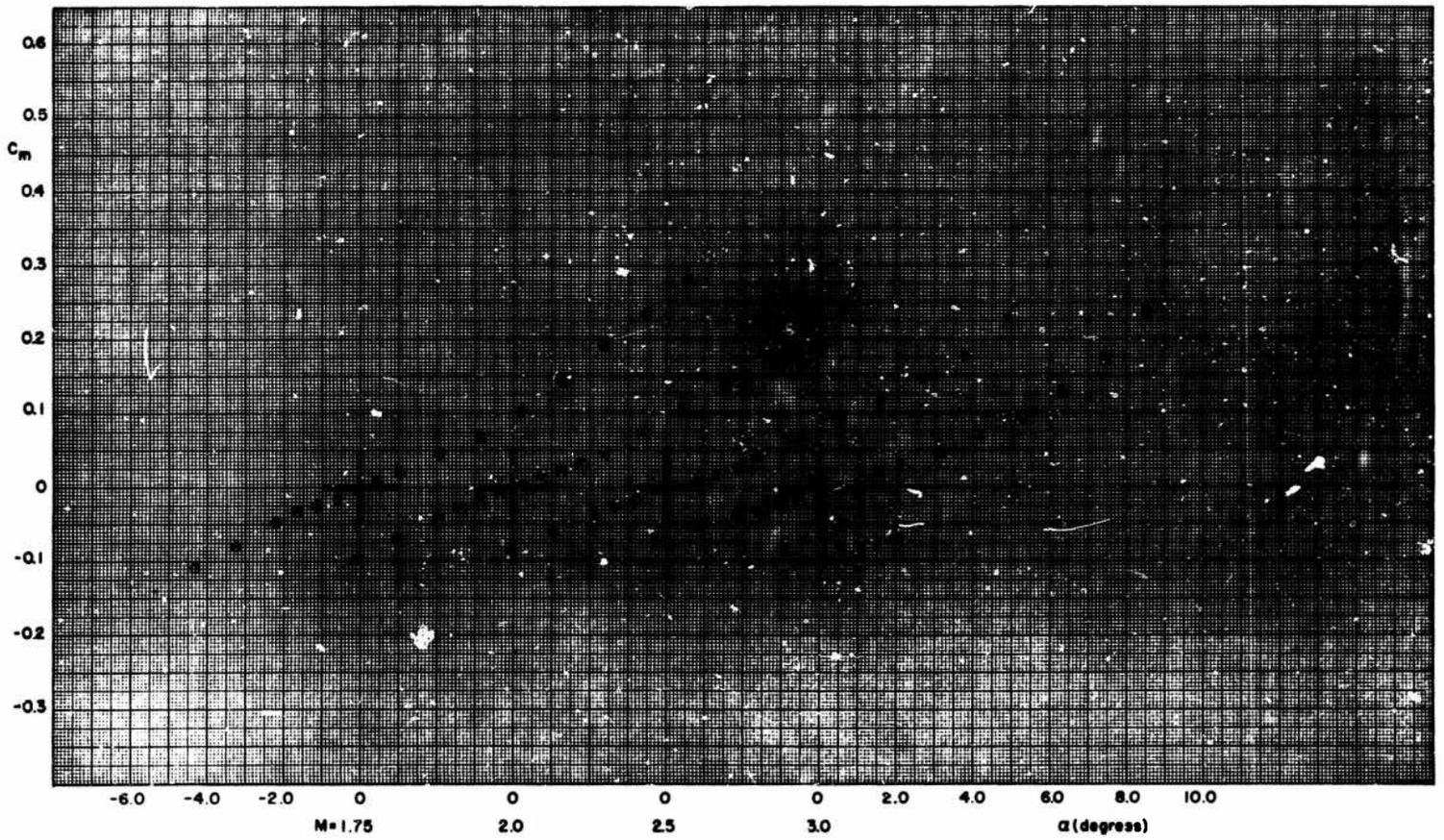

FIGURE A-7. PITCHING MOMENT VERSUS ANGLE OF ATTACK, F8.12 (Continued)

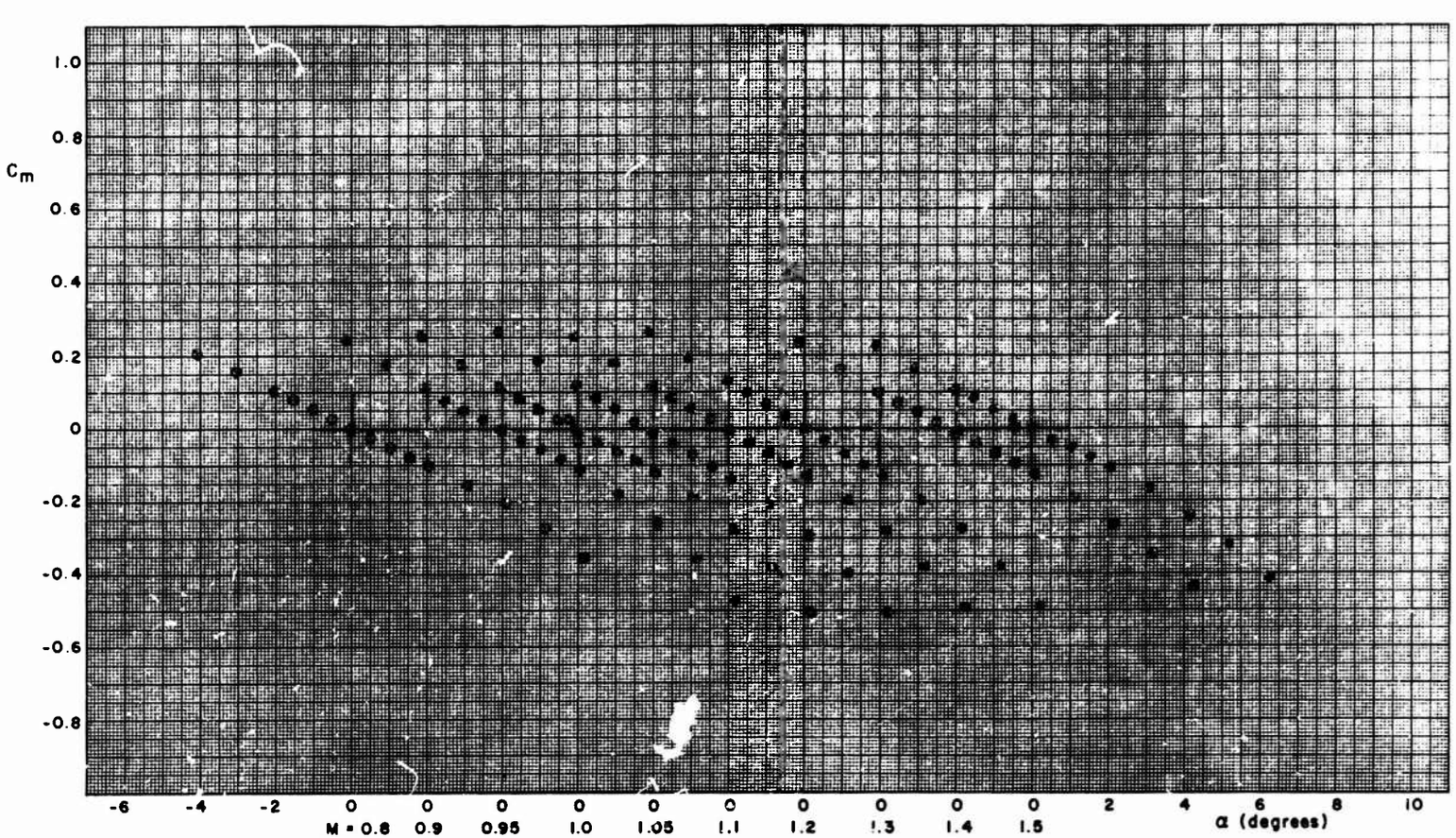

FIGURE A-7. PITCHING MOMENT VERSUS ANGLE OF ATTACK, F8.20 (Continued)

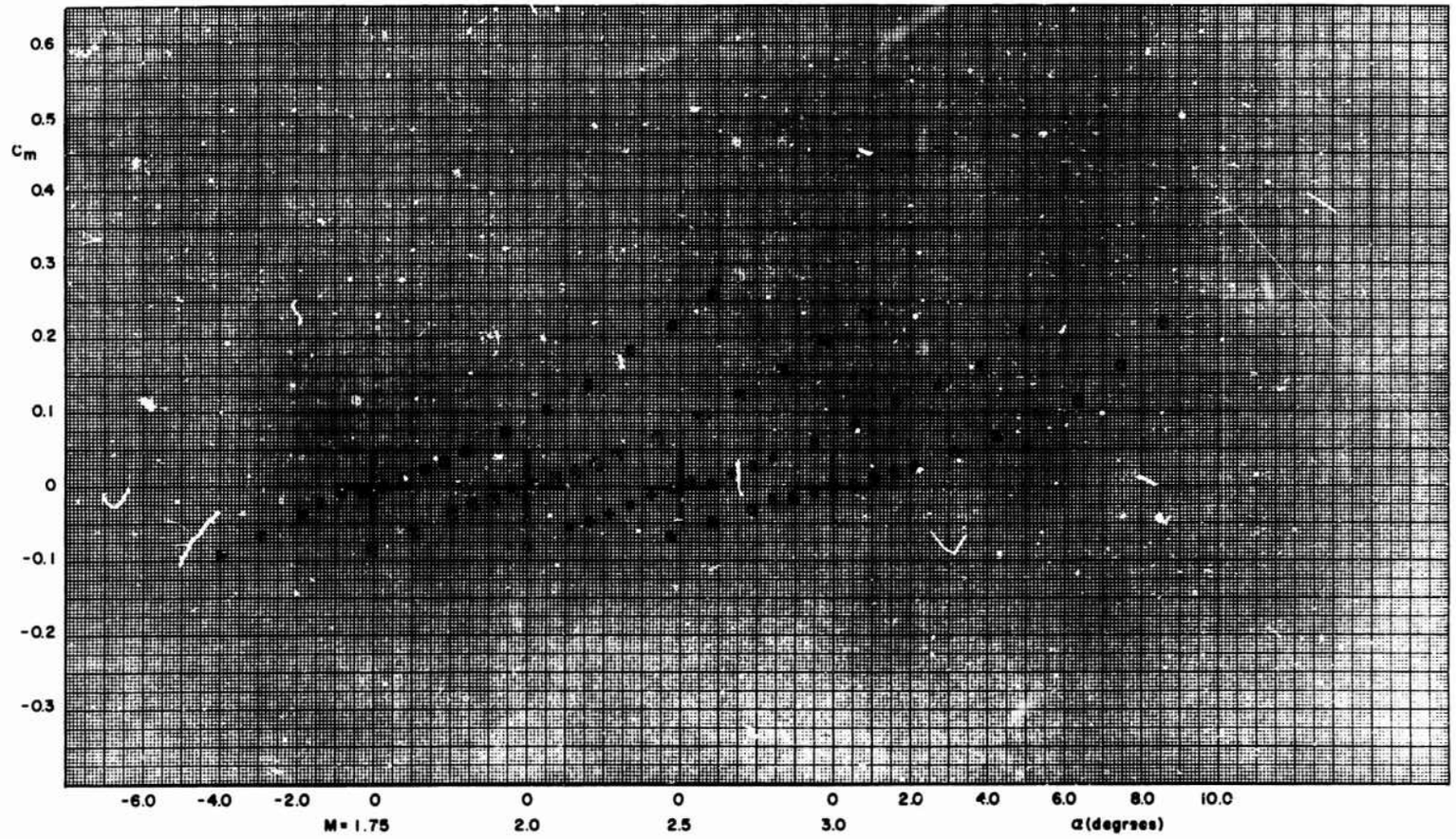

FIGURE A-7. PITCHING MOMENT VERSUS ANGLE OF ATTACK, F8.20 (Concluded)

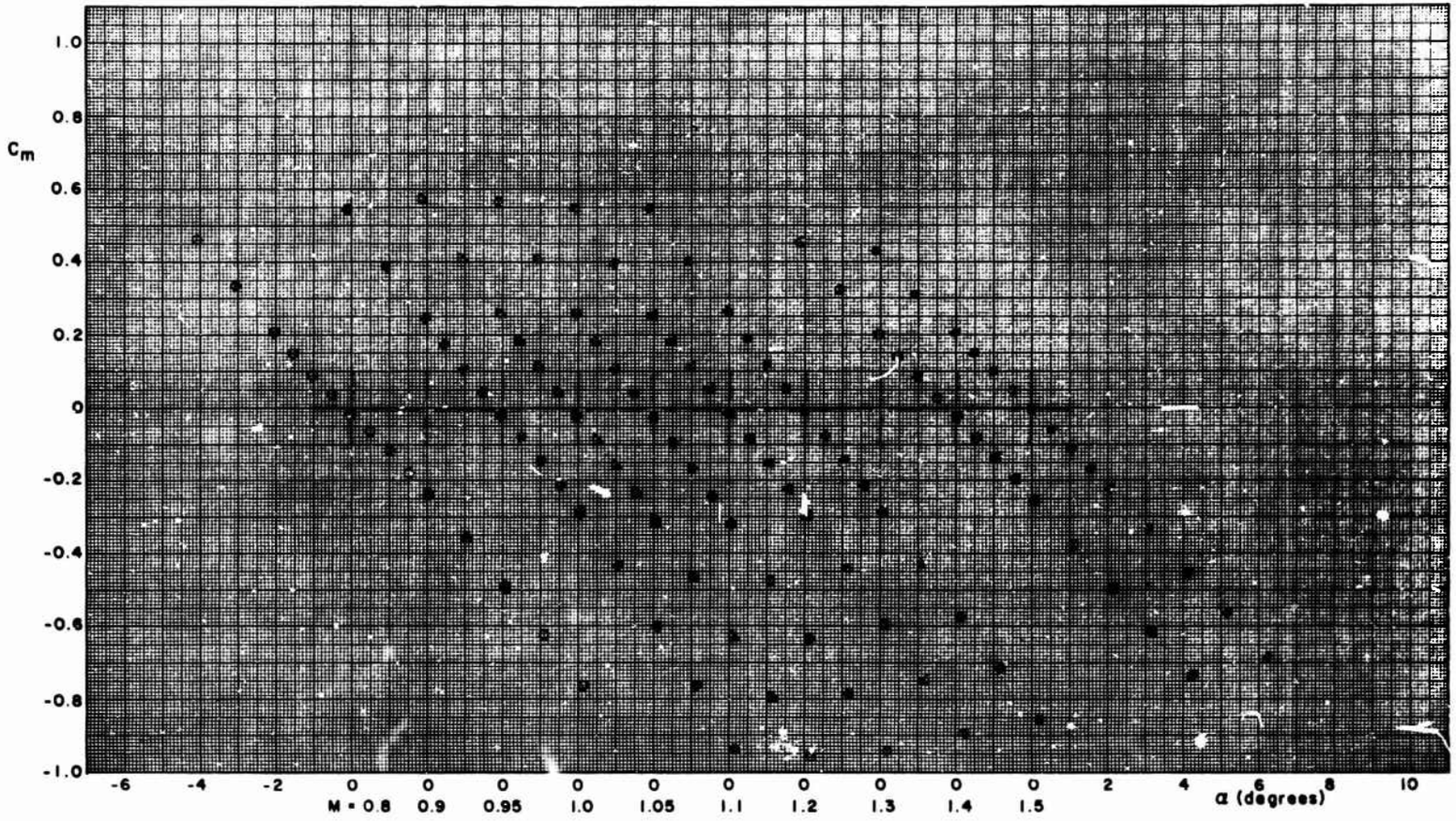

FIGURE A-8. PITCHING MOMENT VERSUS ANGLE OF ATTACK, FD. 00

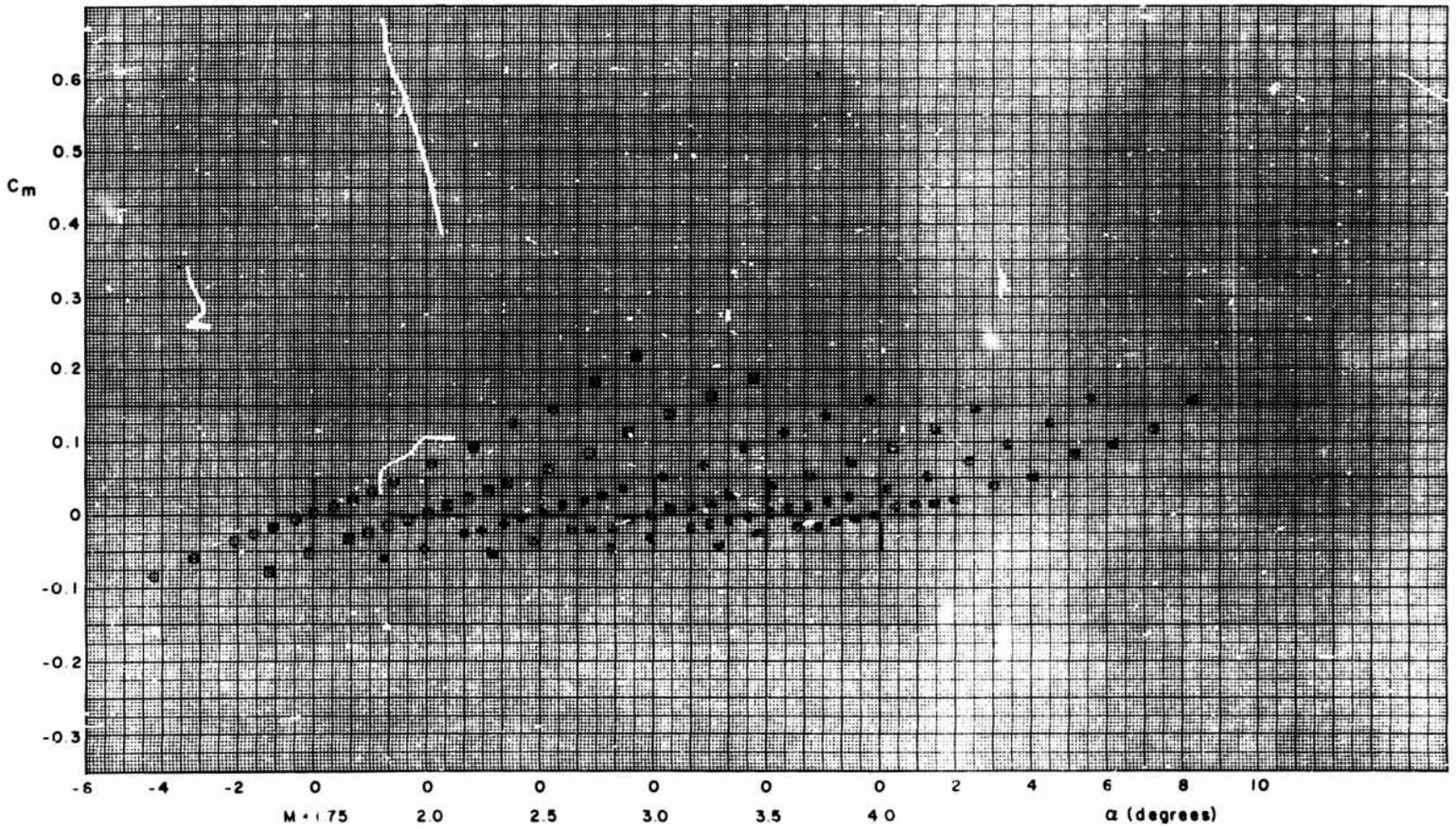

FIGURE A-8. PITCHING MOMENT VERSUS ANGLE OF ATTACK, FD. 00 (Continued)

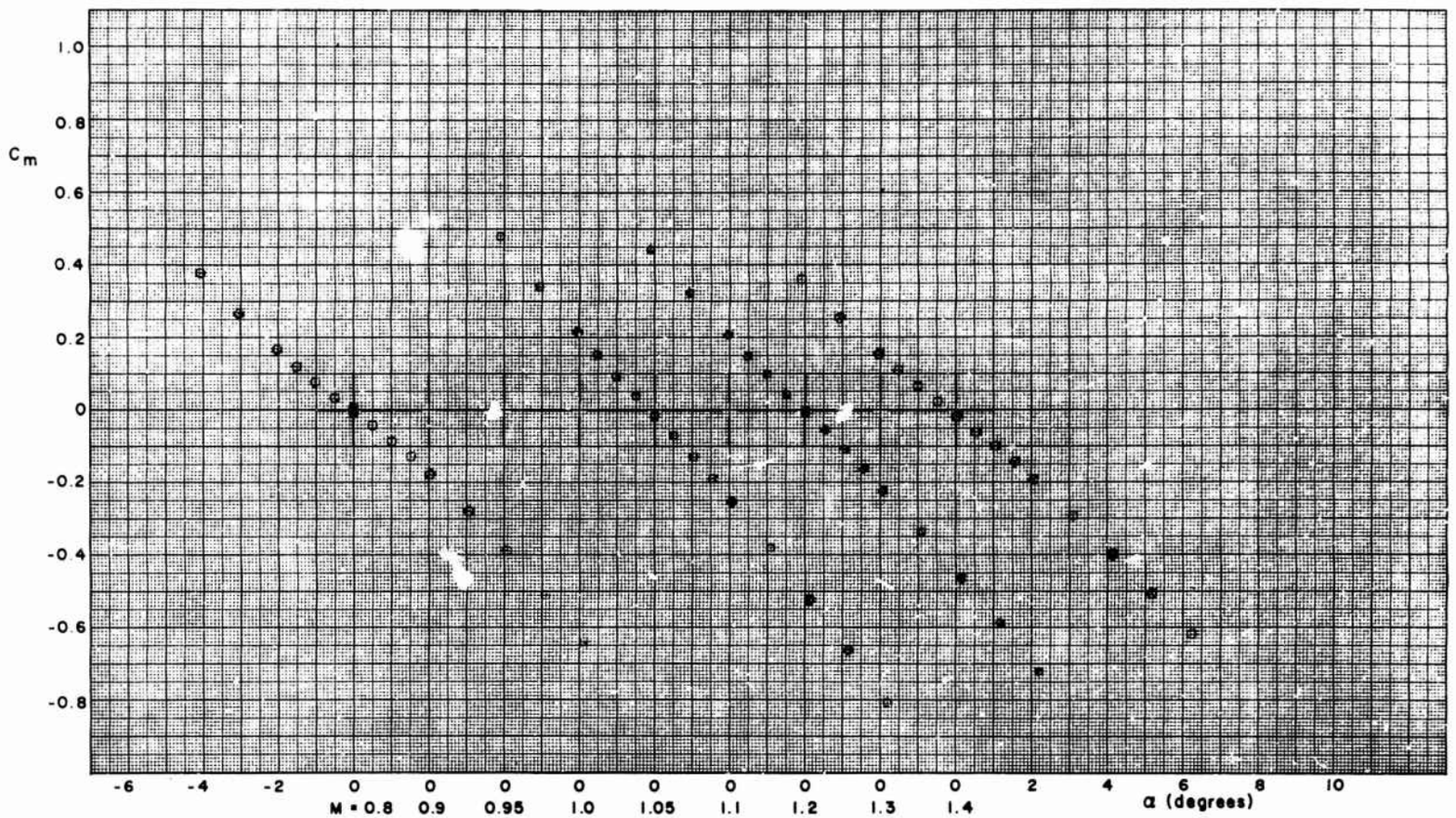

FIGURE A-8. PITCHING MOMENT VERSUS ANGLE OF ATTACK, FD. 06 (Continued)

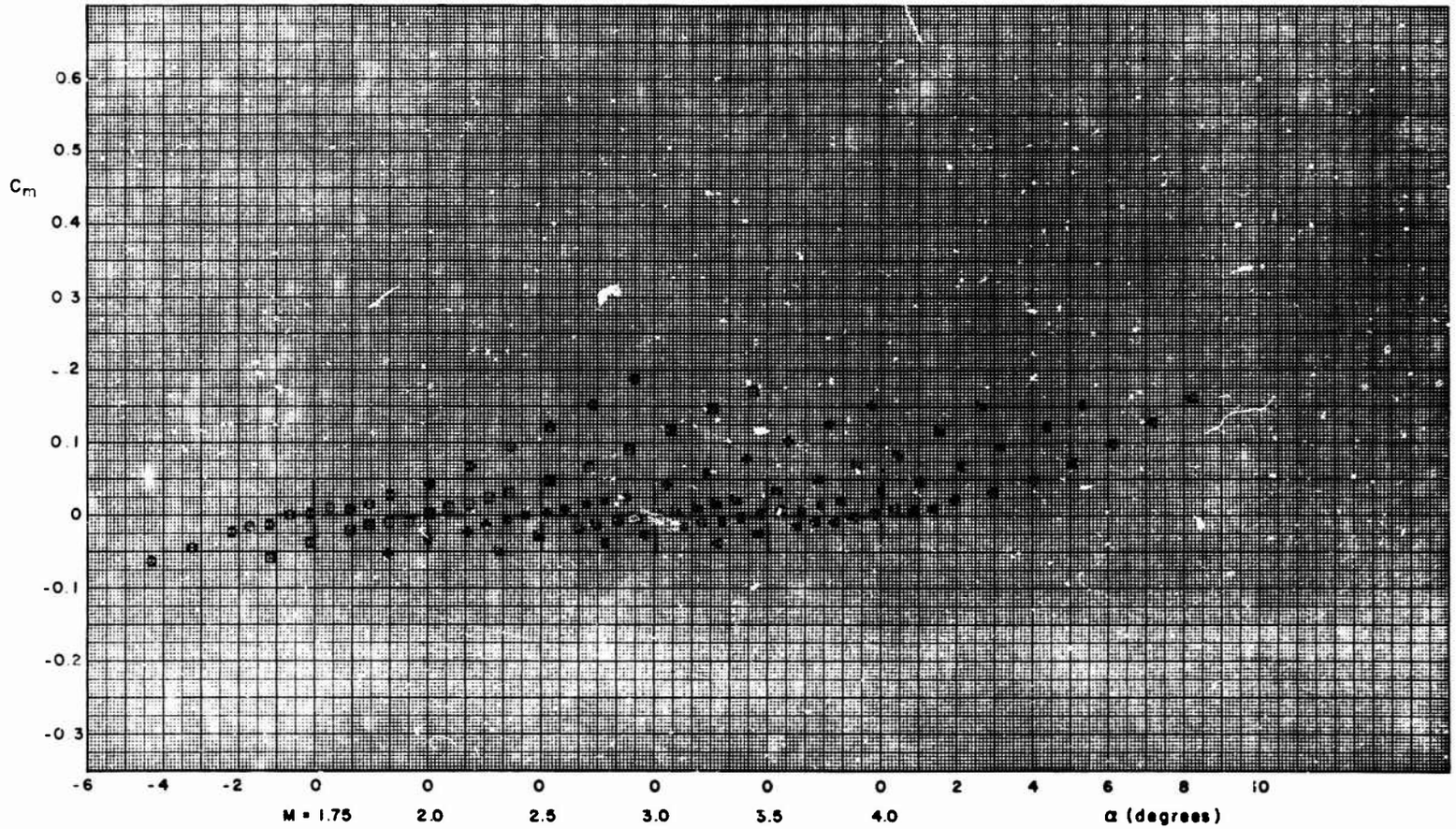

FIGURE A-8. PITCHING MOMENT VERSUS ANGLE OF ATTACK, FD. 06 (Continued)

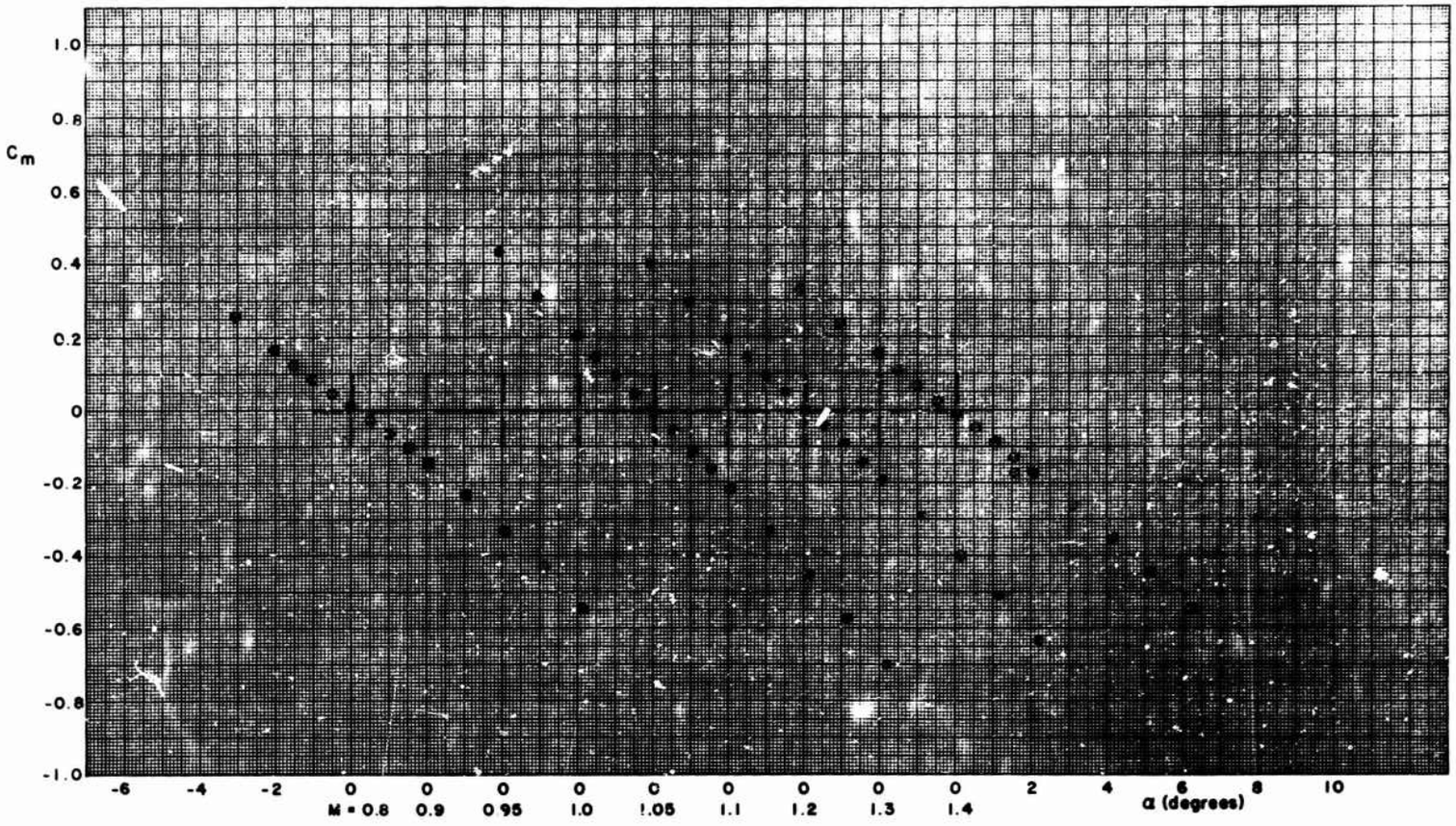

FIGURE A-8. PITCHING MOMENT VERSUS ANGLE OF ATTACK, FD. 12 (Continued)

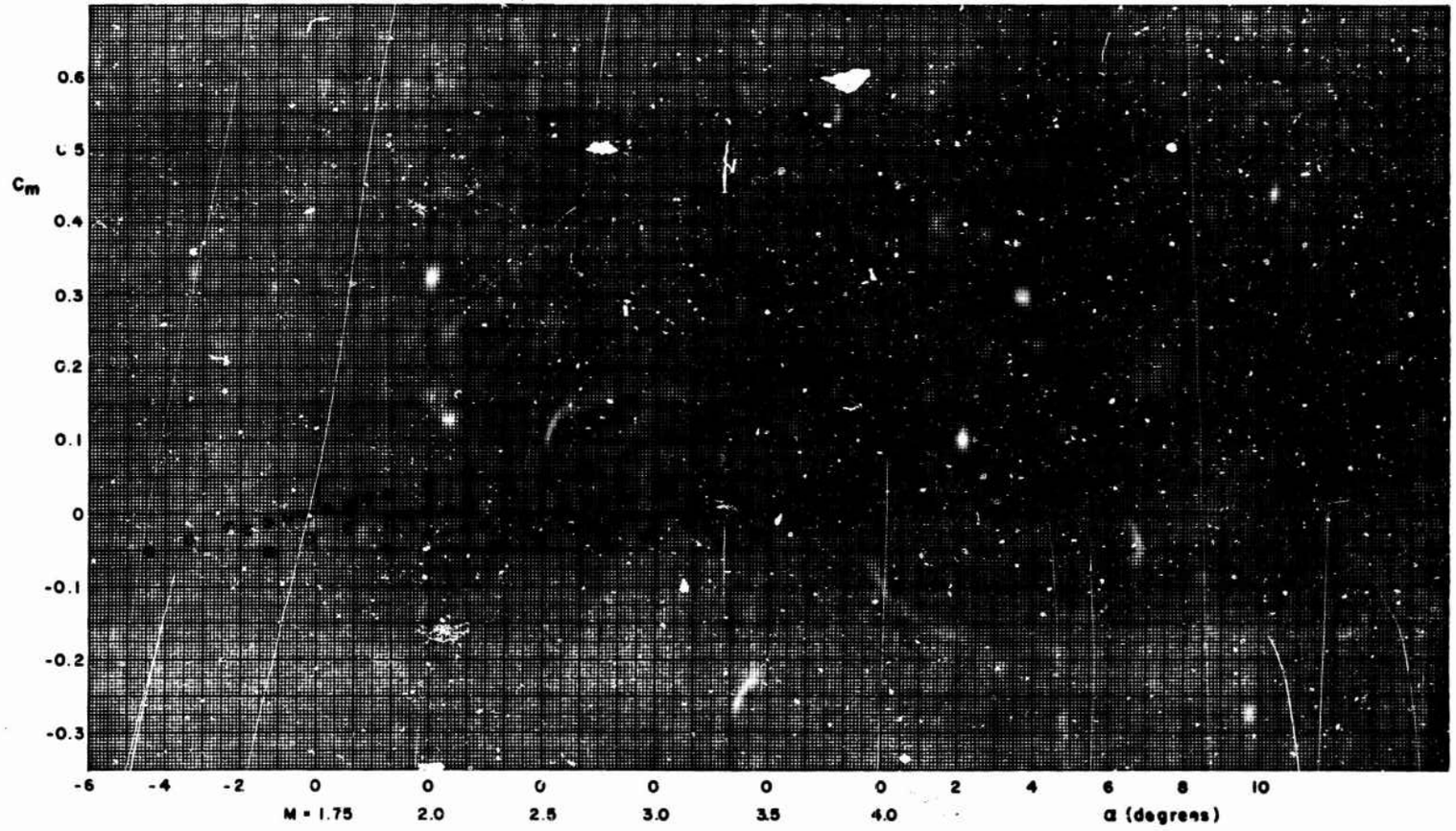

FIGURE A-8. PITCHING MOMENT VERSUS ANGLE OF ATTACK, FD. 12 (Continued)

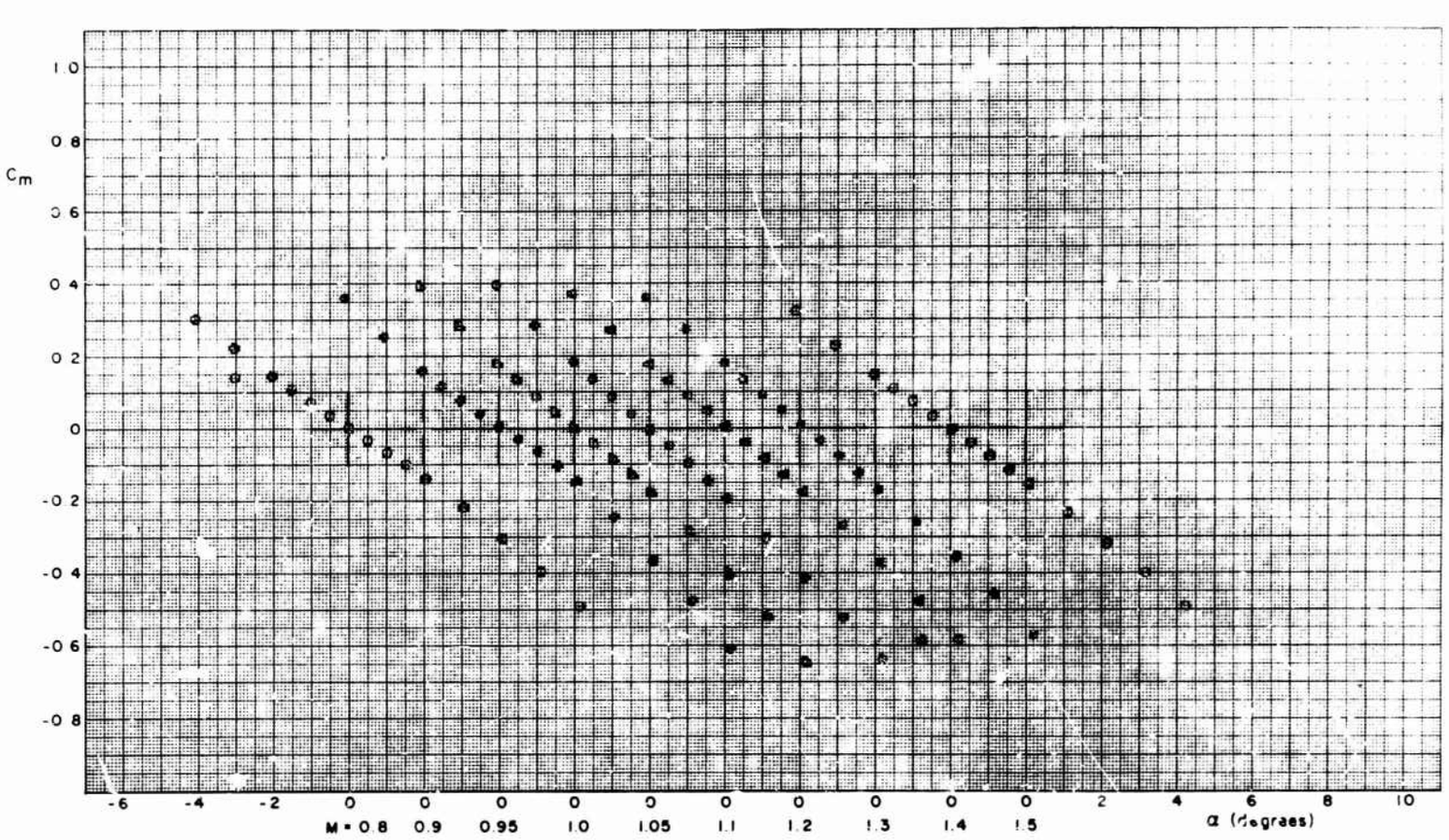

FIGURE A-8. PITCHING MOMENT VERSUS ANGLE OF ATTACK, FD. 20 (Continued)

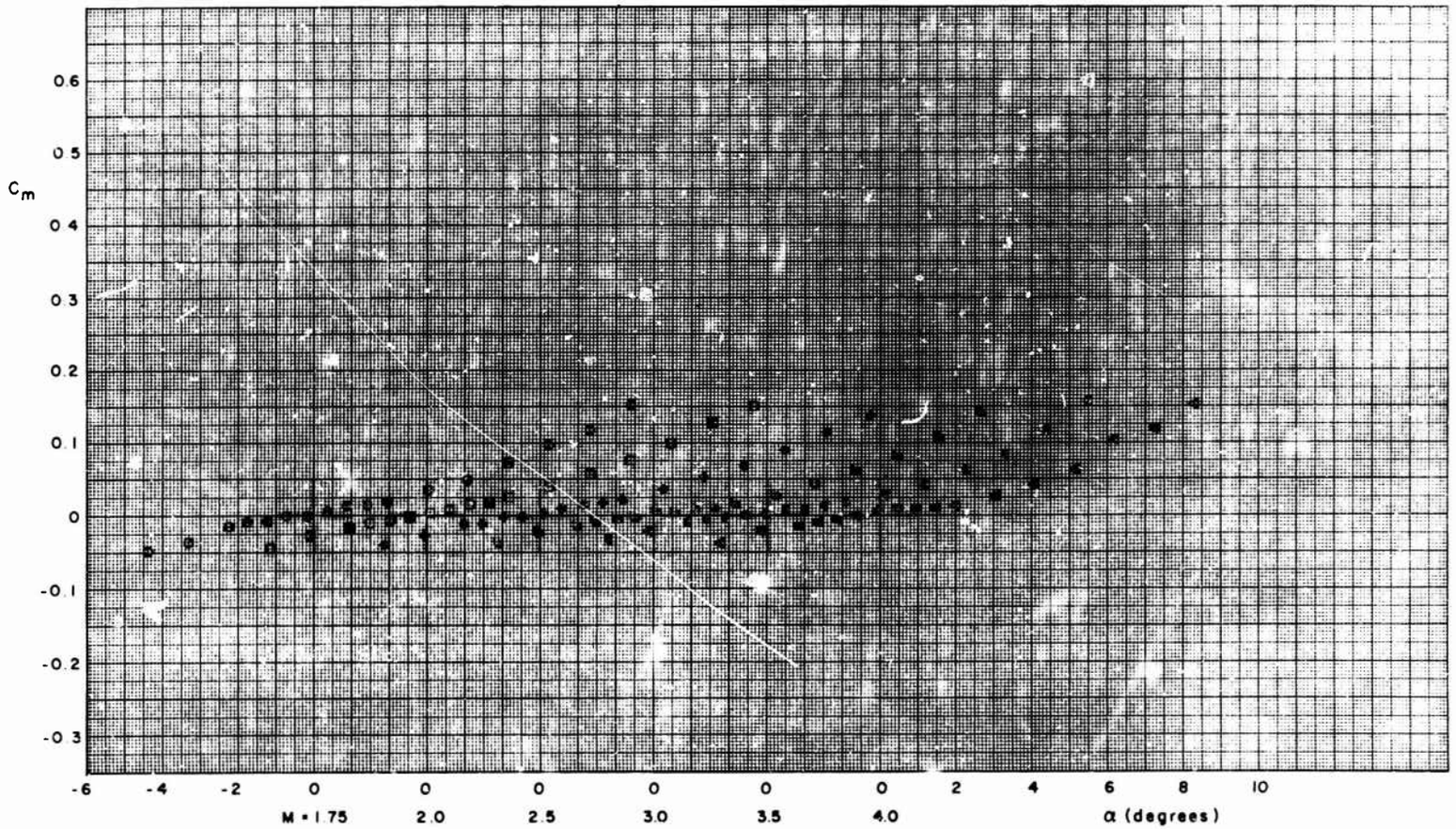

FIGURE A-8. PITCHING MOMENT VERSUS ANGLE OF ATTACK, FD. 20 (Concluded)

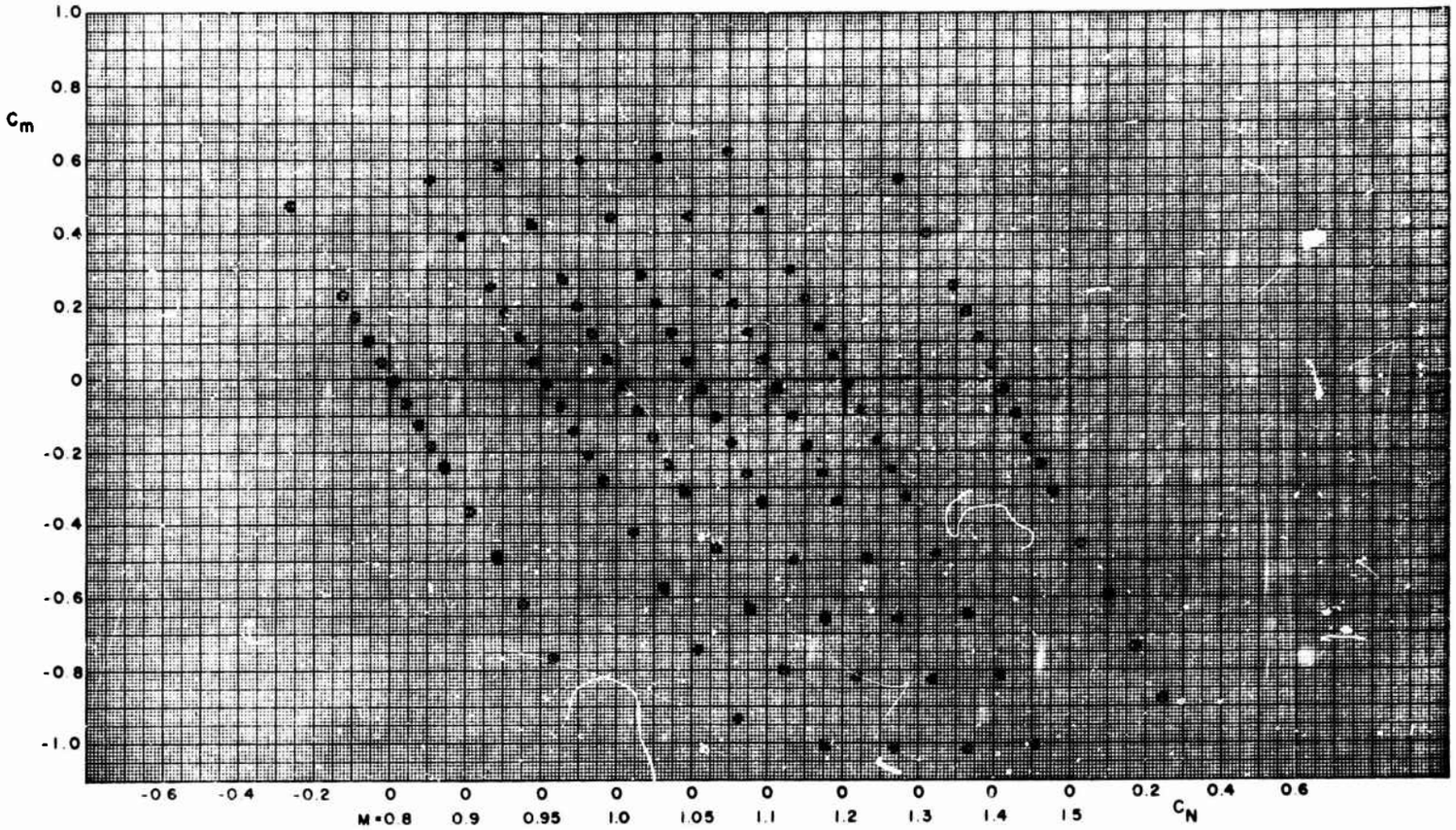

FIGURE A-9. PITCHING MOMENT VERSUS NORMAL FORCE COEFFICIENT, F4.00

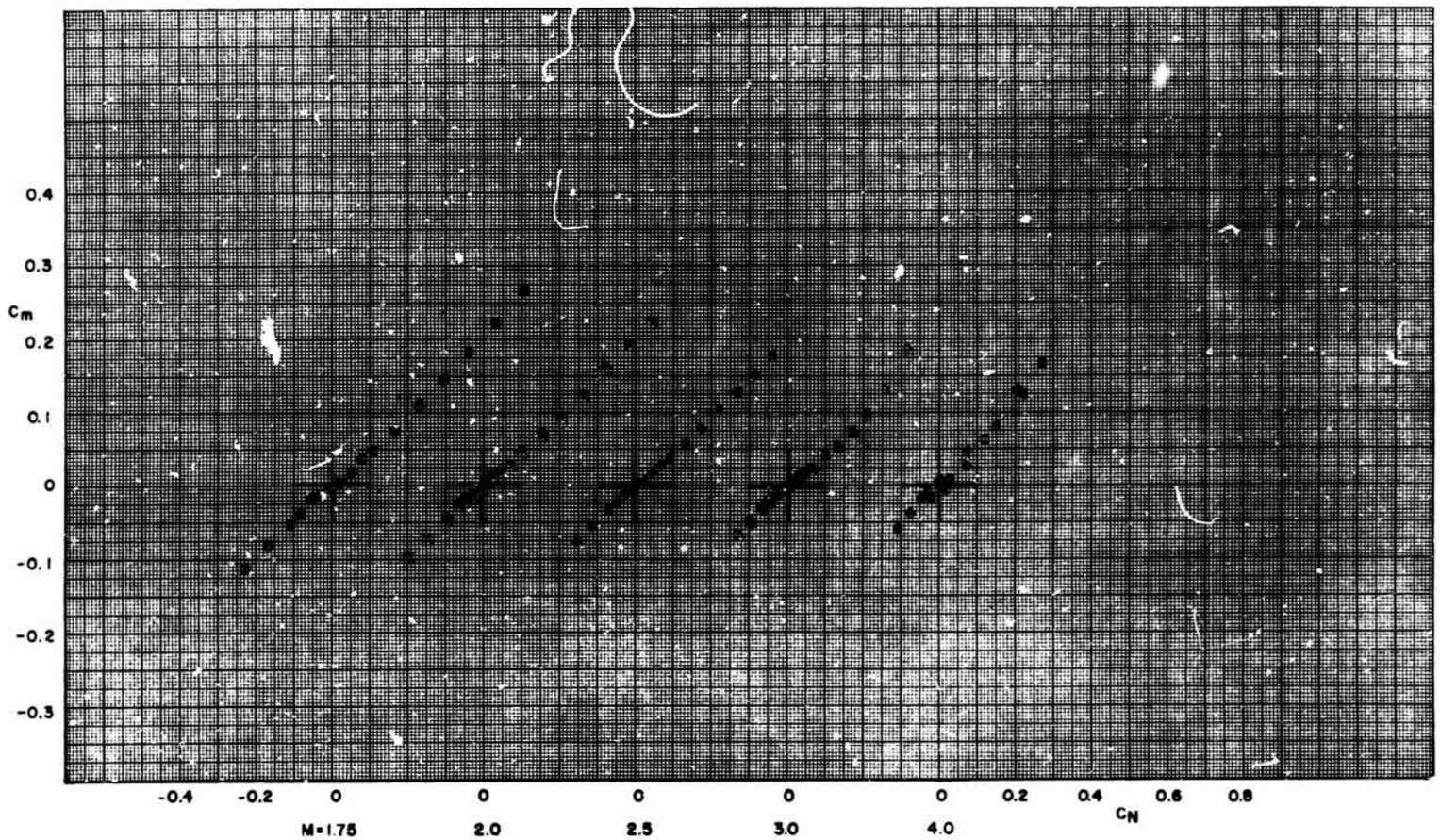

FIGURE A-9. PITCHING MOMENT VERSUS NORMAL FORCE COEFFICIENT, F4.00 (Continued)

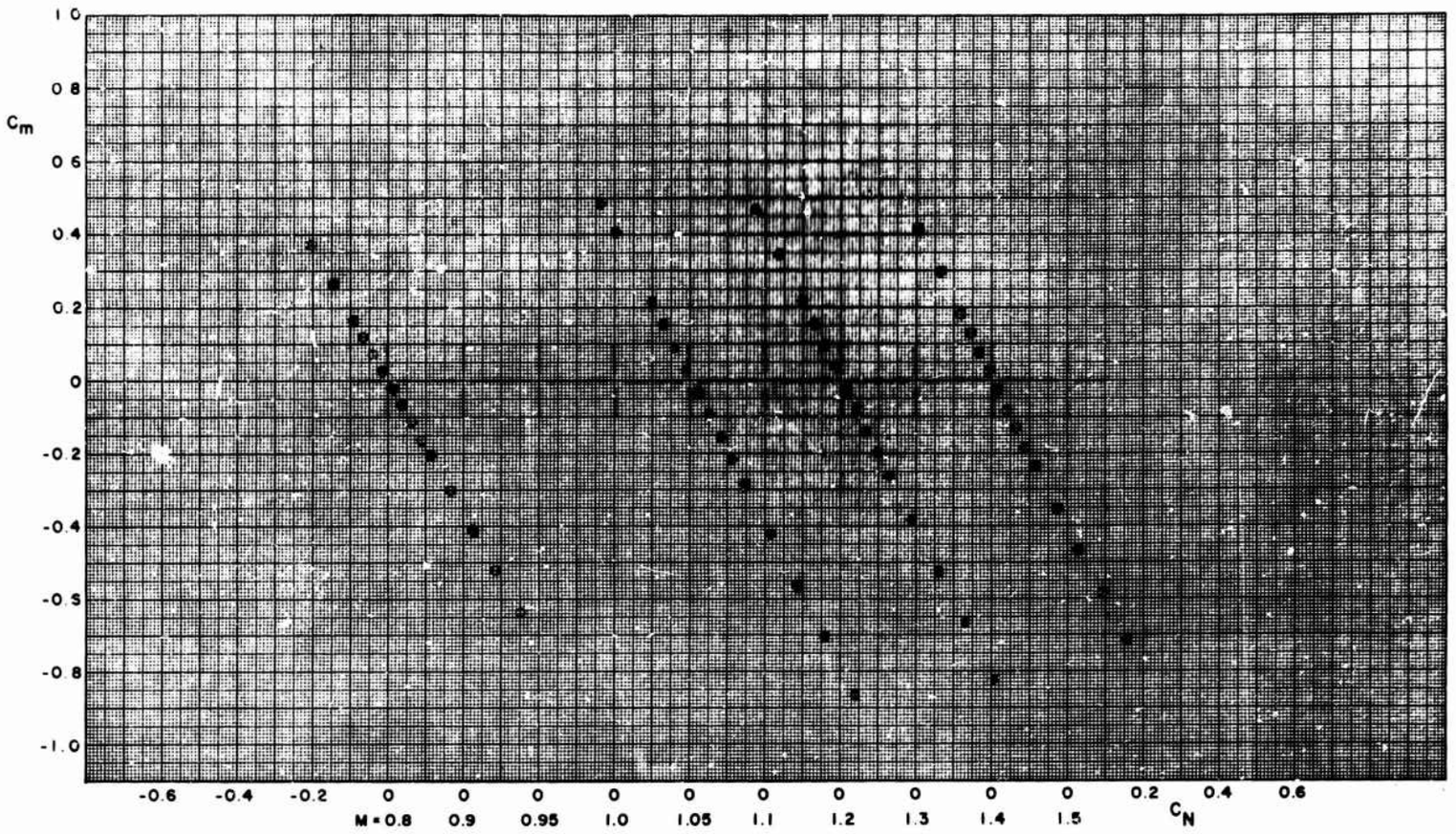

FIGURE A-9. PITCHING MOMENT VERSUS NORMAL FORCE COEFFICIENT, F4.08 (Continued)

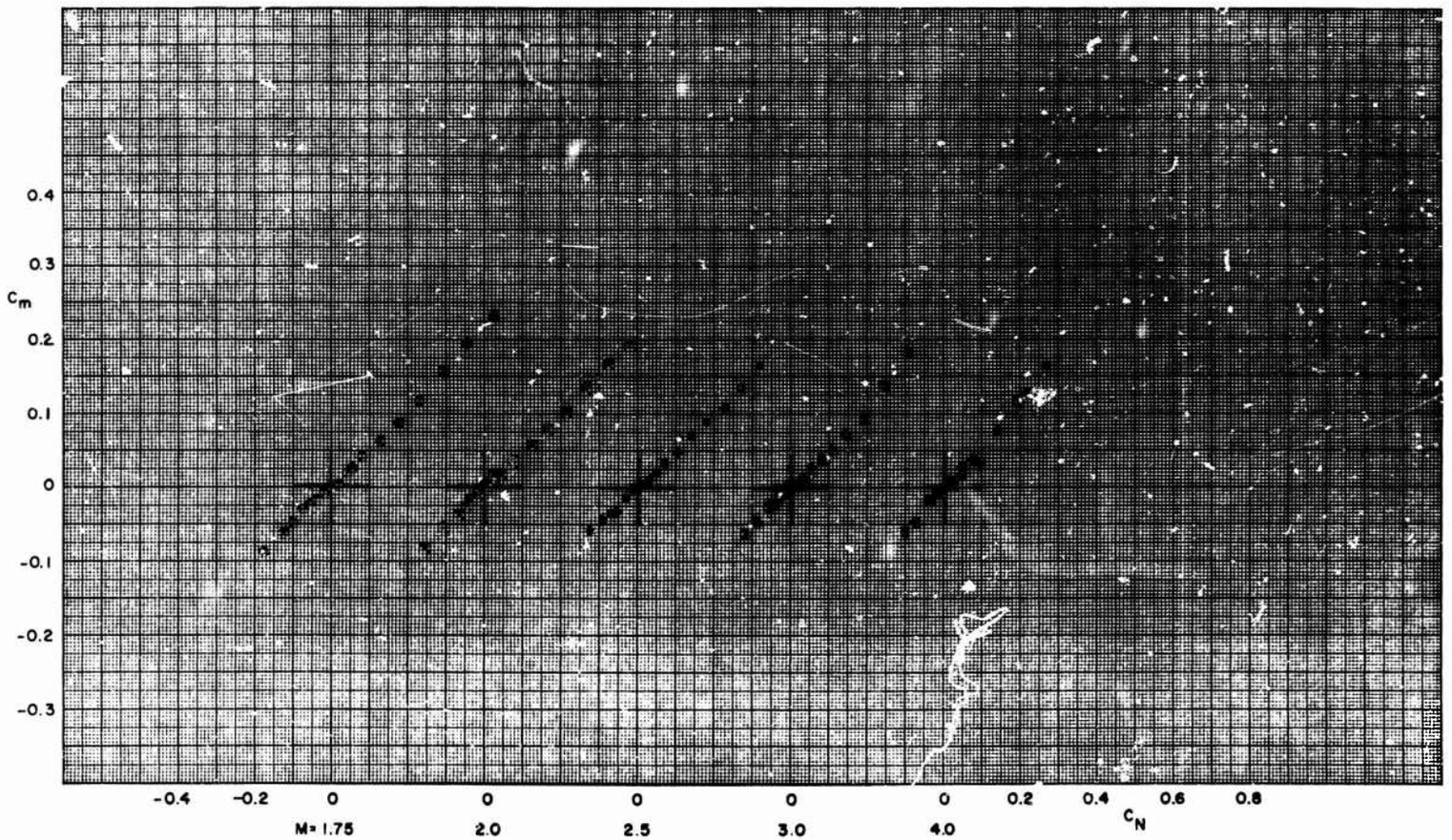

FIGURE A-9. PITCHING MOMENT VERSUS NORMAL FORCE COEFFICIENT, F4.08 (Continued)

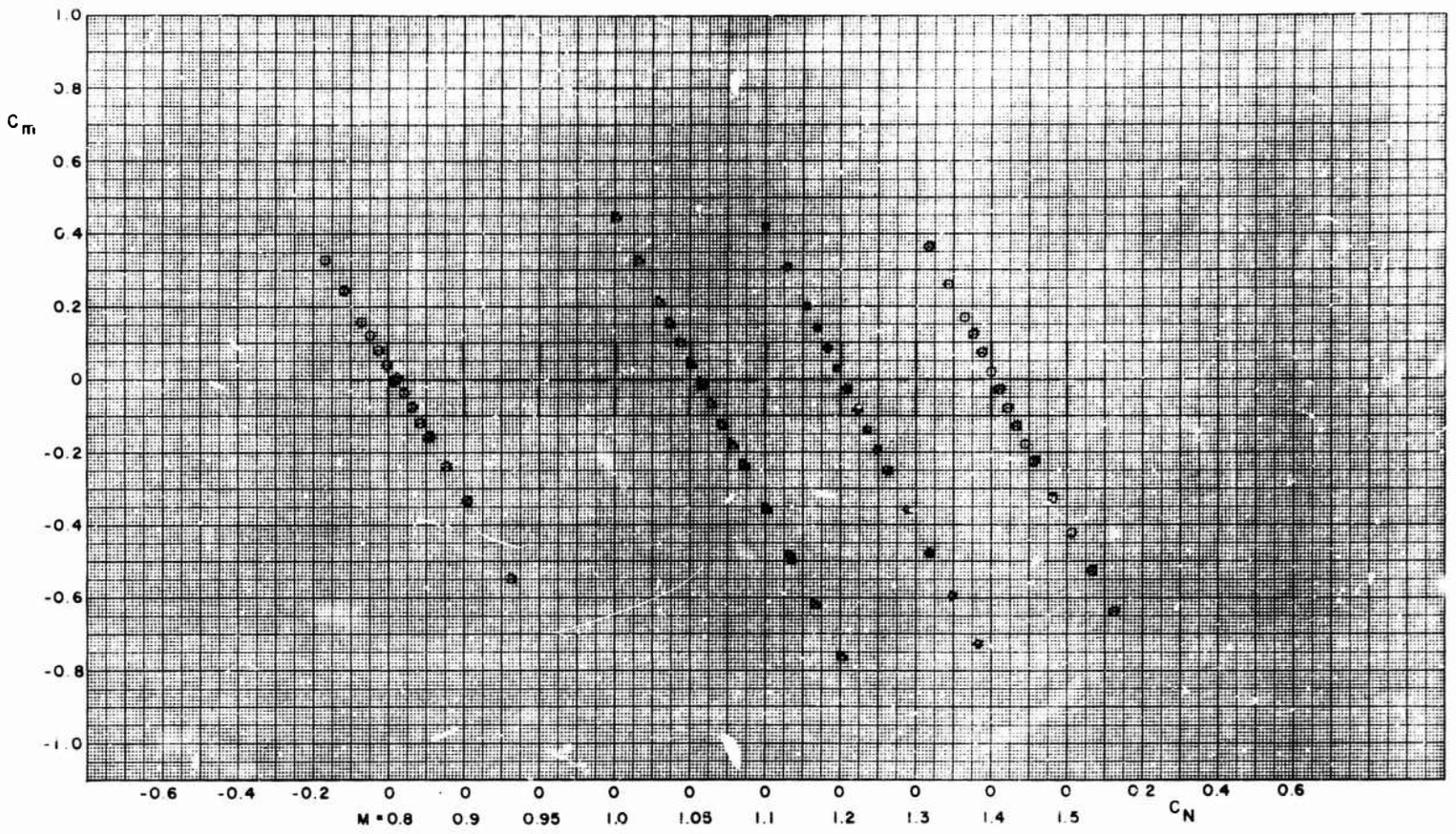

FIGURE A-9. PITCHING MOMENT VERSUS NORMAL FORCE COEFFICIENT, F4.16 (Continued)

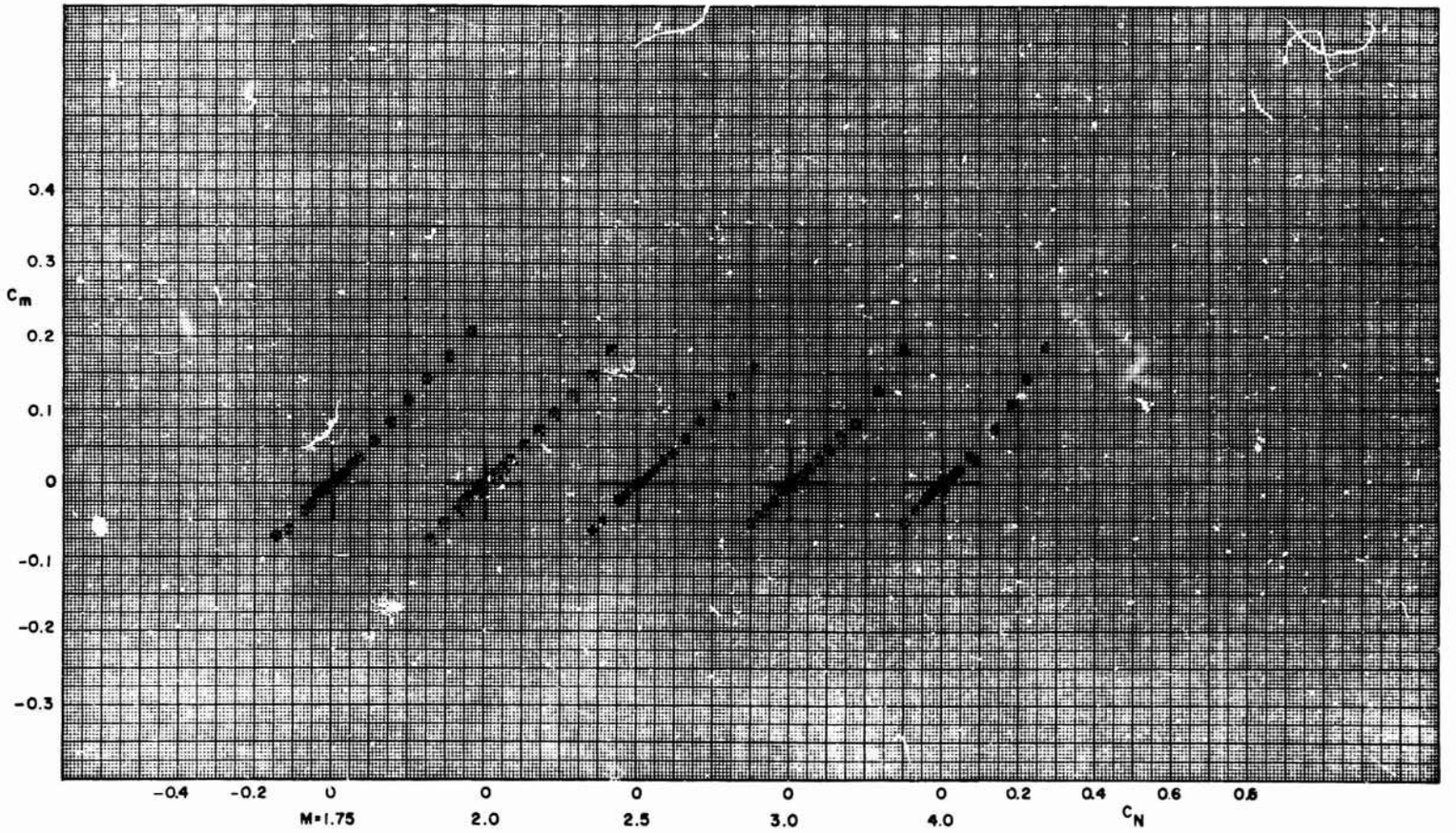

FIGURE A-9. PITCHING MOMENT VERSUS NORMAL FORCE COEFFICIENT, F4.16 (Continued)

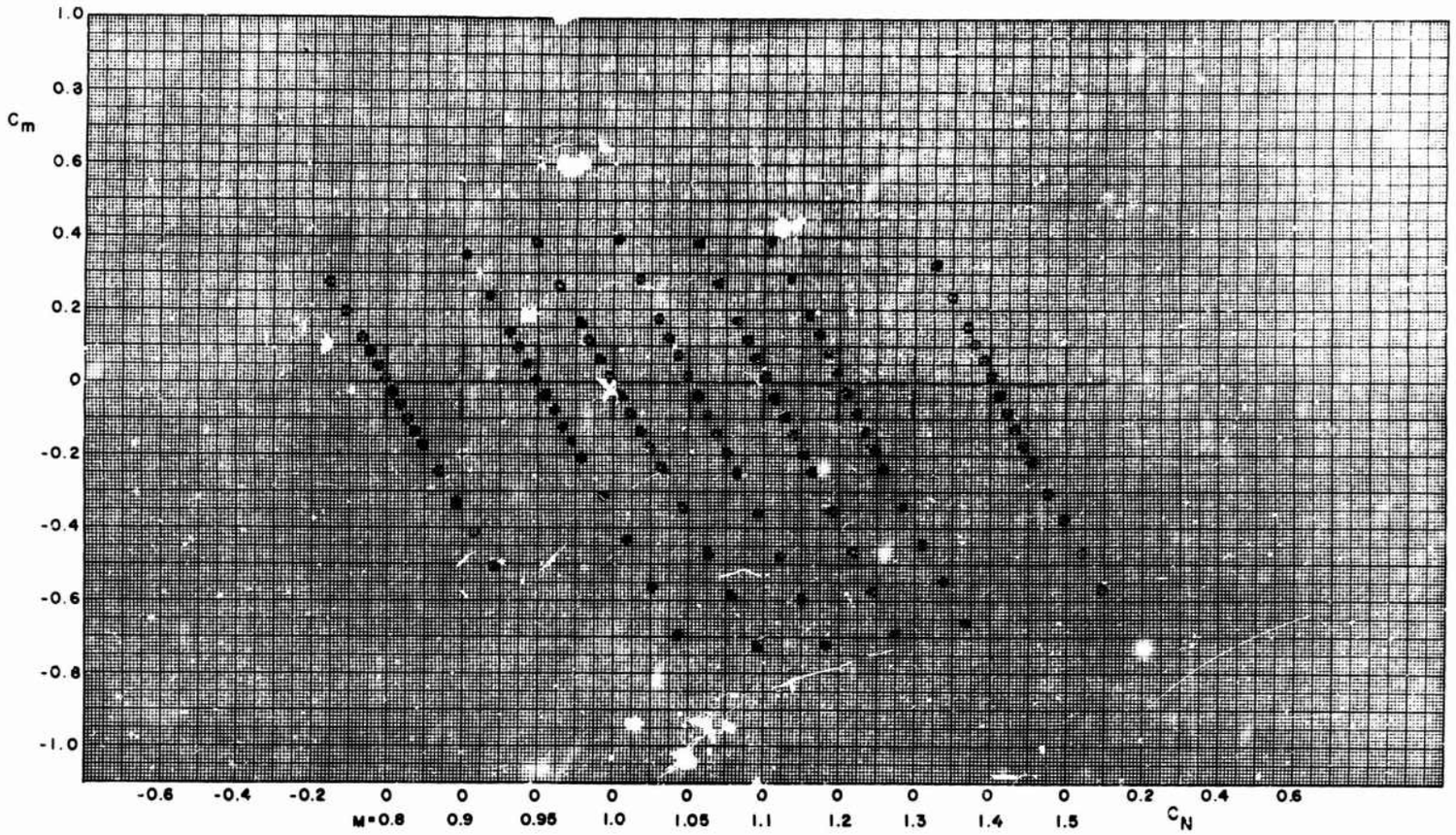

FIGURE A-9. PITCHING MOMENT VERSUS NORMAL FORCE COEFFICIENT, F4.25 (Continued)

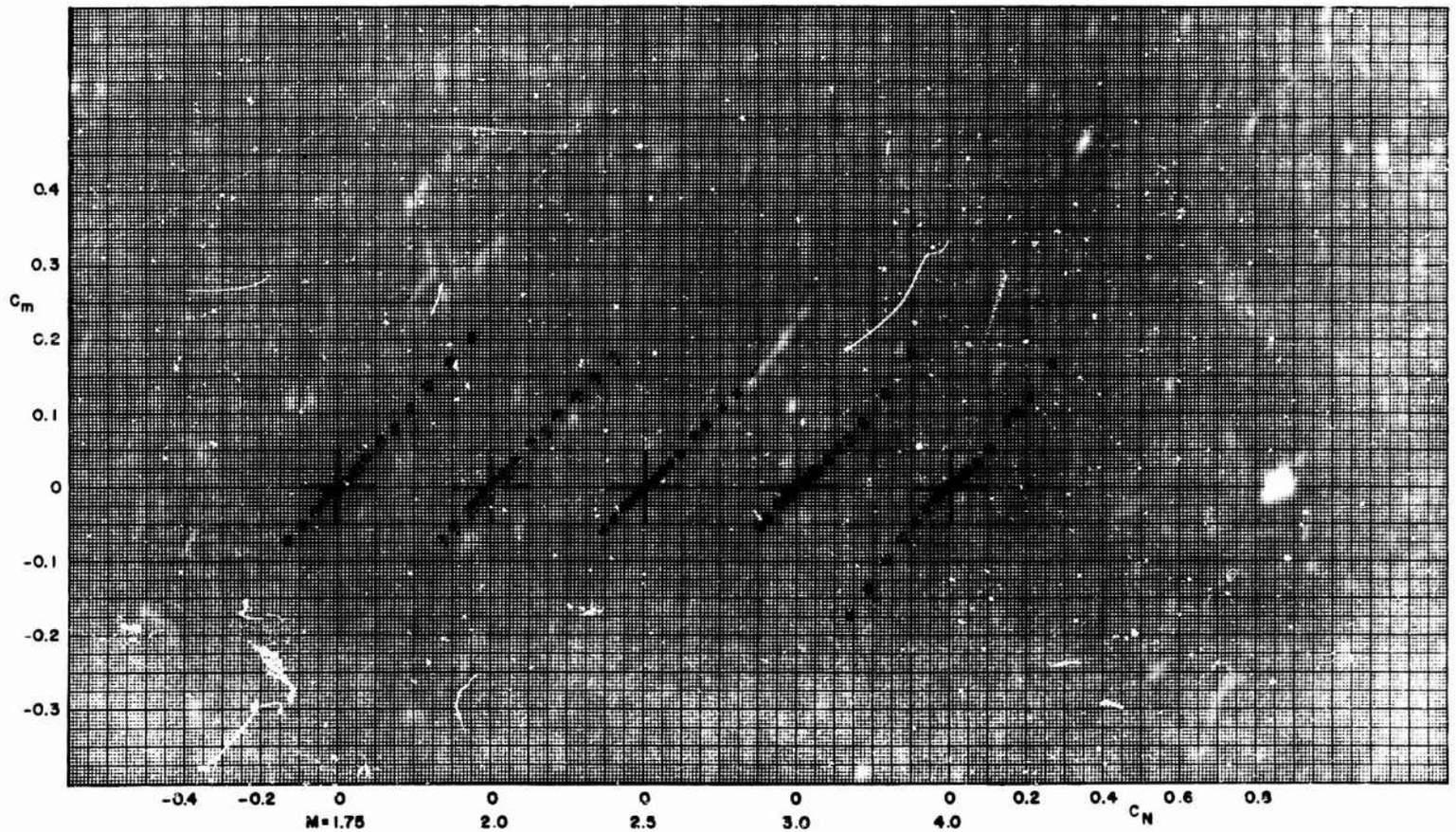

FIGURE A-9. PITCHING MOMENT VERSUS NORMAL FORCE COEFFICIENT, F4. (Concluded)

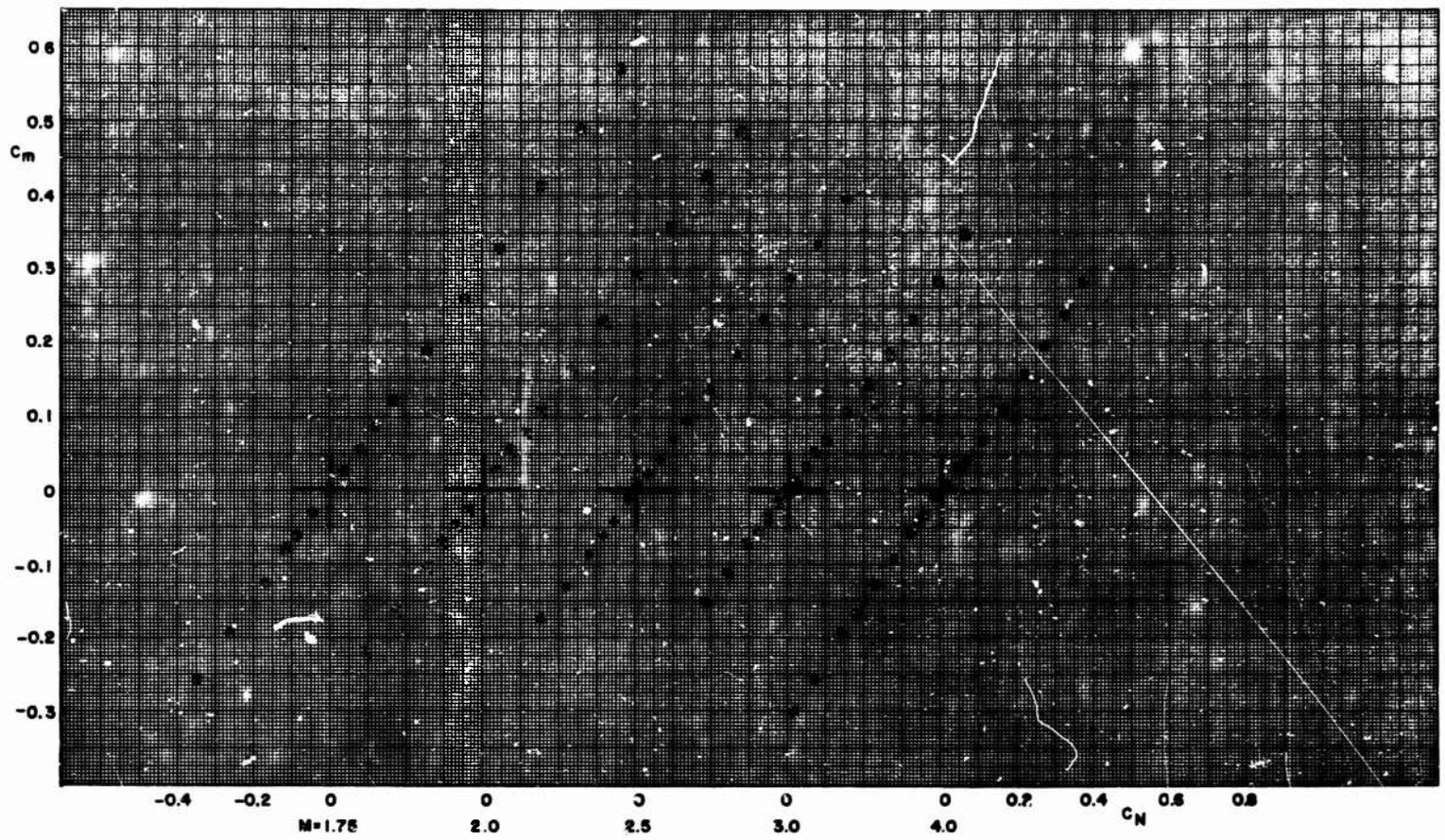

FIGURE A-10. PITCHING MOMENT VERSUS NORMAL FORCE COEFFICIENT, F7.00

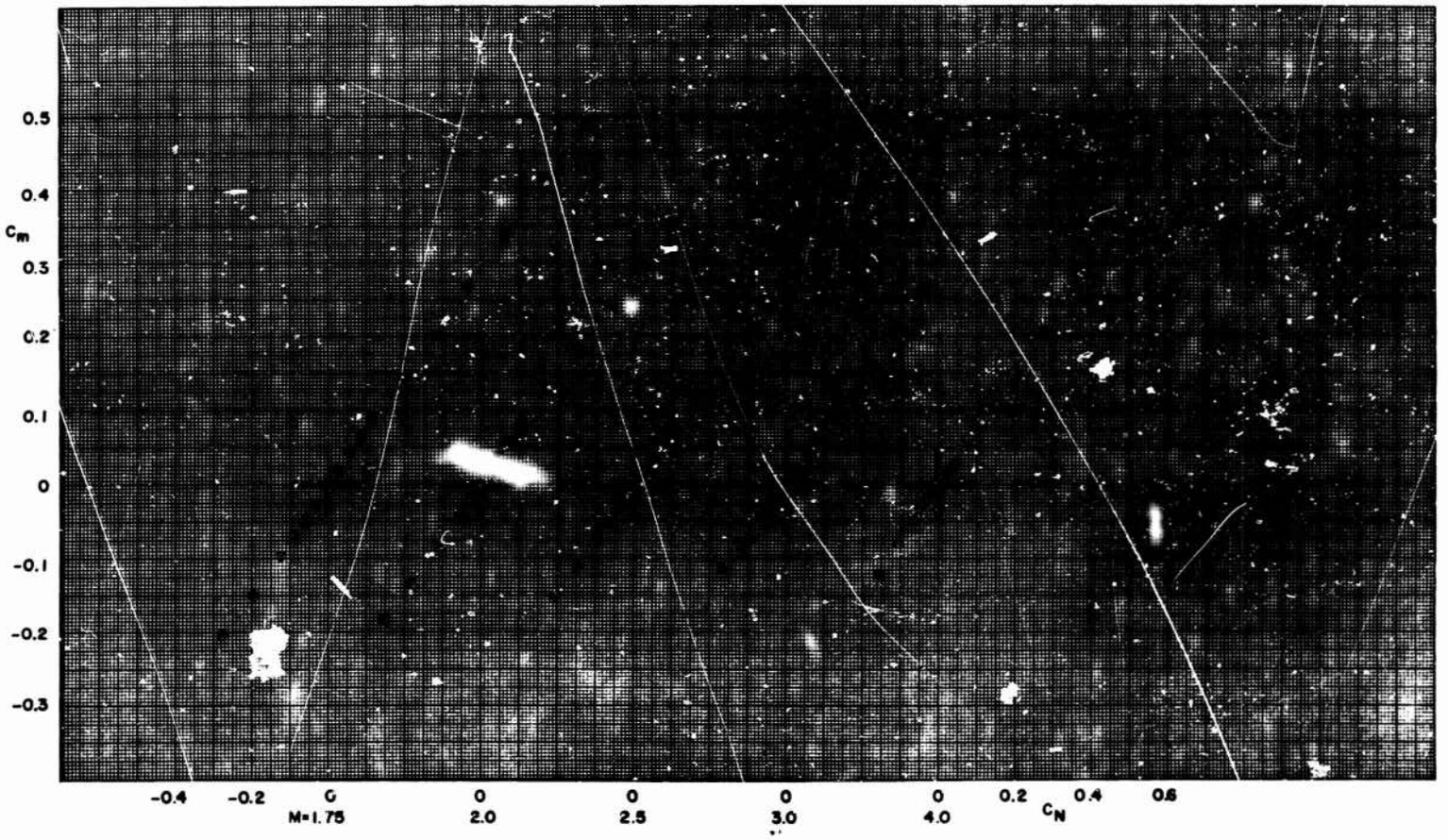

FIGURE A-10. PITCHING MOMENT VERSUS NORMAL FORCE COEFFICIENT, F7.06 (Continued)

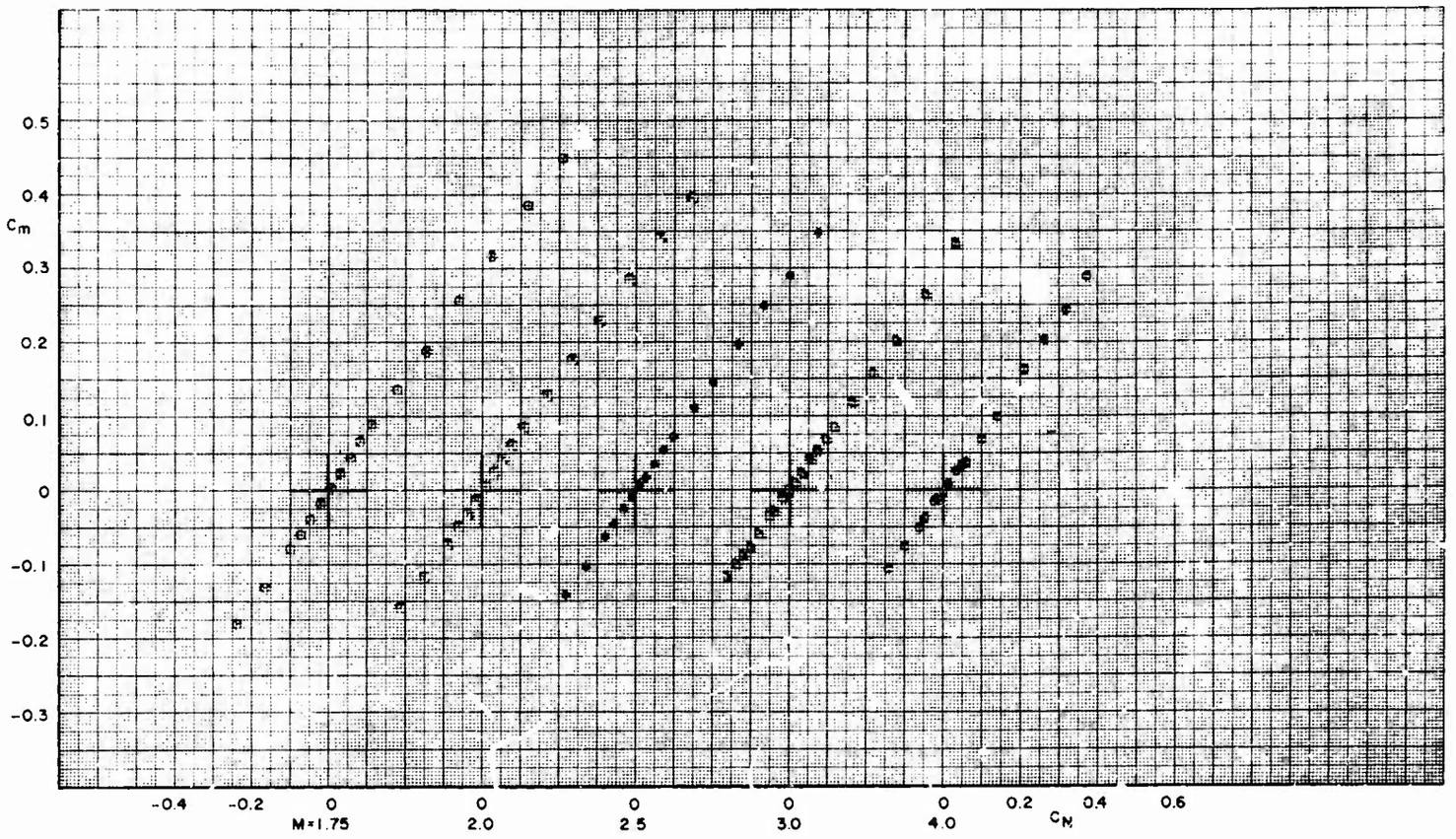

FIGURE A-10. PITCHING MOMENT VERSUS NORMAL FORCE COEFFICIENT, F7.12 (Continued)

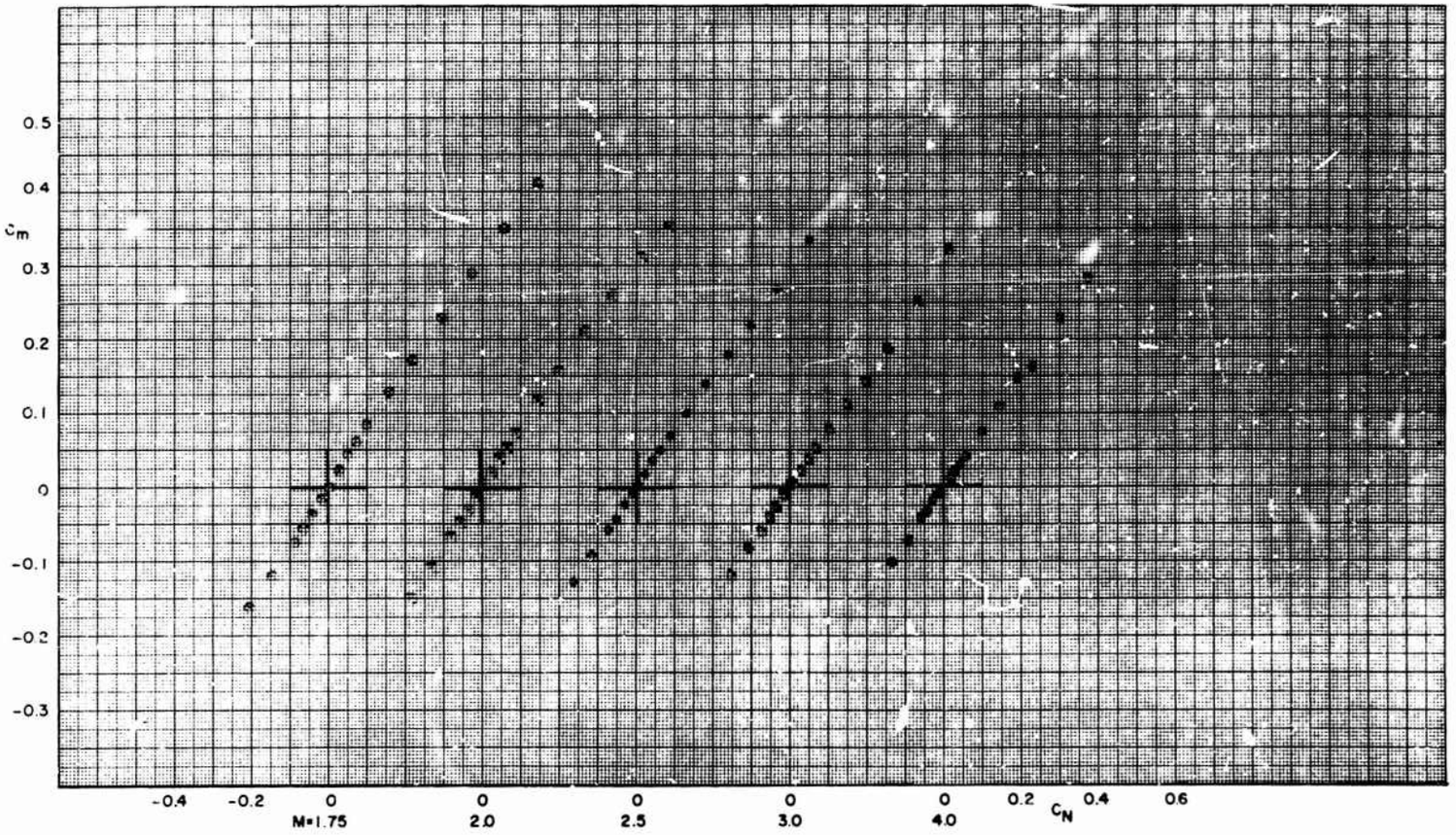

FIGURE A-10. PITCHING MOMENT VERSUS NORMAL FORCE COEFFICIENT, F7.20 (Concluded)

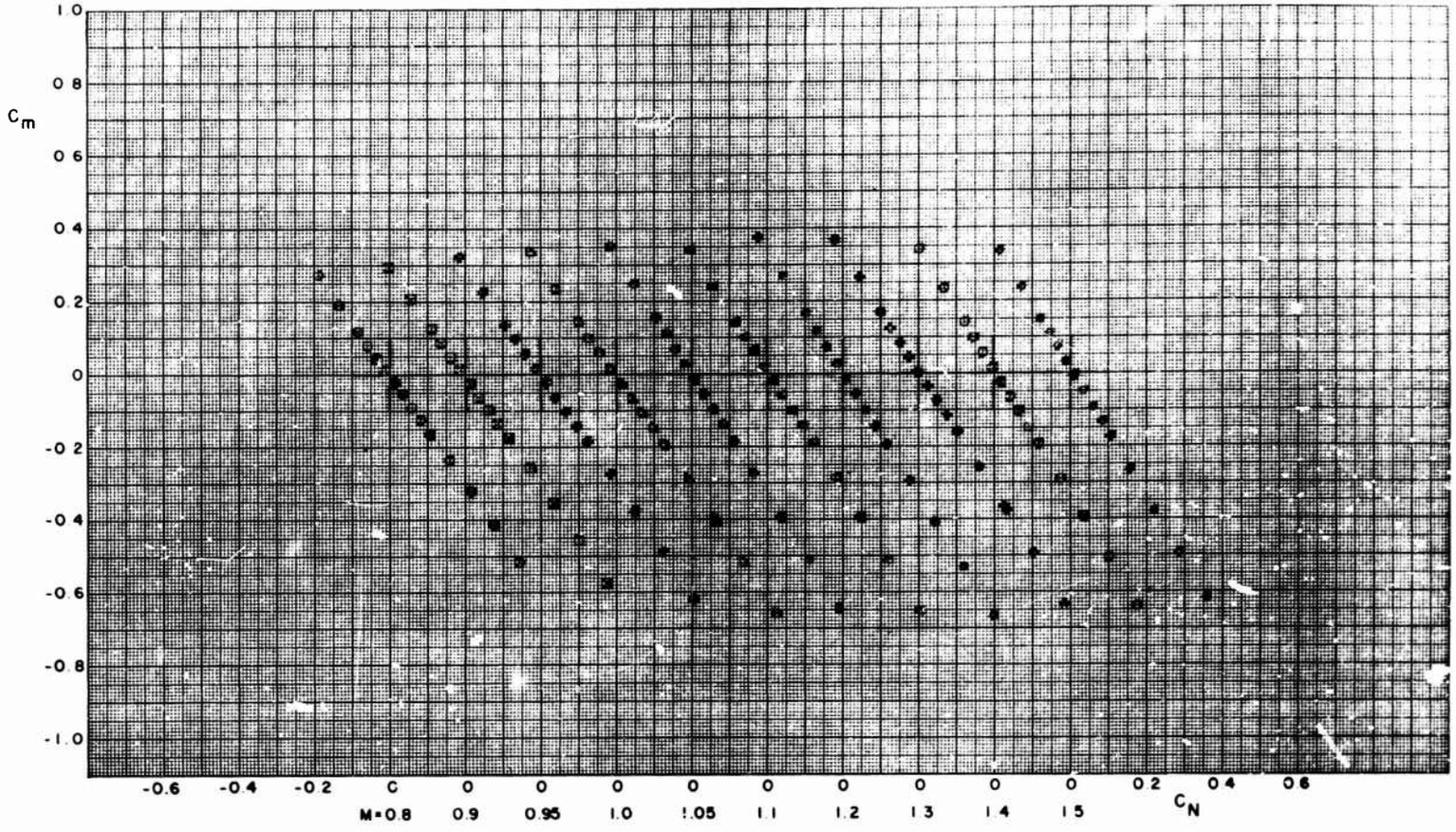

FIGURE A-11. PITCHING MOMENT VERSUS NORMAL FORCE COEFFICIENT, F8.00

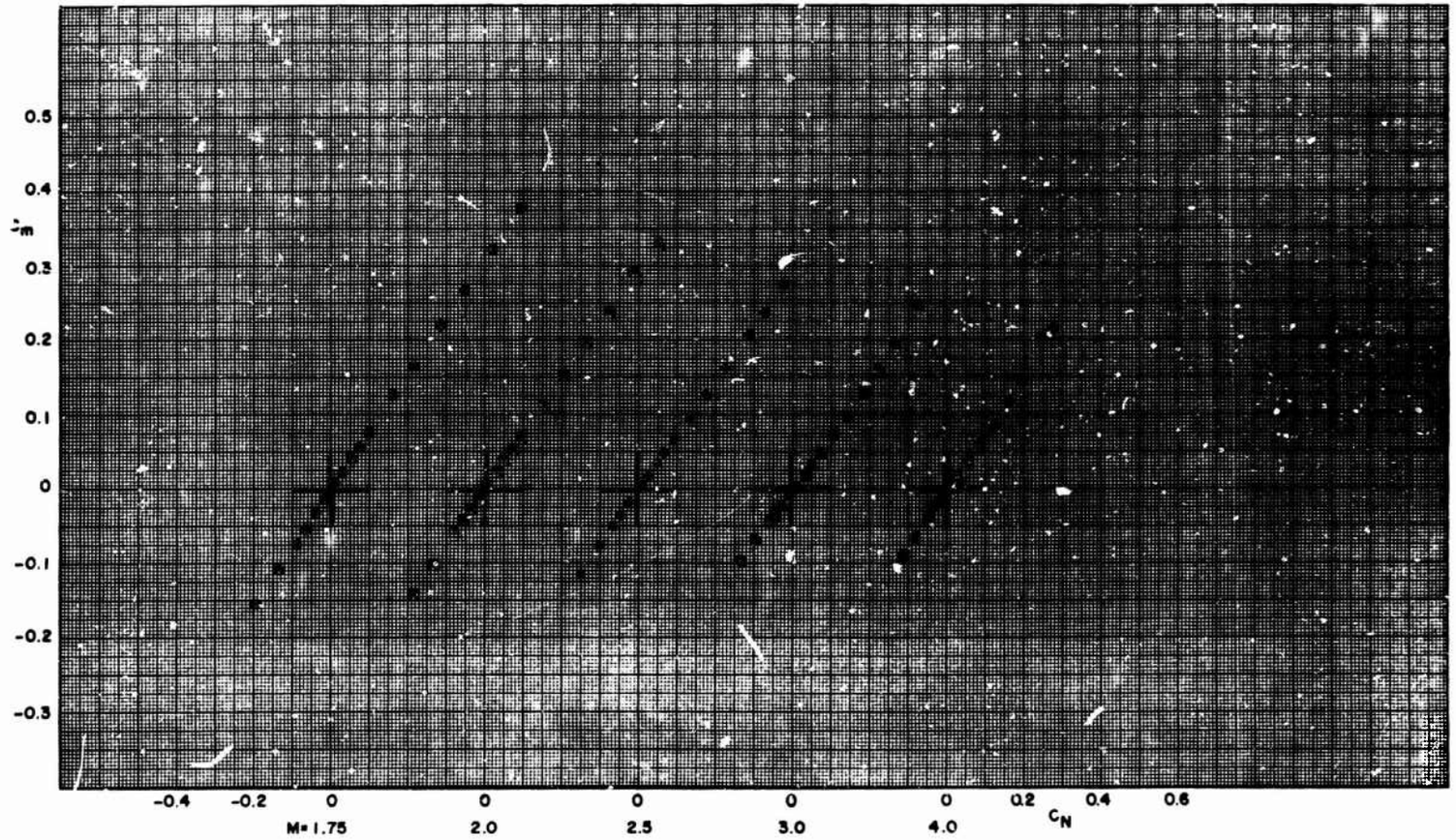

FIGURE A-11. PITCHING MOMENT VERSUS NORMAL FORCE COEFFICIENT, F8.00 (Continued)

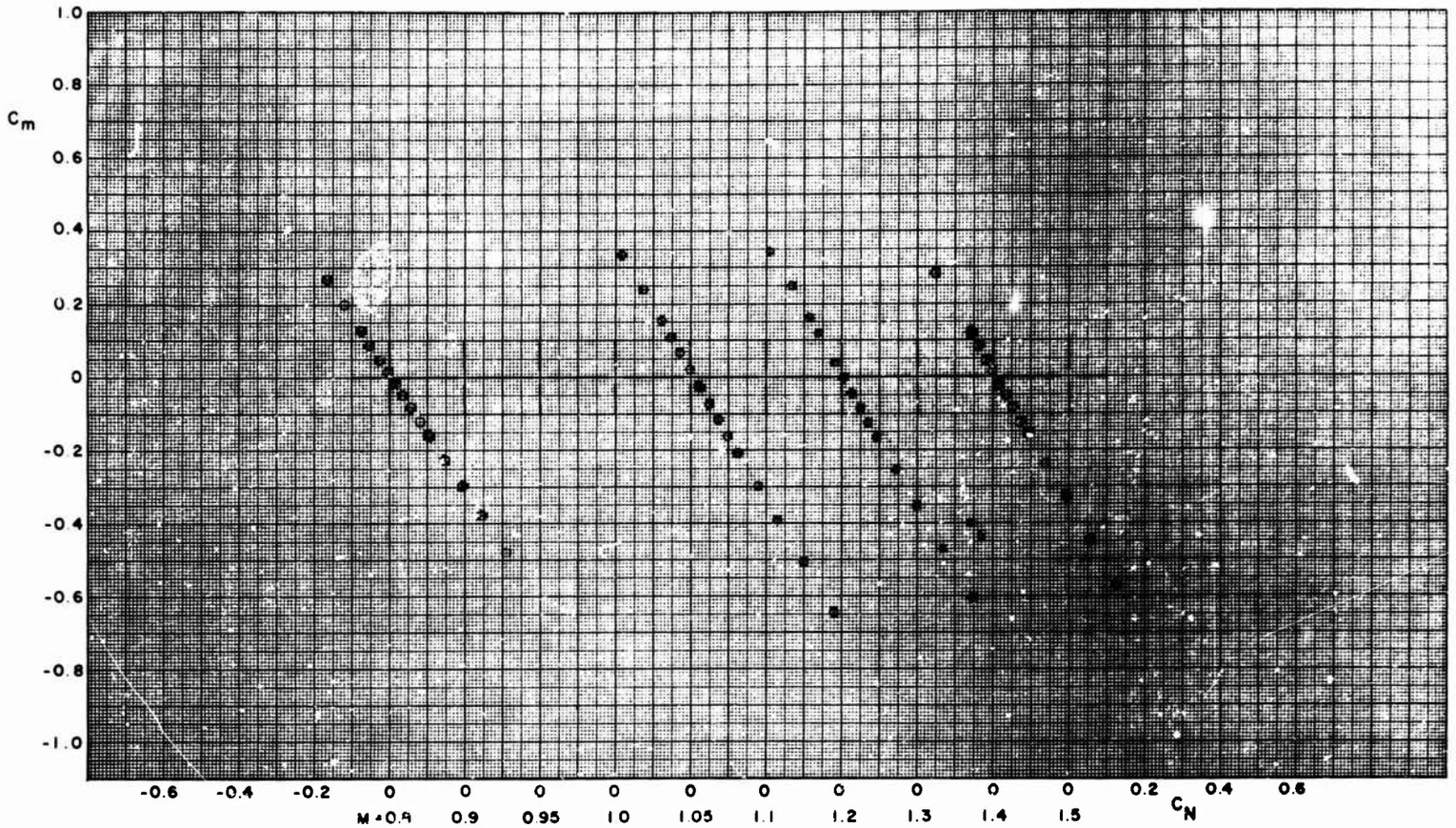

FIGURE A-11. PITCHING MOMENT VERSUS NORMAL FORCE COEFFICIENT, F8.06 (Continued)

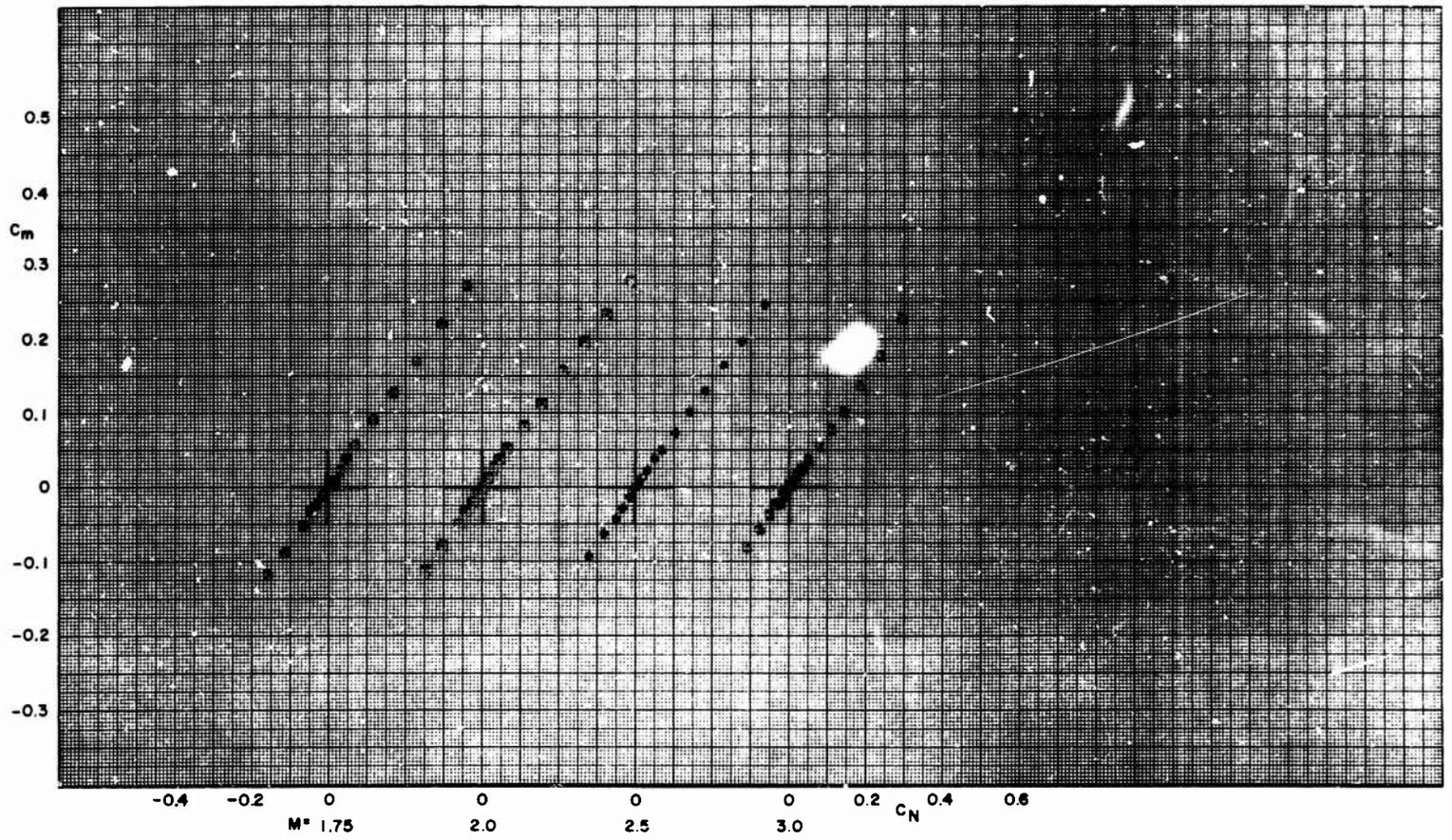

FIGURE A-11. PITCHING MOMENT VERSUS NORMAL FORCE COEFFICIENT, F8.06 (Continued)

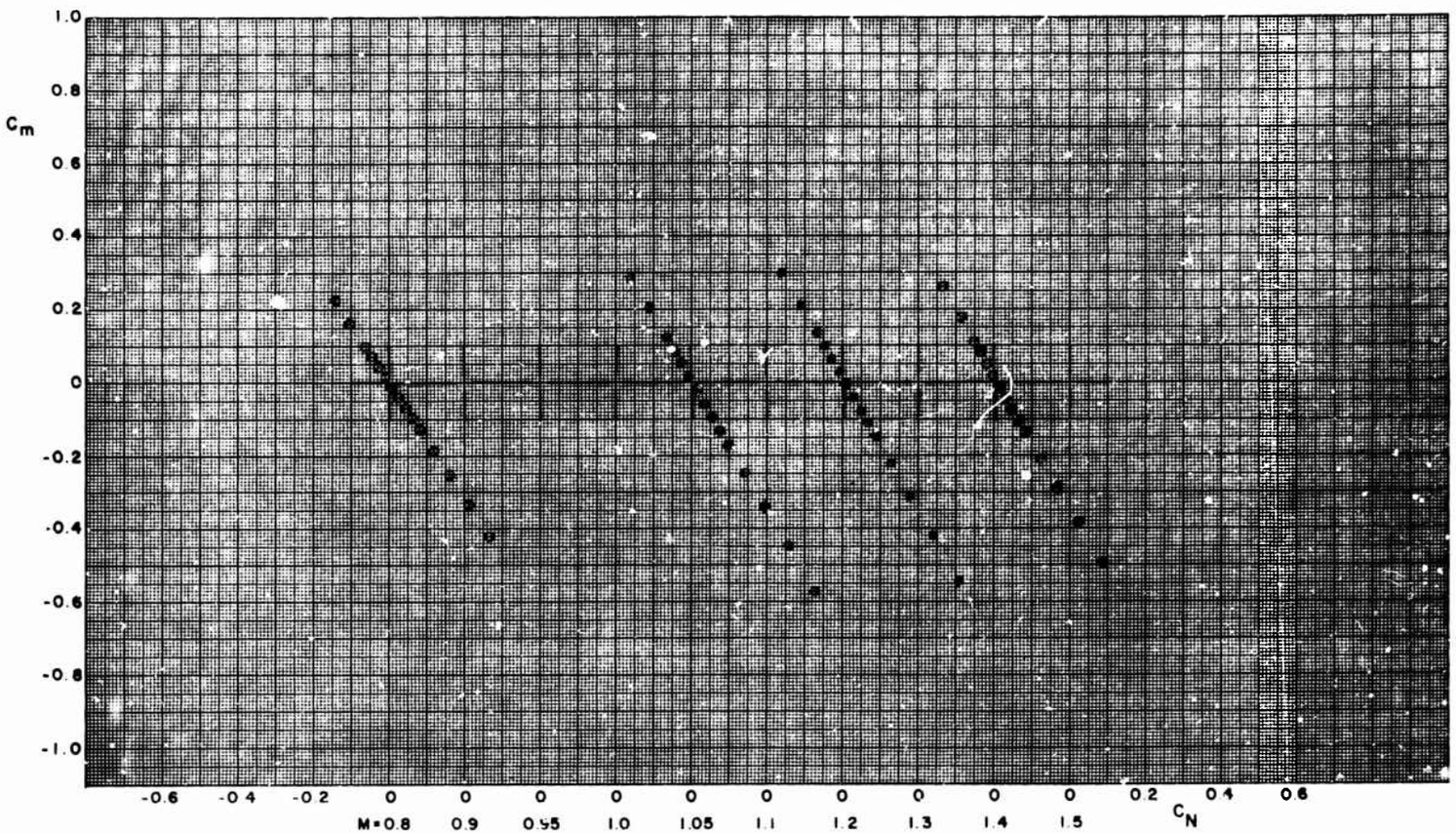

FIGURE A-11. PITCHING MOMENT VERSUS NORMAL FORCE COEFFICIENT, F8.12 (Continued)

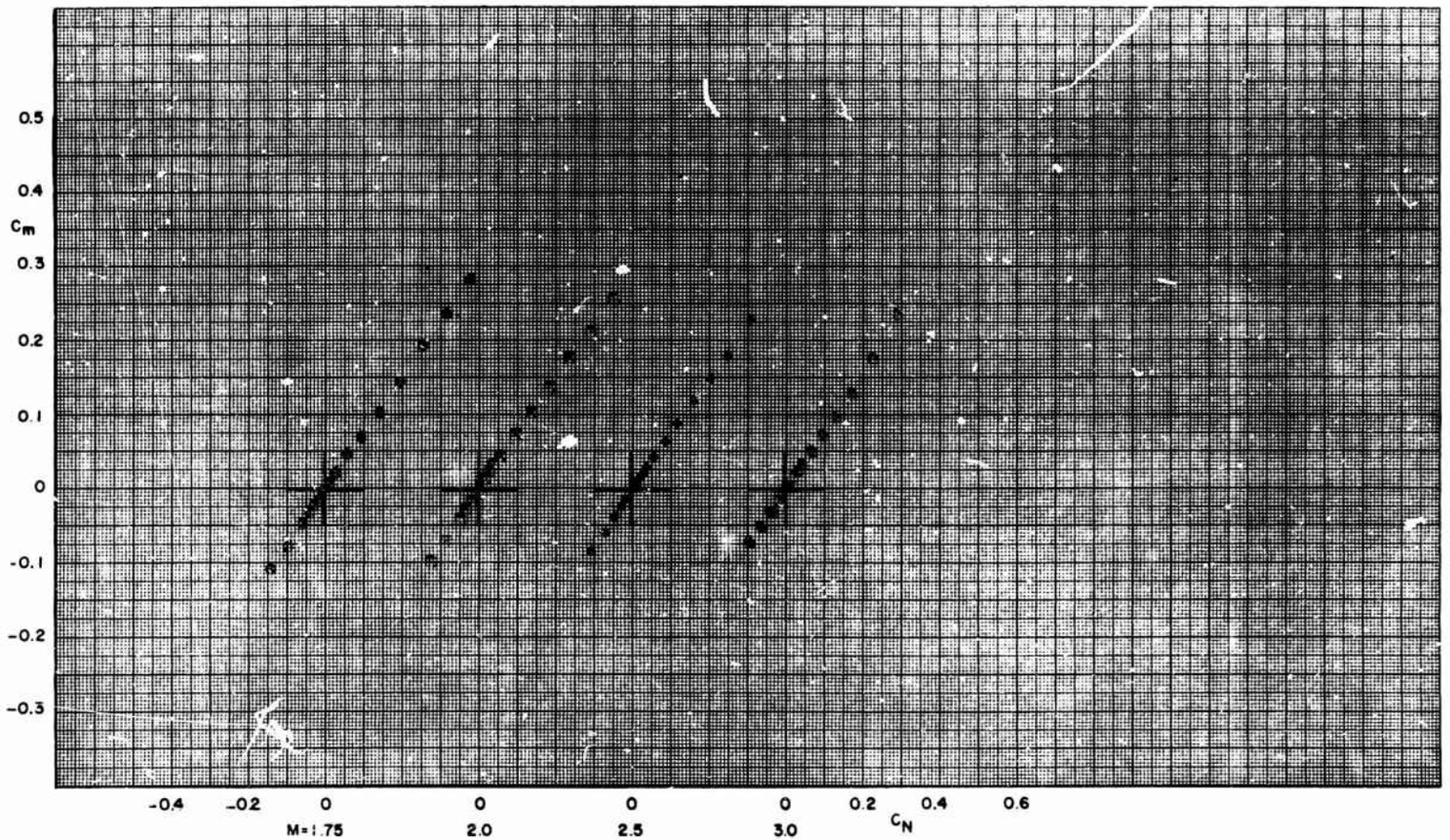

FIGURE A-11. PITCHING MOMENT VERSUS NORMAL FORCE COEFFICIENT, F8.12 (Continued)

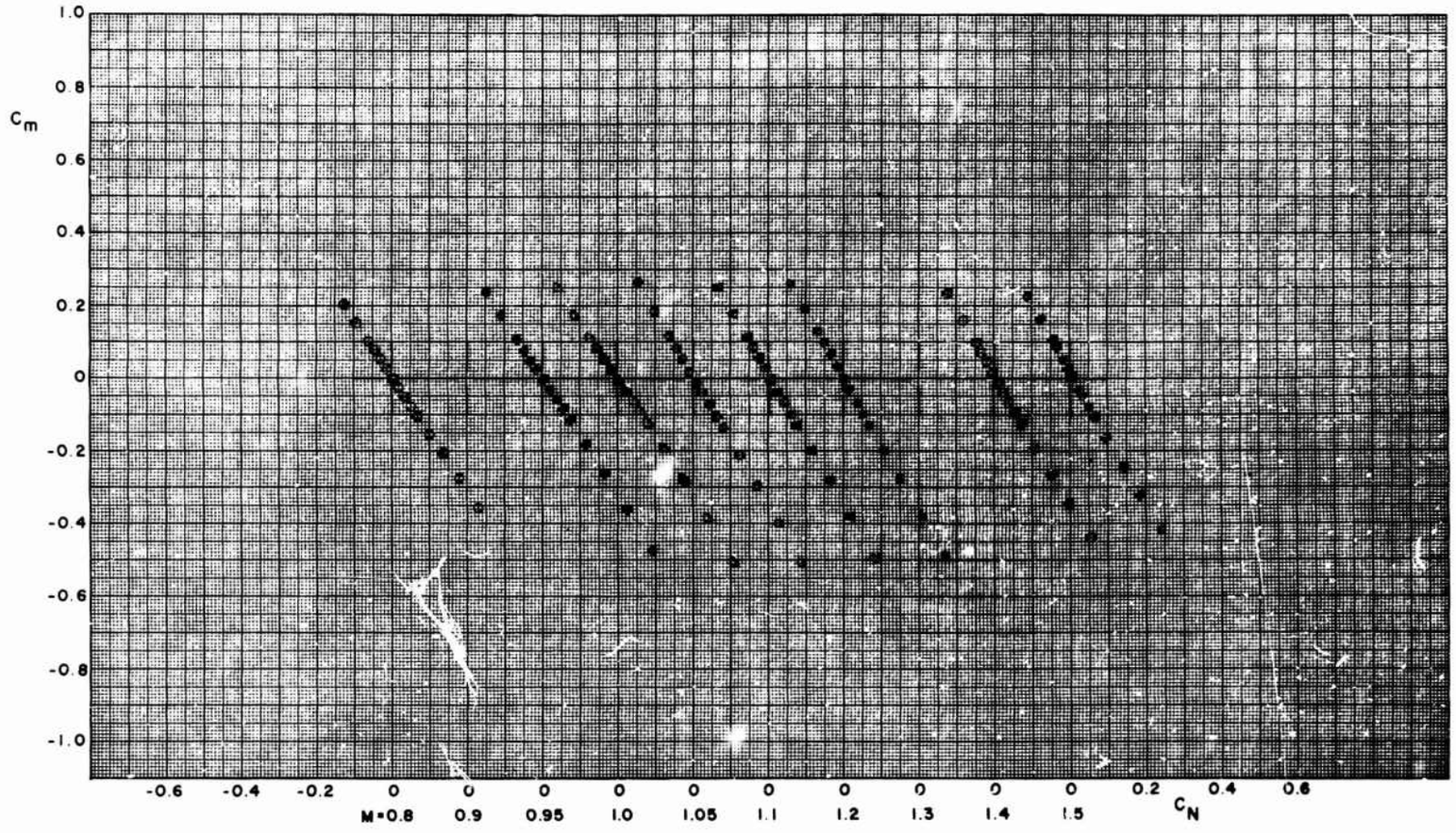

FIGURE A-11. PITCHING MOMENT VERSUS NORMAL FORCE COEFFICIENT, F8.20 (Continued)

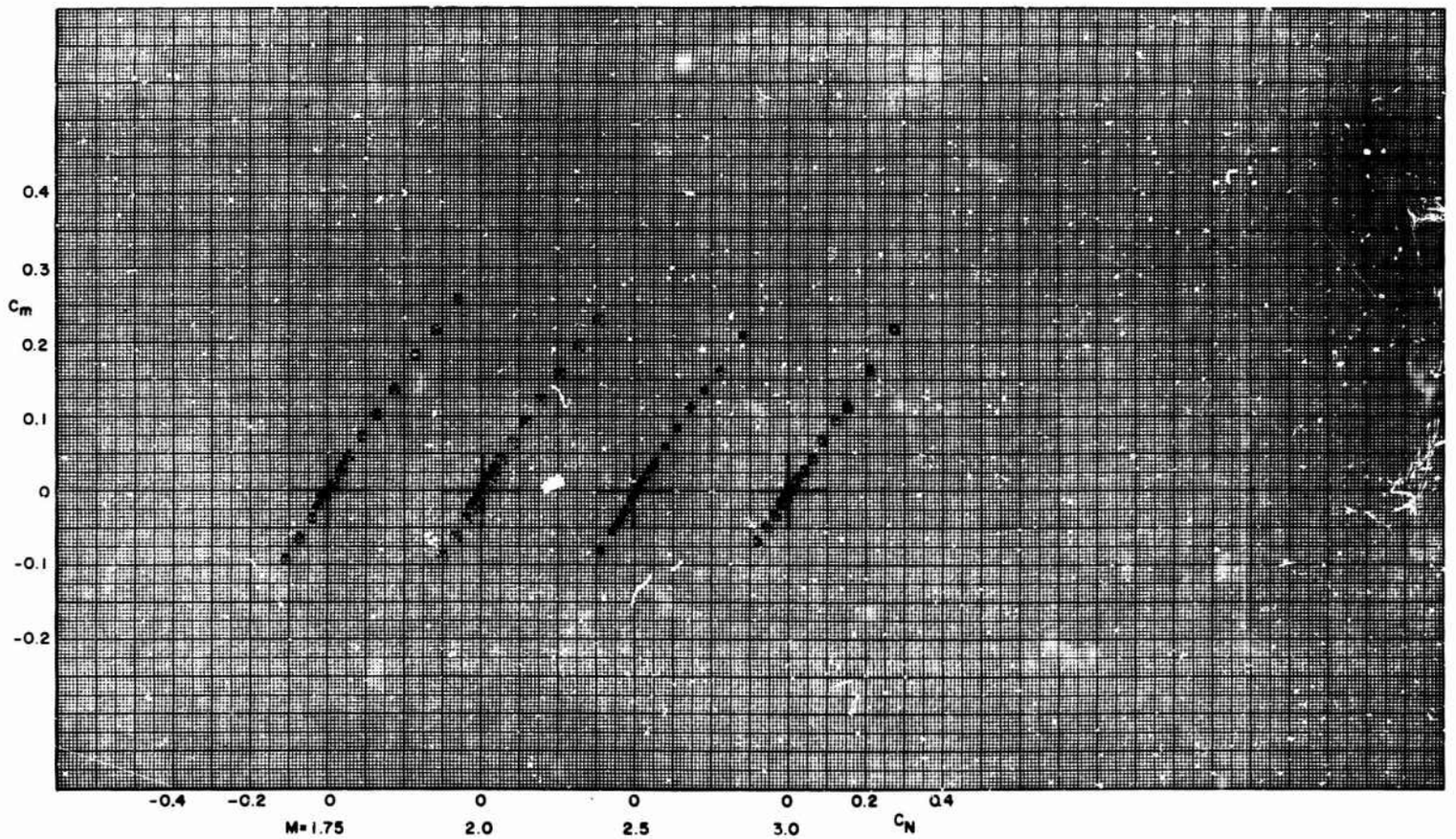

FIGURE A-11. PITCHING MOMENT VERSUS NORMAL FORCE COEFFICIENT, F8.20 (Concluded)

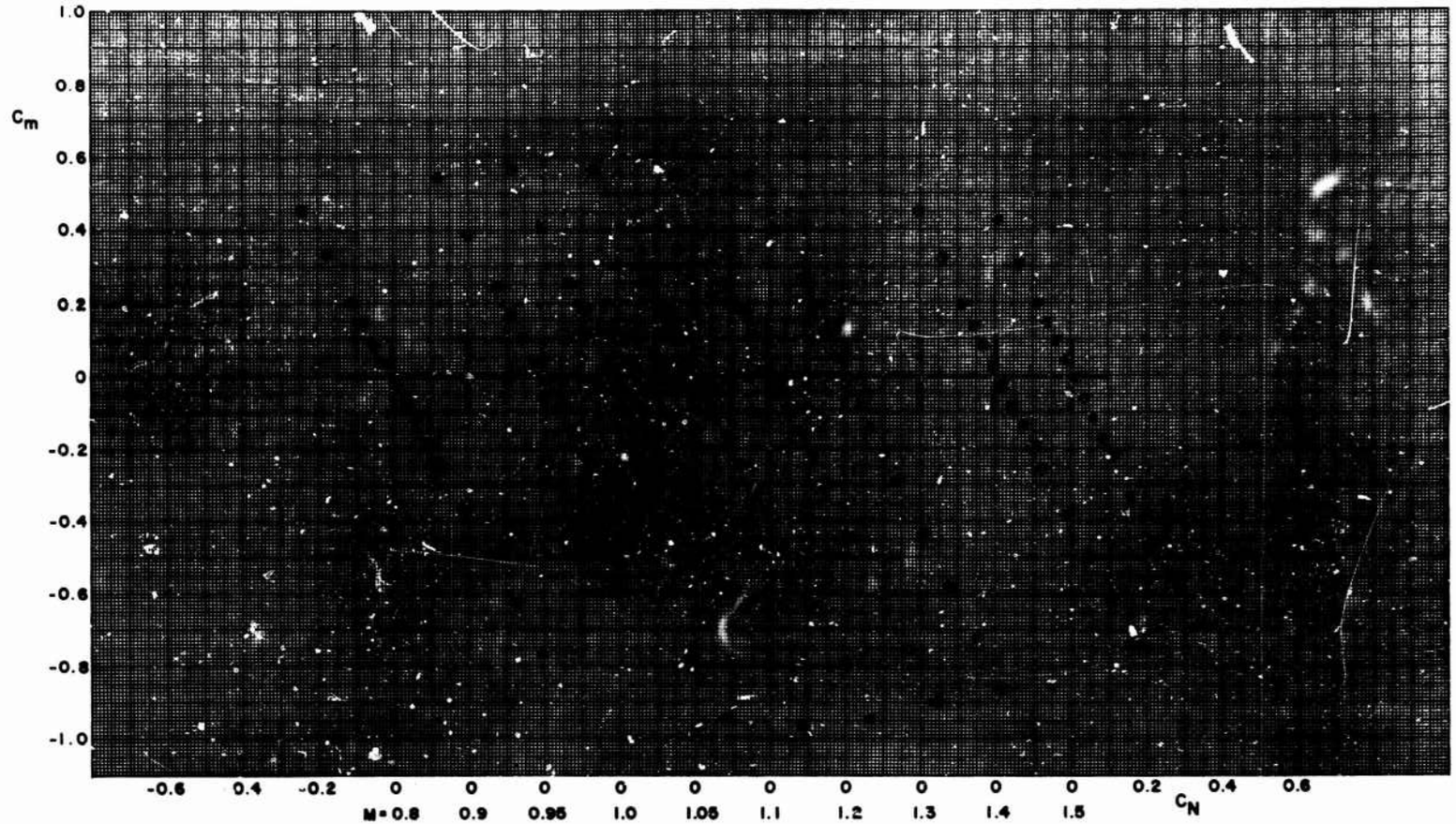

FIGURE A-12. PITCHING MOMENT VERSUS NORMAL FORCE COEFFICIENT, FD.00

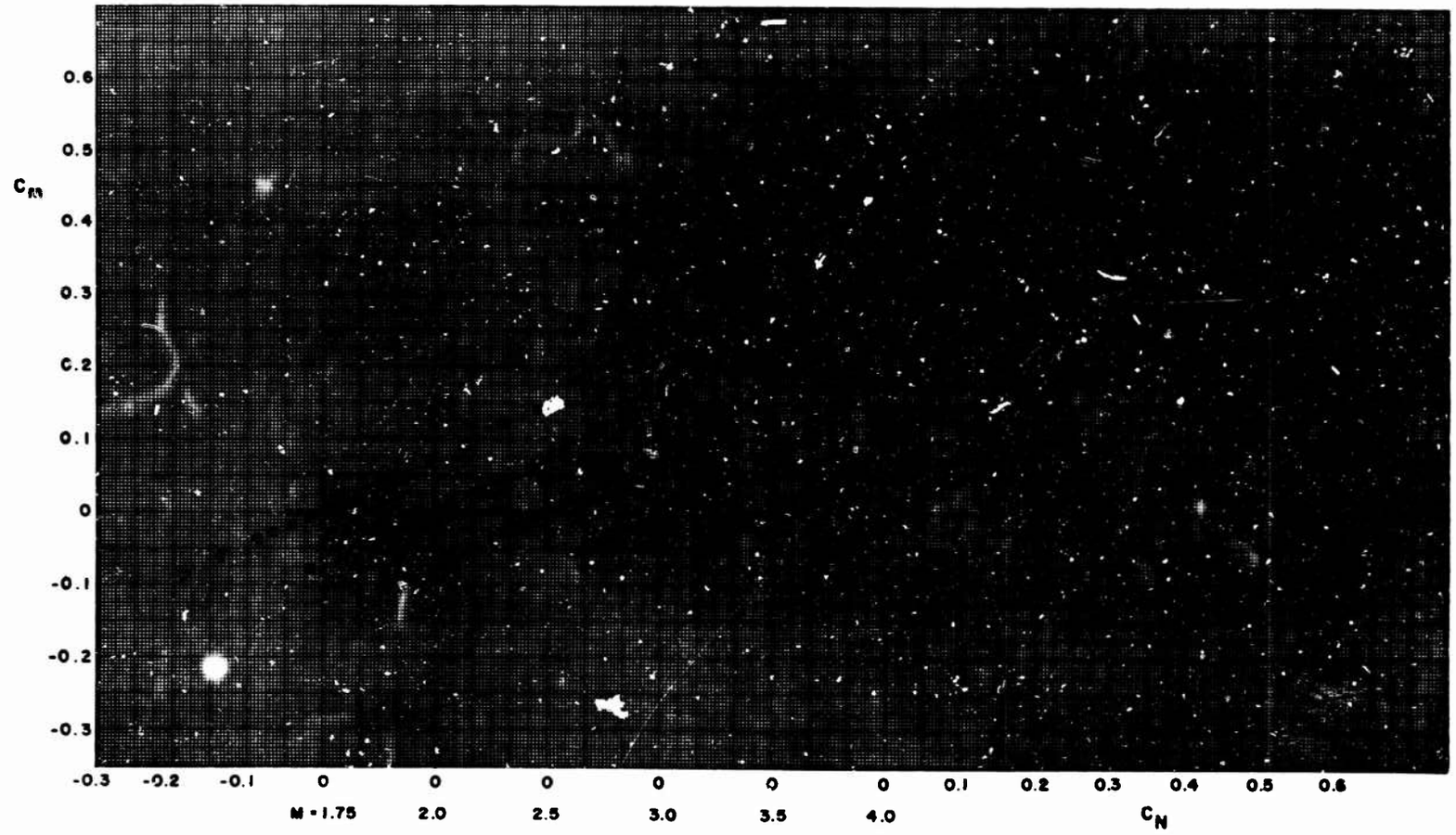

FIGURE A-12. PITCHING MOMENT VERSUS NORMAL FORCE COEFFICIENT, FD. 00 (Continued)

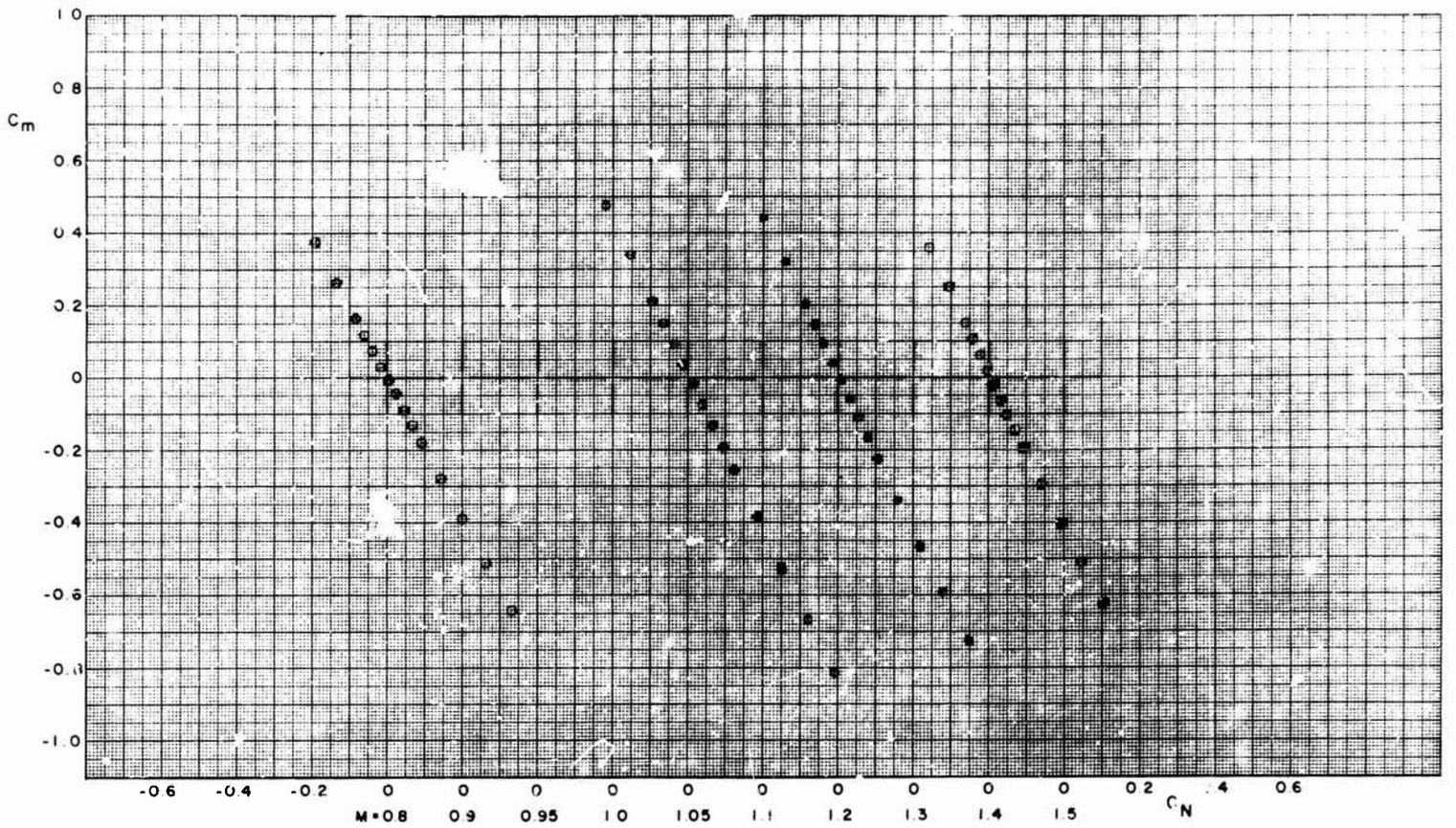

FIGURE A-12. PITCHING MOMENT VERSUS NORMAL FORCE COEFFICIENT, FD. 06 (Continued)

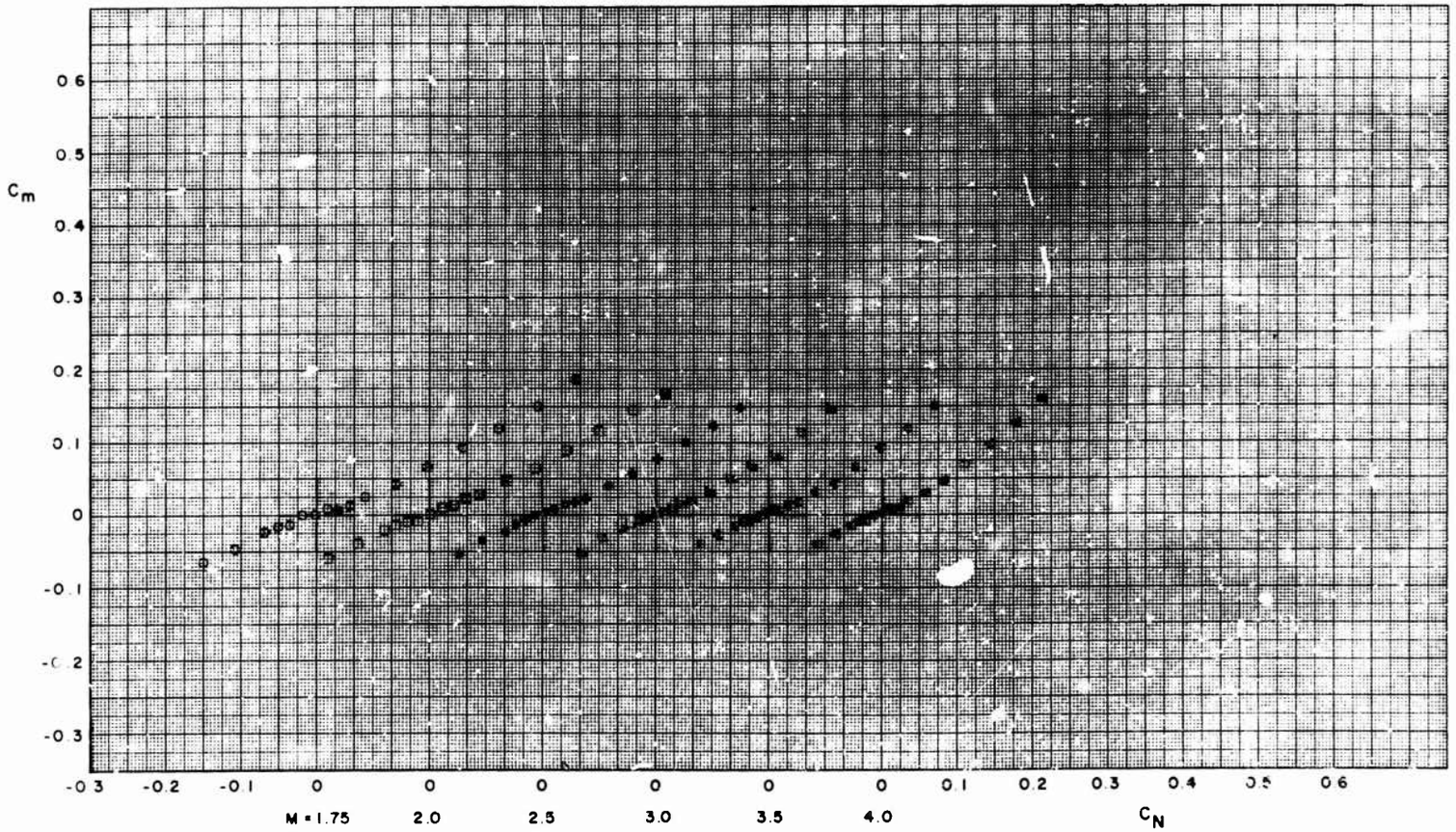

FIGURE A-12. PITCHING MOMENT VERSUS NORMAL FORCE COEFFICIENT, FD. 06 (Continued)

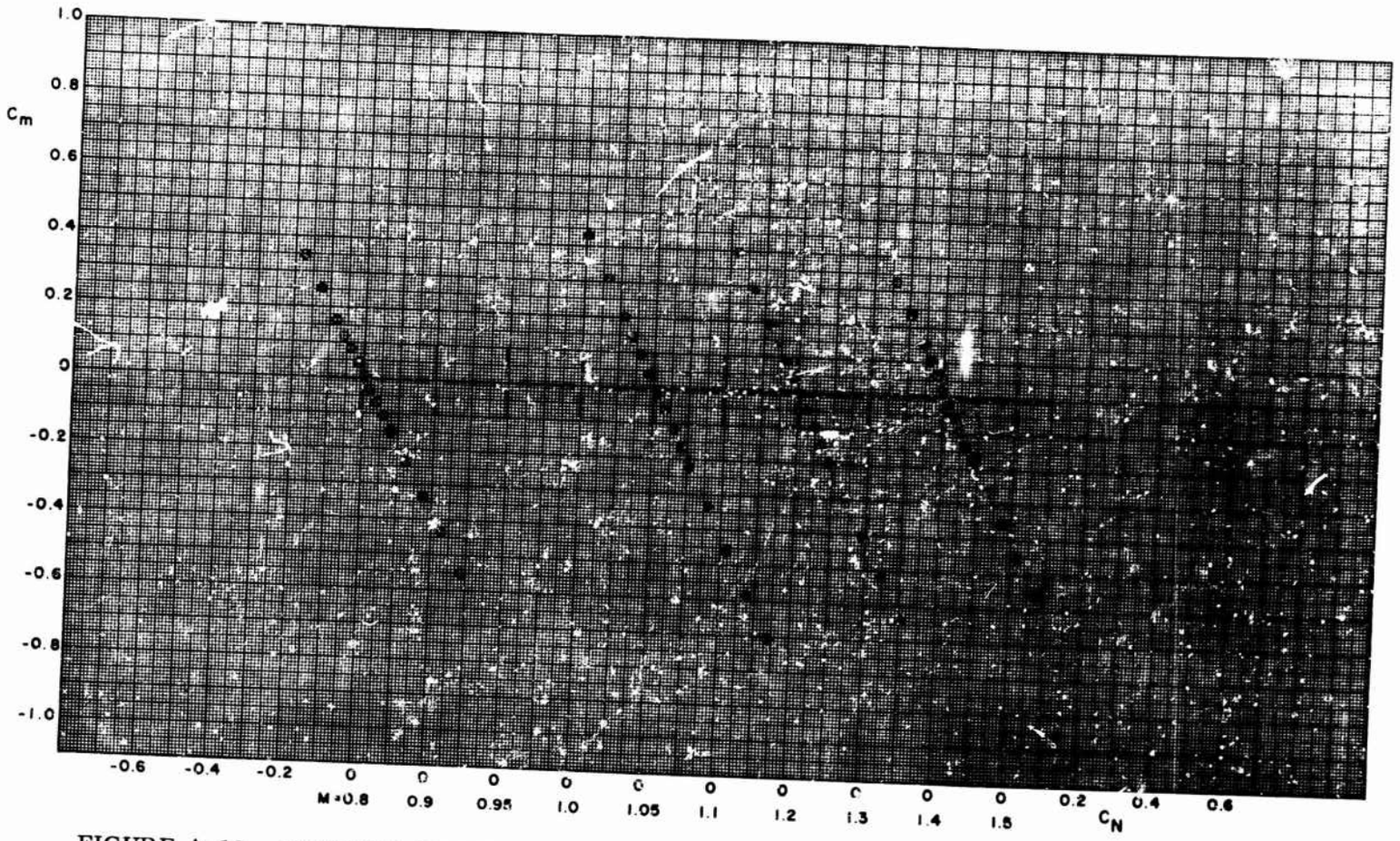

FIGURE A-12. PITCHING MOMENT VERSUS NORMAL FORCE COEFFICIENT, FD.12 (Continued)

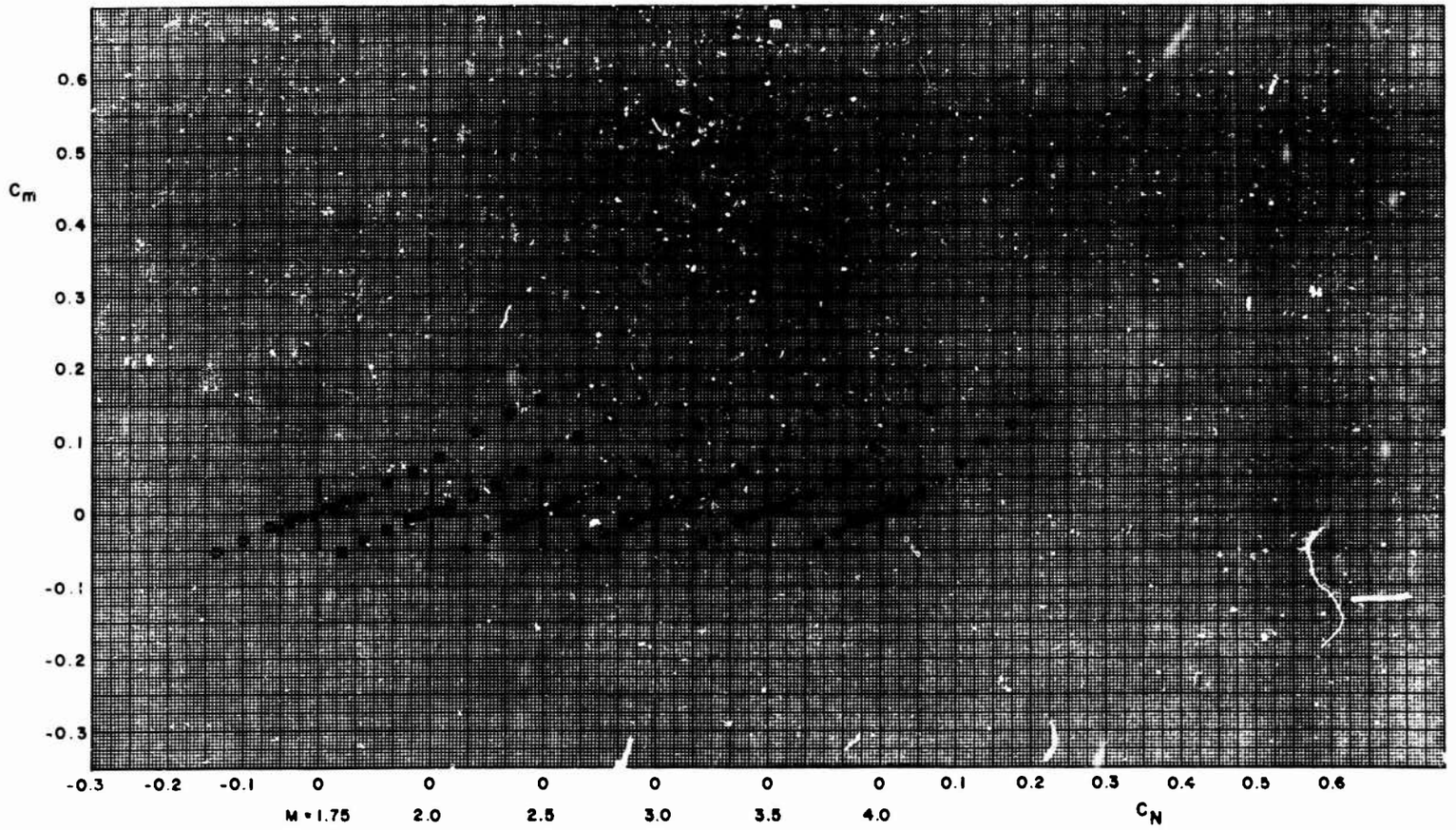

FIGURE A-12. PITCHING MOMENT VERSUS NORMAL FORCE COEFFICIENT, FD. 12 (Continued)

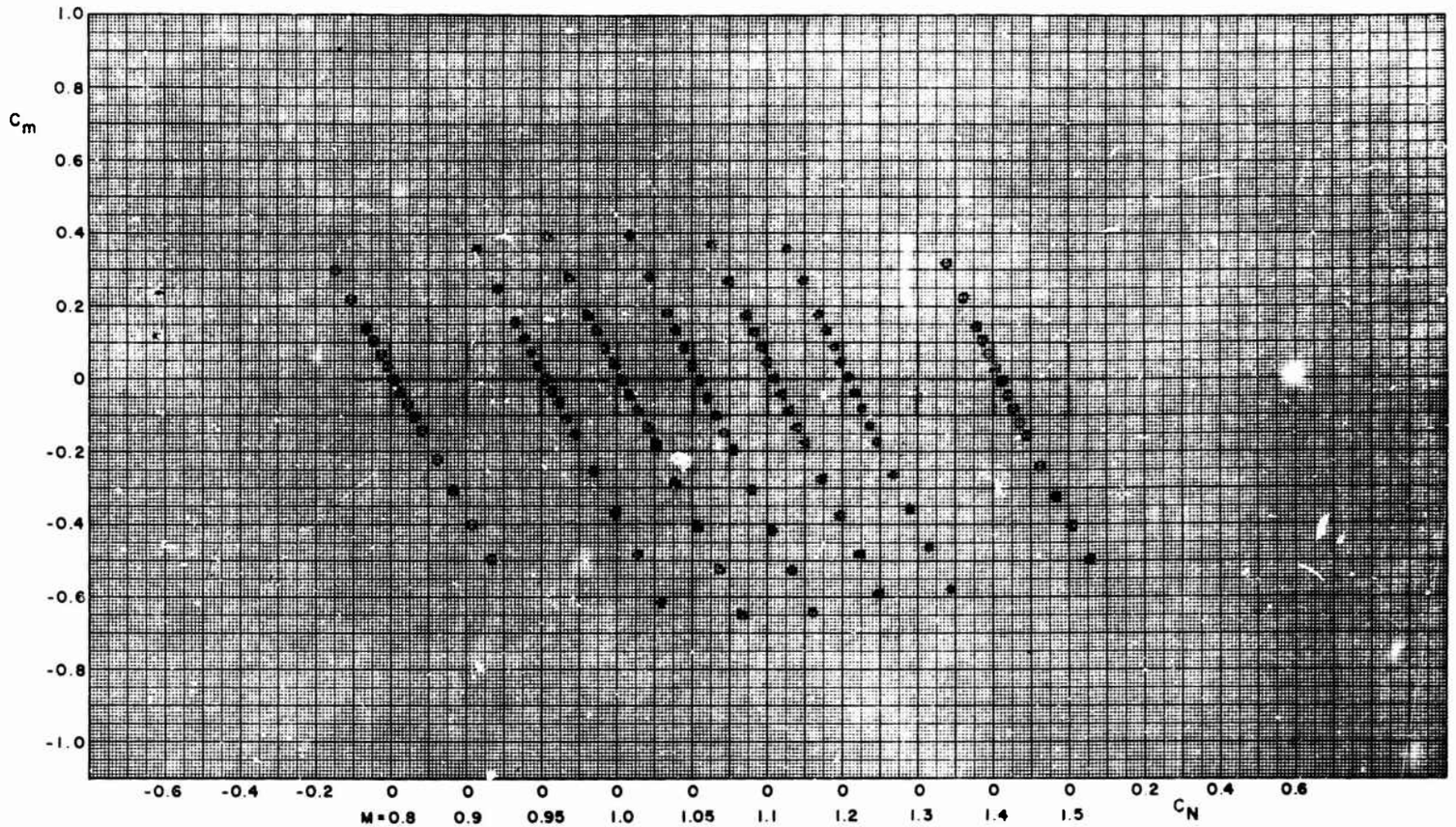

FIGURE A-12. PITCHING MOMENT VERSUS NORMAL FORCE COEFFICIENT, FD. 20 (Continued)

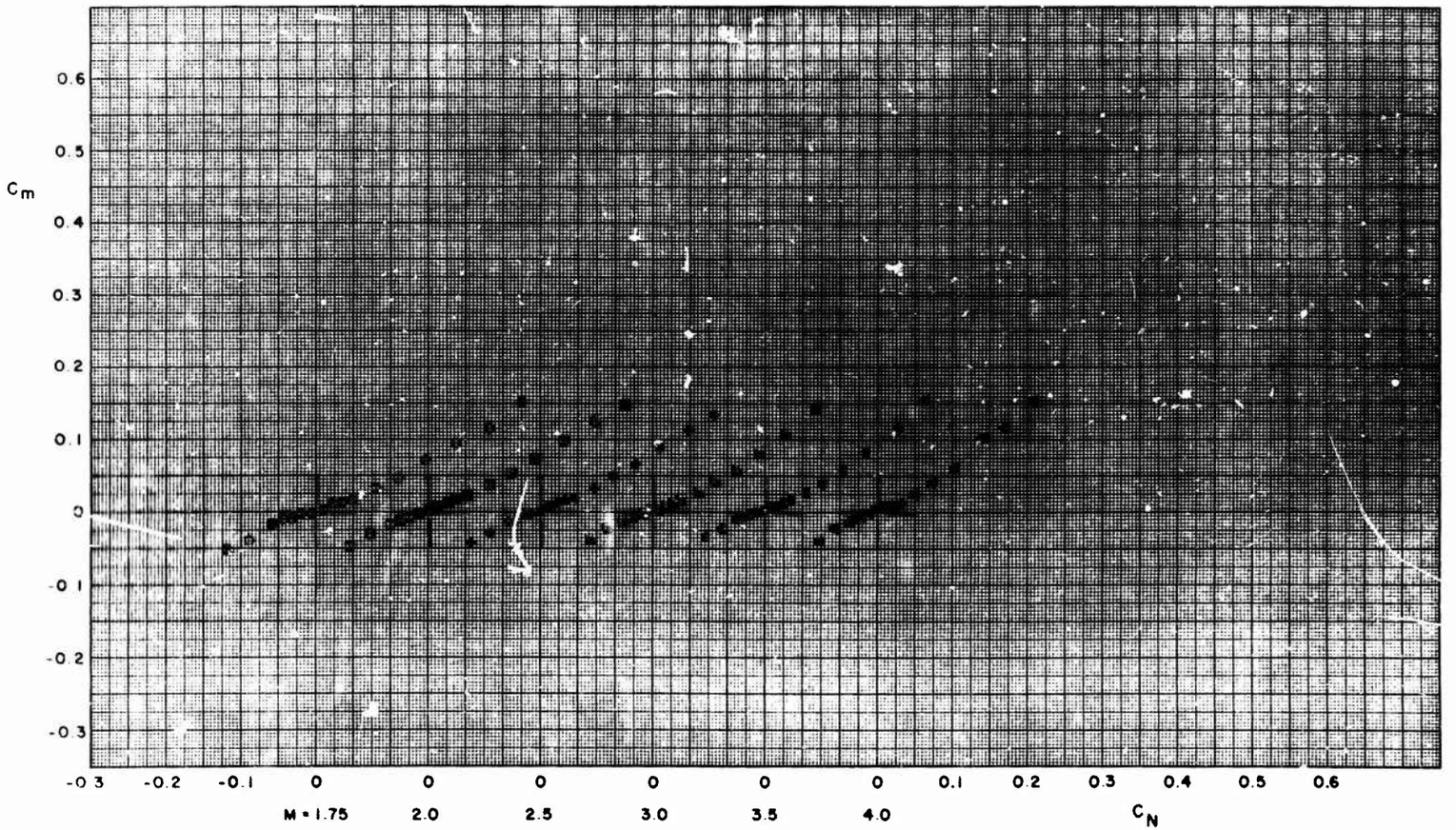

FIGURE A-12. PITCHING MOMENT VERSUS NORMAL FORCE COEFFICIENT, FD.20 (Concluded)

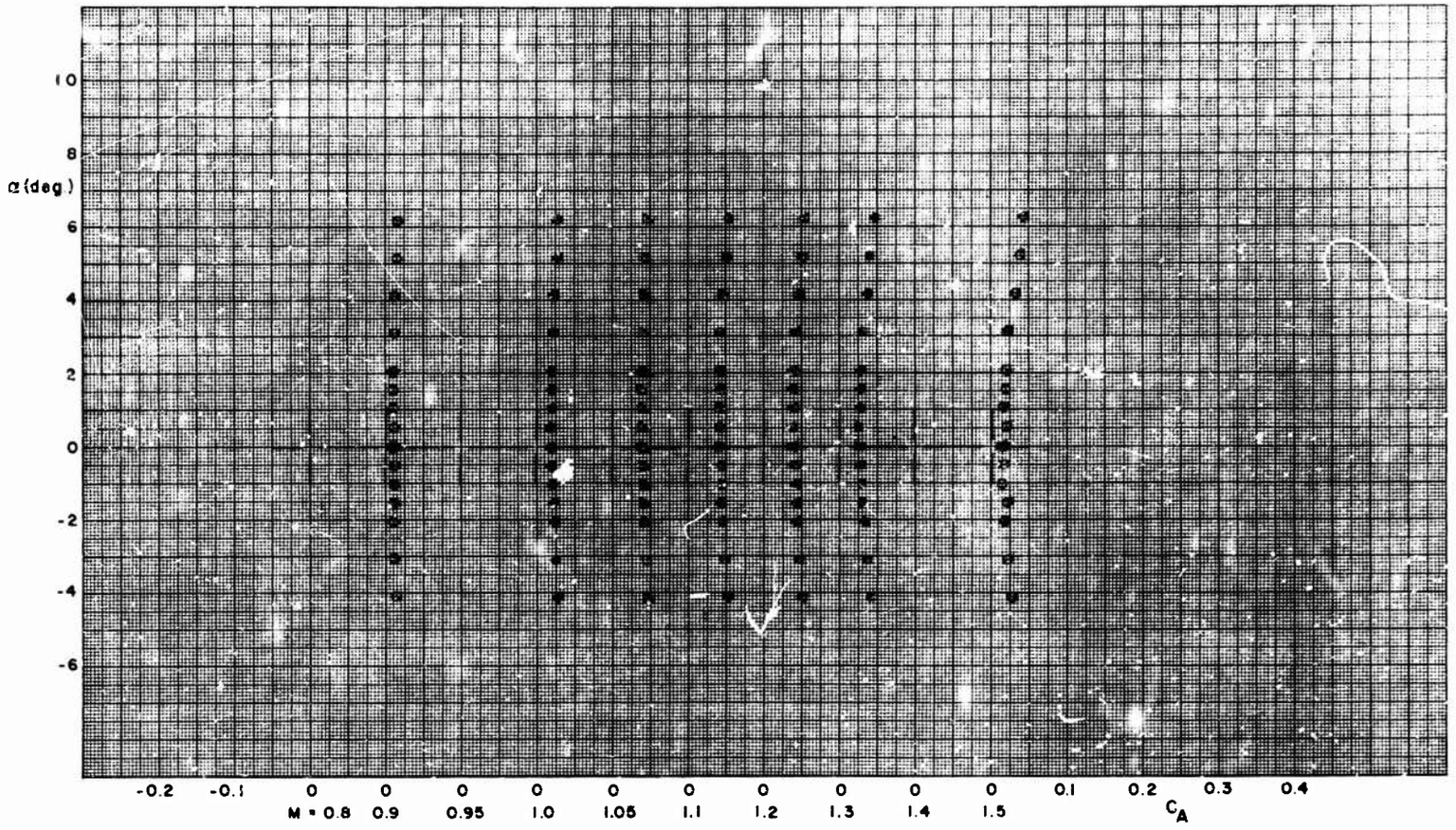

FIGURE A-13. ANGLE OF ATTACK VERSUS AXIAL FORCE COEFFICIENT, F4.00

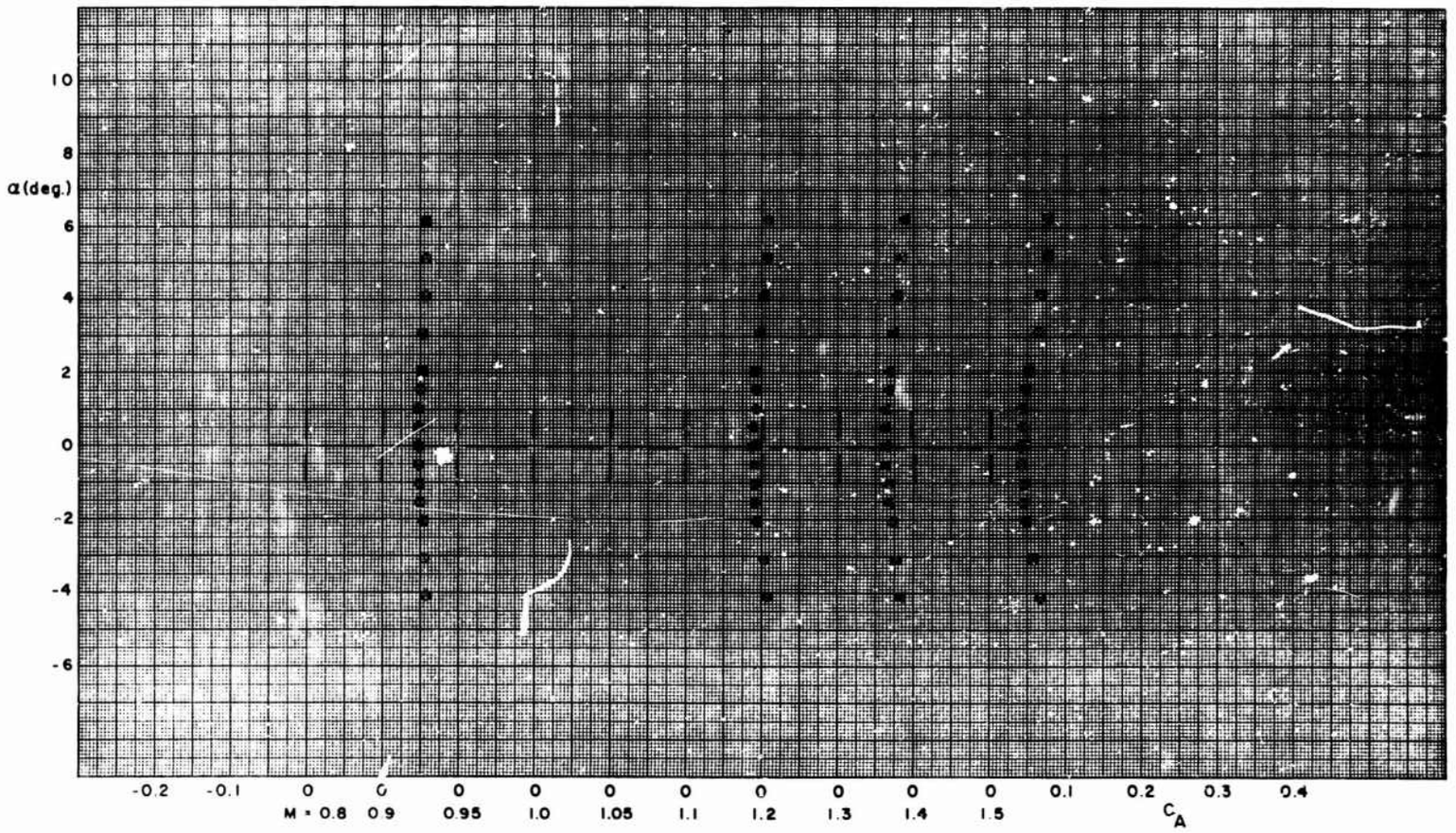

FIGURE A-13. ANGLE OF ATTACK VERSUS AXIAL FORCE COEFFICIENT, F4.08 (Continued)

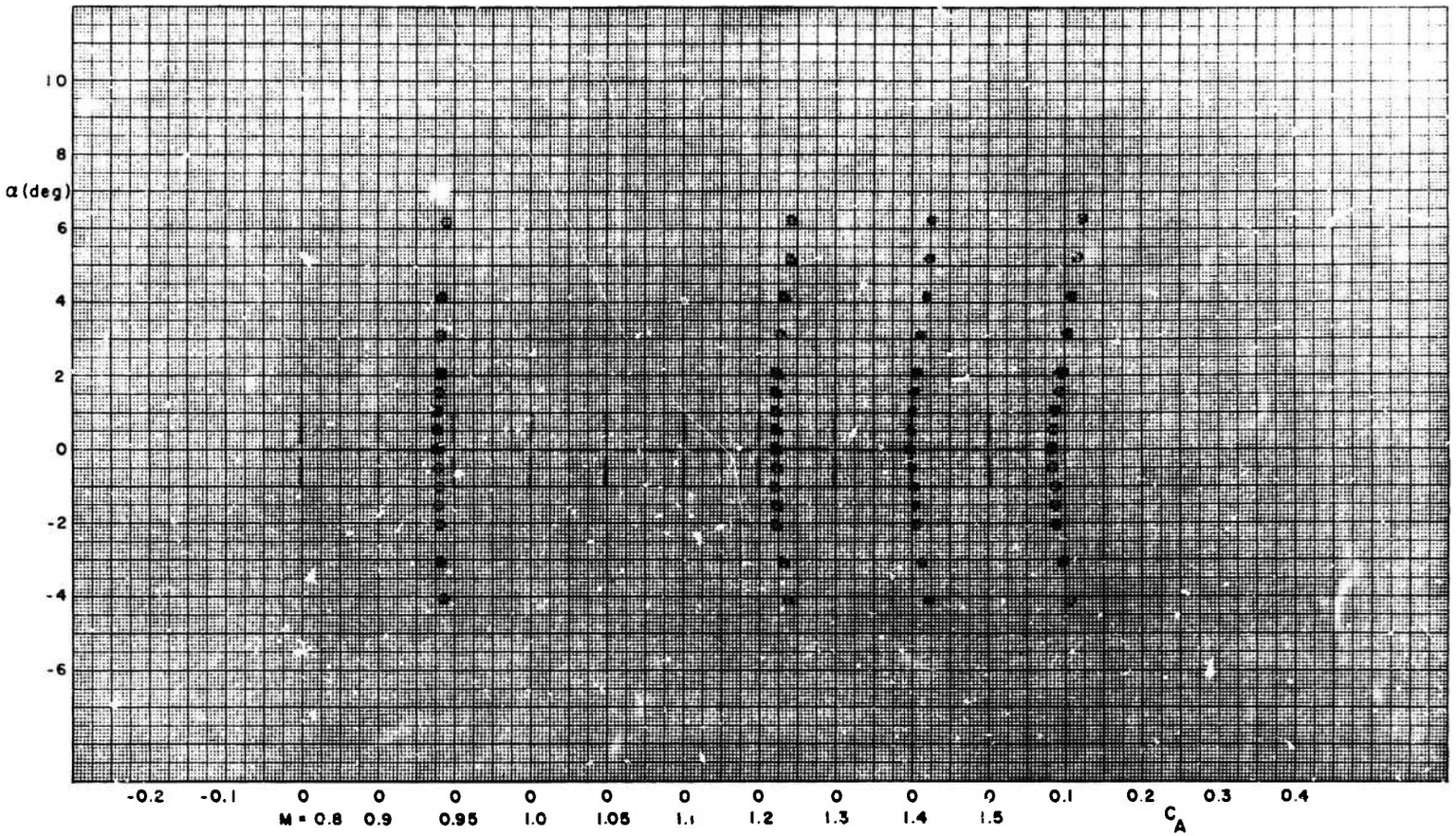

FIGURE A-13. ANGLE OF ATTACK VERSUS AXIAL FORCE COEFFICIENT, F4.16 (Continued)

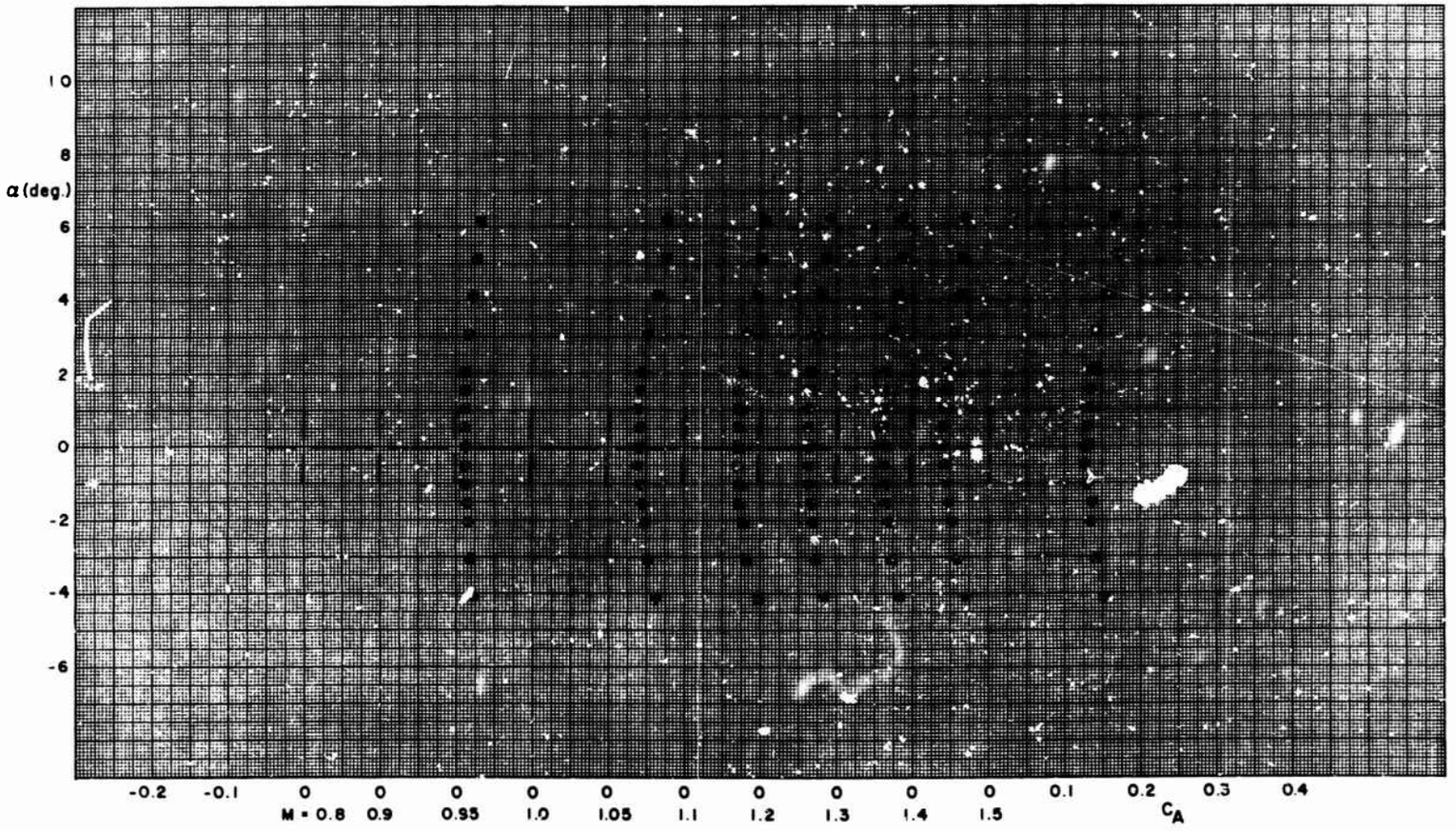

FIGURE A-13. ANGLE OF ATTACK VERSUS AXIAL FORCE COEFFICIENT, F4.25 (Concluded)

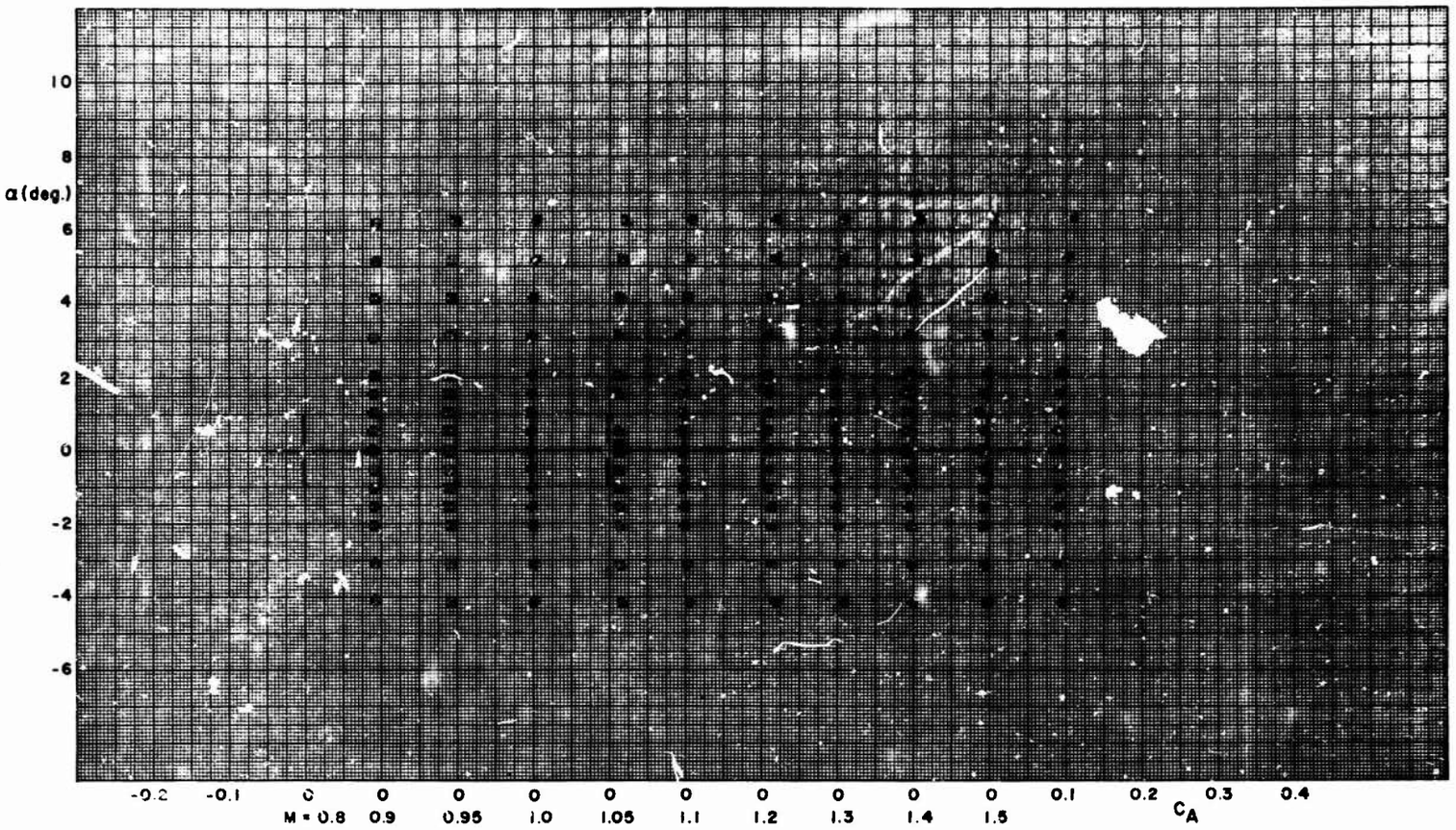

FIGURE A-14. ANGLE OF ATTACK VERSUS AXIAL FORCE COEFFICIENT, F8.00

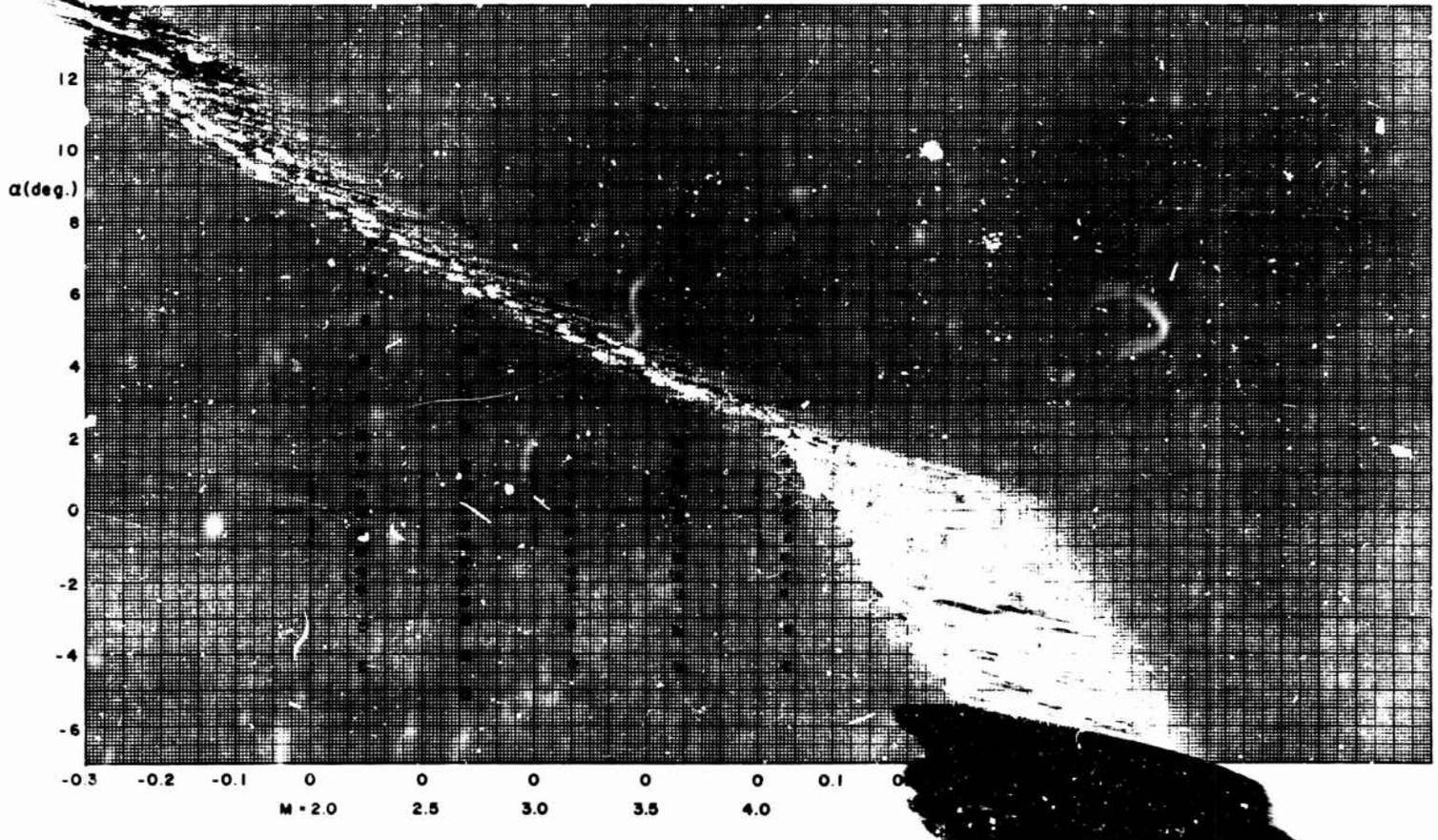

FIGURE A-14. ANGLE OF ATTACK VERSUS AXIAL FORCE COEF[illegible]ed)

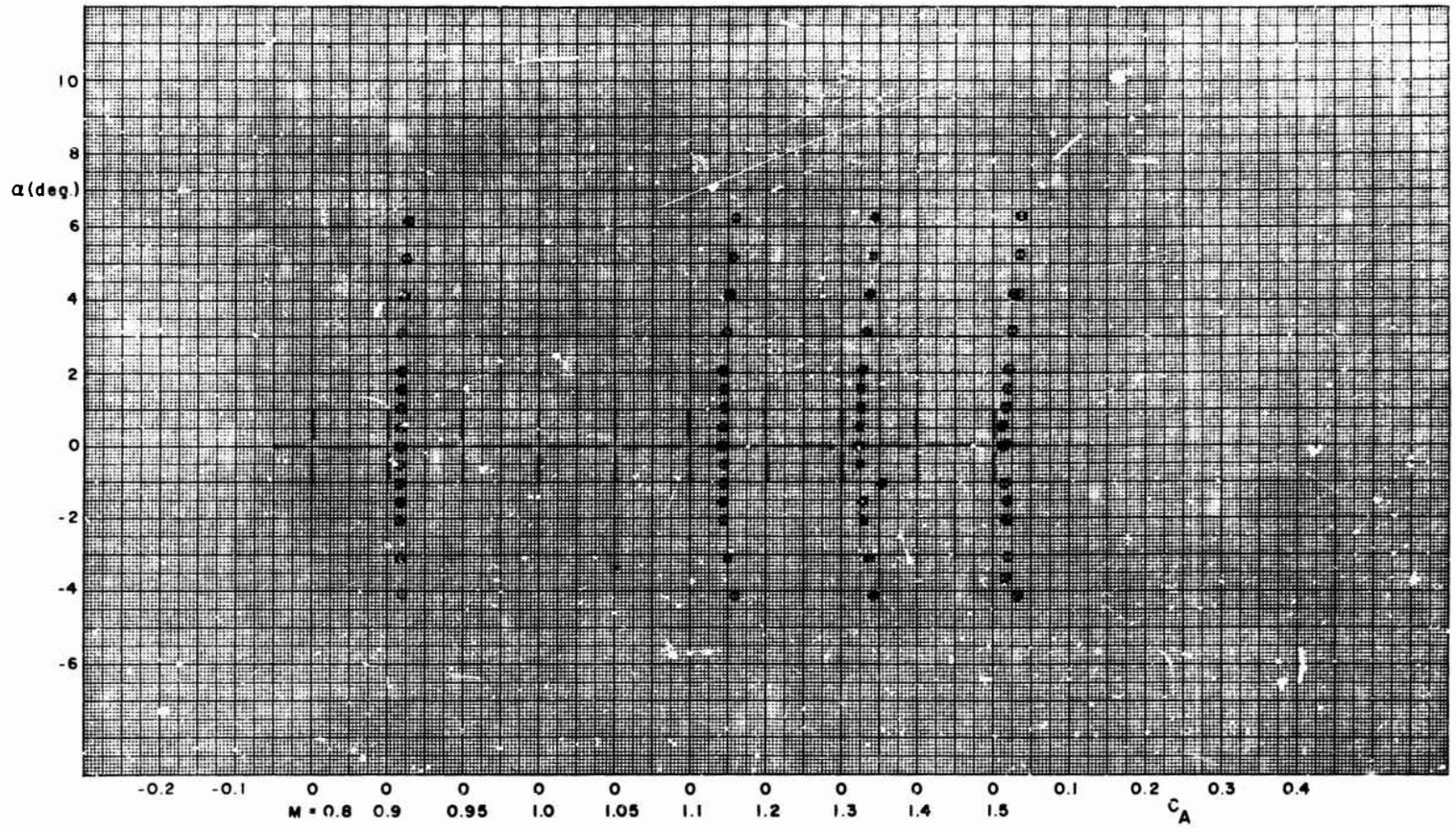

FIGURE A-14. ANGLE OF ATTACK VERSUS AXIAL FORCE COEFFICIENT, F8.06 (Continued)

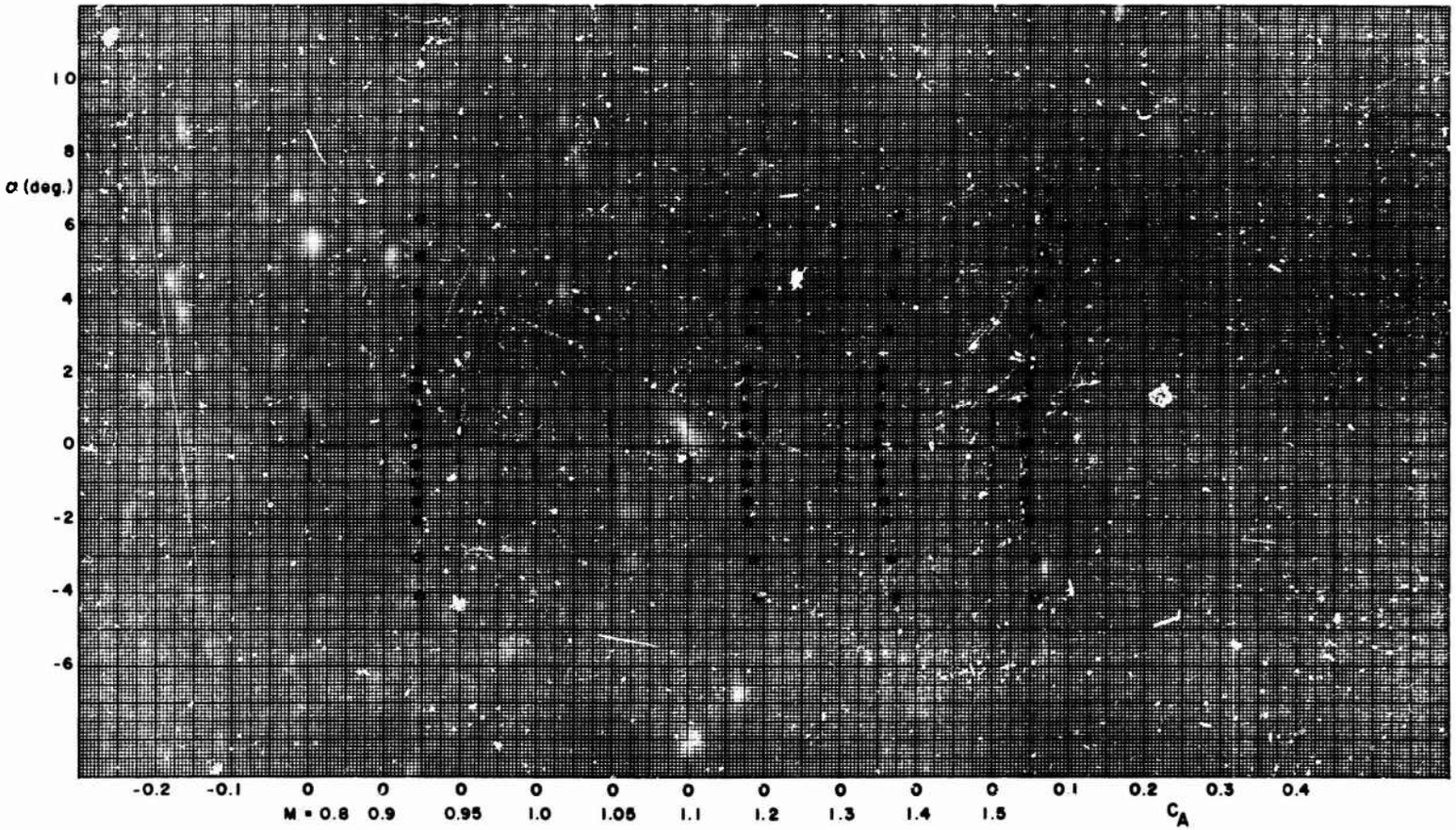

FIGURE A-14. ANGLE OF ATTACK VERSUS AXIAL FORCE COEFFICIENT, F8.12 (Continued)

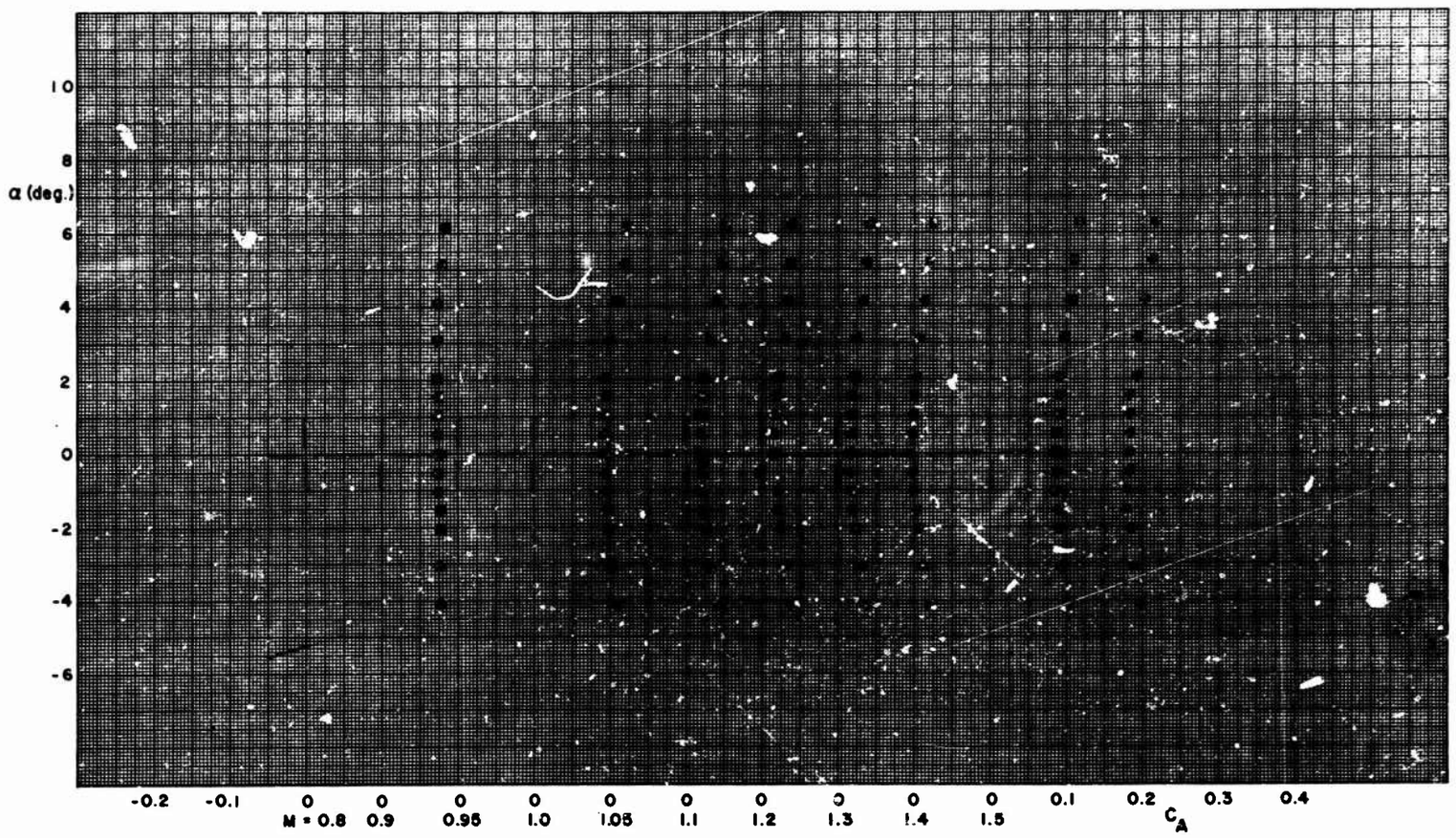

FIGURE A-14. ANGLE OF ATTACK VERSUS AXIAL FORCE COEFFICIENT, F8.20 (Concluded)

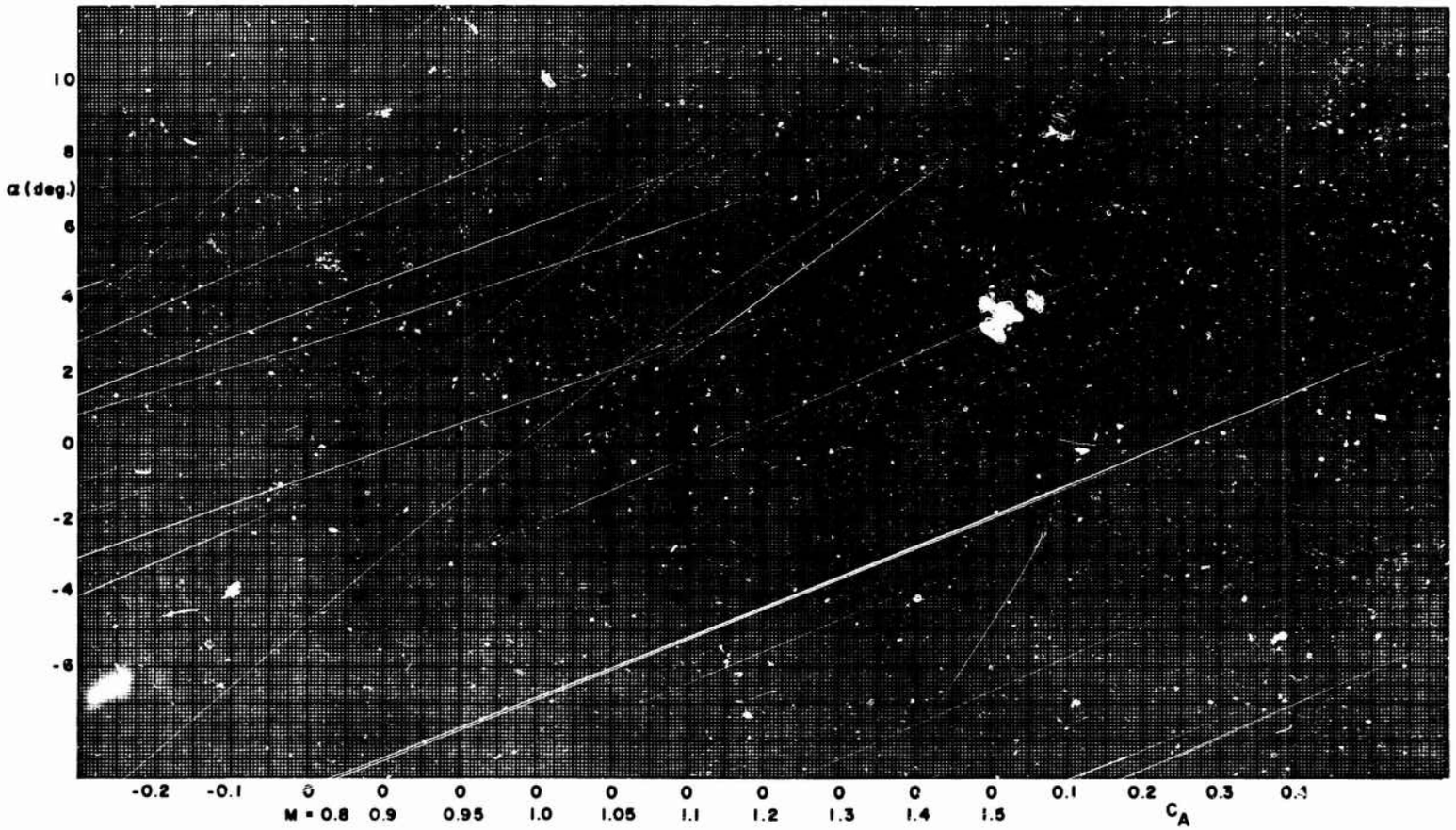

FIGURE A-15. ANGLE OF ATTACK VERSUS AXIAL FORCE COEFFICIENT, FD. 00

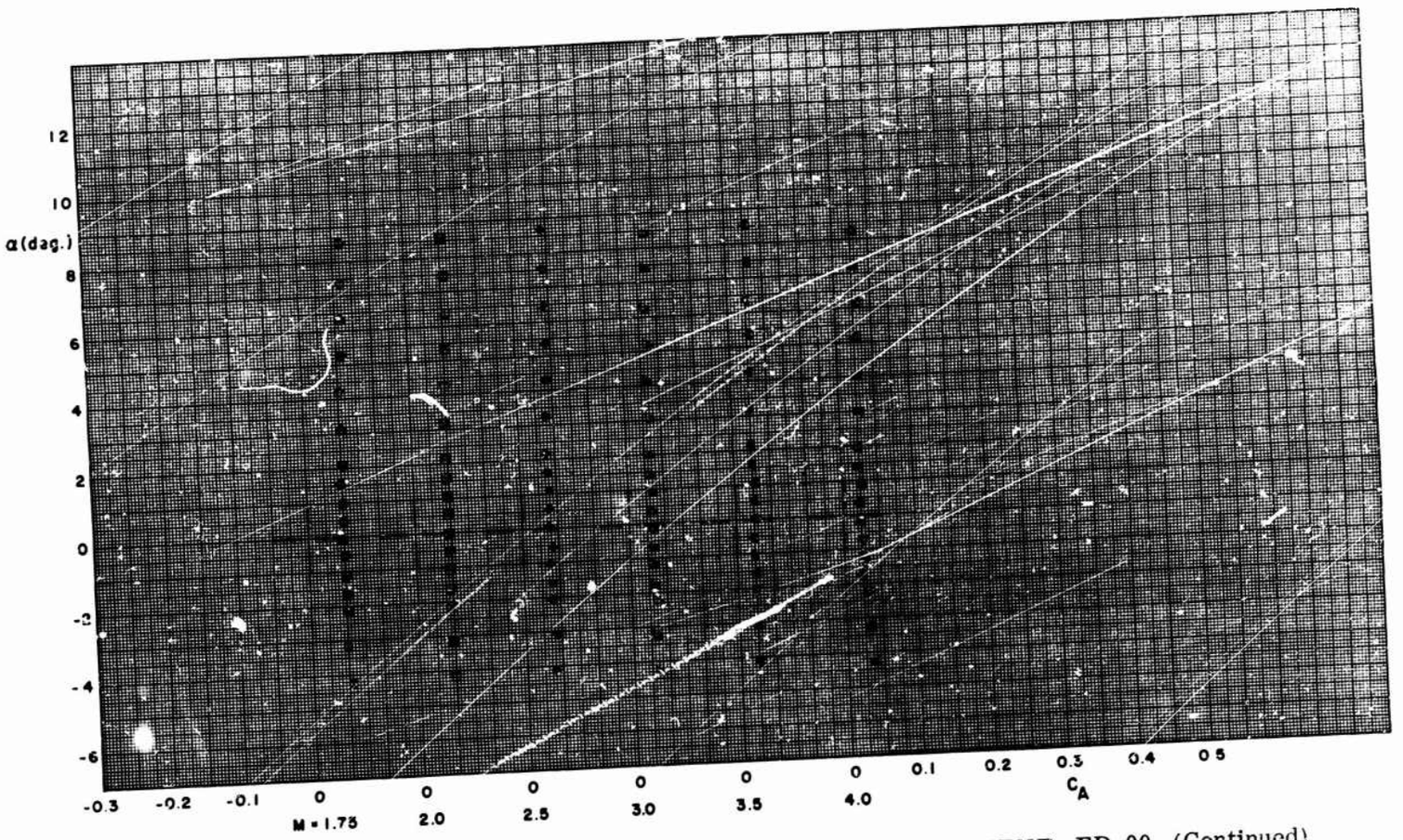

FIGURE A-15. ANGLE OF ATTACK VERSUS AXIAL FORCE COEFFICIENT, FD. 00 (Continued)

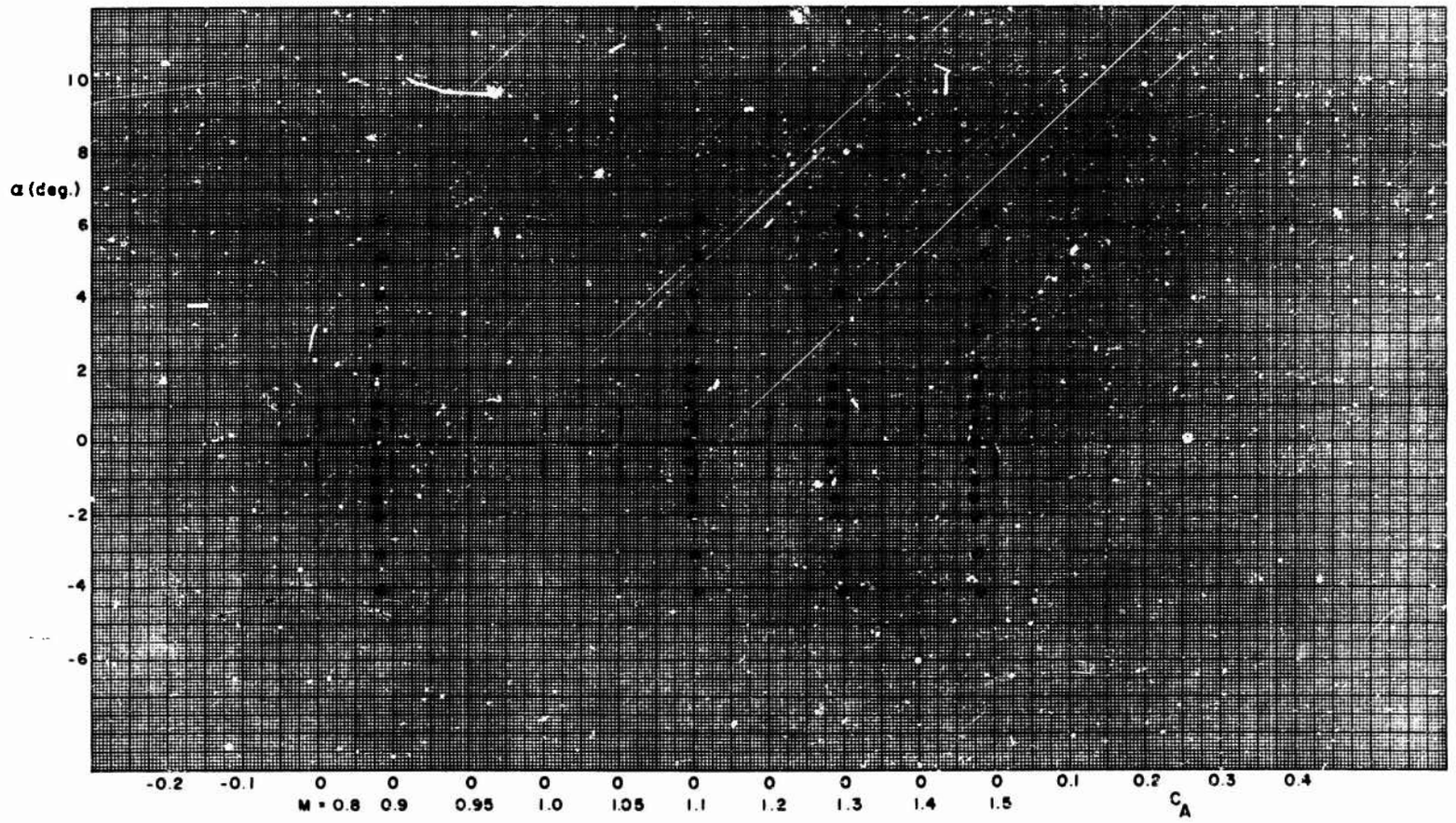

FIGURE A-15. ANGLE OF ATTACK VERSUS AXIAL FORCE COEFFICIENT, FD. 06 (Continued)

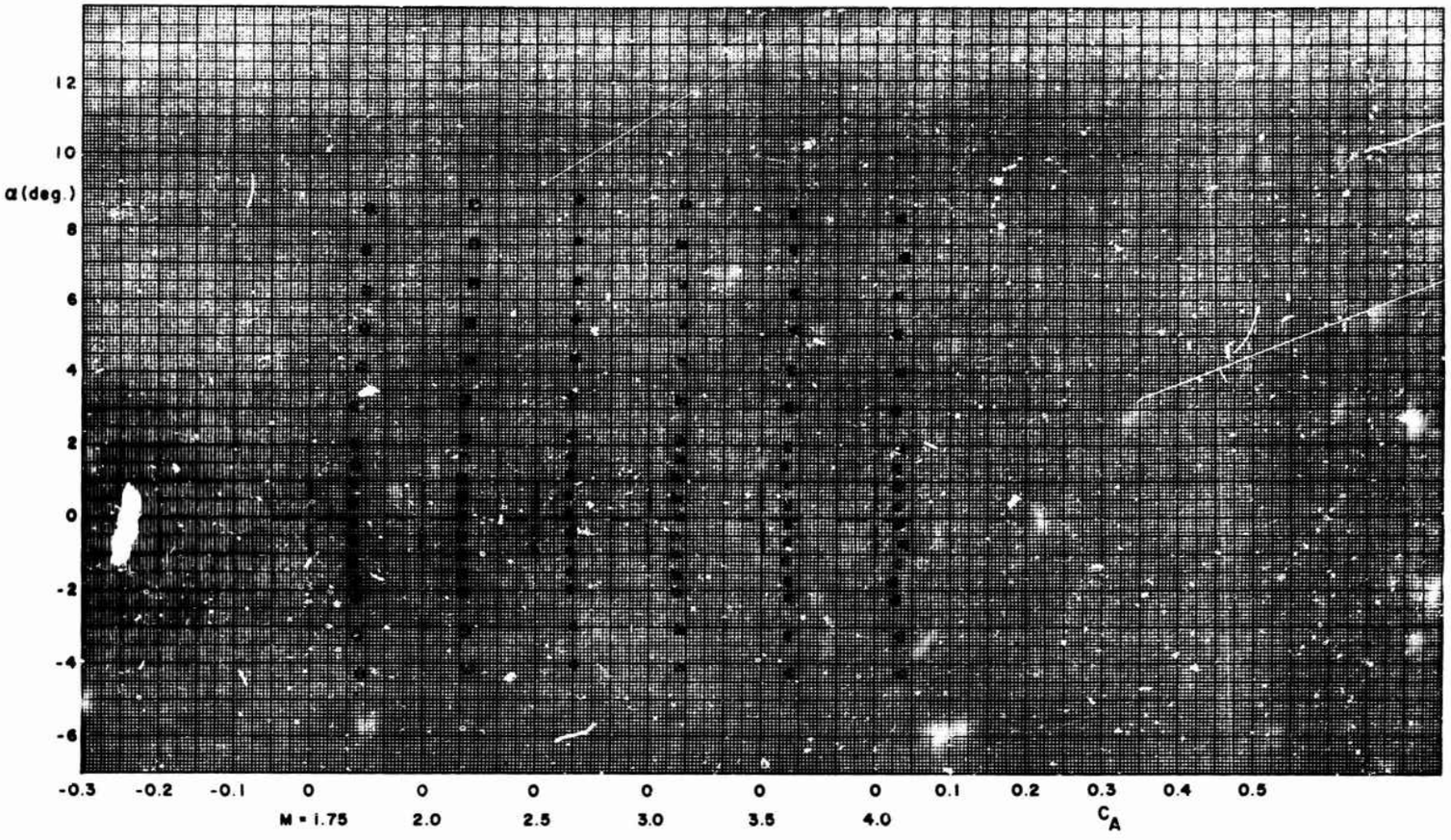

FIGURE A-15. ANGLE OF ATTACK VERSUS AXIAL FORCE COEFFICIENT, FD. 06 (Continued)

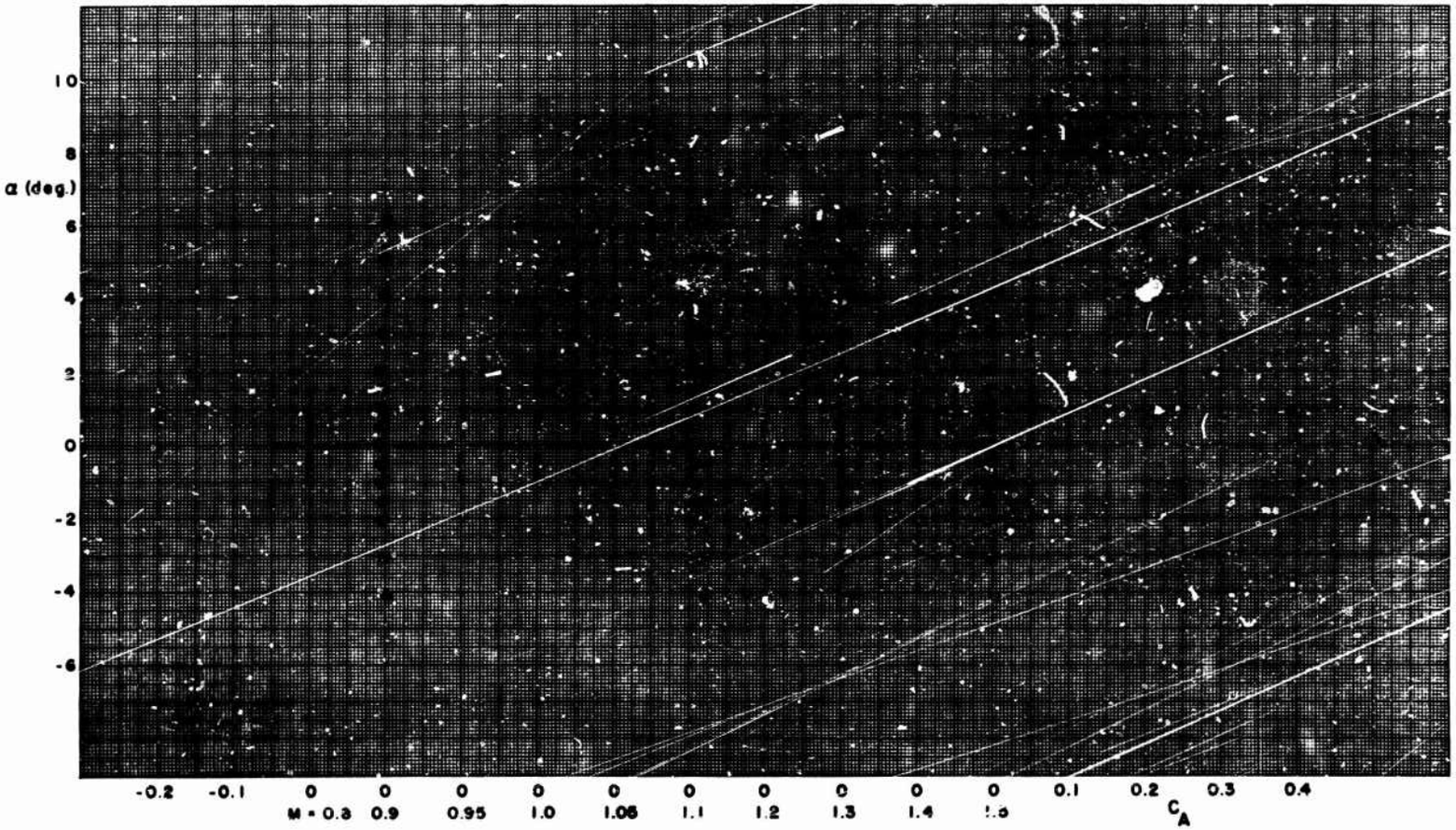

FIGURE A-15. ANGLE OF ATTACK VERSUS AXIAL FORCE COEFFICIENT, FD. 12 (Continued)

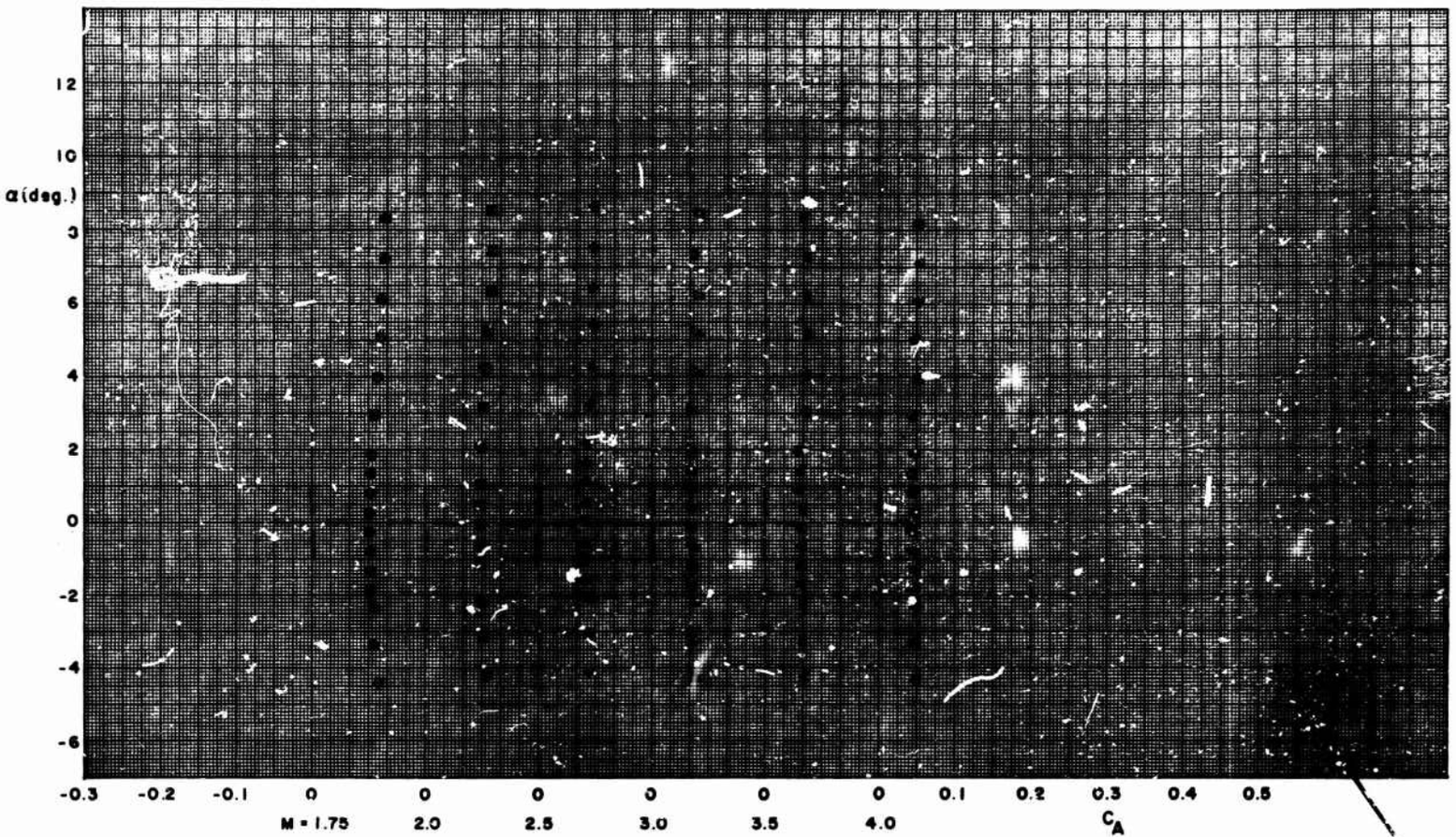

FIGURE A-15. ANGLE OF ATTACK VERSUS AXIAL FORCE COEFFICIENT, FD. 12 (Continued)

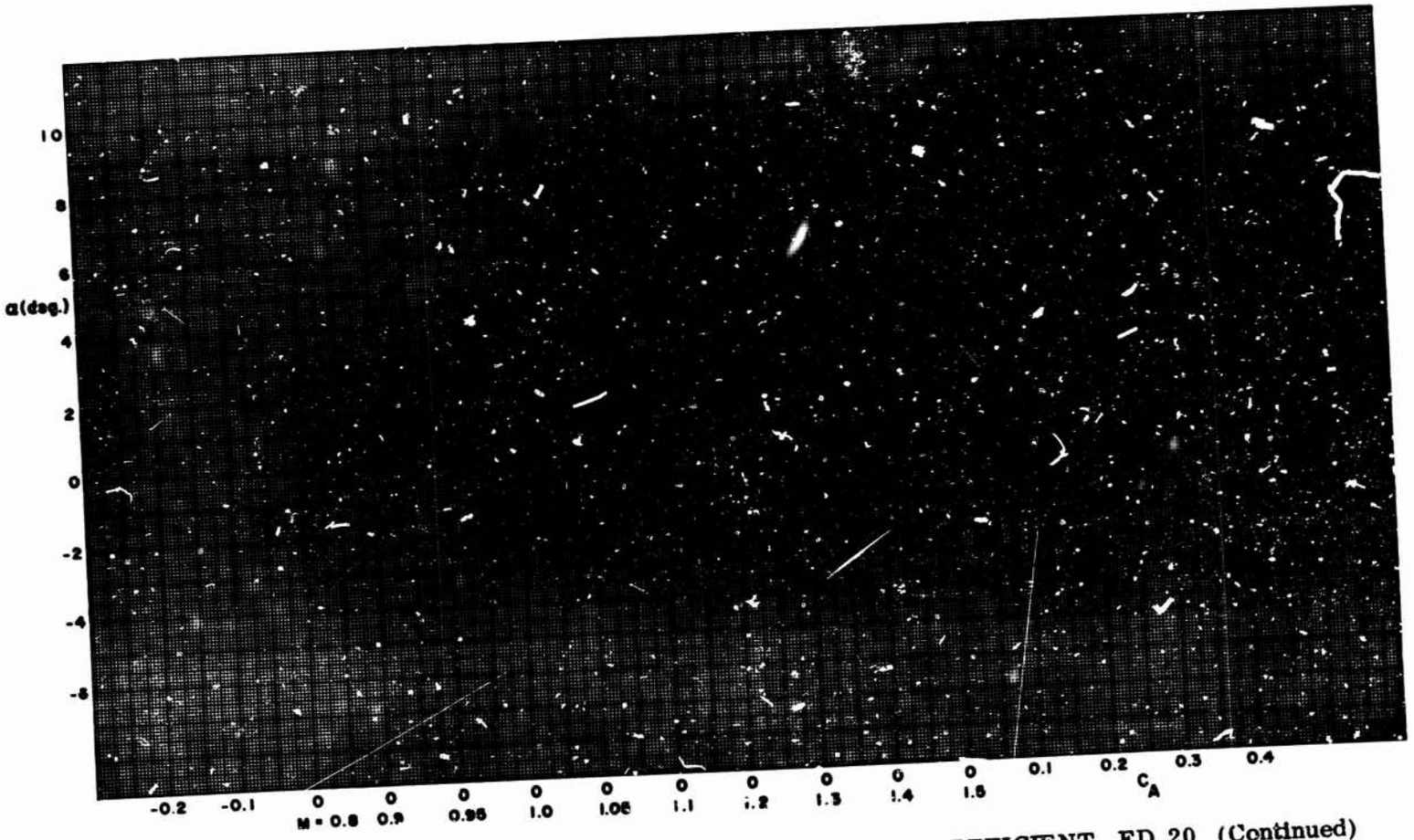

FIGURE A-15. ANGLE OF ATTACK VERSUS AXIAL FORCE COEFFICIENT, FD. 20 (Continued)

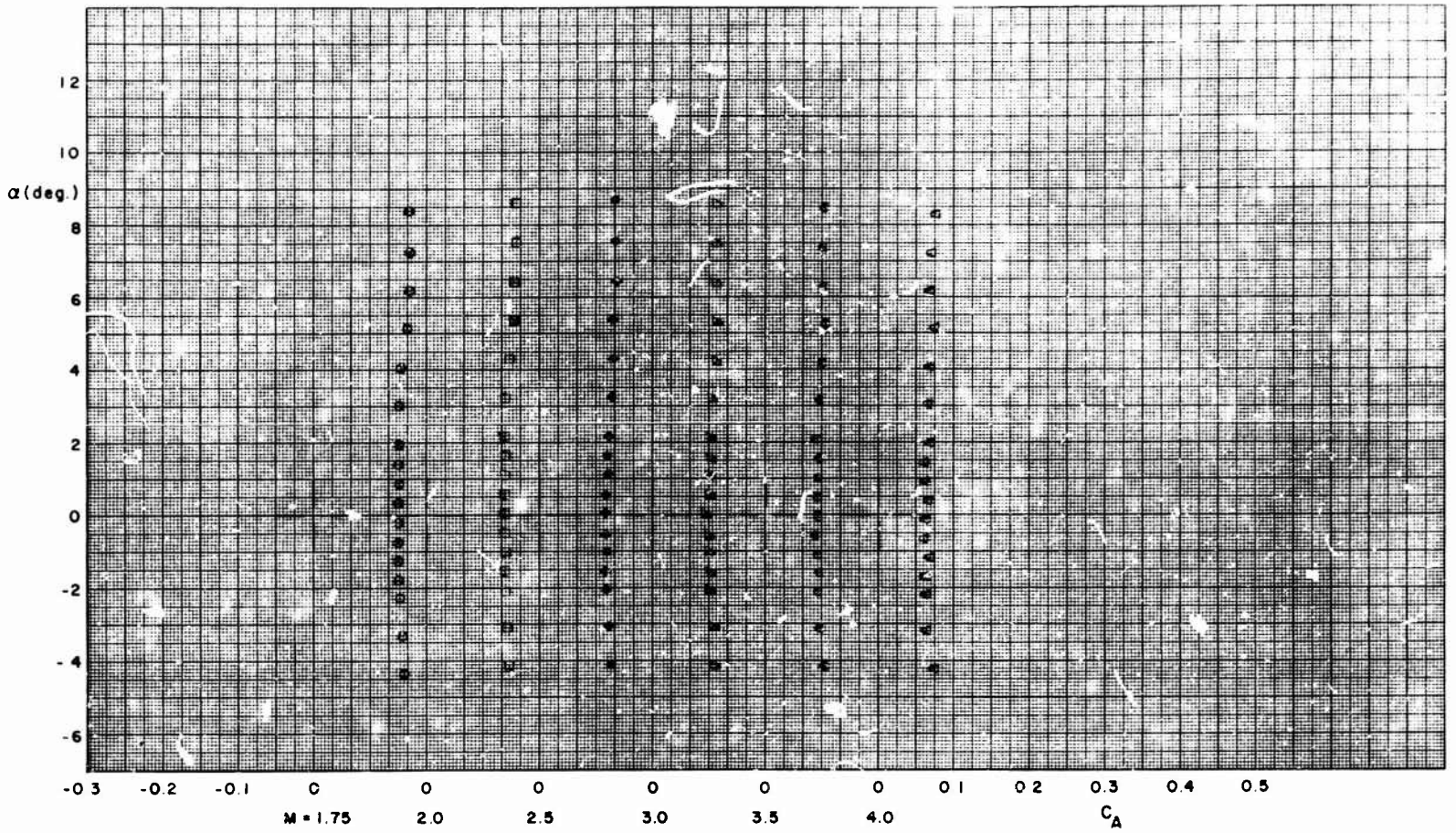

FIGURE A-15. ANGLE OF ATTACK VERSUS AXIAL FORCE COEFFICIENT, FD. 20 (Concluded)

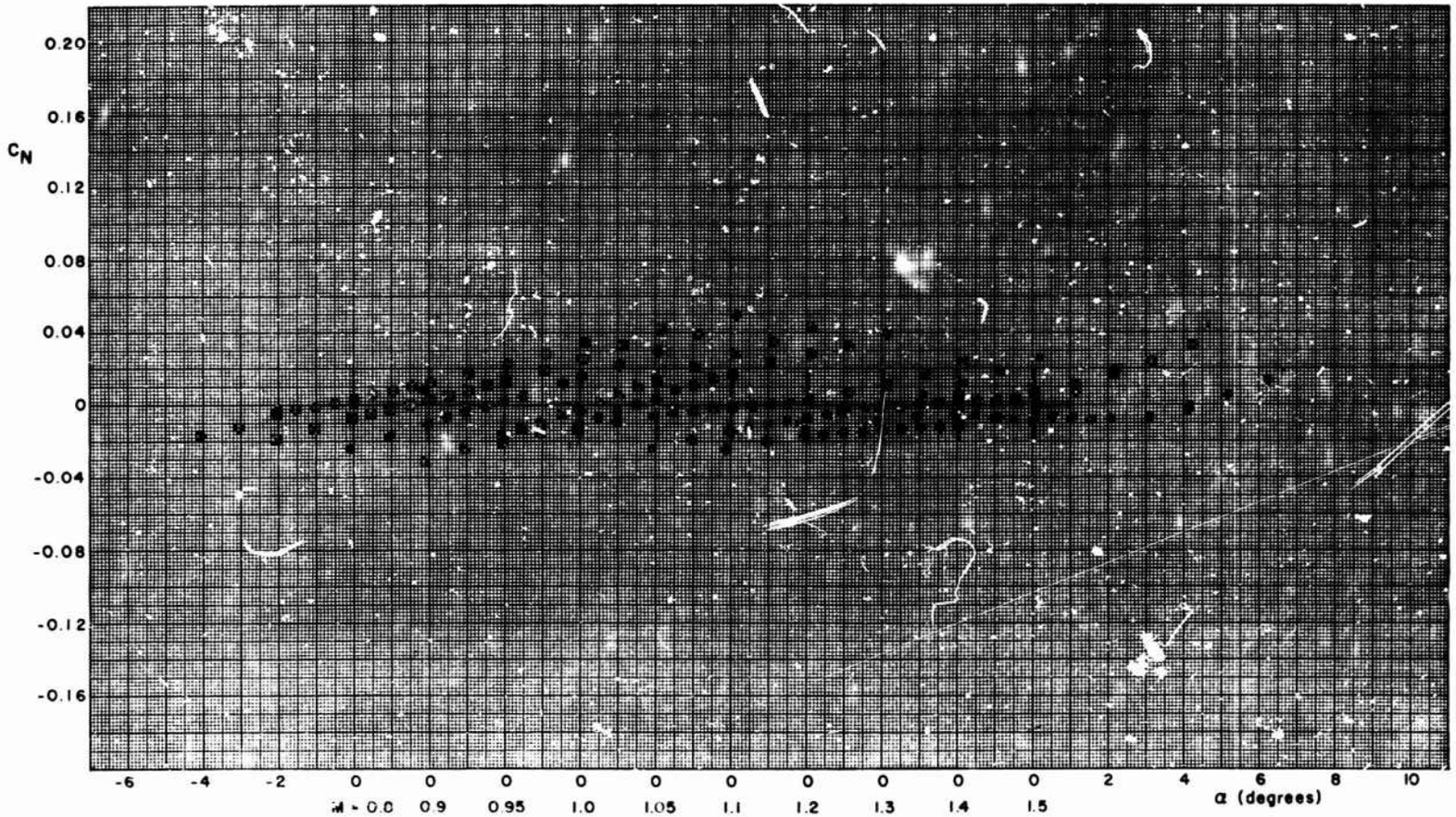

FIGURE A-16a. NORMAL FORCE COEFFICIENT VERSUS ANGLE OF ATTACK, 0000

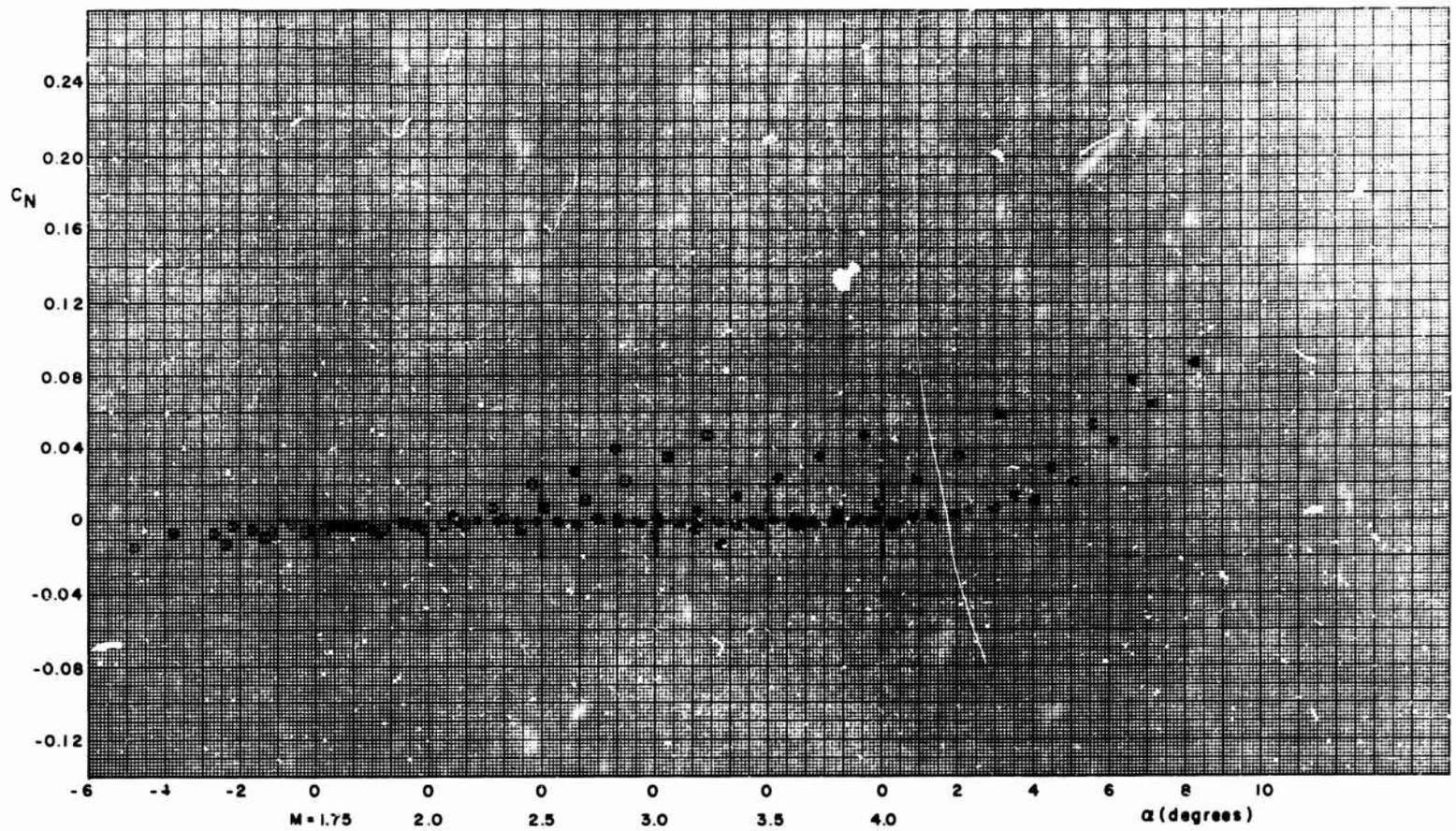

FIGURE A-16a. NORMAL FORCE COEFFICIENT VERSUS ANGLE OF ATTACK, 0000 (Concluded)

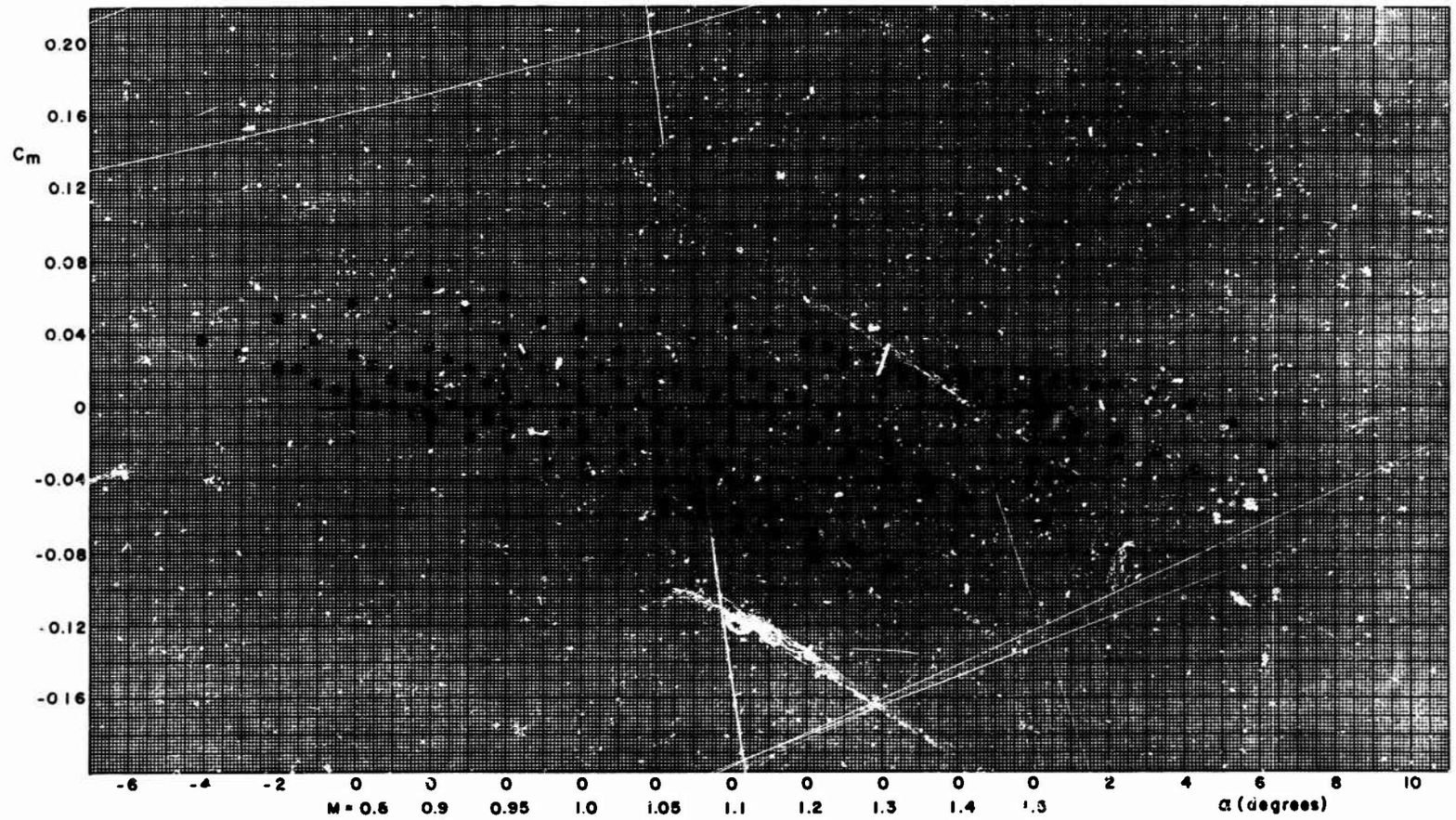

FIGURE A-16b. PITCHING MOMENT VERSUS ANGLE OF ATTACK, 0000

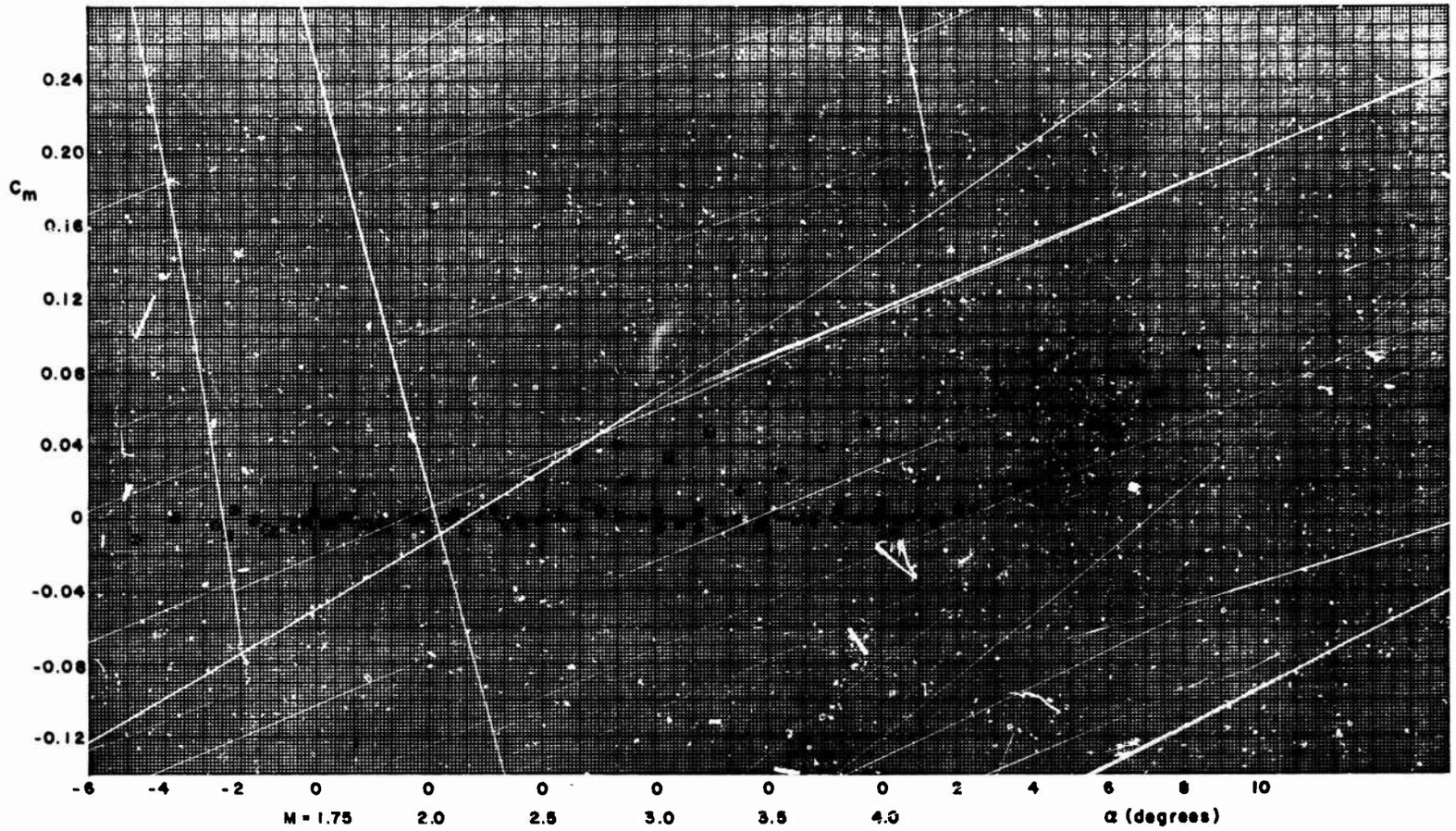

FIGURE A-16b. PITCHING MOMENT VERSUS ANGLE OF ATTACK, 0000 (Concluded)

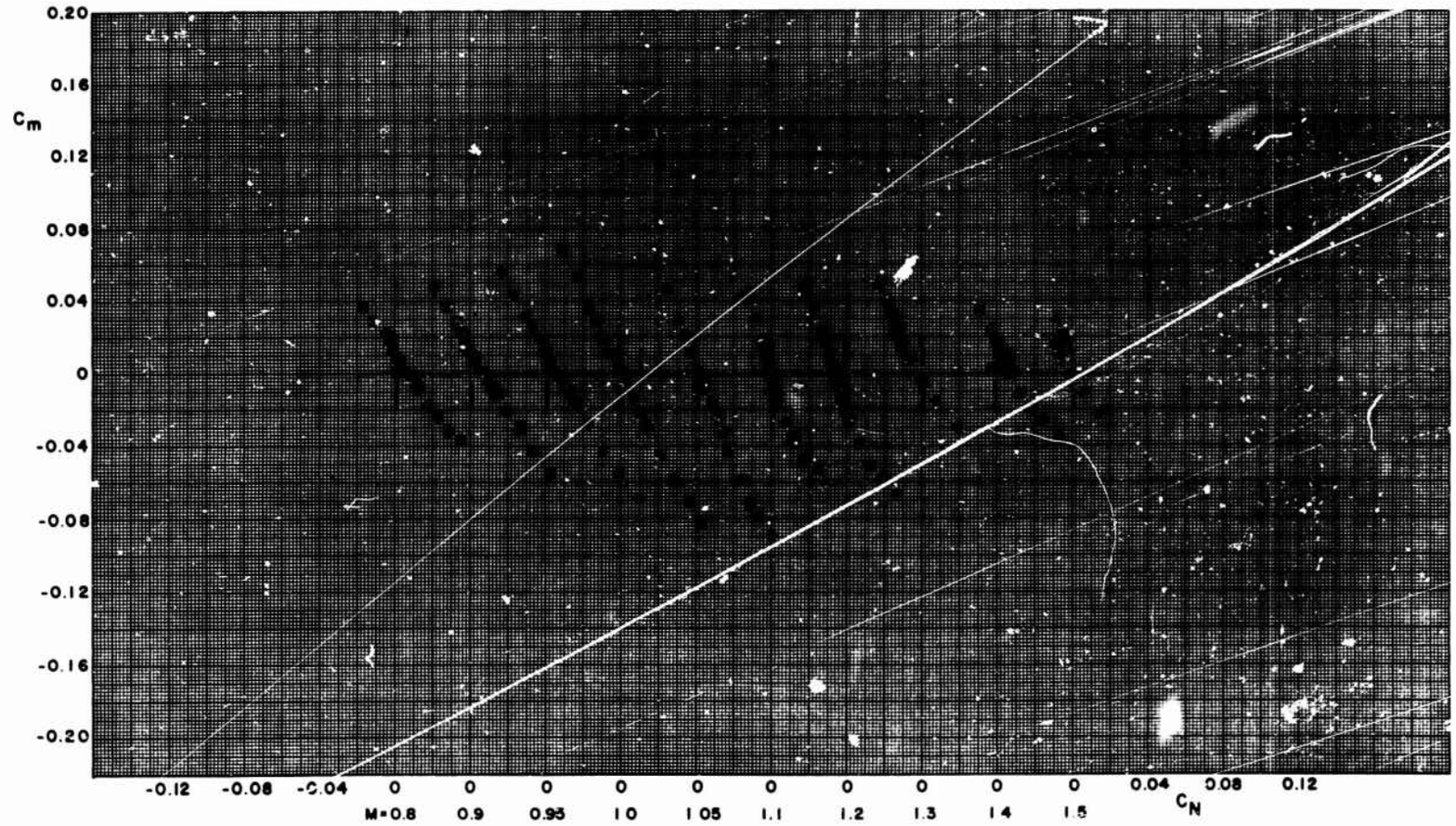

FIGURE A-16c. PITCHING MOMENT VERSUS NORMAL FORCE COEFFICIENT, 0000

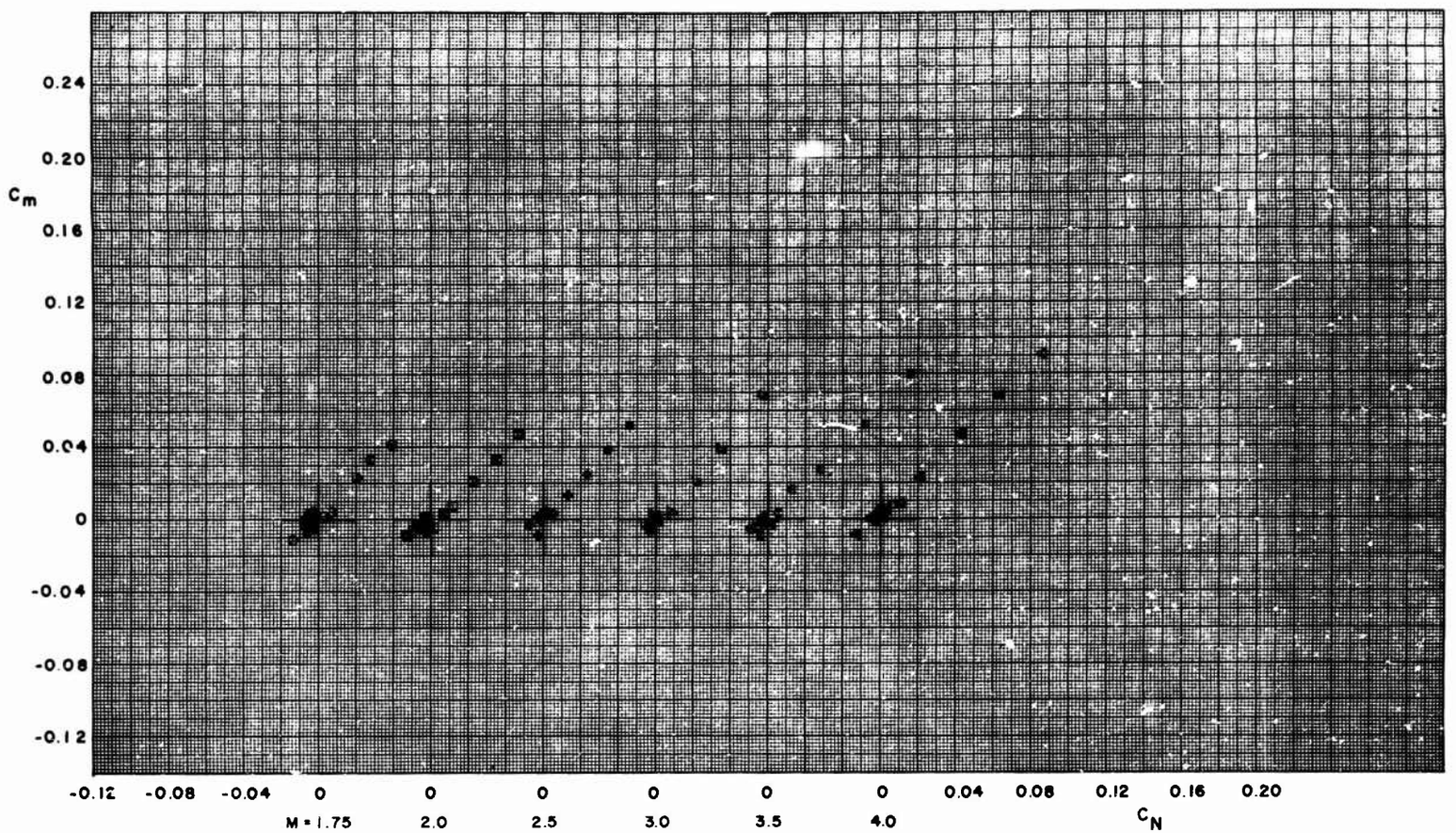

FIGURE A-16c. PITCHING MOMENT VERSUS NORMAL FORCE COEFFICIENT, 0000 (Concluded)

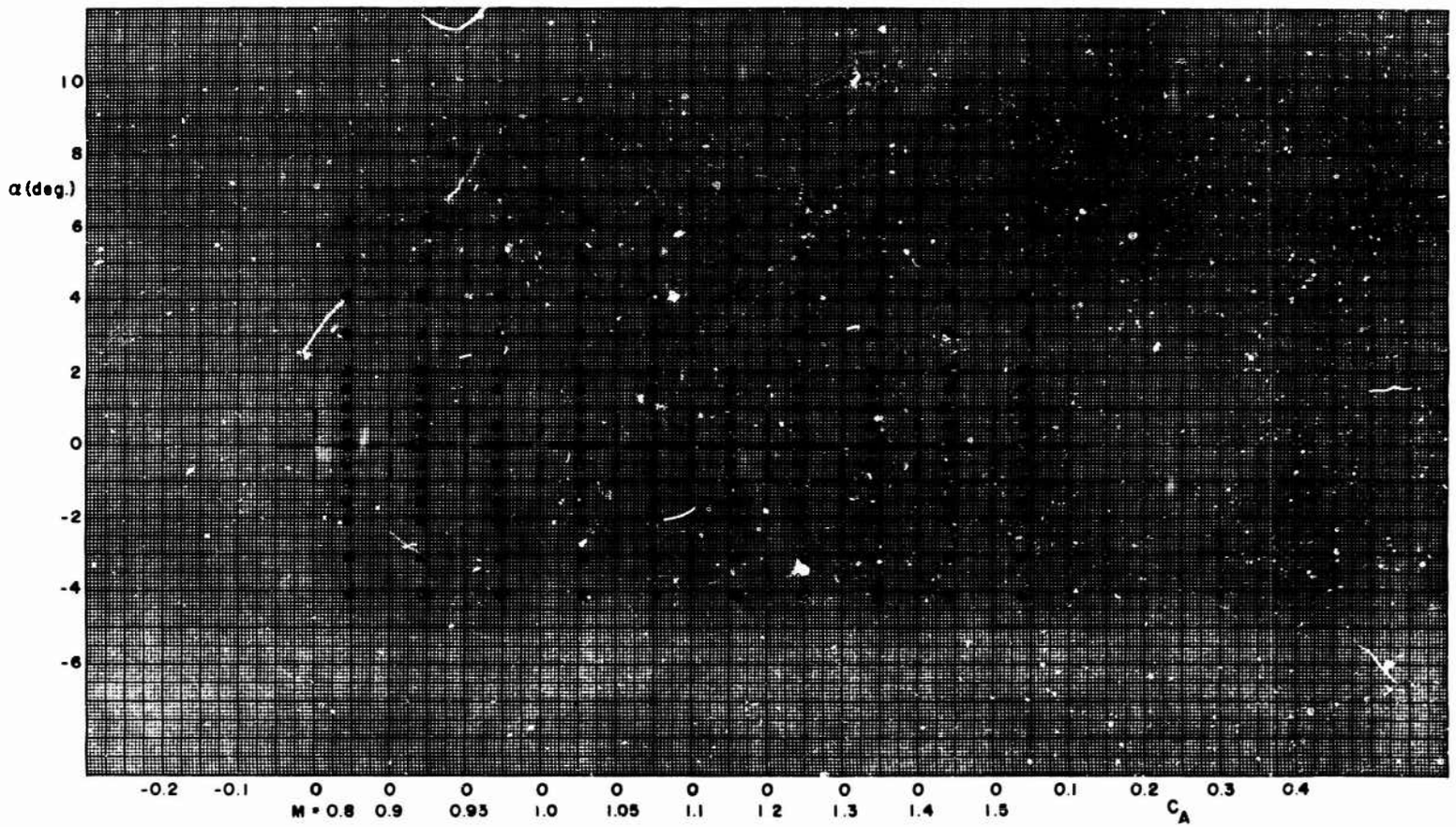

FIGURE A-16d. ANGLE OF ATTACK VERSUS AXIAL FORCE COEFFICIENT, 0000

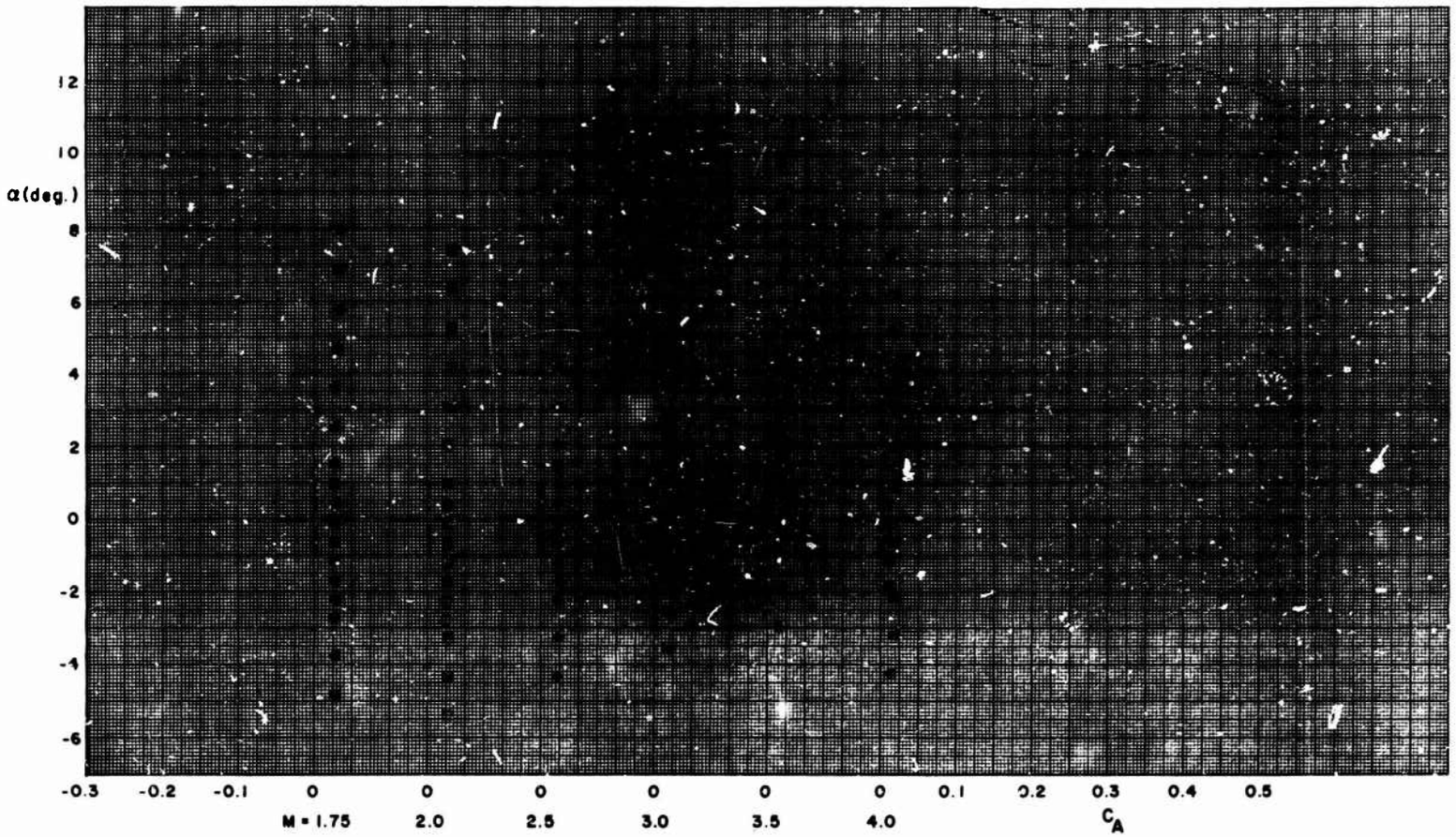

FIGURE A-16d. ANGLE OF ATTACK VERSUS AXIAL FORCE COEFFICIENT, 0000 (Concluded)

References

1. Pettis, W., Aerodynamic Characteristics of Multiple Fins of Rectangular Planform on a Body of Revolution at Mach Numbers of 1.48 to 2.22, U. S. Army Missile Command, Redstone Arsenal, Alabama, July 1967, Report No. RD-TM-67-5.

2. Jackson, F. M., Calibration of the AEDC-PWT 1-Ft. Transonic Tunnel With Variable Porosity Test Section Walls, Arnold Engineering Development Center, Arnold Air Force Station, Tennessee, July 1967, AEDC-TR-67-133.

3. McMullen, J. C., Wind Tunnel Testing Facilities at the Ballistic Research Laboratories, Ballistic Research Laboratories, Aberdeen Proving Grounds, Maryland, July 1960, Memo Report No. 1292.

4. Shadow, T. O., Wind Tunnel Study of the Effects of Fin Gap and Number of Fins on Tail Loads for an Ogive Cylinder Model at Transonic Speeds, Arnold Engineering Development Center, Arnold Air Force Station, Tennessee, July 1967, AEDC-TR-67-133.

UNCLASSIFIED

Security Classification

DOCUMENT CONTROL DATA - R & D

(Security classification of title, body of abstract and indexing annotation must be entered when the overall report is classified)

1. ORIGINATING ACTIVITY (Corporate author) Advanced Systems Laboratory Research and Engineering Directorate U. S. Army Missile Command Redstone Arsenal, Alabama 35809	2a. REPORT SECURITY CLASSIFICATION Unclassified 2b. GROUP NA

3. REPORT TITLE

NORMAL FORCE EFFECTIVENESS OF SEVERAL FIN PLANFORMS WITH STREAMWISE GAPS AT MACH NUMBERS OF 0.8 TO 5.0

4. DESCRIPTIVE NOTES (Type of report and inclusive dates)

Technical Report

5. AUTHOR(S) (First name, middle initial, last name)

C. W. Dahlke
W. Pettis

6. REPORT DATE	7a. TOTAL NO. OF PAGES	7b. NO. OF REFS
24 April 1970	151	4

8a. CONTRACT OR GRANT NO.	9a. ORIGINATOR'S REPORT NUMBER(S)
b. PROJECT NO. (DA) 1M262301A206 c. AMC Management Structure Code No. 5221.11.14800 d.	RD-TR-70-8 (Revision) 9b. OTHER REPORT NO(S) (Any other numbers that may be assigned this report) AD_____

10. DISTRIBUTION STATEMENT

This document is subject to special export controls and each transmittal to foreign governments or foreign nationals may be made only with prior approval of this Command, ATTN: AMSMI-RD.

11. SUPPLEMENTARY NOTES	12. SPONSORING MILITARY ACTIVITY
None	Same as No. 1

13. ABSTRACT

This report contains the results and analysis of a series of wind-tunnel tests for several rectangular and one delta fin planform with streamwise gaps between the fin root chord and body. The tests were conducted at free-stream Mach numbers from 0.8 to 1.5 with fin to body gap variation of 0.00 to 0.25 body diameter. The normal force effectiveness force effectiveness for the fin-gap configuration is presented as normal force coefficient slopes at zero angle of attack. Small gaps are shown to cause significant loss in fin effectiveness especially at transonic Mach numbers.

DD FORM 1 NOV 65 1473 REPLACES DD FORM 1473, 1 JAN 64, WHICH IS OBSOLETE FOR ARMY USE.

UNCLASSIFIED

Security Classification

14. KEY WORDS	LINK A		LINK B		LINK C	
	ROLE	WT	ROLE	WT	ROLE	WT
Fin planforms Streamwise gaps Wind-tunnel tests Supersonic and transonic Mach numbers						